


March 2019

## Design and Self-Assembly of Responsive Scaffolds for Food and Sensing Applications

Uma Sridhar

Follow this and additional works at: [https://scholarworks.umass.edu/dissertations\\_2](https://scholarworks.umass.edu/dissertations_2)

 Part of the [Materials Chemistry Commons](#), [Organic Chemistry Commons](#), and the [Polymer Chemistry Commons](#)

---

### Recommended Citation

Sridhar, Uma, "Design and Self-Assembly of Responsive Scaffolds for Food and Sensing Applications" (2019). *Doctoral Dissertations*. 1503.  
[https://scholarworks.umass.edu/dissertations\\_2/1503](https://scholarworks.umass.edu/dissertations_2/1503)

This Open Access Dissertation is brought to you for free and open access by the Dissertations and Theses at ScholarWorks@UMass Amherst. It has been accepted for inclusion in Doctoral Dissertations by an authorized administrator of ScholarWorks@UMass Amherst. For more information, please contact [scholarworks@library.umass.edu](mailto:scholarworks@library.umass.edu).

**DESIGN AND SELF-ASSEMBLY OF RESPONSIVE SCAFFOLDS FOR  
FOOD AND SENSING APPLICATIONS**

A Dissertation presented

by

UMA SRIDHAR

Submitted to the graduate school of the

University of Massachusetts, Amherst

In partial fulfillment of the requirements for the degree of

DOCTOR OF PHILOSOPHY

February 2019

Chemistry

© Copyright by Uma Sridhar 2019

All Rights Reserved

DESIGN AND SELF-ASSEMBLY OF RESPONSIVE SCAFFOLDS FOR FOOD  
AND SENSING APPLICATIONS

A Dissertation Presented

By

UMA SRIDHAR

Approved as to style and content by:

---

Sankaran Thayumanavan, Chair

---

Dhandapani Venkataraman, Member

---

Ricardo Metz, Member

---

Eric Decker, Member

---

Richard Vachet, Head  
Department of Chemistry

## **DEDICATION**

Dedicated to Amma, Daddy and Shweta

## ACKNOWLEDGEMENTS

It is a pleasure to thank those who made this thesis possible. First and foremost, I would like to thank my advisor Prof. Sankaran Thayumanavan for his immense support and guidance. I feel privileged to be among his students. He celebrates research in the truest sense of the term. I would also like to thank him for providing us with such an excellent opportunity, and also for his encouragement throughout the duration of the project. Despite his busy schedule, he always found time to discuss with us and guide us throughout. His guidance has been an extraordinary learning experience. I would like to thank our group assistant Karen Hakala for going out of the way to help, support all of us and the selfless love she bestows upon all the Thai group members.

I would also like to thank my committee members, Prof. Dhandapani Venkataraman, Prof. Ricardo Metz and Prof. Eric Decker, for their valuable inputs provided, especially during the prospectus and original research proposal. Next, I would like to thank Prof. Nicholas Abbott from University of Wisconsin-Madison with whom I had a chance to collaborate and learn a zillion things about liquid crystal interfaces and Dr Christophe Galopin (Director R&D, Taste Discovery for Sugar Reduction) for his input and insights during telephonic and face-to-face meetings. I must also thank Prof. William Woolridge and Dr. Birton Cowden from the Berthiaume Center for Entrepreneurship for their support and encouragement during the UMass Innovation Challenge pitch competitions.

I am ever grateful to my mentors, Dr. Krishna Reddy Raghupathi and Dr. Mijanur Rahaman Molla, for training me scientifically, and providing moral support during my initial years in graduate

school. A special thank you to Dr. Jiaming Zhuang and Dr. Hui Wang for also mentoring me, providing constructive criticism and helpful inputs for my research.

I would like to express my gratitude to all my collaborators and colleagues, Krishna Raghupathi, Priyaa Prasad, Poornima Rangadurai, Thameez Koyasseril, Kishore Raghupathi, Vikash Kumar, Piyachai Khomein, Manisha Chahar, Khushboo Singh, Bo Zhao, Bin Liu, Kazuki Iwabata and Chulsoon Park (University of Wisconsin, Madison) for their insightful discussions and time to help me understand my research problems better. I also would like to thank Kevin Byrne, Marina Franc and Margareta Ianosi-Irimie, undergraduate researchers for their contributions. Thanks, are in order to the past and present members of the Dendrimer/ (Dis)assembly/ Biomimetic subgroup, especially for their inputs during sub-group meetings. A big thank you to the UMass Chemistry staff Dennis Glick, J.M. Stowe, Kristina Knight, Robert Sabola and Ryan Feyrer for their support and assistance.

I would like to thank my dearest friends Poornima Rangadurai, Priyaa Prasad, Thameez Koyasseril who have stood by me through thick and thin and loved me the way I am. I would also like to thank Vikash Kumar, Huan He, Jingjing Gao, Piyachai Khomein, Manisha, Ann Fernandez, Kingshuk Dutta. They have brought incredible fun and joy and grad school wouldn't have been what it was without them. Thanks for believing in me when I have failed to believe in myself and encouraging me!

None of this would have been possible without the love, support and encouragement from my family. A big thank you to my parents who have nurtured my dreams of pursuing science since

childhood and the sacrifices that they have made for us to realize the same. They have encouraged me to chase my dreams, be empathetic, bold, strong-willed and live life on my own terms. I have been away from home for almost ten years now and they have completely supported every decision of mine all along the way. And thanks to my baby sister Shweta, a sister who has made me laugh, punched me, stuck up for me, drove me crazy, annoyed me, hugged me, watched me succeed, saw me fail, picked me back up, cheered me on, wiped my tears, calmed me down, made me strong & is someone I am proud to have in my life. I couldn't have had a better childhood than growing up with you.



## **ABSTRACT**

### **DESIGN AND SELF-ASSEMBLY OF RESPONSIVE SCAFFOLDS FOR FOOD AND SENSING APPLICATIONS**

FEBRUARY 2019

UMA SRIDHAR

INTEGRATED BS-MS, INDIAN INSTITUTE OF SCIENCE EDUCATION  
AND RESEARCH, PUNE

PH.D., UNIVERSITY OF MASSACHUSETTS, AMHERST

Directed by: Professor Sankaran Thayumanavan

Developing an understanding of how molecules, materials and complex systems contribute to biological functions is important since the interpretation of such mechanisms paves the way to further the development of materials that replicate natural functions or impart the observed properties to synthetic materials. The self-assembly of stimuli-responsive scaffolds based on micelles, liposomes, hydrogels and thin films has been of considerable interest. These systems need to be endowed with certain design features which influence the self-assembly and the responsiveness of the scaffold when subjected to external stimuli which could be physical, chemical or biological in nature. This kind of insight is still lacking in our understanding of how these systems respond to various stimuli. In this thesis, our objective is to establish structure-property relationships between the influence of structural design and the target material properties. Of interest to us are pH, temperature (chemical) and enzyme/proteins (biological) as stimuli and we have performed experiments to validate the responsive features of these systems.

The design principles for oligomeric peptides to exhibit a unique temperature-dependent size transition were elucidated and it was found that incorporation of aromatic hydrophobic groups diminishes the thermo-sensitivity of the peptide nanoassemblies. Since these molecules are designed to incorporate FDA (Food and Drug Administration) approved components and the assembly is biodegradable, this system has interesting applications in the food industry and in cryptic catalysis.

Parameters that dictate the morphology of calcium cross-linked alginate gels and the release of an artificial sweetener, aspartame from these hydrogels were studied. We have validated the effect of cross link densities and sizes on the release kinetics of the microgel spheres and bulk hydrogels. The release data was fitted to kinetic models available from literature to elucidate the pathway constraints which were further, found to dictate the release pathway. Lastly, structure-property relationships were developed using libraries of oligomeric amphiphiles to make possible rational design of triggers for amplification via liquid crystal (LC) response. To this end, we synthesized a wide range of amphiphilic oligomers that responded to a protein, carbonic anhydrase (CA II). The mechanism of binding-induced anchoring transition at the LC/aqueous interface was corroborated using addition of inhibitor by modulating the strength of binding. The design rules established here provide insight into the rational design of oligomers with triggers that can couple specific molecular events to LCs to achieve highly amplified responses. This paves way to develop principles based on LCs that permit incorporation of feedback for massive amplification that can be leveraged for targeting, sensing and triggering.

# TABLE OF CONTENTS

	Page
ACKNOWLEDGEMENTS .....	v
ABSTRACT .....	viii
LIST OF TABLES .....	xiii
LIST OF FIGURES .....	xiv
LIST OF SCHEMES .....	xxii
CHAPTER 1 .....	1
INTRODUCTION .....	1
1.1 Supramolecular self-assembly.....	1
1.2 Stimuli responsive supramolecular systems.....	2
1.3 Exogeneous stimuli .....	3
1.3.1 Temperature responsive systems .....	3
1.3.2 Photo responsive systems .....	7
1.4 Endogenous stimuli.....	9
1.4.1 pH responsive systems.....	9
1.4.2 Redox responsive systems .....	11
1.4.3 Protein and enzyme responsive systems.....	13
1.5 Summary and thesis overview.....	16
1.6 References .....	19
CHAPTER 2 .....	28
ROLE OF AROMATICITY IN DETERMINING NANOSCALE THERMO-RESPONSIVE BEHAVIOR OF AMPHIPHILIC PEPTIDES.....	28
2.1 Background and significance .....	28
2.1.1 Thermo and inverse thermo responsive supramolecular assemblies.....	29
2.1.2 Amphiphilic peptides.....	30
2.1.3 Design Objectives.....	31
2.2 Materials and methods .....	33
2.3 Results and discussion.....	40
2.3.1 Characterization of self-assembly of peptides.....	40

2.3.2 Temperature dependent aggregation and circular dichroism .....	41
2.3.3 Role of hydrophobic unit in thermo responsive behavior .....	43
2.3.4 Reversibility of size transition .....	45
2.3.5 Hydrophobic guest encapsulation and release .....	46
2.4 Conclusions .....	47
2.5 References .....	49
2.6 NMR Spectrum of molecules .....	59
<b>CHAPTER 3 .....</b>	<b>64</b>
<b>ALGINATE HYDROGELS FOR THE STABLE ENCAPSULATION AND RELEASE OF ARTIFICIAL SWEETENERS IN BEVERAGES.....</b>	<b>64</b>
3.1 Background and significance .....	64
3.2 Materials and methods .....	68
3.3 Results and discussion.....	72
3.3.1 Microgel beads: Influence of alginate composition, mode of addition, cross-linking time and concentration of cross-linker .....	72
3.3.2 Bulk Hydrogels: Influence of alginate composition, mode of addition, cross-linking time and concentration of cross-linker .....	74
3.3.3 Resolution of aspartame and degradation products by size exclusion chromatography.....	76
3.3.4 Release kinetics and release mechanism of microgel beads.....	77
3.3.5 Mechanism of release of aspartame for microgel beads.....	79
3.3.6 Mechanism of release of aspartame for bulk hydrogels .....	82
3.4 Conclusions .....	88
3.5 References .....	89
<b>CHAPTER 4 .....</b>	<b>95</b>
<b>AMPLIFICATION AND OPTICAL REPORTING OF INTERFACIAL MOLECULAR EVENTS USING LIQUID CRYSTALS .....</b>	<b>95</b>
4.1 Background and significance .....	95
4.1.1 Design objectives.....	97
4.2 Materials and methods .....	99
4.3 Result and discussion .....	116
4.3.1 Characterization of self-assembly and binding-induced disassembly (BID) .....	116

4.3.2 Anchoring transition in the presence of the oligomers at the aqueous-LC interface.....	118
4.3.3 Binding-induced transition at the aqueous-LC interface in the presence of carbonic anhydrase and dimer.....	119
4.3.4 Competitive inhibition experiment to determine kinetics of binding of complementary vs non-complementary proteins.....	124
4.3.5 Digestion of carbonic anhydrase using Thermolysin to probe non-specific binding.....	126
4.4 Conclusions.....	127
4.5 References.....	128
4.6 NMR spectrum of molecules.....	134
CHAPTER 5.....	145
SUMMARY AND FUTURE DIRECTIONS.....	145
5.1 Summary.....	145
5.2 Future directions.....	147
5.2.1 Role of linker in thermo responsive behavior.....	147
5.2.2 pH dependent degradation of peptide nanoassemblies.....	150
5.2.3 Triggerable Multi-Scale Responses via Liquid Crystallinity.....	151
5.2.4 Understanding the mechanism for the dimer to cause the LC homeotropic anchoring.....	152
5.3 Materials and methods.....	153
5.4 NMR spectrum of molecules.....	156
5.5 References.....	158
APPENDIX.....	160
EFFECT OF HOFMEISTER IONS ON THE SIZE, SUB-LCST AND ENCAPSULATION STABILITY OF TRIMERIC OLIGOMERS.....	160
BIBLIOGRAPHY.....	180

## LIST OF TABLES

Table	Page
Table 3.1 Fabrication of calcium cross linked alginate microgel beads I to V.....	72
Table 3.2 Fabrication of calcium cross linked alginate hydrogels.....	74
Table 3.3 Release models and corresponding correlation coefficients for the microgel beads. The release kinetics for the microgel beads I to V obey the Korsmeyer-Peppas model with a $R^2$ value of $> 0.88$ .....	80
Table 3.4 Release models and corresponding correlation coefficients for the hydrogels. Bulk hydrogels obey the Korsmeyer-Peppas model of release with a $R^2$ value $> 0.8$ .....	88
Table 4.1 CACs and sizes of aggregates from oligomers 1-6.....	116
Table 4.2 Molecular weights and pI values of proteins CA II, BSA and lysozyme (Table 1) and Zeta potential measurements of the LC-aqueous interface (Table 2) .....	122

## LIST OF FIGURES

Figure	Page
Figure 1.1 Various intrinsic and extrinsic stimuli.....	2
Figure 1.2 A) Structures of the Amphiphilic Oligomers Used in This Study B) Plot of HT voltage vs temperature for molecules 1–6 in water <sup>21</sup> .....	4
Figure 1.3 A) Structures of the Amphiphilic dendrimers Used in This Study B) large change in the $D_H$ of 1 observed for 25 °C (160 nm) and 10 °C (30 nm) assemblies as revealed by DLS (C) The temperature sensitivity of 1 was shown to have an inverse effect on the guest exchange dynamics with exchange at 4 °C complete within 10 min and virtually no exchange observed at 37°C <sup>22</sup> .....	5
Figure 1.4 Design of Amphiphilic Diblock Copolymer (BCP) and (a) Photograph showing an aqueous solution of BCP; left-at room temperature, right-after heating to 40 °C. (b) Turbidity experiment showing the change in HT voltage with temperature of BCP and PNIPAM (P3) <sup>16</sup> .....	6
Figure 1.5 A) Schematic representation of the light-induced disassembly of amphiphilic dendritic assemblies B) UV/Vis spectra of the G1 dendron upon irradiation with UV light for different time intervals (0–380 s) and plot of the absorbance at 320 nm, which illustrates cleavage of the photolabile ester bond <sup>26</sup> .....	8
Figure 1.6 Substituent effects upon the hydrolysis of benzylidene acetals. (A)Hydrolysis kinetics and the first-order reaction fitting curve, (B) Hammett plot. The hydrolysis was performed under TFA condition. The solid lines are the fitting curves <sup>33</sup> .....	11

Figure 1.7 A) Schematic representation of the formation of a covalent polymer network using the protein as the template and its traceless and triggered release in a reducing environment. B) Chemical Structures of Polymers and the Reaction Scheme for Protein Conjugation, Crosslinking to Generate the Nanoassembly, and Its Release in the Presence of a Reducing Agent <sup>42</sup> .....	12
Figure 1.8 A) Schematic Representation of MMP-9-Responsive Nanogels and Resulting Activated Cell Uptake and GSH Release and (B) Structural Representation of Polymer Nanogels and Stimuli Responsiveness: <sup>47</sup> .....	13
Figure 1.9 A) Binding-induced disassembly with lipophilic ligand containing dendrons. B) a) Sizes of G1–DNP (◇) and G2–DNP (▪) dendrons; b) size changes in G1–DNP and G2–DNP dendron based amphiphilic assemblies due to the presence of anti-DNP IgG; ◆, G1–DNP; □, G2–DNP; ▲, G1 <sup>51</sup> .....	14
Figure 1.10 A) Schematic representation of protein AND enzyme gated supramolecular disassembly. B) Disassembly of 1 (13 μM) in the presence of anti-DNP IgG (1 μM) and PLE (50 nM): Size change after 8 h, monitored by DLS <sup>52</sup> .....	15
Figure 2.1 Critical aggregation concentrations of peptides a) AMD-ALIP and b) AMD-AROM.....	40
Figure 2.2 Temperature-dependent size variation observed using dynamic light scattering (DLS) of a) AMD-ALIP and d) AMD-AROM. Corresponding TEM images of b) AMD-ALIP and e) AMD-AROM at 25 °C and c) AMD-ALIP and f) AMD-AROM at 5 °C indicates spherical assemblies.....	41
Figure 2.3 Temperature dependent circular dichroism (CD) for a) AMD-ALIP indicates formation of β-sheets with significant reduction of intensity at 5 °C while b) AMD-AROM exhibits a signature α-helix conformation with the same intensity at 25 °C and 5 °C.....	42



Figure 2.4 Variable temperature DLS of AMD-AROM and AMD-ALIP where AMD-AROM: AMD-ALIP is 1:1 reveals that incorporation of a peptide containing an aliphatic hydrophobic group(AMD-ALIP) results in a size transition of an aromatic group containing peptide nanoassembly.....44

Figure 2.5 DLS sizes for a) AMD-ALIP and b) AMD-AROM indicate that the size transition is irreversible over several heating and cooling cycles and that the peptide nanoassemblies are ‘kinetically trapped’ at 25 °C.....45

Figure 2.6 Fluorescence spectra of DiI encapsulated in peptide nanoassemblies against pristine DiI in water for AMD-ALIP(a), AMD-AROM(b).....46

Figure 2.7: Guest encapsulation ability at 25 °C and 5 °C for a) AMD-ALIP and b) AMD-AROM.....47

Figure 2.8 <sup>1</sup>H NMR spectrum of starting material (top) and molecule 2 (bottom).....59

Figure 2.9 <sup>1</sup>H NMR spectrum of molecule 3 (top) and molecule 4 (bottom).....60

Figure 2.10 <sup>1</sup>H NMR spectrum of molecule 5 (top) and molecule 6 (bottom).....61

Figure 2.11 <sup>1</sup>H NMR spectrum of molecule 7 (top) and ESI-MS of molecule AMD-ALIP (bottom).....62

Figure 2.12 ESI-MS of molecule AMD-AROM.....63

Figure 3.1 Degradation pathways of aspartame at different pH.....65

Figure 3.2 Loading efficiency and sizes of beads I to V as a function of alginate composition, mode of addition, cross-linking time and concentration of cross-linker.....73

Figure 3.3 SEM images of A) Alginate showing loose networks as compared to B) Gel F which exhibits ordered yet inhomogeneous networks.....75

Figure 3.4 A) Resolution of aspartame and phenylalanine methyl ester using SEC B) Calibration curve for aspartame using SEC.....	76
Figure 3.5 Release profiles of microgel beads I and II. Compared to control I, increase in cross-linking time results in a greatest burst release.....	77
Figure 3.6 Release profiles for microgel beads IV and III.....	78
Figure 3.7 Korsmeyer-Peppas release model fitting for microspheres II and V.....	81
Figure 3.8 Mechanism of release of aspartame from microgel beads II and V.....	81
Figure 3.9 Higuchi release model for microspheres I and III.....	82
Figure 3.10 Cumulative release profiles of aspartame from gels B, C and D at pH 2 and 4.....	83
Figure 3.11 Cumulative release of aspartame from Gels F and H at pH 2 and pH 4.....	84
Figure 3.12 Release of aspartame from Gel H at pH 2 and 4 when fitted to Korsmeyer-Peppas model.....	85
Figure 3.13 Release of aspartame from Gel B at pH 2 and 4 when fitted to Higuchi's model.....	86
Figure 3.14 Schematic for the proposed H-bonding stabilization in Gel H.....	87
Figure 4.1 Illustration of the proposed mechanism for anchoring transition in the presence of oligomeric amphiphiles at the LC-water interface.....	97
Figure 4.2 a CAC(top) and DLS(bottom) profiles for molecule 1(left) and 2(right).....	112
Figure 4.2 b CAC(top) and DLS(bottom) profiles for molecule 3(left) and 4(right).....	113
Figure 4.2 c CAC(top) and DLS(bottom) profiles for molecule 5(left) and 6(right).....	114

Figure 4.3 Principle of binding-induced disassembly (BID) and disassembly of dimer with complementary protein bovine carbonic anhydrase as monitored by DLS.....	117
Figure 4.4 Polarized light microscopy images of aqueous-LC interface decorated with dimeric oligomers exhibiting a homeotropic anchoring transition.....	118
Figure 4.5 Stability of aqueous-LC interface decorated with dimer (A) 0 day, (B) 1 day, (C) 2 day, and (D) 4 day.....	119
Figure 4.6 The images of the response of aqueous-LC interface decorated from H-dimer (20 $\mu\text{M}$ ) with (A) Carbonic anhydrase II (4 $\mu\text{M}$ ), (B) BSA (4 $\mu\text{M}$ ), and (C) lysozyme (4 $\mu\text{M}$ ). The schematic illustrations of the response of aqueous-LC interface to (D) Carbonic anhydrase II (4 $\mu\text{M}$ ), (E) BSA (4 $\mu\text{M}$ ), and (F) lysozyme (4 $\mu\text{M}$ ). All magnified images were represented on the middle and white bar in the magnified images represented 100 $\mu\text{m}$ .....	121
Figure 4.7 (A) The relative intensities of aqueous-LC interface decorated with dimer with different concentration of CA II and BSA.....	123
Figure 4.8 The polarized light microscopy images of anchoring transition of aqueous-LC interface decorated from dimer (20 $\mu\text{M}$ ) with (A) Carbonic anhydrase II (0.4 $\mu\text{M}$ ) – Dimer complex after contacting with BSA (1 $\mu\text{M}$ ), (B) Carbonic anhydrase II (1 $\mu\text{M}$ ) and BSA (1 $\mu\text{M}$ ) simultaneously, and (C) lysozyme (1 $\mu\text{M}$ ) and BSA (1 $\mu\text{M}$ ) simultaneously. Time interval to add CA II (0.4 $\mu\text{M}$ ), BSA (1 $\mu\text{M}$ ), and lysozyme (1 $\mu\text{M}$ ) onto the well. All samples were incubated for 2 hour and observed by polarized light microscopy.....	124
Figure 4.9 The relative intensity of aqueous-LC interface of (A) All control samples, (B) The relative intensity of aqueous-LC interface with different concentration of TLN, (C) the schematic illustration of experimental system with TLN, CA II, and BSA, (D) the schematic illustration of role of TLN in the mixture of CA II (0.4 $\mu\text{M}$ ) and BSA (1 $\mu\text{M}$ ).....	126

Figure 4.10 $^1\text{H}$ NMR of molecules 15(top) and 14(bottom).....	134
Figure 4.11 $^1\text{H}$ NMR of molecules 13(top) and 7(bottom).....	135
Figure 4.12 $^1\text{H}$ NMR of molecules 8(top) and 9(bottom).....	136
Figure 4.13 $^1\text{H}$ NMR of molecules 10(top) and 11(bottom).....	137
Figure 4.14 $^1\text{H}$ NMR of molecules 12(top) and 21(bottom).....	138
Figure 4.15 $^1\text{H}$ NMR of molecules 1(top) and 2(bottom).....	139
Figure 4.16 $^1\text{H}$ NMR of molecules 3(top) and 4(bottom).....	140
Figure 4.17 $^1\text{H}$ NMR of molecules 5(top) and 6(bottom).....	141
Figure 4.18 $^{13}\text{C}$ NMR of molecules 1(top) and 2(bottom).....	142
Figure 4.19 $^{13}\text{C}$ NMR of molecules 3(top) and 4(bottom).....	143
Figure 4.20 $^{13}\text{C}$ NMR of molecules 5(top) and 6(bottom).....	144
Figure 5.1 a) Temperature-dependent size variation for molecule 4 from DLS b) CD spectrum for molecule 4 indicates higher ordered structures at 25 °C with a substantial loss at 5 °C. TEM images for molecule 17 at c) 25 °C and d) 5 °C support the data obtained.....	148
Figure 5.2 DLS sizes for molecule 4 indicate that the size transition is irreversible over several heating and cooling cycles and that the peptide nanoassemblies are kinetically trapped at 25 °C.....	149
Figure 5.3 CD spectra of a) molecule 12, b) molecule 13 and c) molecule 17 upon incubation in acidic medium show that the nanoassemblies adopt a different secondary structure than their native conformation.....	150
Figure 5.4 Simulations indicate that oligomeric dimer disrupts ordering of LC interface.....	151
Figure 5.5 Critical aggregation concentrations of peptide 4.....	154
Figure 5.6 $^1\text{H}$ NMR of molecules 4'(top) and 14(bottom).....	156

Figure 5.7 ESI-MS of molecule EST-AROM(4')	157
Figure A.1 The Hofmeister series showing Kosmotropes and Chaotropes	160
Figure A.2 Effect of Hofmeister Ions on the Size and Encapsulation Stability of Polymer Nanogels	162
Figure A.3 Sub-LCST and trimers exhibiting a change in aggregation properties below sub-LCST	163
Figure A.4 Dynamic light scattering (DLS) of trimer (T) in the presence of kosmotropic (sodium sulfate), weakly kosmotropic (sodium chloride) and chaotropic salts (sodium thiocyanate)	167
Figure A.5 Correlation coefficients as given by Dynamic light scattering (DLS) of trimer (T) in the presence of kosmotropic (sodium sulfate), weakly kosmotropic (sodium chloride) and chaotropic salts (sodium thiocyanate)	168
Figure A.6 Dynamic light scattering (DLS) of cyclic trimer (CT) in the presence of kosmotropic (sodium sulfate), weakly kosmotropic (sodium chloride) and chaotropic salts (sodium thiocyanate)	169
Figure A.7 Correlation coefficients as determined by dynamic light scattering (DLS) of cyclic trimer (CT) in the presence of kosmotropic (sodium sulfate), weakly kosmotropic (sodium chloride) and chaotropic salts (sodium thiocyanate)	170
Figure A.8 Correlation coefficients as determined by dynamic light scattering (DLS) of trimer (T) in the presence of 500 mM kosmotropic (sodium sulfate), weakly kosmotropic (sodium chloride) and chaotropic salts (sodium thiocyanate) at different temperatures	170
Figure A.9 Correlation coefficients as determined by dynamic light scattering (DLS) of cyclic trimer (CT) in the presence of 500 mM kosmotropic (sodium sulfate), weakly kosmotropic (sodium chloride) and chaotropic salts (sodium thiocyanate) at different temperatures	171

Figure A.10 Working principle of the FRET-based method to determine the dynamics of exchange in supramolecular assemblies.....	172
Figure A.11 Absorbance of DiI in dye-loaded trimer (T) upon addition of kosmotrope ( $\text{Na}_2\text{SO}_4$ and $\text{NaCl}$ ) and chaotropes ( $\text{NaSCN}$ ).....	173
Figure A.12 Absorbance of DiI in dye-loaded cyclic trimer (CT) upon addition of kosmotrope ( $\text{Na}_2\text{SO}_4$ and $\text{NaCl}$ ) and chaotropes ( $\text{NaSCN}$ ).....	174
Figure A.13 Overlap integral for DiO and DiI in dye-loaded trimer (T) upon addition of kosmotrope ( $\text{Na}_2\text{SO}_4$ and $\text{NaCl}$ ) and chaotropes ( $\text{NaSCN}$ ).....	175
Figure A.14 Overlap integral for DiO and DiI in dye-loaded cyclic trimer (CT) upon addition of kosmotrope ( $\text{Na}_2\text{SO}_4$ and $\text{NaCl}$ ) and chaotropes ( $\text{NaSCN}$ ).....	176

## LIST OF SCHEMES

Scheme	Page
Scheme 2.1 Structures of different oligomeric peptide amphiphiles used in this study.....	32
Scheme 2.2 Synthesis of amphiphilic aspartic acid from L-Aspartic acid $\beta$ -benzyl ester and 3 from N alpha,N epsilon-Bis(tert-butoxycarbonyl)-L-lysine.....	33
Scheme 2.3 Synthesis of amphiphilic peptides AMD-AROM (13) and AMD-ALIP (12) .....	37
Scheme 3.1 Schematic for alginate and calcium cross-linked microgel beads and hydrogels for aspartame encapsulation and release.....	66
Scheme 4.1 Molecular structure of the dimeric amphiphile with the hydrophobic, hydrophilic moieties along with the sulfonamide ligand (complementary to enzyme carbonic anhydrase)....	98
Scheme 4.2 Synthesis of precursors 13-16.....	100
Scheme 4.3 Synthesis of oligomers 7-12.....	102
Scheme 4.4 Synthesis of sulfonamide-PEG ligand 21.....	104
Scheme 4.5 Synthesis of control PEG linker 23.....	107
Scheme 4.6 Synthesis of oligomer with sulfonamide ligand 1' .....	107
Scheme 4.7 Structures of oligomers with sulfonamide ligand.....	110
Scheme 4.8 Structures of methylated oligomers with sulfonamide ligand.....	111

Scheme 5.1 Synthesis of amphiphilic peptide 4.....	147
Scheme 5.2 Synthesis of control molecule 5.....	149
Scheme A.1 Structures of the trimeric amphiphiles used in the study.....	16



# CHAPTER 1

## INTRODUCTION

### 1.1 Supramolecular self-assembly

The study of amphiphilic molecules has garnered significant attention in the past decade due to its implications in biomimetic architectures. Developing an understanding of how molecules, materials and complex systems contribute to biological functions is important since the interpretation of such mechanisms paves the way to further the development of materials that replicate natural functions or impart the observed properties to synthetic materials.

The supramolecular assemblies arising out of the spontaneous organization of these amphiphilic molecules is governed by non-covalent interactions such as hydrogen-bonding, ion-dipole interactions, van der waals forces, pi-pi interactions, electrostatic interactions and hydrophobic effect<sup>1,2</sup>. Supramolecular self-assembly is dynamic in nature since the moieties involved are bridged through reversible interactions and undergo spontaneous assembly-disassembly process in response to environmental cues. Owing to the reversible and dynamic nature of non-covalent interactions, supramolecular scaffolds have the inherent ability to respond to their environment and makes them unique candidates for supramolecular materials. Also, a favorable hydrophilic-lipophilic balance (HLB) between the hydrophilic and lipophilic moieties in an amphiphiles is understood to be the major driving force that governs the assembly-disassembly of the amphiphilic molecules to supramolecular scaffolds<sup>3</sup>.

In this thesis, we focus on the design strategies to structure macromolecular scaffolds by means of self-assembly that can be leveraged to introduce stimuli-responsive elements within these scaffolds.

## 1.2 Stimuli responsive supramolecular systems

The self-assembly of stimuli-responsive scaffolds based on micelles, liposomes, hydrogels and thin films has been of considerable interest in areas such as diagnostics<sup>4,5</sup>, sensing<sup>6,7</sup>, drug delivery<sup>8,9</sup> and cryptic catalysis<sup>10,11</sup>. These systems need to be endowed with certain design features which influence the self-assembly and the responsiveness of the scaffold when subjected to external stimuli which could be physical, chemical or biological in nature.

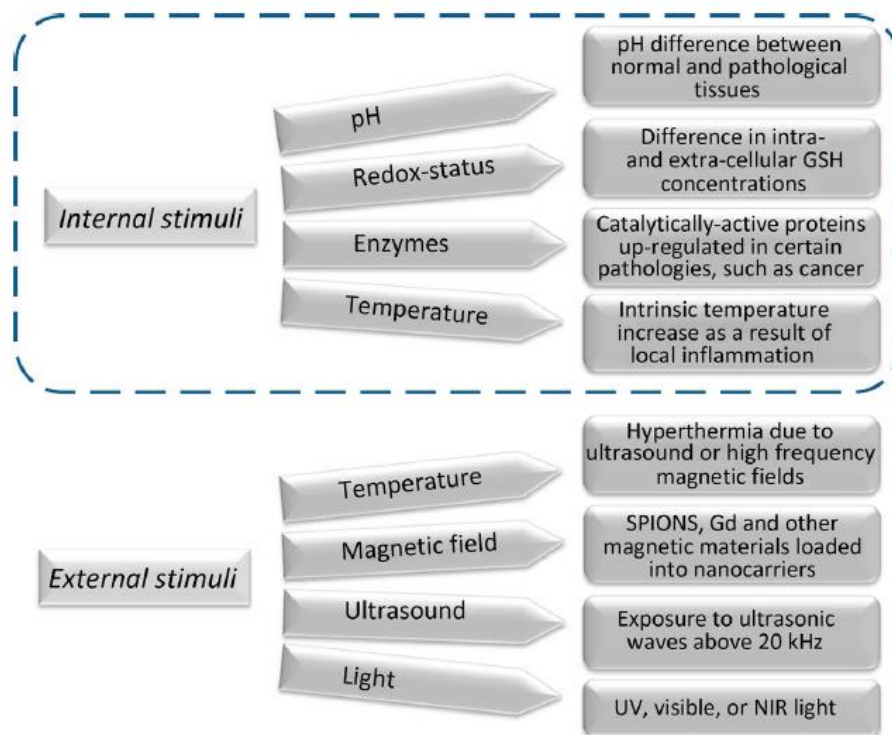


**Figure 1.1** Various intrinsic and extrinsic stimuli

Stimuli that can be exploited for triggering these responsiveness supramolecular scaffolds are diverse but are broadly classified as intrinsic/endogenous and extrinsic/exogenous. Intrinsic stimuli represent any physiological or pathological variations that occur in target cells or tissues in the body. This includes pH, redox, oxidative stress, enzyme and temperature<sup>12</sup>. External stimuli encompass inducements that are externally applied to biological systems such as temperature, ultrasound, light, magnetic and electric field<sup>13</sup>.

### **1.3 Exogeneous stimuli**

Exogenous stimuli confer the advantage of being non-invasive unlike their endogenous counterparts that has applications *in vivo*. In addition, since they are applied from an external source they can be maneuvered such that the location and the rate of response can be easily adjusted.

#### **1.3.1 Temperature responsive systems**

Thermo-responsive systems that undergo a temperature dependent solubility change have been widely studied and explored. Such systems are designed by incorporating a thermo-responsive component with poly(N-isopropylacrylamide) (PNIPAM) and poly ethylene glycol (PEG) being the most investigated thermo-responsive moieties<sup>14,15,16,17</sup>.

The underlying reason for the observed dispersibility is attributed to their propensity to hydrogen bond with water. At elevated temperatures, the hydrogen bonding network is disrupted and their solubility in the aqueous phase is affected leading to a phase transition that is commonly referred to as Lower Critical Solution Temperature (LCST). This differential hydration of PEG/PNIPAM-containing amphiphiles leads to a change in the hydrophilic-lipophilic balance (HLB) of the amphiphile and affects the overall assembly behavior of these amphiphiles<sup>18</sup>. It is important to note that hydrogen bonding is a dynamic process and that makes these phase transitions reversible and reproducible. PEG containing assemblies, in addition to their thermo-responsive behavior also

confer the advantage of preventing them from being opsonized when in circulation owing to PEG's stealth properties and this has paved way for it to be used in drug delivery, theranostics and sensing applications<sup>19</sup>.

Dendrons G1-G3 containing a temperature responsive poly ethylene glycol (PEG) as the hydrophilic group and decyl group as the hydrophobic moiety were synthesized. In aqueous solution, these dendrons were found to self-assemble to form micelle-type aggregates as revealed

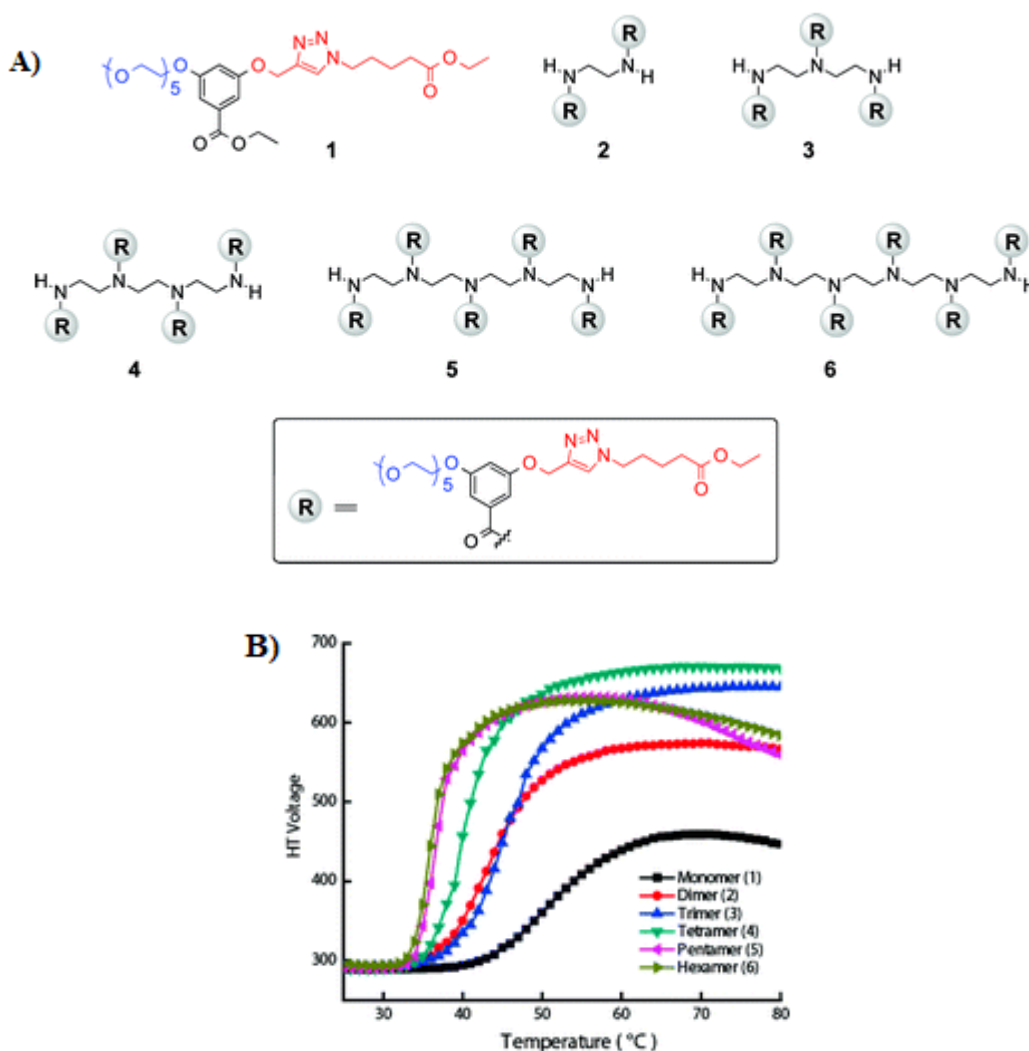


**Figure 1.2** A) Structures of the Amphiphilic Oligomers Used in This Study B) Plot of HT voltage vs temperature for molecules 1–6 in water.<sup>21</sup>

by dynamic light scattering (DLS) and transmission electron microscopy (TEM)<sup>20</sup>.

Also, the LCST transition for the PEG-containing dendrons namely G1, G2 and G3 were found to be 42, 32 and 31 °C respectively. The dependence of the transition temperature on the generation of dendron was indeed surprising given that all the dendrons formed assemblies of nearly the same size. We further, studied this using a set of linear oligomeric amphiphiles. It was found that the covalent attachment of PEG groups provided cooperativity in temperature sensitivity and this manifests in temperature sensitivity as well.<sup>21</sup>

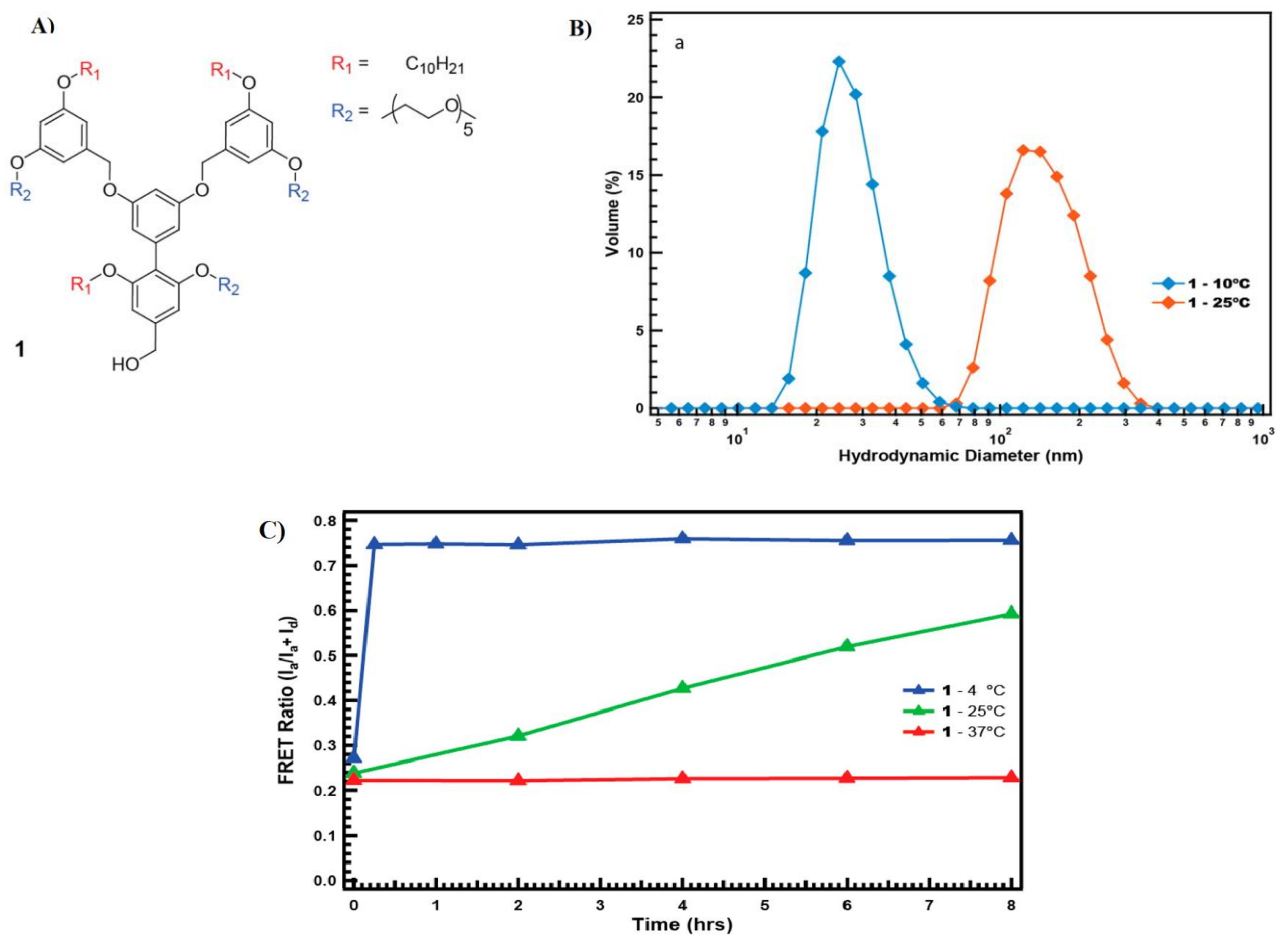


**Figure 1.3** A) Structures of the Amphiphilic dendrimers Used in This Study B) large change in the  $D_H$  of 1 observed for 25 °C (160 nm) and 10 °C (30 nm) assemblies as revealed by DLS (C) The temperature sensitivity of 1 was shown to have an inverse effect on the guest exchange dynamics with exchange at 4 °C complete within 10 min and virtually no exchange observed at 37 °C.<sup>22</sup>

While most of the LCST transition in literature describes a phase change at elevated temperatures wherein the soluble molecules fall out of solution, there have been no investigations on the fate of these molecules below LCST. Particularly, we found that the first-generation dendron (G1) exhibited another temperature responsive transition at a much lower temperature (17.5 °C, termed

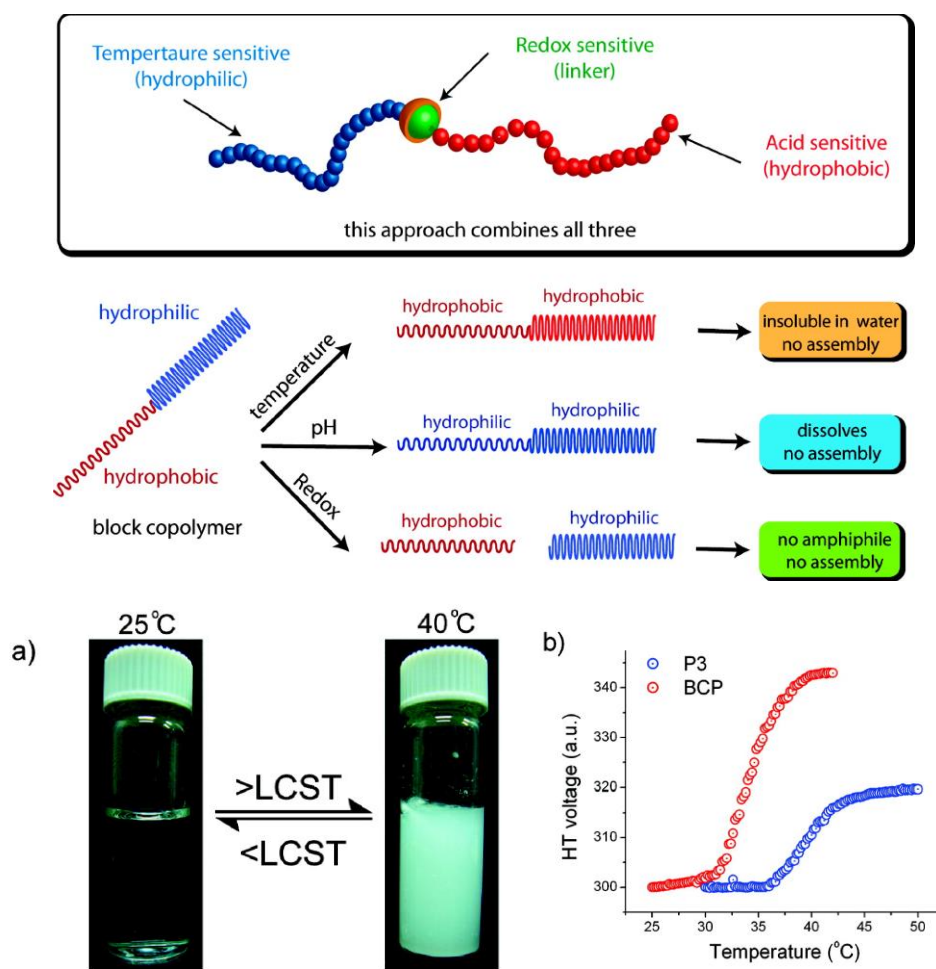


**Figure 1.4** Design of Amphiphilic Diblock Copolymer (BCP) and (a) Photograph showing an aqueous solution of BCP; left-at room temperature, right-after heating to 40 °C. (b) Turbidity experiment showing the change in HT voltage with temperature of BCP and PNIPAM (P3).<sup>16</sup>

as sub-LCST) below the LCST wherein the size of these aggregates changed from ~160 nm to ~30 nm as indicated by DLS. By means of a fluorescence resonance energy transfer based (FRET) technique, it was found that the encapsulation stability of the amphiphilic dendrons changed in

response to temperature and the guest molecules were found to exchange faster at lower temperatures than at higher temperatures. This was presumed to be because of the PEG units being hydrated better at lower temperatures due to stronger hydrogen bonding with water and would result in the decreased residence time of the amphiphile in the aggregate. The hypothesis was validated using a pyrene label and we found that the dendrons in the aggregate exchange faster at lower temperatures<sup>22</sup>. The generalization of this sub-LCST in PEG containing amphiphilic assemblies is one of the current foci and is being pursued in the Thayumanavan laboratory.

### **1.3.2 Photo responsive systems**

Light sensitive systems have continued to be promising owing to their potential to be site-specific and non-invasive. Therefore, they are used in applications such as drug delivery, theranostics and photodynamic therapy (PDT)<sup>23,24,25</sup>. Our group has reported on amphiphilic dendrons that are composed of a hydrophobic PEG group and a hydrophobic alkyl chain that contains a photodegradable linker. The nanoassemblies formed by these dendrons encapsulate hydrophobic guest molecules and upon UV irradiation, the amphiphilic molecules release the encapsulated dye molecules<sup>26</sup>.

The change in HLB owing to the cleavage of the ortho-nitrobenzyl group in response to light results in the formation of carboxylic acid in the amphiphile and the ortho-nitrosobenzaldehyde byproduct. This renders the dendron hydrophilic on both the faces and results in disassembly and subsequent release of the guest molecule. Similarly, the light-dependent cross-linking of hydrophobic coumarin units was observed to result in the stabilization of micellar aggregates that could be used to tune the release of guest molecules<sup>27</sup>.

Recently, our group has investigated a supramolecular nano-machine that is capable of performing work in the presence of energy input in the form of light and changes structurally when the energy

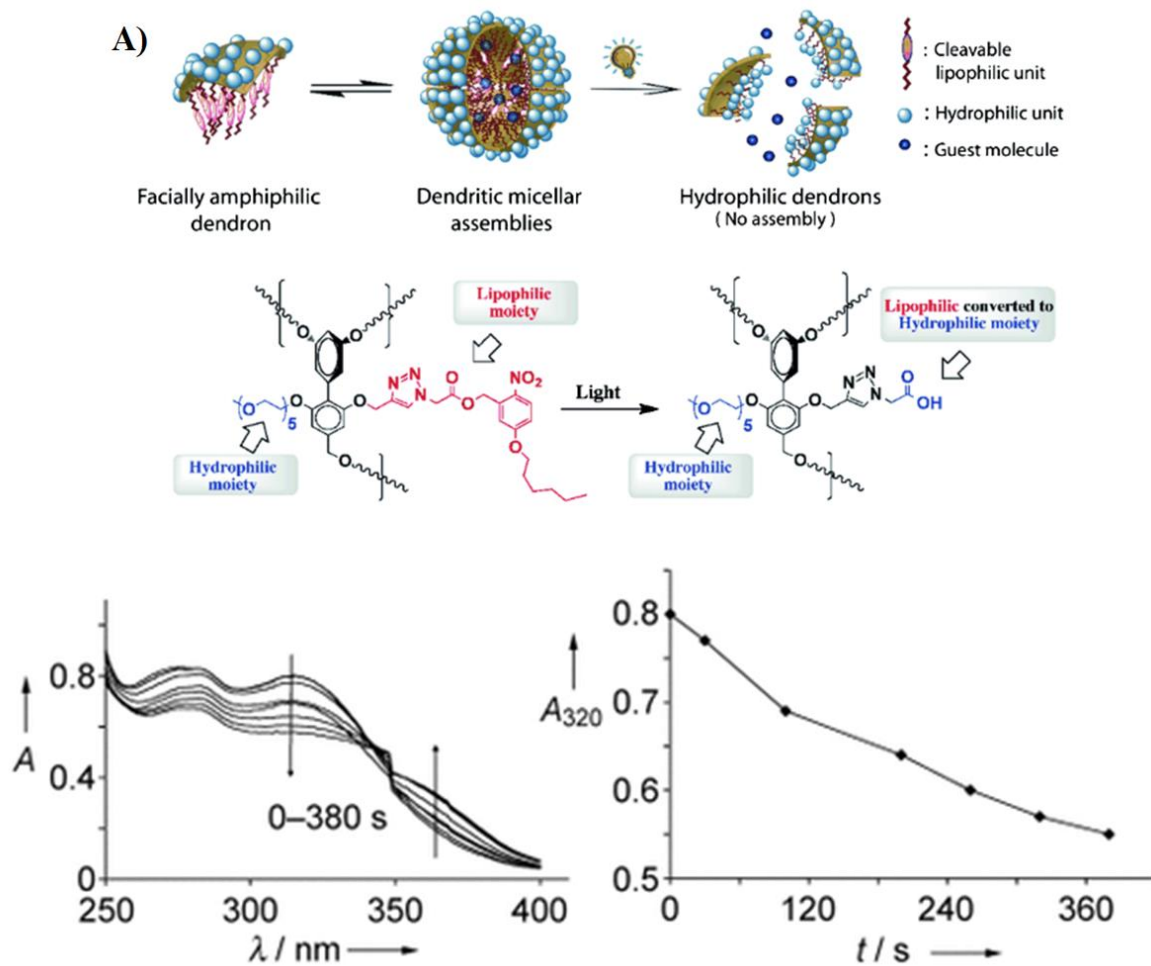


**Figure 1.5** A) Schematic representation of the light-induced disassembly of amphiphilic dendritic assemblies B) UV/Vis spectra of the G1 dendron upon irradiation with UV light for different time intervals (0–380 s) and plot of the absorbance at 320 nm, which illustrates cleavage of the photolabile ester bond.<sup>26</sup>

source is removed. It falls back into a thermodynamic minimum and can be manipulated to perform work when required. To this end, an azobenzene containing block copolymer was designed and the hypothesis was validated by means of extensive MD simulations and mechanistic investigations<sup>28</sup>.



## **1.4 Endogenous stimuli**

Endogenous stimuli pertain to an environment that is characteristic of a certain physiological condition or a certain pathological state<sup>29</sup>. These include changes in pH, redox gradient and enzyme concentration and are discussed below.

### **1.4.1 pH responsive systems**

While the physiological pH in the body is 7.4, tumor microenvironments, gastrointestinal tract and the lysosomal, endosomal components of a cell are known to be acidic in nature. These pH gradation at the cellular and sub-cellular levels provide for opportunities in drug delivery by means of responsive molecular designs. Molecules containing ionizable groups such as amines, carboxylic acids serve to be the best candidates for this purpose<sup>30</sup>. Since the charge is directly associated with solubility, variations in pH can be exploited to trigger a charge generation or removal that alters the HLB. pH responsive assemblies also regularly employ functional groups such as acetals, ketals, hydrazines and imines which alter assembly properties upon cleavage owing to a change in HLB<sup>31,32</sup>.

Our group has reported a facile method to prepare polymeric nanogels that generate a surface charge upon decrease in pH. This was achieved by incorporating a 2-diisopropylamino (DPA) unit which undergoes a rapid protonation owing to its  $pK_b$  which is reminiscent of the extracellular environment of solid tumors. These nanogels exhibited enhance uptake in an acidic pH environment owing to the surface charge generation<sup>33</sup>. Such materials are of considerable interest in drug delivery.

In addition to various features that are essential in a nanocarrier, size and surface charge have been found to play a crucial role in determining its biological fate. In a study, polymeric nanoparticles that respond to small changes in pH have been designed and found to exhibit surface charge and size variation features. This was achieved using a pH sensitive interparticle In a study, polymeric

nanoparticles that respond to small changes in pH have been designed and found to exhibit surface charge and size variation features. This was achieved using a pH sensitive interparticle cross-linking through a reversible imine bond formation. The conversion of amine to imine brought about the concomitant burial of the imine moieties leading to the surface charge to be less positive resulting in enhanced cellular uptake at pH 6.5 as compared to 7.4<sup>34</sup>.

In another study, an amphiphilic homopolymer that can degrade both at the side and the main chains was designed and subjecting the nanoassemblies arising out of the homopolymer to a pH change causes it to lose its encapsulation properties due to the degradation of the  $\beta$ -thioester side chain functionalities<sup>35</sup>. This is interesting because degradable amphiphiles have attracted a lot of attention for their implications in drug delivery and diagnostics.

The effect of substituents on the pH sensitivity of acetal and ketal-based linkers on their degradation kinetics was studied using a structure-activity relationship study. A systematic investigation through the structural fine-tuning of the linkers allowed for the kinetics of degradation to be varied up to more than six orders of magnitude. The trends observed in the small molecules also translate to the encapsulation stability of the guest molecules within these linkers when incorporated in polymeric nanogels<sup>36</sup>.

Nanoscope systems comprising of polymers and proteins are being actively pursued for protein delivery. A polymeric nanogel has been used to sequester and silence a lysosomal protein,  $\alpha$ -glucosidase that has been implicated in the Pompe disease which can be treated by delivery of a recombinant enzyme.

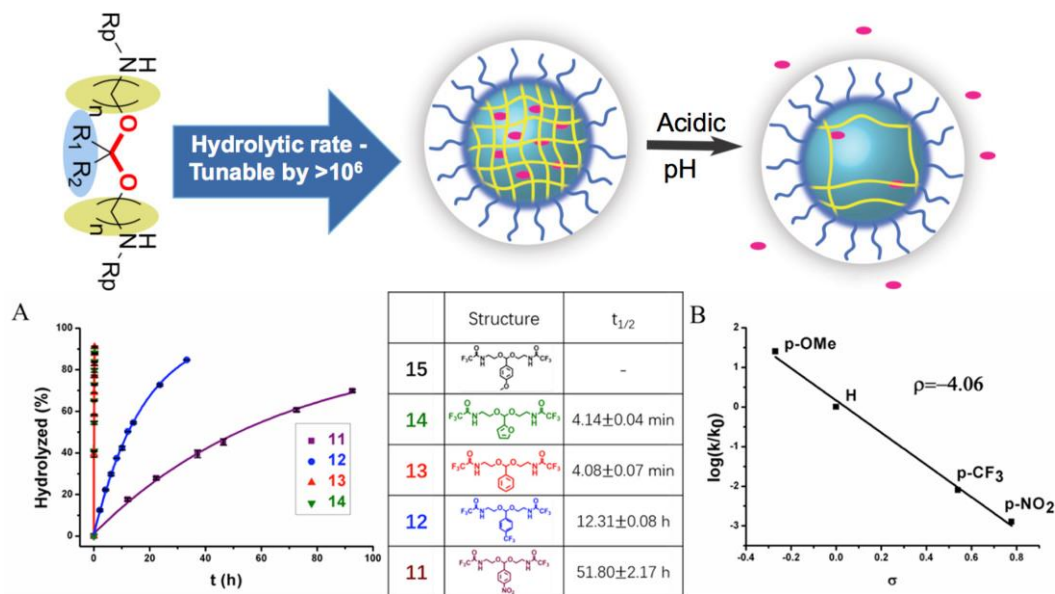


**Figure 1.6** Substituent effects upon the hydrolysis of benzylidene acetals. (A) Hydrolysis kinetics and the first-order reaction fitting curve, (B) Hammett plot. The hydrolysis was performed under TFA condition. The solid lines are the fitting curves.<sup>33</sup>

The encapsulation turns off the enzyme's activity but is recovered ( $\sim 75\%$ ) upon reducing the pH to 5. The recovered activity is attributed to the degradation of  $\beta$ -thiopropionate cross-linker upon decrease in pH that leads to swelling of the nanogel and a subsequent release of the enzyme<sup>37</sup>. Such strategies for sequestering protein molecules and releasing them at physiological pH opens new avenues for CRISPR-Cas9, siRNA, dsRNA and other biologically relevant proteins.

#### 1.4.2 Redox responsive systems

Redox responsive systems leverage the difference in the redox potentials that exist in extracellular environment ( $\sim 2-10 \mu\text{M}$  Glutathione(GSH)) vs the intracellular milieu ( $\sim 2-10 \text{mM}$  Glutathione (GSH)). This is especially true for the tumor microenvironment where the concentration of GSH is much higher than in normal tissues. Therefore, they are lucrative options for intracellular delivery and tumor-directed delivery. This is also a viable system for intracellular gene delivery involving a plasmid DNA or siRNA since, they need to be protected from the extracellular components and

cross the cell membrane to reach cytosol to achieve better transfection efficiencies. Commonly used redox-responsive units are disulfide, diselenide or ditellurium bonds<sup>38,39,40</sup>.

N-acetyl-L-cysteine (NAC) is an anti-inflammatory drug that needs to be administered in high doses and causes many side effects. This was circumvented by conjugating NAC to PAMAM

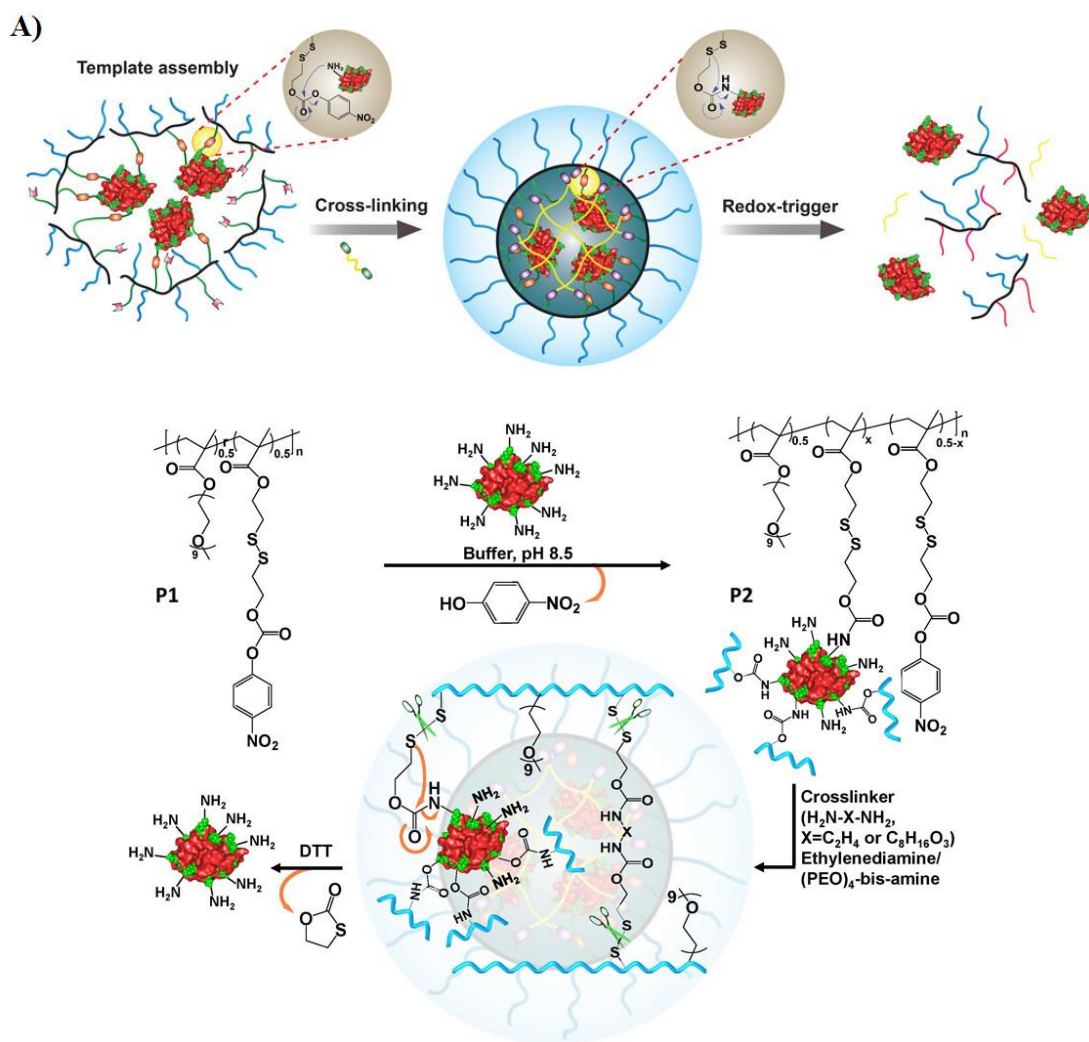


**Figure 1.7** A) Schematic representation of the formation of a covalent polymer network using the protein as the template and its traceless and triggered release in a reducing environment. B) Chemical Structures of Polymers and the Reaction Scheme for Protein Conjugation, Crosslinking to Generate the Nanoassembly, and Its Release in the Presence of a Reducing Agent.<sup>42</sup>

dendrimers by means of a disulfide linkage, that can cleave in the presence of GSH to release NAC<sup>41</sup>. Thayumanavan group has reported cross-linked polymeric nanogels synthesized through RAFT that comprise of oligoethylene glycol methacrylate (OEGMA) and pyridyl disulfide ethyl methacrylate (PDSMA). Their redox-responsive nature was investigated using the addition of dithiothreitol (DTT). We have exploited this strategy to shrink-wrap proteins and deliver it into an intracellular space in response to a redox stimulus<sup>42</sup>.

### 1.4.3 Protein and enzyme responsive systems

Pathological imbalances are understood to be brought about by aberrations in protein activity and

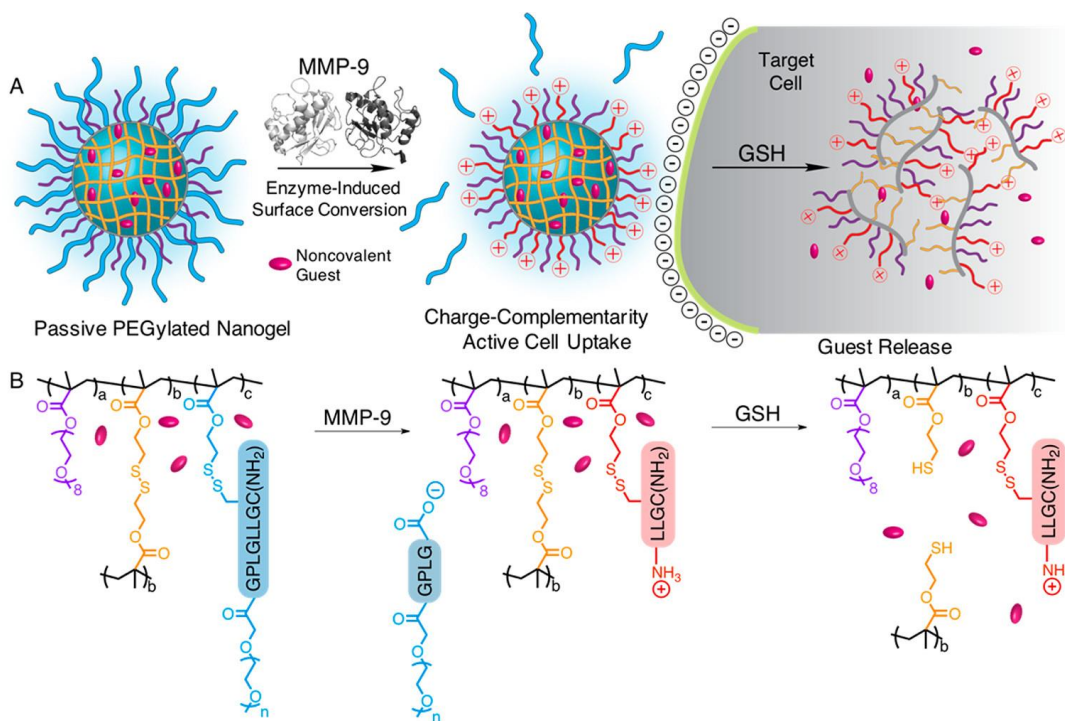


**Figure 1.8** A) Schematic Representation of MMP-9-Responsive Nanogels and Resulting Activated Cell Uptake and GSH Release and (B) Structural Representation of Polymer Nanogels and Stimuli Responsiveness.<sup>47</sup>

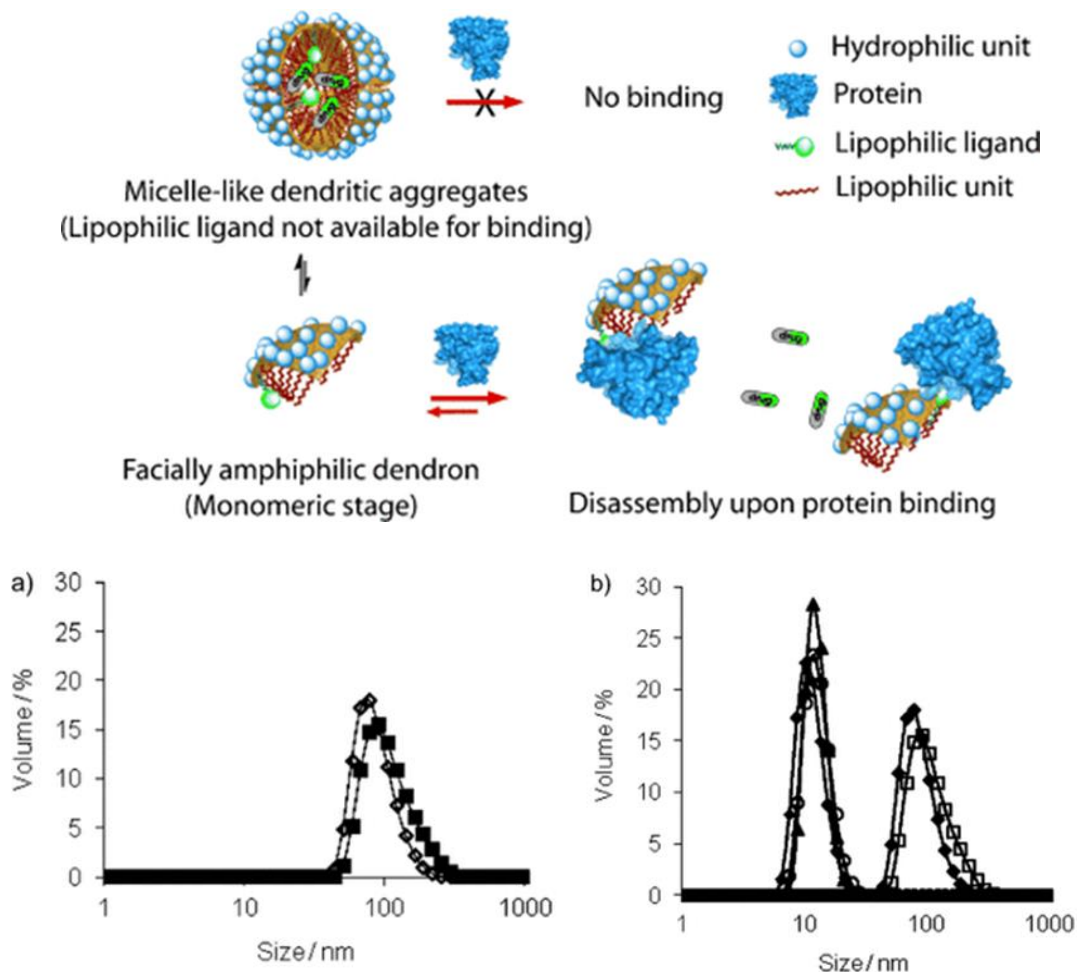


**Figure 1.9** A) Binding-induced disassembly with lipophilic ligand containing dendrons. B) a) Sizes of G1–DNP ( $\diamond$ ) and G2–DNP ( $\blacksquare$ ) dendrons; b) size changes in G1–DNP and G2–DNP dendron based amphiphilic assemblies due to the presence of anti-DNP IgG;  $\blacklozenge$ , G1–DNP;  $\square$ , G2–DNP;  $\blacktriangle$ , G1<sup>51</sup>

supramolecular scaffolds that can respond to variations in protein concentrations are of great significance but relatively underexplored<sup>43</sup>. In this context, non-covalent interaction-based changes in the assembly properties of amphiphiles presents greater opportunities since it encompasses a larger number of proteins that are implicated in signal transduction pathways.

The design strategy for such supramolecular assemblies commonly employs the disruption of HLB by influencing the molecular interactions through either a cleavage of a functional group (ester, amides) or by means of non-covalent interactions<sup>44,45,46</sup>. Matrix metalloproteinase (MMP), Thermolysin and Chymotrypsin are few examples of enzymes prompting extracellular drug release

when conjugated to supramolecular assemblies<sup>47,48,49,50</sup>. In our group, we have incorporated enzyme-cleavable functional group into the hydrophobic part of a facially amphiphilic dendrimer. We hypothesized that the conversion of the hydrophobic group to hydrophilic upon enzymatic cleavage would cause a disassembly owing to the disruption of HLB<sup>51</sup>. Indeed, we have shown that this disassembly is accompanied by a release of guest molecule. In addition, we partially cross-

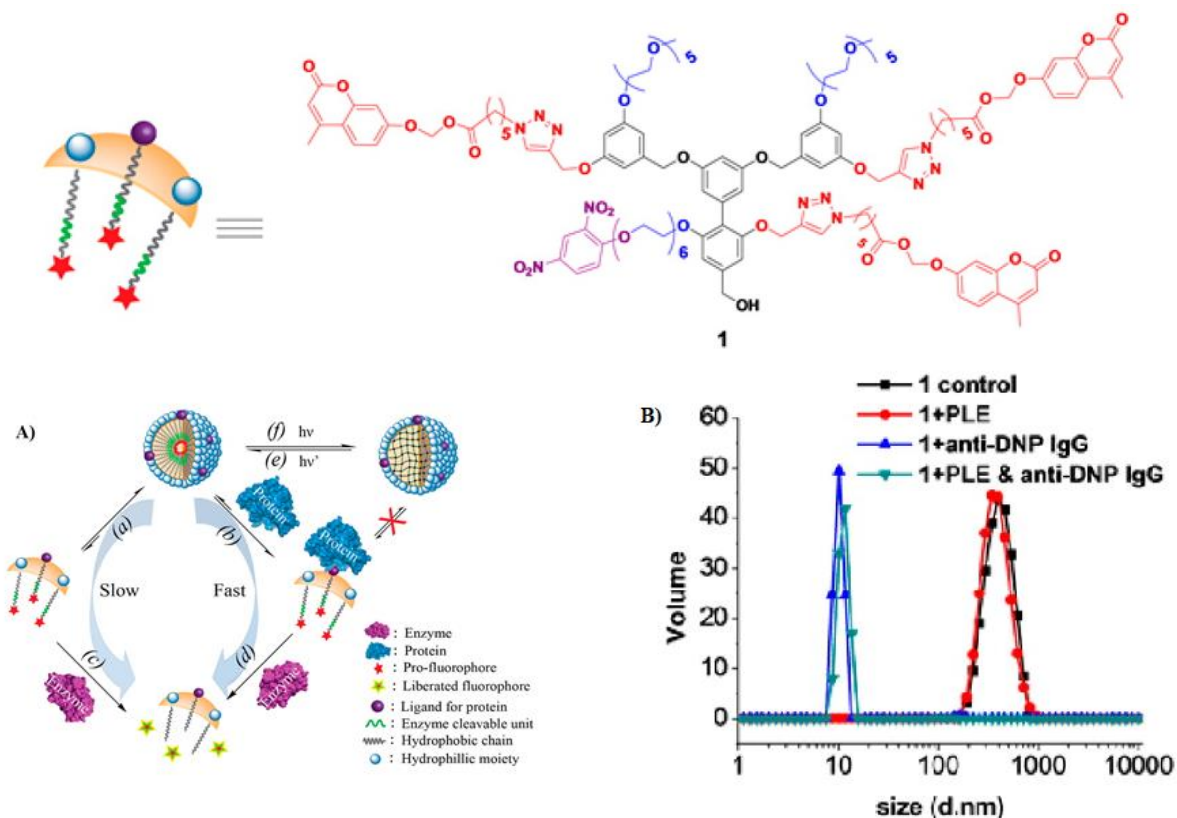


**Figure 1.10** A) Schematic representation of protein AND enzyme gated supramolecular disassembly. B) Disassembly of 1 (13  $\mu$ M) in the presence of anti-DNP IgG (1  $\mu$ M) and PLE (50 nM): Size change after 8 h, monitored by DLS.<sup>52</sup>

linked these amphiphilic assemblies and monitored the enzymatic cleavage using the release of a covalently conjugated fluorophore, 4-methyl umbelliferone (MUF). A clear correlation between the kinetics of the enzymatic reaction and that of the guest molecule release was revealed by



concurrently monitoring the fluorescence of MUF and that of a non-covalently encapsulated fluorophore<sup>27</sup>.

In yet another approach, we synthesized dendrons that contain a single biotin ligand at the focal point on its hydrophilic face to study an approach called binding-induced disassembly (BID). Studies revealed that an amphiphilic dendron had a very different HLB compared to the dendron-protein complex which resulted in the binding-induced disassembly and concomitant release of a non-covalent guest molecule<sup>52,53</sup>. We were next, interested in determining whether the placement of a hydrophobic ligand that is likely to be buried in the pockets of the micellar aggregate would still be available for BID. To test this, we placed the ligand on the hydrophobic part and were able to show that BID did exist and was attributed to the equilibrium between the unimeric and the aggregated states of the amphiphilic dendrimer assembly<sup>54</sup>. These results were also validated using other oligomeric amphiphiles as well as polymeric systems<sup>55,56,57</sup>. The design principle was extended to a 'AND' logic gate-based system that responded to the simultaneous presence of two proteins<sup>58,59</sup>.

## **1.5 Summary and thesis overview**

In this chapter, an introduction to responsive systems that are built on the fundamentals of supramolecular self-assembly were discussed. The self-assembly of stimuli-responsive scaffolds based on micelles, liposomes, hydrogels and thin films has been of considerable interest in areas such as diagnostics, sensing, drug delivery and cryptic catalysis<sup>60,61,62</sup>. Developing an understanding of how molecules, materials and complex systems contribute to biological functions is important since the interpretation of such mechanisms paves the way to further the development of materials that replicate natural functions or impart the observed properties to synthetic materials. In stimuli responsive applications, the dynamic nature of non-covalent interactions can be utilized



to disrupt self-assembly to achieve a response in the presence of a specific stimulus<sup>63,64,65,66</sup>. The origin, significance of each stimulus, the molecular design parameters and a few reported examples were explained.

These systems need to be endowed with certain design features which influence the self-assembly and the responsiveness of the scaffold when subjected to external stimuli which could be physical, chemical or biological in nature<sup>67,68,69,70</sup>. This kind of insight is still lacking in our understanding of how these systems respond to various stimuli. In this thesis, our objective is to establish structure-property relationships between the influence of structural design and the target material properties. Of interest to us are pH, temperature (chemical) and enzyme/proteins (biological) as stimuli and we have performed experiments to validate the responsive features of these systems.

In Chapter 2, we have established the design principles for oligomeric peptides to exhibit a unique size transition well below the LCST. We have found that incorporation of aromatic hydrophobic groups diminishes the thermo-sensitivity of the peptide nanoassemblies. The size transition is brought about by a loss of secondary structures at low temperatures and the temperature-dependent aggregation properties also gave rise to disparity in terms of guest encapsulation ability upon changing temperature. Since these molecules are designed to incorporate FDA approved components and the assembly is biodegradable, this system has interesting applications in the food industry and in cryptic catalysis.

In Chapter 3, we have established structure-property relationships pertaining to the release of an artificial sweetener, aspartame from microgels and bulk hydrogels of aspartame encapsulated calcium cross linked alginate gels. We have, in particular, studied the different parameters that dictate the gel architecture and hence, the morphology and the structure of the gels. We have validated the effect of cross link densities and sizes on the release kinetics of the microgel spheres

and bulk hydrogels. The release data was fitted to kinetic models available from literature to elucidate the pathway constraints dictated the release pathway.

In Chapter 4, structure-property relationships were developed using libraries of polymeric and oligomer amphiphiles to make possible rational design of triggers for amplification via LC response. To this end, we synthesized a wide range of stimuli-responsive amphiphilic oligomers that responded to a protein, carbonic anhydrase (CA II). Dimer was the only amphiphilic oligomer that was found to adsorb at the aqueous-LC interface to trigger a homeotropic anchoring transition. Moreover, CA II was found to bind to sulfonamide on the interface stronger than BSA resulting in the blocking of non-specific binding of bovine serum albumin (BSA) on aqueous-LC interface. This mechanism was corroborated using addition of inhibitor which enhanced the release of CA II from aqueous-LC interface by modulating the strength of binding. The design rules established here provide insight into the rational design of oligomers with triggers that can couple specific molecular events to LCs to achieve highly amplified responses. This paves way to develop principles based on LCs that permit incorporation of feedback for massive amplification that can be leveraged for targeting and triggering.

## 1.6 References

- (1) Webber, M. J.; Appel, E. A.; Meijer, E. W.; Langer, R. Supramolecular Biomaterials. *Nat. Mater.* **2015**, *15* (1), 13–26.
- (2) Stupp, S. I.; Palmer, L. C. Supramolecular Chemistry and Self-Assembly in Organic Materials Design. *Chem. Mater.* **2014**, *26* (1), 507–518.
- (3) Kunz, W.; Testard, F.; Zemb, T. Correspondence between Curvature, Packing Parameter, and Hydrophilic-Lipophilic Deviation Scales around the Phase-Inversion Temperature. *Langmuir* **2009**, *25* (1), 112–115.
- (4) Lee, J. H.; Yigit, M. V.; Mazumdar, D.; Lu, Y. Molecular Diagnostic and Drug Delivery Agents Based on Aptamer-Nanomaterial Conjugates. *Adv. Drug Deliv. Rev.* **2010**, *62* (6), 592–605.
- (5) Stuart, M. A. C.; Huck, W. T. S.; Genzer, J.; Müller, M.; Ober, C.; Stamm, M.; Sukhorukov, G. B.; Szleifer, I.; Tsukruk, V. V.; Urban, M.; et al. Emerging Applications of Stimuli-Responsive Polymer Materials. *Nat. Mater.* **2010**, *9* (2), 101–113.
- (6) Wang, H.; Zhuang, J.; Raghupathi, K. R.; Thayumanavan, S. A Supramolecular Dissociation Strategy for Protein Sensing. *Chem. Commun.* **2015**, *51* (97), 17265–17268.
- (7) González, D. C.; Savariar, E. N.; Thayumanavan, S. Fluorescence Patterns from Supramolecular Polymer Assembly and Disassembly for Sensing Metallo- and Nonmetalloproteins. *J. Am. Chem. Soc.* **2009**, *131* (22), 7708–7716.
- (8) Salim, M.; Minamikawa, H.; Sugimura, A.; Hashim, R. Amphiphilic Designer Nano-Carriers for Controlled Release: From Drug Delivery to Diagnostics. *Med. Chem. Commun.* **2014**, *5* (11), 1602–1618.

- (9) Torchilin, V. P. Structure and Design of Polymeric Surfactant-Based Drug Delivery Systems. *J. Control. Release* **2001**, *73* (2–3), 137–172.
- (10) Ramström, O.; Mosbach, K. Synthesis and Catalysis by Molecularly Imprinted Materials. *Curr. Opin. Chem. Biol.* **1999**, *3* (6), 759–764.
- (11) Jun, H. W.; Paramonov, S. E.; Hartgerink, J. D. Biomimetic Self-Assembled Nanofibers. *Soft Matter* **2006**, *2* (3), 177–181.
- (12) Hatakeyama, H. Recent Advances in Endogenous and Exogenous Stimuli-Responsive Nanocarriers for Drug Delivery and Therapeutics. *Chem. Pharm. Bull* **2017**, *65* (7), 612–617.
- (13) Cheng, W.; Gu, L.; Ren, W.; Liu, Y. Stimuli-Responsive Polymers for Anti-Cancer Drug Delivery. *Mater. Sci. Eng. C* **2015**, *45*, 600–608.
- (14) Hocine, S.; Li, M.-H. Thermoresponsive Self-Assembled Polymer Colloids in Water. *Soft Matter* **2013**, *9* (25), 5839.
- (15) Hocine, S.; Li, M.-H. Thermoresponsive Self-Assembled Polymer Colloids in Water. *Soft Matter* **2013**, *9* (25), 5839.
- (16) Klaikherd, A.; Nagamani, C.; Thayumanavan, S. Multi-Stimuli Sensitive Amphilic Block Copolymer Assemblies. *J. Am. Chem. Soc.* **2009**, *131* (13), 4830–4838.
- (17) Chen, C.; Wang, Z.; Li, Z. Thermoresponsive Polypeptides from Pegylated Poly-L-Glutamates. *Biomacromolecules* **2011**, *12* (8), 2859–2863.
- (18) Meijer, J. T.; Henckens, M. J. A. G.; Minten, I. J.; Löwik, D. W. P. M.; Van Hest, J. C. M. Disassembling Peptide-Based Fibres by Switching the Hydrophobic-Hydrophilic Balance. *Soft Matter* **2007**, *3* (9), 1135–1137.

- (19) Settanni, G.; Zhou, J.; Suo, T.; Schöttler, S.; Landfester, K.; Schmid, F.; Mailänder, V. Protein Corona Composition of PEGylated Nanoparticles Correlates Strongly with Amino Acid Composition of Protein Surface. **2016**.
- (20) Aathimankandan, S. V.; Savariar, E. N.; Thayumanavan, S. Temperature-Sensitive Dendritic Micelles. *J. Am. Chem. Soc.* **2005**, *127* (42), 14922–14929.
- (21) Wang, F.; Klaukherd, A.; Thayumanavan, S. Temperature Sensitivity Trends and Multi-Stimuli Sensitive Behavior in Amphiphilic Oligomers. *J. Am. Chem. Soc.* **2011**, *133* (34), 13496–13503.
- (22) Fuller, J. M.; Raghupathi, K. R.; Ramireddy, R. R.; Subrahmanyam, A. V.; Yesilyurt, V.; Thayumanavan, S. Temperature-Sensitive Transitions below LCST in Amphiphilic Dendritic Assemblies: Host-Guest Implications. *J. Am. Chem. Soc.* **2013**, *135* (24), 8947–8954.
- (23) Hu, X.; Tian, J.; Liu, T.; Zhang, G.; Liu, S. Photo-Triggered Release of Caged Camptothecin Prodrugs from Dually Responsive Shell Cross-Linked Micelles. *Macromolecules* **2013**, *46* (15), 6243–6256.
- (24) Kumar, S.; Dory, Y. L.; Lepage, M.; Zhao, Y. Surface-Grafted Stimuli-Responsive Block Copolymer Brushes for the Thermo-, Photo- and PH-Sensitive Release of Dye Molecules. *Macromolecules* **2011**, *44* (18), 7385–7393.
- (25) Gaplovsky, M.; Il'ichev, Y. V.; Kamdzhilov, Y.; Kombarova, S. V.; Mac, M.; Schwörer, M. A.; Wirz, J. Photochemical Reaction Mechanisms of 2-Nitrobenzyl Compounds: 2-Nitrobenzyl Alcohols Form 2-Nitroso Hydrates by Dual Proton Transfer. *Photochem. Photobiol. Sci.* **2005**, *4* (1), 33–42.
- (26) Yesilyurt, V.; Ramireddy, R.; Thayumanavan, S. Photoregulated Release of Noncovalent

- Guests from Dendritic Amphiphilic Nanocontainers. *Angew. Chemie - Int. Ed.* **2011**, *50* (13), 3038–3042.
- (27) Raghupathi, K. R.; Azagarsamy, M. A.; Thayumanavan, S. Guest-Release Control in Enzyme-Sensitive, Amphiphilic-Dendrimer-Based Nanoparticles through Photochemical Crosslinking. *Chem. - A Eur. J.* **2011**, *17* (42), 11752–11760.
- (28) Molla, M. R.; Rangadurai, P.; Pavan, G. M.; Thayumanavan, S. Experimental and Theoretical Investigations in Stimuli Responsive Dendrimer-Based Assemblies. *Nanoscale* **2015**, *7* (9), 3817–3837.
- (29) Ramireddy, R. R.; Raghupathi, K. R.; Torres, D. A.; Thayumanavan, S. Stimuli Sensitive Amphiphilic Dendrimers. *New J. Chem.* **2012**, *36* (2), 340–349.
- (30) Pennakalathil, J.; Jahja, E. Red Emitting, Cucurbituril-Capped, PH-Responsive Conjugated Oligomer-Based Nanoparticles for Drug Delivery and Cellular Imaging. **2014**.
- (31) Raghupathi, K. R.; Guo, J.; Munkhbat, O.; Rangadurai, P.; Thayumanavan, S. Supramolecular Disassembly of Facially Amphiphilic Dendrimer Assemblies in Response to Physical, Chemical, and Biological Stimuli. *Acc. Chem. Res.* **2014**, *47* (7), 2200–2211.
- (32) Xiao, Z.; Liu, W.; Zhu, G.; Zhou, R.; Niu, Y.; Tamura, A.; Ikeda, G.; Seo, J. H.; Tsuchiya, K.; Yajima, H.; et al. Micellar Interpolyelectrolyte Complexes. *Soft Matter* **2013**, *8* (21), 6888–6901.
- (33) Li, L.; Raghupathi, K.; Yuan, C.; Thayumanavan, S. Surface Charge Generation in Nanogels for Activated Cellular Uptake at Tumor-Relevant PH. *Chem. Sci.* **2013**, *4* (9), 3654–3660.
- (34) Raghupathi, K.; Li, L.; Ventura, J.; Jennings, M.; Thayumanavan, S. pH Responsive Soft Nanoclusters with Size and Charge Variation Features. *Polym. Chem.* **2014**, *5* (5), 1737–

1742.

- (35) Rangadurai, P.; Molla, M. R.; Prasad, P.; Caissy, M.; Thayumanavan, S. Temporal and Triggered Evolution of Host-Guest Characteristics in Amphiphilic Polymer Assemblies. *J. Am. Chem. Soc.* **2016**, *138* (24), 7508–7511.
- (36) Liu, B.; Thayumanavan, S. Substituent Effects on the pH Sensitivity of Acetals and Ketals and Their Correlation with Encapsulation Stability in Polymeric Nanogels. *J. Am. Chem. Soc.* **2017**, *139* (6), 2306–2317.
- (37) Molla, M. R.; Marcinko, T.; Prasad, P.; Deming, D.; Garman, S. C.; Thayumanavan, S. Unlocking a Caged Lysosomal Protein from a Polymeric Nanogel with a pH Trigger. *Biomacromolecules* **2014**, *15* (11), 4046–4053.
- (38) Balce, D. R.; Yates, R. M. Redox-Sensitive Probes for the Measurement of Redox Chemistries within Phagosomes of Macrophages and Dendritic Cells. *Redox Biol.* **2013**, *1* (1), 467–474.
- (39) You, Y.; Zhou, Q.; Manickam, D. S.; Wan, L.; Mao, G.; Oupicky, D. Dually Responsive Multiblock Copolymers via Reversible Addition-Fragmentation Chain Transfer Polymerization: Synthesis of Temperature- and Redox-Responsive Copolymers of Poly ( N-Isopropylacrylamide ) and Poly ( 2- ( Dimethylamino ) Ethyl Methacrylate ). *Macromolecules* **2007**, *40*, 8617–8624.
- (40) Ghosh, S.; Irvin, K.; Thayumanavan, S. Tunable Disassembly of Micelles Using a Redox Trigger. *Langmuir* **2007**, *23* (15), 7916–7919.
- (41) Stasko, N. A.; Fischer, T. H.; Schoenfisch, M. H. S-Nitrosothiol-Modified Dendrimers as Nitric Oxide Delivery Vehicles. *Biomacromolecules* **2008**, *9* (3), 834–841.
- (42) Dutta, K.; Hu, D.; Zhao, B.; Ribbe, A. E.; Zhuang, J.; Thayumanavan, S. Templated Self-

- Assembly of a Covalent Polymer Network for Intracellular Protein Delivery and Traceless Release. *J. Am. Chem. Soc.* **2017**, *139* (16), 5676–5679.
- (43) Ventura, J.; Eron, S. J.; González-Toro, D. C.; Raghupathi, K.; Wang, F.; Hardy, J. A.; Thayumanavan, S. Reactive Self-Assembly of Polymers and Proteins to Reversibly Silence a Killer Protein. *Biomacromolecules* **2015**, *16* (10), 3161–3171.
- (44) Jiang, L.; Yan, Y.; Drechsler, M.; Huang, J. Enzyme-Triggered Model Self-Assembly in Surfactant-Cyclodextrin Systems. *Chem. Commun.* **2012**, *48* (59), 7347–7349.
- (45) Tamura, A.; Ikeda, G.; Seo, J. H.; Tsuchiya, K.; Yajima, H.; Sasaki, Y.; Akiyoshi, K.; Yui, N. Molecular Logistics Using Cytocleavable Polyrotaxanes for the Reactivation of Enzymes Delivered in Living Cells. *Sci. Rep.* **2013**, *3*, 22–24.
- (46) Lindhoud, S.; de Vries, R.; Norde, W.; Stuart, M. a C. Structure and Stability of Complex Coacervate Core Micelles with Lysozyme. *Biomacromolecules* **2007**, *8* (7), 2219–2227.
- (47) Gordon, M. R.; Zhao, B.; Anson, F.; Fernandez, A.; Singh, K.; Homyak, C.; Canakci, M.; Vachet, R. W.; Thayumanavan, S. Matrix Metalloproteinase-9-Responsive Nanogels for Proximal Surface Conversion and Activated Cellular Uptake. *Biomacromolecules* **2018**, *19* (3), 860–871.
- (48) Ulijn, R. V. Enzyme-Responsive Materials: A New Class of Smart Biomaterials. *J. Mater. Chem.* **2006**, *16* (23), 2217–2225.
- (49) Wang, H.; Raghupathi, K. R.; Zhuang, J.; Thayumanavan, S. Activatable Dendritic <sup>19</sup>F Probes for Enzyme Detection. *ACS Macro Lett.* **2015**, *4* (4), 422–425.
- (50) Liu, Y.; Terrell, J. L.; Tsao, C. Y.; Wu, H. C.; Javvaji, V.; Kim, E.; Cheng, Y.; Wang, Y.; Ulijn, R. V.; Raghavan, S. R.; et al. Biofabricating Multifunctional Soft Matter with Enzymes and Stimuli-Responsive Materials. *Adv. Funct. Mater.* **2012**, *22* (14), 3004–3012.



- (51) Azagarsamy, M. A.; Yesilyurt, V.; Thayumanavan, S. Disassembly of Dendritic Micellar Containers Due to Protein Binding. *J. Am. Chem. Soc.* **2010**, *132* (13), 4550–4551.
- (52) Savariar, E. N.; Ghosh, S.; González, D. C.; Thayumanavan, S. Disassembly of Noncovalent Amphiphilic Polymers with Proteins and Utility in Pattern Sensing. *J. Am. Chem. Soc.* **2008**, *130* (16), 5416–5417.
- (53) Azagarsamy, M. A.; Sokkalingam, P.; Thayumanavan, S. Enzyme-Triggered Disassembly of Dendrimer-Based Amphiphilic Nanocontainers. *J. Am. Chem. Soc.* **2009**, *131* (40), 14184–14185.
- (54) Yesilyurt, V.; Ramireddy, R.; Azagarsamy, M. A.; Thayumanavan, S. Accessing Lipophilic Ligands in Dendrimer-Based Amphiphilic Supramolecular Assemblies for Protein-Induced Disassembly. *Chem. - A Eur. J.* **2012**, *18* (1), 223–229.
- (55) Molla, M. R.; Prasad, P.; Thayumanavan, S. Protein-Induced Supramolecular Disassembly of Amphiphilic Polypeptide Nanoassemblies. *J. Am. Chem. Soc.* **2015**, *137* (23), 7286–7289.
- (56) Amado Torres, D.; Garzoni, M.; Subrahmanyam, A. V.; Pavan, G. M.; Thayumanavan, S. Protein-Triggered Supramolecular Disassembly: Insights Based on Variations in Ligand Location in Amphiphilic Dendrons. *J. Am. Chem. Soc.* **2014**, *136* (14), 5385–5399.
- (57) Amado Torres, D.; Azagarsamy, M. A.; Thayumanavan, S. Supramolecular Displacement-Mediated Activation of a Silent Fluorescence Probe for Label-Free Ligand Screening. *J. Am. Chem. Soc.* **2012**, *134* (17), 7235–7237.
- (58) Gao, J.; Liu, X.; Secinti, H.; Jiang, Z.; Munkhbat, O.; Xu, Y.; Guo, X.; Thayumanavan, S. Photoactivation of Ligands for Extrinsically and Intrinsically Triggered Disassembly of Amphiphilic Nanoassemblies. *Chem. - A Eur. J.* **2018**, *24* (8), 1789–1794.

- (59) Guo, J.; Zhuang, J.; Wang, F.; Raghupathi, K. R.; Thayumanavan, S. Protein and Enzyme Gated Supramolecular Disassembly. *J. Am. Chem. Soc.* **2014**, *136* (6), 2220–2223.
- (60) Liu, X.; Hu, D.; Jiang, Z.; Zhuang, J.; Xu, Y.; Guo, X.; Thayumanavan, S. Multi-Stimuli-Responsive Amphiphilic Assemblies through Simple Postpolymerization Modifications. *Macromolecules* **2016**, *49* (17), 6186–6192.
- (61) Bai, W.; Jiang, Z.; Ribbe, A. E.; Thayumanavan, S. Smart Organic Two-Dimensional Materials Based on a Rational Combination of Non-Covalent Interactions. *Angew. Chemie - Int. Ed.* **2016**, *55* (36), 10707–10711.
- (62) Zhuang, J.; Gordon, M. R.; Ventura, J.; Li, L.; Thayumanavan, S. Multi-Stimuli Responsive Macromolecules and Their Assemblies. *Chem. Soc. Rev.* **2013**, *42* (17), 7421–7435.
- (63) Ryu, J. H.; Roy, R.; Ventura, J.; Thayumanavan, S. Redox-Sensitive Disassembly of Amphiphilic Copolymer Based Micelles. *Langmuir* **2010**, *26* (10), 7086–7092.
- (64) Ryu, J.-H.; Chacko, R. T.; Jiwanich, S.; Bickerton, S.; Babu, R. P.; Thayumanavan, S. Self-Cross-Linked Polymer Nanogels: A Versatile Nanoscopic Drug Delivery Platform Supporting Info. *J. Am. Chem. Soc.* **2010**, *3* (c), 2–10.
- (65) Israelachvili, J. N.; Mitchell, D. J.; Ninham, B. W. Theory of Self-Assembly of Hydrocarbon Amphiphiles into Micelles and Bilayers. *J. Chem. Soc. Faraday Trans. 2* **1976**, *72*, 1525.
- (66) Mu, Y.; Yu, M. Effects of Hydrophobic Interaction Strength on the Self-Assembled Structures of Model Peptides. *Soft Matter* **2014**, *10* (27), 4956–4965.
- (67) Jeong, B.; Gutowska, A. Lessons from Nature : Stimuli- Responsive Polymers and Their Biomedical Applications. *TRENDS Biotechnol.* **2002**, *20* (7), 305–311.
- (68) Li, M.-H.; Keller, P. Stimuli-Responsive Polymer Vesicles. *Soft Matter* **2009**, *5* (5), 927–

937.

- (69) de Las Heras Alarcon, C.; Pennadam, S.; Alexander, C. Stimuli Responsive Polymers for Biomedical Applications. *Chem. Soc. Rev.* **2005**, *34* (3), 276–285.
- (70) Roy, D.; Cambre, J. N.; Sumerlin, B. S. Future Perspectives and Recent Advances in Stimuli-Responsive Materials. *Prog. Polym. Sci.* **2010**, *35* (1–2), 278–301.

## CHAPTER 2

### ROLE OF AROMATICITY IN DETERMINING NANOSCALE THERMO-RESPONSIVE BEHAVIOR OF AMPHIPHILIC PEPTIDES

#### 2.1 Background and significance

Supramolecular assemblies that exhibit excellent biocompatibility and possess dynamic stimuli-responsive properties present themselves as smart biomaterials<sup>1,2</sup>. The designs for such systems are derived from nature and have important implications in the field of bioimaging, theranostics, drug delivery and tissue engineering<sup>3,4</sup>. Stimuli-responsive polymers emulate biological systems wherein an external stimulus results in an observable macroscopic change<sup>5,6,7</sup>. This includes a change in conformation, change in solubility, alteration of the hydrophilic/hydrophobic balance or release of a guest molecule<sup>8,9</sup>. Temperature responsive polymers exhibit a volume phase transition at a certain temperature and this result of change in their hydration state<sup>10,11,12</sup>. Polymers that become insoluble upon heating are known to exhibit Lower Critical Solution Temperature (LCST)<sup>13,14,15,16</sup> and those which become soluble upon heating are known to exhibit Upper Critical Solution Temperature (UCST)<sup>17,18,19</sup>. This macroscopic response of the polymer is a result of several cooperative interactions that manifests as a large structural change and reflects the nature of hydrogen bonding in the polymer in contrast to their solubilization by water<sup>20,21,22</sup>. This is an outcome of an intricate balance between the entropic and enthalpic effects. While entropic effects are ascribed to the dissolution process and the ordering of water molecules near the polymer, enthalpic effects arise due to a combination of intramolecular and intermolecular forces and due to solvation (Hydrogen bonding and hydrophobic interactions)<sup>23</sup>. The transition temperature is strongly dependent on factors such as solvent quality, salt concentration, and molecular weight

and concentration<sup>24,5</sup>. While their self-assembly is determined by a delicate balance of several non-covalent forces such as hydrogen bonding and hydrophobic interactions, it is possible to integrate parameters that evoke a response upon introduction of a stimulus.

### **2.1.1 Thermo and inverse thermo responsive supramolecular assemblies**

Oligo and Poly ethylene glycol based hydrophilic functional groups are renowned for exhibiting LCST behavior<sup>25,16</sup>. In our group, we were interested in determining the factors that account for the temperature sensitivity of PEG groups and embarked in a study to investigate the thermosensitive properties of oligo ethylene based supramolecular assemblies below the LCST. A sub-LCST was observed well below the LCST of oligo ethylene glycol based dendrons which was accompanied by a change in size of these supramolecular assemblies<sup>26</sup>. It was interesting to note that the host-guest properties were significantly altered at low temperature that affected the guest encapsulation stability indicating that the assemblies became a lot more dynamic at low temperatures.

However, the mere presence of PEG groups could not endow these molecules with temperature sensitive properties. Therefore, we were inquisitive to investigate the effect of the shape of the amphiphiles on their assembly properties and their concurrent temperature-sensitive behavior. Design and synthesis of a set of trimeric amphiphiles which differed only in the nature of the amide backbone revealed that intra-molecular hydrogen bonding could bestow the amphiphiles with conformational rigidity and the size transition so observed correlated with the guest encapsulation properties at lower temperatures. The hypothesis was validated using a linear trimeric amphiphiles that had conformational rigidity due to the covalently bound backbone. It has been discovered of late that trimeric amphiphilic assemblies containing OEG units are also capable of exhibiting a morphological transition commonly referred to as sub-LCST, which occurs at temperatures well below the LCST. Rigidity of the backbone was found to be imperative for these

trimeric amphiphiles to exhibit a sub-LCST behavior which was understood to be brought about by intramolecular hydrogen-bonding<sup>27</sup>. However, most of these systems are neither biocompatible nor biodegradable which undermines its use in a lot of biological applications. Therefore, there is a growing interest to turn to materials that offer competitive advantages in terms of biocompatibility.

### **2.1.2 Amphiphilic peptides**

Amphiphilic peptides are an interesting class of supramolecular materials that can undergo spontaneous conformational transitions in response to environmental cues such as pH, redox, ion concentration and temperature<sup>28,29,30,31</sup>. Peptides containing amide bonds can self-assemble through supramolecular interactions such as H-bonding,  $\pi$ -stacking and hydrophobic interactions<sup>32,33,34,35</sup> and are biocompatible and biodegradable<sup>36,37,38</sup>. The design of peptide-based self-assembled materials relies on secondary structures such as  $\alpha$ -helices and  $\beta$ -sheets<sup>14,39,32,40,41</sup>. Transitions from one conformation to another can be brought about by change of temperature through reorganization of hydrogen bonds<sup>42,43</sup>. Therefore, they can also show LCST behavior since these changes the hydrophilic-lipophilic balance (HLB) leading to a conformational transition and an eventual spatial redistribution of hydrophobic and hydrophilic residues. Imparting thermo-sensitivity to these materials is of considerable interest and peptides modified with oligo ethylene glycol (OEG) based functional groups have been explored quite heavily in the recent past owing to their lower critical solution temperature (LCST) behavior<sup>44,45,46</sup>.

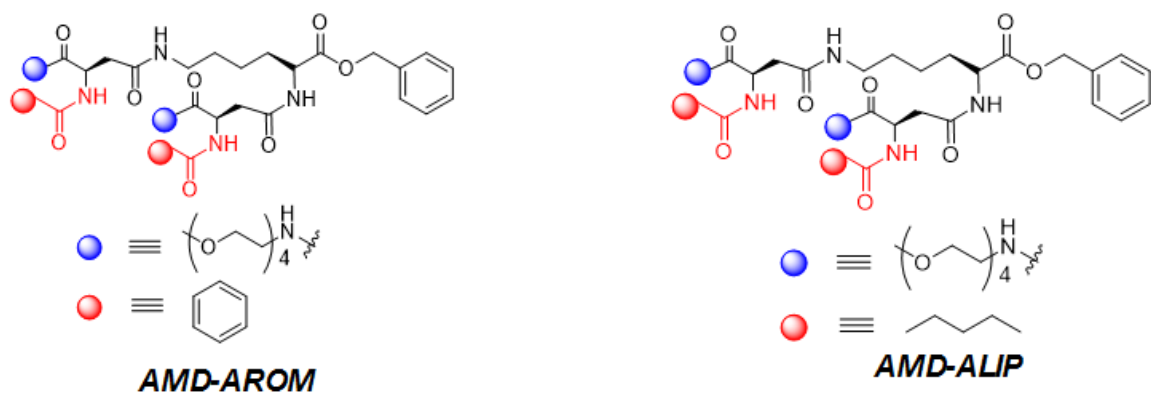
Elastin-like polypeptides (ELP) are a class of biopolymers that are made up of a pentameric repeat unit (Val-Pro-Gly-X-Gly) where X is any guest residue except proline<sup>47,48,49</sup>. ELPs are known to undergo a reversible phase transition in aqueous solutions ( $T_t$ ) depending on the nature of the guest residue<sup>48,15,50</sup>. While hydrophobic amino acids lower the transition temperature ( $T_t$ ), polar/charged amino acids raise  $T_t$ <sup>51</sup>. The LCST is understood by model proposed by Urry

wherein, the free ELP chains remain in a disordered random coil and are fully hydrated below the transition temperature ( $T_t$ ). Above  $T_t$ , the chains fold due to the hydrophobic effect and adopt a  $\beta$ -spiral structure<sup>17,52</sup>. Similarly, Poly-(L-Lysine) displayed a thermal helix-sheet transition between 20 °C and 40 °C depending on the molecular weight. Below transition temperature,  $\alpha$ -helix was found to be the predominant structure and a progressive organization into anti-parallel  $\beta$ -sheets was observed above  $T_t$ <sup>53,54</sup>. However, the design of these strategies involves the use of recombinant DNA technology.

While most of the temperature sensitivity is understood to arise only from OEG units, no investigations have been done to ascertain the role of hydrophobic units in the aggregation properties of peptide nanoassemblies at temperatures below the LCST of OEG units. These observations constitute as the preliminary findings of this communication (Scheme 1).

### **2.1.3 Design Objectives**

To this end, we synthesized a trimeric peptide AMD-ALIP from lysine and aspartic acid which was rendered amphiphilic owing to the choice of tetraethylene glycol (hydrophilic unit) and a hydrophobic hexyl unit. The peptide was designed in a way such that the individual components of the assembly were biodegradable and the by-products that were formed were also non-toxic i.e. GRAS. GRAS (Generally Recognized as Safe) molecules are recognized by the U.S. Food and Drug Administration (FDA) to be used as food additives or as medical devices<sup>55</sup>. The synthetic strategy adapted here makes it amenable for various hydrophobic units to be grafted on to the amphiphilic peptide in a facile manner. In addition, we also synthesized molecule AMD-AROM which differed from AMD-ALIP only in the choice of an aromatic hydrophobic unit (Scheme 2 and 3). We envisioned that this difference would help us understand the influence of hydrophobicity versus aromaticity in dictating the aggregation properties as a function of temperature for these peptide nanoassemblies.

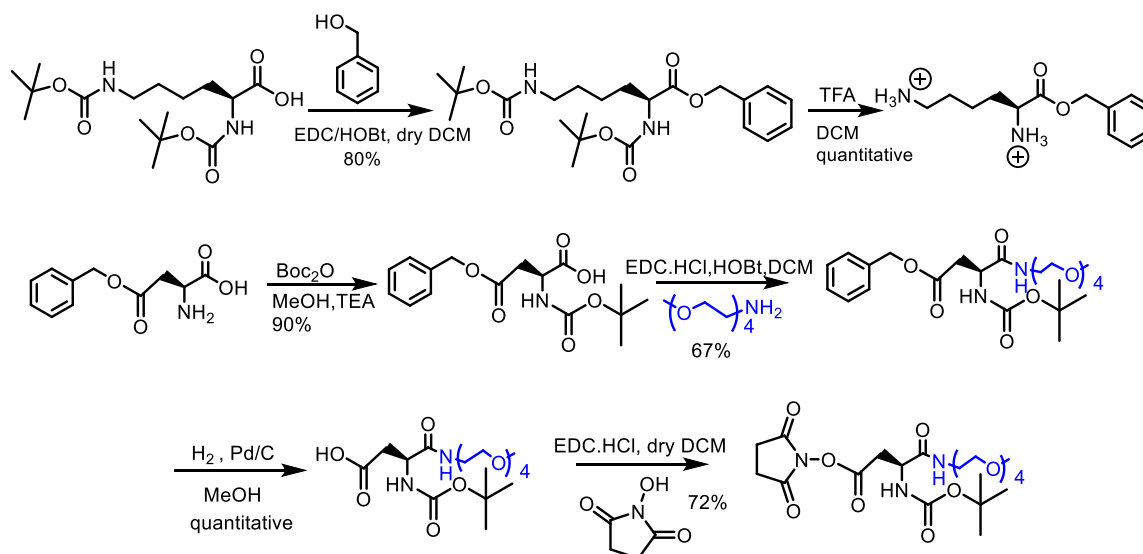


**Scheme 2.1:** Structures of different oligomeric peptide amphiphiles used in this study



## 2.2 Materials and methods

All chemicals and reagents were purchased from commercial sources and were used as received, unless mentioned otherwise. <sup>1</sup>H NMR spectra were recorded on 400 MHz NMR spectrometer using the residual proton resonance of the solvent as the internal standard. Chemical shifts are reported in parts per million (ppm). When peak multiplicities are given the following abbreviations are used: s, singlet; d, doublet; t, triplet; m, multiplet.



**Scheme 2.2:** Synthesis of amphiphilic aspartic acid from L-Aspartic acid  $\beta$ -benzyl ester and 3 from N- $\alpha$ ,N- $\epsilon$ -bis(tert-butoxycarbonyl)-L-lysine

- **Synthesis of 2:** 3 g (0.0084 mol) of N- $\alpha$ , N- $\epsilon$ -bis(tert-butoxycarbonyl)-L-lysine was dissolved in anhydrous dichloromethane in a round bottom flask and cooled to 0 °C under inert atmosphere. To this solution, (3-dimethylaminopropyl)-N'-ethylcarbodiimide hydrochloride (1.93 g, 0.01 mol), hydroxybenzotriazole (1.35g, 0.01 mol) and 4-dimethylamino pyridine (0.205 g, 0.00168 mol) were added and the solution was left to stir for 30 minutes. Benzyl alcohol (0.79 mL, 0.0076 mol) was added dropwise to the stirring solution and the reaction was further left to stir overnight. The reaction mixture was concentrated in vacuo, extracted using dichloromethane and water, followed by washing with 1N hydrochloric acid. The

combined extracts were dried over anhydrous  $\text{Na}_2\text{SO}_4$  and the crude product was purified by silica gel chromatography using hexane and ethyl acetate as eluents to afford **2** in 80 % yield.  $^1\text{H}$  NMR ( $\text{CDCl}_3$ , 400 MHz, TMS):  $\delta$  (ppm) = 7.35(m, 5H), 5.05-5.3 (m,3H), 4.5(broad s, 1H), 4.25 (broad s, 1H), 3.0 (broad d, 2 H), 1.55-1.8(m, 2H),1.49(s, 18H),1.25(m,2H) ( $\text{M}+\text{Na}^+$ ) from ESI spectroscopy: 459.26

- **Synthesis of 3:** To a solution of **2** in anhydrous dichloromethane in a round bottom flask, trifluoroacetic acid (1:1 vol% DCM: TFA) was added and the reaction was left to stir for 4 hours. The reaction mixture was concentrated in vacuo followed by pouring into ice cold diethyl ether. The product was isolated as a precipitate and washed with diethyl ether twice to afford a white dry product **3** in quantitative yield and used as it is.  $^1\text{H}$  NMR (Acetone- $d_6$ , 400 MHz, TMS):  $\delta$  (ppm) = 7.35(m, 5H), 5.25(m, 2H), 4.3(m, 1H), 3.7(m,1H), 3.1(t, 1 H), 2.5 (m, 2H), 1.6 (m, 2H), 1.7(m,2H) ( $\text{M}+\text{Na}^+$ ) from ESI spectroscopy: 489.13
- **Synthesis of 4:** 5 g (0.0223 mol) of L-Aspartic acid  $\beta$ -benzyl ester was dissolved in anhydrous methanol in a round bottom flask and cooled to 0 °C under inert atmosphere. To this solution, triethylamine (4 mL, 0.025 mol) and di-tert-butyl-dicarbonate (5.38 g, 0.025 mol) were added and the solution was left to stir overnight. The reaction mixture was concentrated in vacuo, extracted using ethyl acetate and water, followed by washing with saturated  $\text{NaHCO}_3$ . The combined extracts were dried over anhydrous  $\text{Na}_2\text{SO}_4$  to afford **4** in 90% yield and was used as it is.  $^1\text{H}$  NMR ( $\text{CDCl}_3$ , 400 MHz, TMS):  $\delta$  (ppm) = 7.35(m, 5H), 5.5(broad d, 1H), 5.1(d,2H), 4.5(broad m, 1H), 3.1(broad m, 1H), 2.9(dd, 1H), 1.5(s,9H) ( $\text{M}+\text{Na}^+$ ) from ESI spectroscopy: 346.14
- **Synthesis of 5:** 1.55 g (0.0048 mol) of **4** was dissolved in anhydrous dichloromethane in a round bottom flask and cooled to 0 °C under inert atmosphere. To this solution, (3-

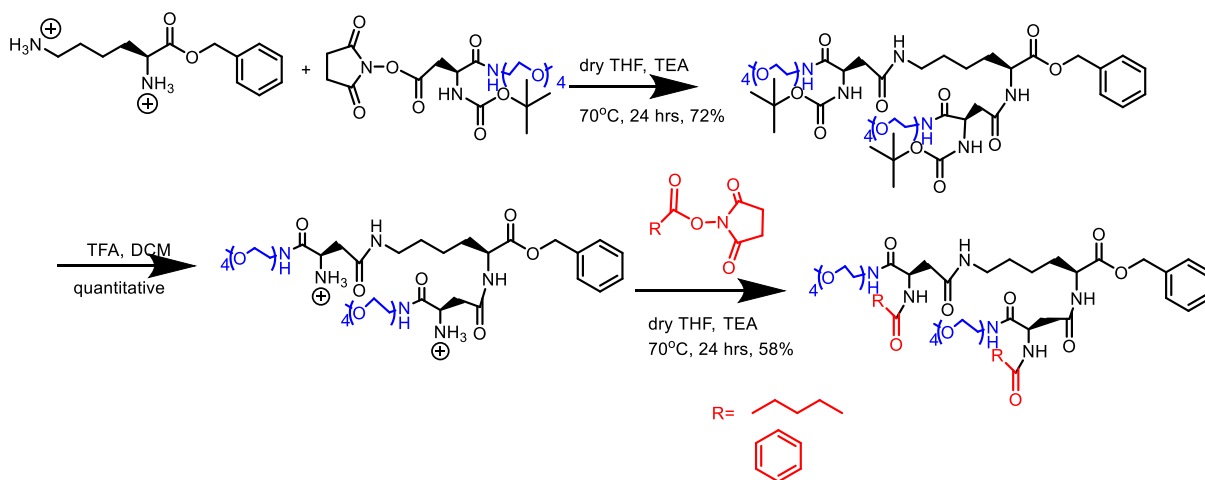
dimethylaminopropyl)-N'-ethylcarbodiimide hydrochloride (1.104 g, 0.0057 mol), hydroxybenzotriazole (0.78 g, 0.00576 mol) and 4-dimethylamino pyridine (0.12 g, 0.00096 mol) were added and the solution was left to stir for 30 minutes. Tetraethylene glycol amine monomethyl ether (1 g, 0.0048 mol) was added dropwise to the stirring solution and the reaction was further left to stir overnight. The reaction mixture was concentrated in vacuo, extracted using dichloromethane and water, followed by washing with 1N hydrochloric acid. The combined extracts were dried over anhydrous Na<sub>2</sub>SO<sub>4</sub> and the crude product was purified by silica gel chromatography using hexane and ethyl acetate as eluents to afford **5** in 67 % yield. <sup>1</sup>H NMR (CDCl<sub>3</sub>, 400 MHz, TMS): δ (ppm) = 7.35(m, 5H), 6.8(broad peak, 1H), 5.6(broad d, 1H), 5.1(d, 2H), 4.5(broad peak, 1H), 3.49-3.65(m, 13H), 3.4(m, 2H), 3.3(s, 3H), 3.0(broad m, 1H), 2.7(broad dd, 1H), 1.5(s,9H) (M+Na<sup>+</sup>) from ESI spectroscopy: 535.27

- **Synthesis of 6:** Compound **5** (1 g) was dissolved in anhydrous methanol and Pd/C (100mg) was added to the reaction mixture. This was left on a Parr apparatus under hydrogen at 45 psi for 12 hours. The reaction mixture was filtered over celite and the solvent was evaporated to afford an oily viscous liquid **6** in quantitative yield and used as it is. <sup>1</sup>H NMR (CD<sub>2</sub>Cl<sub>2</sub>, 400 MHz, TMS): 6.8(broad peak, 1H), 6.0(broad d, 1H), 4.5(broad peak, 1H), 3.49-3.65(m, 13H), 3.4(m, 2H), 3.3(s, 3H), 3.0(broad m, 1H), 2.7(broad dd, 1H), 1.5(s,9H) (M+Na<sup>+</sup>) from ESI spectroscopy: 445.23
- **Synthesis of 7:** **6**(1 g, 0.00246 mol) and N-hydroxy succinimide(0.34 g, 0.0030 mol) were dissolved in anhydrous dichloromethane in a round bottom flask and cooled to 0 °C under inert atmosphere. To this, (3-dimethylaminopropyl)-N'-ethylcarbodiimide hydrochloride (0.7 g, 0.00369 mol) was added and the reaction was further left to stir overnight. The reaction mixture was extracted using dichloromethane and water and further, washed with saturated NaHCO<sub>3</sub>,

saturated NaCl, dried over anhydrous Na<sub>2</sub>SO<sub>4</sub> and concentrated to afford **7** in 72% yield. <sup>1</sup>H NMR (CDCl<sub>3</sub>, 400 MHz, TMS): 6.8(broad peak, 1H), 5.6(broad d, 1H), 4.5(broad peak, 1H), 3.49-3.65(m, 13H), 3.4(m, 2H), 3.3(s, 3H), 3.0(broad m, 1H), 2.85(s, 4H), 2.7(broad dd, 1H), 1.5(s, 9H) (M+Na<sup>+</sup>) from ESI spectroscopy: 542.24

- **Synthesis of 8:** **3**(0.308 g, 0.00130 mol) and **7**(1.309 g, 0.00260 mol) were dissolved in dry tetrahydrofuran in a round bottom flask under inert atmosphere. To this, triethylamine (0.72 mL, 0.0052 mol) was added and was refluxed overnight under inert atmosphere. The reaction mixture was extracted using ethyl acetate and water. The organic layers were further washed with 1 N HCl and saturated NaHCO<sub>3</sub>. The crude product was purified by silica gel chromatography using dichloromethane and methanol as eluents to afford **8** in 72 % yields. <sup>1</sup>H NMR was attempted by dissolving the compound in various solvents. However, it was found to be sparingly soluble. <sup>1</sup>H NMR in acetone denotes all the characteristic peaks for the product but the integration does not come out as expected owing to low solubility of the compound. (M+Na<sup>+</sup>) from ESI spectroscopy: 1067.50

- Synthesis of 12(AMD-AROM) and 13(AMD-ALIP):** To a solution of **8** in anhydrous dichloromethane in a round bottom flask, trifluoroacetic acid (1:1 vol% DCM: TFA) was added and the reaction was left to stir for 4 hours. The reaction mixture was concentrated in vacuo to afford **9.9**(0.103g, 0.000105 mol) and **10**(0.046 g, 0.000211 mol) or **11** (0.043 g, 0.000205 mol) were dissolved in anhydrous tetrahydrofuran along with triethylamine (50  $\mu$ L, 0.00041 mol) and the reaction mixture was refluxed under inert atmosphere overnight. The reaction mixture was extracted using ethyl acetate and water. The organic layers were further



**Scheme 2.3:** Synthesis of amphiphilic peptides AMD-AROM (**13**) and AMD-ALIP (**12**)

washed with 1 N HCl

and saturated  $\text{NaHCO}_3$ . The crude product was purified by silica gel chromatography using dichloromethane and methanol as eluents to afford **12** and **13** in 58% and 62% yield respectively. **12**( $\text{M}+\text{Na}^+$ ) from ESI spectroscopy: 1063.62, purity from HPLC and **13**( $\text{M}+\text{Na}^+$ ) from ESI spectroscopy: 1075.53, purity from HPLC

- Temperature dependent Dynamic light scattering study (DLS):** The stock solutions of AMD-ALIP (1.23 mM), AMD-AROM (1.86 mM) respectively, were made by a standard

method of dispersing the weighed compound in required amount of HPLC grade water in a scintillation vial with a stir bar followed by sonication and vortex for 5 minutes. DLS was performed on a Malvern nano-zeta sizer instrument with a 637 nm laser with non-invasive backscattering technology detected at 173°. All sizes are reported as the hydrodynamic diameter ( $D_H$ ) and were repeated in triplicate. Variable temperature DLS experiments were performed by equilibrating the aqueous solutions for 5 minutes at the respective temperature before the size measurements.

- **Temperature dependent Transmission electron microscopy (TEM) study:** For TEM studies, concentrations same as that for DLS measurements were used. Briefly, one drop (10 $\mu$ L) of each sample was drop casted on carbon coated Cu grid and allowed to dry for 24 hours (at ambient temperature) before imaging them. For the size measurement at low temperature, the same sample was incubated at 5°C following which it was drop casted and allowed to dry before imaging. TEM images were recorded on a JEOL-2000FX machine operating at an accelerating voltage of 100 kV.
- **Temperature dependent Circular Dichroism (CD) studies:** CD spectra of the peptide nano assemblies were recorded on JASCO J-1500 spectrophotometer. In a typical experiment, 200  $\mu$ L of the peptide amphiphiles solution (concentrations same as that in DLS and TEM measurements) was injected into a quartz cuvette of 1-mm path length, equilibrated at 25 °C and 5 °C for 5 min and scanned from 180 to 250 nm (scan rate: 20 nm/min, interval: 0.2 nm, average of three spectra).
- **Fluorescence study to determine temperature, pH and salt dependent guest release:** The stock solutions of AMD-ALIP (1.23 mM) and AMD-AROM (1.86 mM) respectively, were made by a standard method of dispersing the weighed compound in required amount of HPLC

grade water and diluted with pH 3 phosphate-citrate buffer (500mM) just before the measurement in a scintillation vial with a stir bar. 100  $\mu$ L of DiI stock (1mM in acetone) was then added to the vial in a dropwise manner. The contents were sonicated for 5 minutes and vortexed for 2 minutes, following which they were left to stir for 8 hours at room temperature uncapped to facilitate the evaporation of acetone. The excess insoluble DiI was removed by filtration using a membrane with a pore size of 0.450 $\mu$ m. The solution was then transferred to a cuvette and emission spectrum was recorded at specified time intervals at 25 °C and 5 °C. Concomitant DLS size measurements were also performed to corroborate the guest release.

- **pH dependent DLS:** The peptide nanoassemblies were incubated in 1N HCl (1 mL) for 30 minutes following which the DLS was recorded at 25 °C and 5 °C.
- **pH dependent CD and degradation studies:** The peptide nanoassemblies were incubated in 1N HCl (1 mL) for 30 minutes following which the CD spectra was recorded at 25 °C and 5 °C. For the degradation studies, samples were prepared in the above-mentioned way and then lyophilized. The samples were dissolved in water and methanol mixture and the degradation products were studied using ESI mass spectroscopy.
- **Salt dependent DLS and CD studies:** The peptide nanoassemblies were incubated with kosmotropic salt (Sodium sulfate was made as a 2M stock in HPLC grade water) and chaotropic salts (Sodium thiocyanate and Urea was made as a 2M stock in HPLC grade water) and diluted with the peptide assemblies such that their concentration in the final solution was 1M. The solutions were left to sit for 15 minutes before performing DLS and CD measurements. The solutions were found to become turbid in about 30 minutes after adding the respective salts.

## 2.3 Results and discussion

### 2.3.1 Characterization of self-assembly of peptides

To study the aggregation properties of AMD-ALIP and AMD-AROM, the peptides were dispersed in water at different concentrations and the critical aggregation concentrations (CAC) were calculated using DiI, a hydrophobic dye as a spectroscopic probe<sup>11</sup>. The stock solutions of AMD-

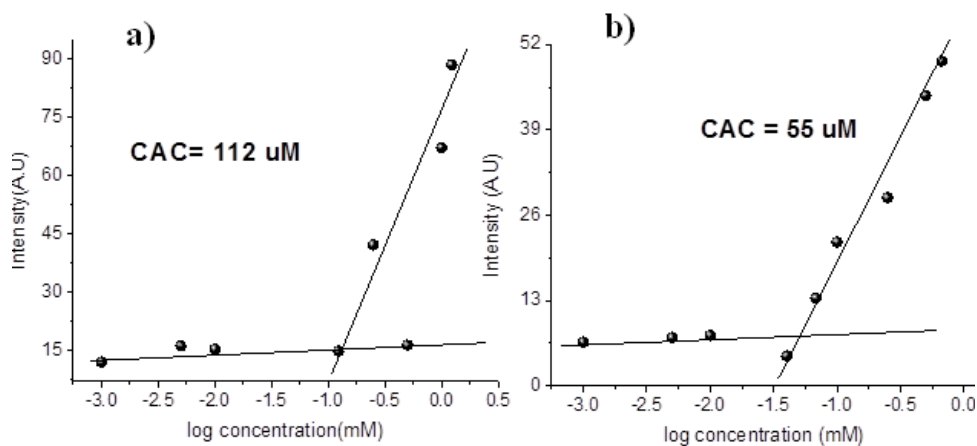


**Figure 2.1:** Critical aggregation concentrations of peptides a) AMD-ALIP and b) AMD-AROM

ALIP (1.23 mM), AMD-AROM (1mM) respectively, were made by a standard method of dispersing the weighed compound in required amount of HPLC grade water in a scintillation vial with a stir bar followed by sonication and vortex for 5 minutes.

The contents were sonicated for 5 minutes and vortexed for 2 minutes, following which they were left to stir for 8 hours at room temperature uncapped to facilitate the evaporation of acetone. The excess insoluble DiI was removed by filtration using a membrane with a pore size of 0.450 $\mu$ m. The intensity at the maxima (584 nm for AMD-AROM and 569 nm for AMD-



ALIP) were plotted as a function of concentration of the peptide amphiphiles and the inflexion point was noted to be the critical aggregation concentration or CAC (Figure 1).

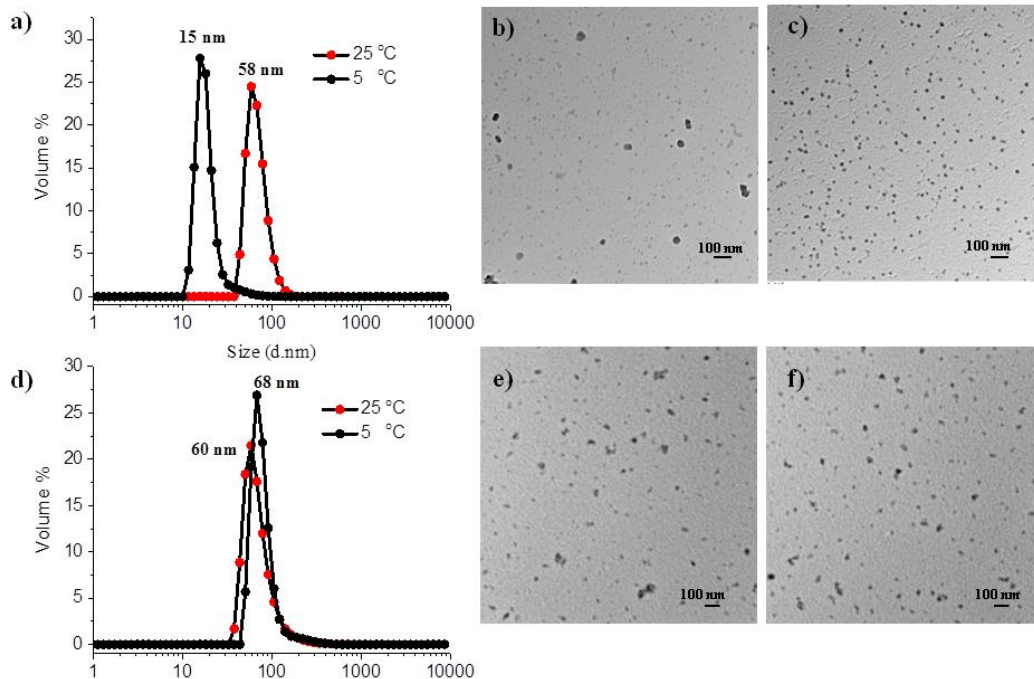


**Figure 2.2:** Temperature-dependent size variation observed using dynamic light scattering (DLS) of a) AMD-ALIP and d) AMD-AROM reveals a temperature dependent size transition at 5 °C in case of AMD-ALIP assemblies. Corresponding TEM images of b) AMD-ALIP and e) AMD-AROM at 25 °C and c) AMD-ALIP and f) AMD-AROM at 5 °C indicates spherical assemblies

### 2.3.2 Temperature dependent aggregation and circular dichroism

We, then, investigated the size of these assemblies (AMD-ALIP and AMD-AROM) at different temperatures above the CAC using dynamic light scattering (DLS). Both molecules were found to self-assemble into aggregates ~58 nm and ~70 nm in size at 25 °C. When the temperature was decreased, we found the peptide nanoassembly formed by molecule AMD-ALIP to have a sudden size transition at 5 °C with the assemblies now having a size of 15 nm.

Interestingly, nanoassemblies formed by molecule AMD-AROM did not exhibit this kind of a sharp transition and their size changed from about 68 nm at 25 °C to 60 nm at 5 °C which was a

rather small change compared to molecule AMD-ALIP (Figure 2). It must be noted here that the molecules AMD-ALIP and AMD-AROM were structurally very similar and the only contrast was with respect to their hydrophobic units. We reasoned that this observation could arise out of the change in the hydrodynamic radius of these assemblies at lower temperatures. This arises from the

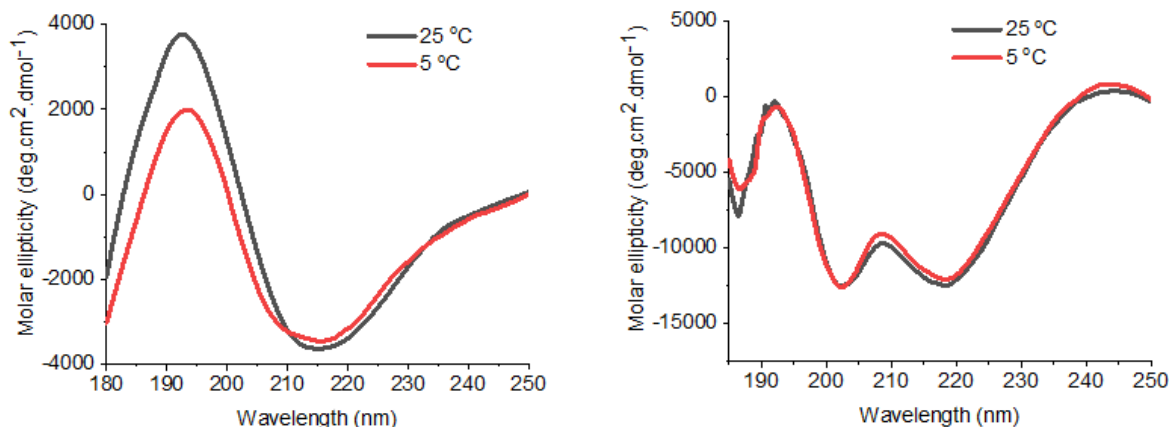


**Figure 2.3:** Temperature dependent circular dichroism (CD) for a) AMD-ALIP indicates formation of  $\beta$ -sheet like structures with significant reduction of intensity at 5 °C while b) AMD-AROM exhibits a signature  $\alpha$ -helix like conformation with the same intensity at 25 °C and 5 °C.

fact that peptide amphiphiles are known to exhibit polymorphism<sup>56</sup>. So, we subjected these peptide nanoassemblies to examination using Transmission Electron Microscopy (TEM) and found that the assemblies exist as spherical non-hollow aggregates and sizes corroborate with that obtained from DLS (Figure 2b-f).

Intrigued by this observation, we hypothesized that this could arise due to the nature of secondary structures that were formed by molecules AMD-ALIP and AMD-AROM at 25 °C and 5 °C that gave rise to different hydrodynamic volumes that manifested in their different sizes as observed by light scattering. The hypothesis arises from the fact that the self-assembly of peptides is known to depend heavily on temperature and peptides are known to undergo irreversible changes in the assembly characteristics upon heating or cooling to extreme temperatures accompanied by a concomitant loss in activity<sup>57,58,59</sup>. To test this hypothesis, we utilized circular dichroism wherein

we characterized solutions of molecules AMD-ALIP and AMD-AROM at 25 °C. While assemblies formed by molecule AMD-ALIP exhibited a typical  $\beta$ -sheet secondary structure<sup>60,61,62,63,64</sup> organization, the assemblies arising from molecule AMD-AROM was found to exist as  $\alpha$ -helix<sup>63,65,66,67,68</sup> (Figure 3). We, further, investigated the evolution of secondary structures at 5 °C. Interestingly, the intensity of  $\beta$ -sheet organization was found to decrease substantially at 5 °C for amphiphilic assemblies of molecule AMD-ALIP alluding to the role of the hydrophobic units in the molecular organization of the peptide nanoassemblies since hydrophobic interactions are known to be stronger at higher temperature<sup>23,69,70,57</sup>. On the other hand, the intensity of the secondary structure i.e.  $\alpha$ -helix for assemblies of molecule AMD-AROM at 5 °C was found to be the same as that at 25 °C alluding to the role of the aromatic group in imparting rigidity to the assemblies making them less sensitive to temperature changes<sup>71,63,72</sup>. Aromatic interactions have indeed, been reported to diminish temperature responsive behavior of dendrimer-based amphiphilic assemblies<sup>73</sup>.

### **2.3.3 Role of hydrophobic unit in thermo responsive behavior**

To allow for a direct correlation between the influence of aromatic hydrophobic groups and temperature sensitivity, solutions of AMD-ALIP and AMD-AROM were mixed to see if there is a sharp transition upon gradual introduction of the temperature-insensitive AMD-AROM peptide into the AMD-ALIP solution.

The temperature of a single mixed micelle solution was decreased from 25 °C to 5 °C in 5 °C intervals. The AMD-ALIP and AMD-AROM solutions were allowed to equilibrate at each temperature and the presence or absence of a temperature-dependent size transition was observed by DLS.

As observed before, the AMD-ALIP peptide nanoassemblies showed a size transition at 5 °C which was absent in case of AMD-AROM. Upon addition of AMD-AROM peptide nanoassemblies into a solution of AMD-ALIP peptide nanoassemblies (1:1 volume:volume ratio), we observed aggregates of sizes ~140 nm from DLS which was understood to arise from the mixed assemblies formed from AMD-ALIP and AMD-AROM. Further, upon decreasing the temperature of the solution, a gradual decrease in size was observed with the assemblies now, exhibiting a size of ~80 nm at 5 °C. This indeed, reveals that the introduction of a temperature-sensitive AMD-ALIP

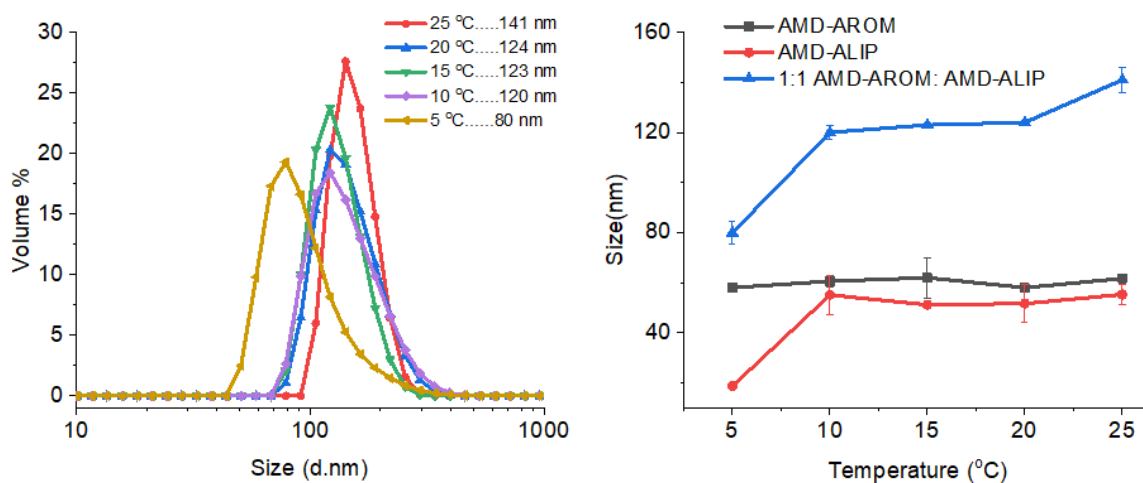


**Figure 2.4:** Variable temperature DLS of AMD-AROM and AMD-ALIP where AMD-AROM: AMD-ALIP is 1:1 reveals that incorporation of a peptide containing an aliphatic hydrophobic group (AMD-ALIP) results in a size transition of an aromatic group containing peptide nanoassembly.

assemblies into the temperature-insensitive AMD-AROM assemblies results in a temperature-sensitive size transition. This suggests that incorporation of aromatic hydrophobic units in a peptide diminishes the temperature sensitivity of the nanoassemblies

### 2.3.4 Reversibility of size transition

It is also interesting to note that the size transition observed for molecules AMD-ALIP and AMD-AROM are sharp yet irreversible over repeated heating and cooling cycles (Figure 4). Concomitantly, circular dichroism studies for the molecules suggest that the extent of secondary structure formation reaches a minimum at 5 °C and does not revert to its original intensity even after several cycles of heating and cooling (Figure 4). These studies indeed, reveal that the peptide nanoassemblies are ‘kinetically trapped’ at 25 °C indicating the possibility of transition between the kinetic traps and thermodynamic states under appropriate external stimuli<sup>74,75,76</sup>.

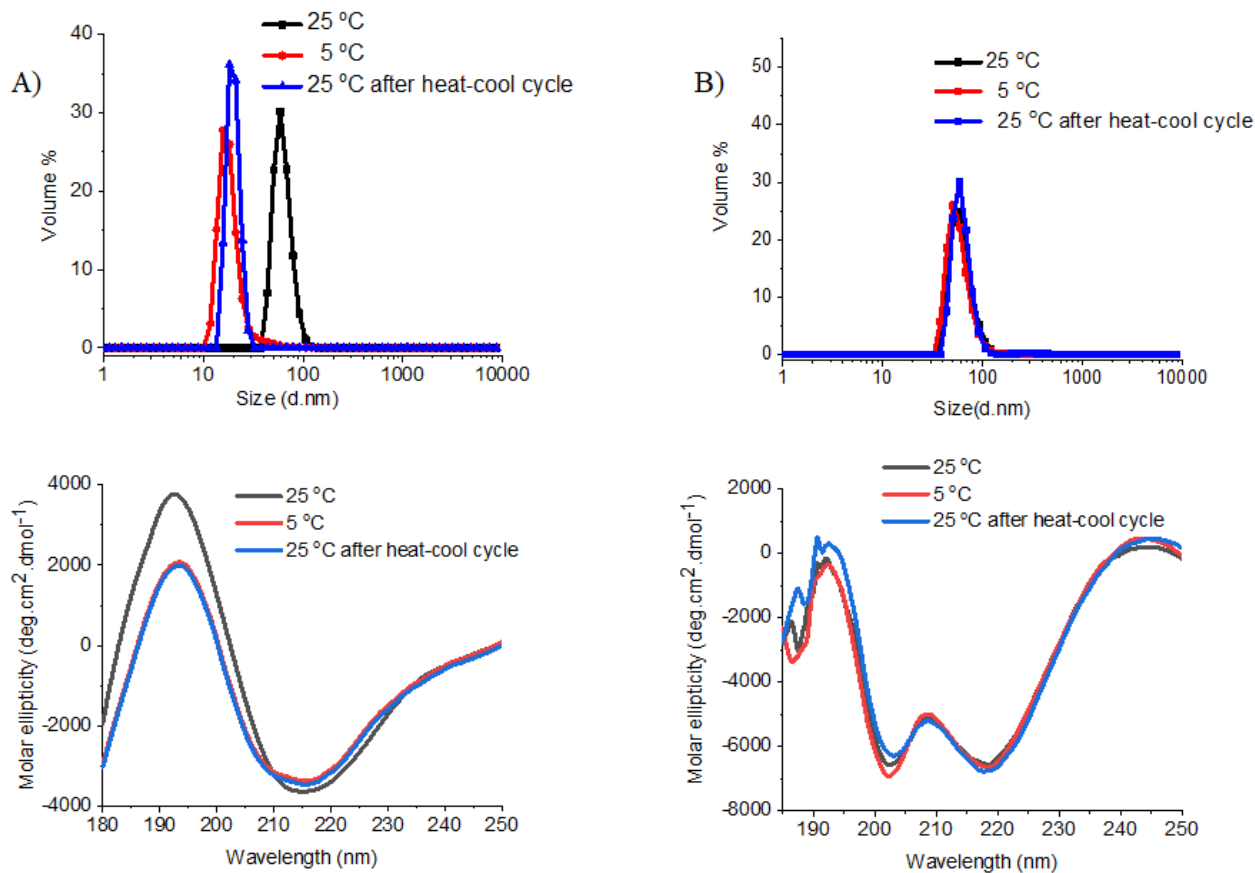


**Figure 2.5:** DLS sizes for a) AMD-ALIP and b) AMD-AROM indicate that the size transition is irreversible over several heating and cooling cycles and that the peptide nanoassemblies are ‘kinetically trapped’ at 25 °C

Kinetics affects the mode of molecular packing; such that different pathways lead to different morphologies and function.

### 2.3.5 Hydrophobic guest encapsulation and release

The stock solutions of AMD-ALIP (1.23 mM), AMD-AROM (1.86 mM) respectively, were made by a standard method of dispersing the weighed compound in required amount of HPLC grade water in a scintillation vial with a stir bar. 40  $\mu$ L of DiI stock (1mM in acetone) was then added to the vial in a dropwise manner. The contents were sonicated for 5 minutes and vortexed for 2 minutes, following which they were left to stir for 8 hours at room temperature uncapped to facilitate the evaporation of acetone.

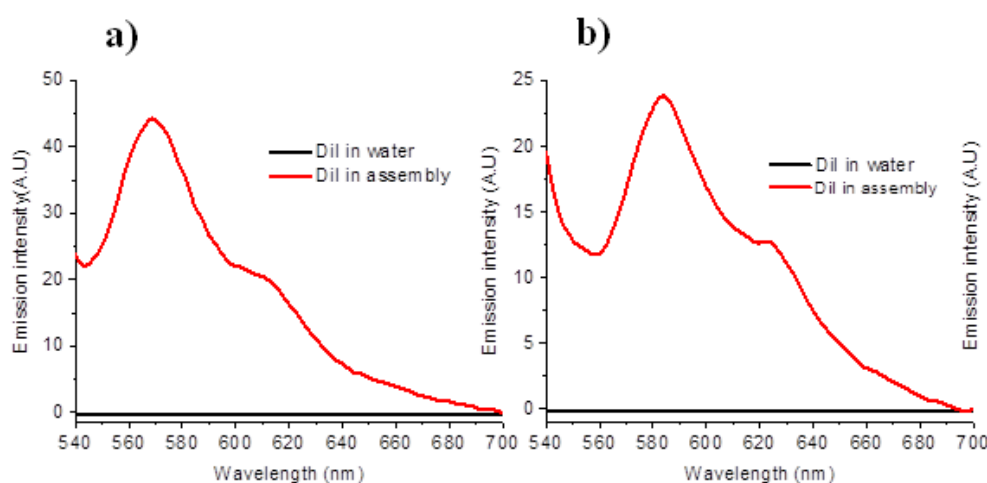


**Figure 2.6:** Fluorescence spectra of DiI encapsulated in peptide nanoassemblies against pristine DiI in water for AMD-ALIP(a), AMD-AROM(b)

The excess insoluble DiI was removed by filtration using a membrane with a pore size of 0.450 $\mu$ m. The emission wavelength of pristine DiI in water and that of DiI encapsulated in the amphiphilic peptide assemblies is shown in Figure 5. Finally, we were interested in investigating the implications of the temperature dependent aggregation properties of the peptide nanoassemblies in their encapsulation stabilities the implications of the temperature dependent aggregation properties of the peptide nanoassemblies in their encapsulation stabilities

We expected that the difference in their aggregation properties would manifest in different encapsulation stabilities at 25 °C and 5 °C since host-guest interactions are driven by solvophobic interactions<sup>77</sup>. Indeed, we observed that the change in the aggregation properties at 5 °C for molecule AMD-ALIP was accompanied by release of the guest, DiI indicating that the assemblies at 5 °C had a weak propensity to encapsulate hydrophobic guests as compared to the ones at 25 °C. Meanwhile, molecule AMD-AROM which did not exhibit a size transition was found to have similar guest encapsulation properties at 25 °C and 5 °C (Figure 6).

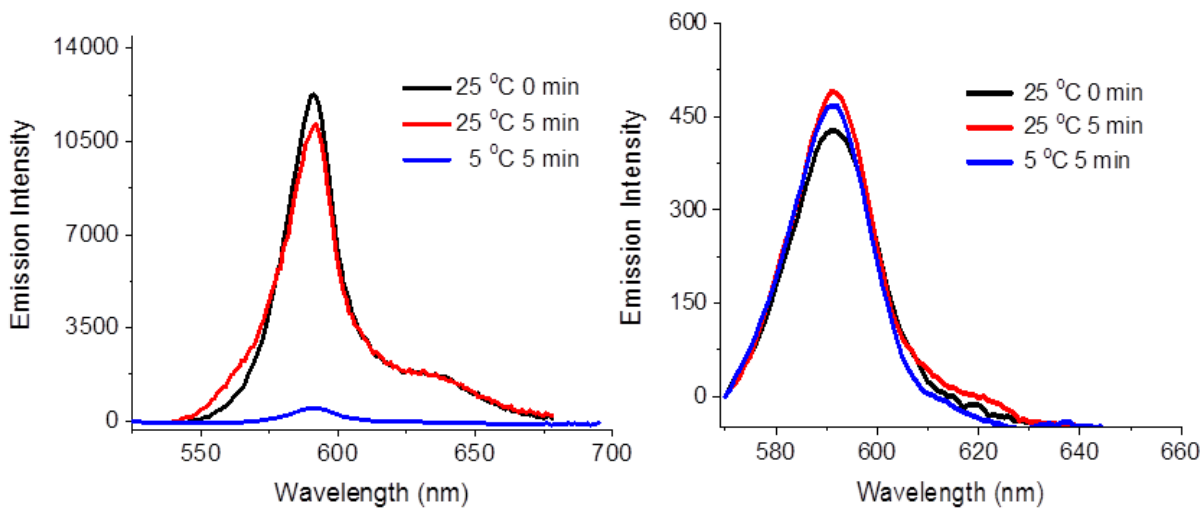


**Figure 2.7:** Guest encapsulation ability at 25 °C and 5 °C for a) AMD-ALIP and b) AMD-AROM

## 2.4 Conclusions

In summary, we have established the design principles for oligomeric peptides to exhibit a unique size transition well below the LCST. We have found that incorporation of aromatic hydrophobic groups diminishes the thermo-sensitivity of the peptide nanoassemblies. The size transition is understood to be brought about by a significant loss of secondary structures at low temperatures which results in assemblies with a different hydrodynamic volume than those at ambient temperatures that is manifested in their aggregation properties. Concurrently, the peptide nanoassemblies were found to degrade under acidic conditions owing to the presence of ester and

amide linkages in the backbone. The temperature-dependent aggregation properties of these peptide nanoassemblies also gave rise to disparity in terms of guest encapsulation ability upon decreasing temperature. Because the molecules are designed to incorporate FDA approved components, the assembly is biodegradable, and the degraded by-products are safe. The supramolecular structural requirements established in this study have drawn significant attention since these assemblies offer themselves as excellent means for the release of flavor molecules at low temperatures when encapsulated in these assemblies and this is currently being pursued in collaboration with a beverage industry.



## 2.5 References

- (1) Stupp, S. I.; Palmer, L. C. Supramolecular Chemistry and Self-Assembly in Organic Materials Design. *Chem. Mater.* **2014**, *26* (1), 507–518.
- (2) Webber, M. J.; Appel, E. A.; Meijer, E. W.; Langer, R. Supramolecular Biomaterials. *Nat. Mater.* **2015**, *15* (1), 13–26.
- (3) Cheng, C.-C.; Wang, J.-H.; Chuang, W.-T.; Liao, Z.-S.; Huang, J.-J.; Huang, S.-Y.; Fan, W.-L.; Lee, D.-J. Dynamic Supramolecular Self-Assembly: Hydrogen Bonding-Induced Contraction and Extension of Functional Polymers. *Polym. Chem.* **2017**, *8* (21), 3294–3299.
- (4) Middleton, J. C.; Tipton, A. J. Synthetic Biodegradable Polymers as Orthopedic Devices. *Biomaterials* **2000**, *21* (23), 2335–2346.
- (5) Schmaljohann, D. Thermo- and PH-Responsive Polymers in Drug Delivery. *Adv. Drug Deliv. Rev.* **2006**, *58* (15), 1655–1670.
- (6) Li, M.-H.; Keller, P. Stimuli-Responsive Polymer Vesicles. *Soft Matter* **2009**, *5* (5), 927–937.
- (7) Torchilin, V. P. Structure and Design of Polymeric Surfactant-Based Drug Delivery Systems. *J. Control. Release* **2001**, *73* (2–3), 137–172.
- (8) de Las Heras Alarcon, C.; Pennadam, S.; Alexander, C. Stimuli Responsive Polymers for Biomedical Applications. *Chem. Soc. Rev.* **2005**, *34* (3), 276–285.
- (9) Cabral, H.; Nishiyama, N.; Kataoka, K. Supramolecular Nanodevices: From Design Validation to Theranostic Nanomedicine. *Acc. Chem. Res.* **2011**, *44* (10), 999–1008.
- (10) Hocine, S.; Li, M.-H. Thermoresponsive Self-Assembled Polymer Colloids in Water. *Soft Matter* **2013**, *9* (25), 5839.
- (11) Dan, K.; Bose, N.; Ghosh, S. Vesicular Assembly and Thermo-Responsive Vesicle-to-

- Micelle Transition from an Amphiphilic Random Copolymer. *Chem. Commun.* **2011**, 47 (46), 12491.
- (12) Jain, K.; Vedarajan, R.; Watanabe, M.; Ishikiriyama, M.; Matsumi, N. Tunable LCST Behavior of Poly(N-Isopropylacrylamide/Ionic Liquid) Copolymers. *Polym. Chem.* **2015**, 6 (38), 6819–6825.
- (13) Kashyap, S.; Jayakannan, M. Super LCST Thermo-Responsive Nanoparticle Assembly for ATP Binding through the Hofmeister Effect. *J. Mater. Chem. B* **2015**, 00, 1–11.
- (14) Nuhn, H.; Klok, H. A. Secondary Structure Formation and LCST Behavior of Short Elastin-like Peptides. *Biomacromolecules* **2008**, 9 (10), 2755–2763.
- (15) Hyun, J.; Lee, W. K.; Nath, N.; Chilkoti, A.; Zauscher, S. Capture and Release of Proteins on the Nanoscale by Stimuli-Responsive Elastin-like Polypeptide “Switches.” *J. Am. Chem. Soc.* **2004**, 126 (23), 7330–7335.
- (16) Aathimanikandan, S. V.; Savariar, E. N.; Thayumanavan, S. Temperature-Sensitive Dendritic Micelles. *J. Am. Chem. Soc.* **2005**, 127 (42), 14922–14929.
- (17) Luo, T.; Kiick, K. L. Noncovalent Modulation of the Inverse Temperature Transition and Self-Assembly of Elastin-b-Collagen-like Peptide Bioconjugates. *J. Am. Chem. Soc.* **2015**, 137 (49), 15362–15365.
- (18) Saito, N.; Kobayashi, H.; Yamaguchi, M. “Inverse” Thermoresponse: Heat-Induced Double-Helix Formation of an Ethynylhelicene Oligomer with Tri(Ethylene Glycol) Termini. *Chem. Sci.* **2016**, 7 (6), 3574–3580.
- (19) Ukpebor, O. T.; Shah, A.; Bazov, E.; Boutis, G. S. Inverse Temperature Transition of Elastin like Motifs in Major Ampullate Dragline Silk: MD Simulations of Short Peptides and NMR Studies of Water Dynamics. *Soft Matter* **2014**, 10 (5), 773–785.

- (20) Rajdev, P.; Molla, M. R.; Ghosh, S. Understanding the Role of H-Bonding in Aqueous Self-Assembly of Two Naphthalene Diimide (NDI)-Conjugated Amphiphiles. *Langmuir* **2014**, *30* (8), 1969–1976.
- (21) Feil, H.; Bae, Y. H.; Feijen, J.; Kim, S. W. Effect of Comonomer Hydrophilicity and Ionization on the Lower Critical Solution Temperature of N-Isopropylacrylamide Copolymers. *Macromolecules* **1993**, *26* (10), 2496–2500.
- (22) Jones, S. T.; Walsh-Korb, Z.; Barrow, S. J.; Henderson, S. L.; Del Barrio, J.; Scherman, O. A. The Importance of Excess Poly(N-Isopropylacrylamide) for the Aggregation of Poly(N-Isopropylacrylamide)-Coated Gold Nanoparticles. *ACS Nano* **2016**, *10* (3), 3158–3165.
- (23) Rudolph, T.; Kumar Allampally, N.; Fernández, G.; Schacher, F. H. Controlling Aqueous Self-Assembly Mechanisms by Hydrophobic Interactions. *Chem. - A Eur. J.* **2014**, *20* (43), 13871–13875.
- (24) Yamaoka, T.; Tamura, T.; Seto, Y.; Tada, T.; Kunugi, S.; Tirrell, D. a. Mechanism for the Phase Transition of a Genetically Engineered Elastin Model Peptide (VPGIG)<sub>40</sub> in Aqueous Solution. *Biomacromolecules* **2003**, *4* (6), 1680–1685.
- (25) Hocine, S.; Li, M.-H. Thermoresponsive Self-Assembled Polymer Colloids in Water. *Soft Matter* **2013**, *9* (25), 5839.
- (26) Fuller, J. M.; Raghupathi, K. R.; Ramireddy, R. R.; Subrahmanyam, A. V.; Yesilyurt, V.; Thayumanavan, S. Temperature-Sensitive Transitions below LCST in Amphiphilic Dendritic Assemblies: Host-Guest Implications. *J. Am. Chem. Soc.* **2013**, *135* (24), 8947–8954.
- (27) Raghupathi, K. R.; Sridhar, U.; Byrne, K.; Raghupathi, K.; Thayumanavan, S. Influence of Backbone Conformational Rigidity in Temperature-Sensitive Amphiphilic Supramolecular

- Assemblies. *J. Am. Chem. Soc.* **2015**, 150420131555003.
- (28) Mart, R. J.; Osborne, R. D.; Stevens, M. M.; Ulijn, R. V. Peptide-Based Stimuli-Responsive Biomaterials. *Soft Matter* **2006**, 2 (10), 822.
- (29) Ulijn, R. V.; Smith, A. M. Designing Peptide Based Nanomaterials. *Chem. Soc. Rev.* **2008**, 37 (4), 664–675.
- (30) Liu, C. W.; Su, M.; Li, X. L.; Xue, T.; Liu, N.; Yin, J.; Zhu, Y. Y.; Wu, Z. Q. Multi-Stimuli-Responsive Chiral Organogels Based on Peptide Derivatives. *Soft Matter* **2015**, 11 (28), 5727–5737.
- (31) Wang, H.; Yang, Z. Short-Peptide-Based Molecular Hydrogels: Novel Gelation Strategies and Applications for Tissue Engineering and Drug Delivery. *Nanoscale* **2012**, 4 (17), 5259–5267.
- (32) Gazit, E. Self-Assembled Peptide Nanostructures: The Design of Molecular Building Blocks and Their Technological Utilization. *Chem. Soc. Rev.* **2007**, 36 (8), 1263–1269.
- (33) Miravet, J. F.; Escuder, B.; Segarra-Maset, M. D.; Tena-Solsona, M.; Hamley, I. W.; Dehsorkhi, A.; Castelletto, V. Self-Assembly of a Peptide Amphiphile: Transition from Nanotape Fibrils to Micelles. *Soft Matter* **2013**, 9 (13), 3558.
- (34) Hatip Koc, M.; Cinar Ciftci, G.; Baday, S.; Castelletto, V.; Hamley, I. W.; Guler, M. O. Hierarchical Self-Assembly of Histidine-Functionalized Peptide Amphiphiles into Supramolecular Chiral Nanostructures. *Langmuir* **2017**, 33 (32), 7947–7956.
- (35) Colombo, G.; Soto, P.; Gazit, E. Peptide Self-Assembly at the Nanoscale: A Challenging Target for Computational and Experimental Biotechnology. *Trends Biotechnol.* **2007**, 25 (5), 211–218.
- (36) Krishna, O. D.; Kiick, K. L. Protein- and Peptide-Modified Synthetic Polymeric

- Biomaterials. *Biopolymers* **2010**, *94* (1), 32–48.
- (37) Wong, S.; Shim, M. S.; Kwon, Y. J. Synthetically Designed Peptide-Based Biomaterials with Stimuli-Responsive and Membrane-Active Properties for Biomedical Applications. *J. Mater. Chem. B* **2014**, *2* (6), 595.
- (38) Jonker, A. M.; Löwik, D. W. P. M.; Van Hest, J. C. M. Peptide- and Protein-Based Hydrogels. *Chem. Mater.* **2012**, *24* (5), 759–773.
- (39) Marine, J. E.; Song, S.; Liang, X.; Watson, M. D.; Rudick, J. G. Bundle-Forming  $\alpha$ -Helical Peptide–dendron Hybrid. *Chem. Commun.* **2015**, *51* (76), 14314–14317.
- (40) Rajagopal, K.; Lamm, M. S.; Haines-Butterick, L. a.; Pochan, D. J.; Schneider, J. P. Tuning the PH Responsiveness of  $\beta$ -Hairpin Peptide Folding, Self-Assembly, and Hydrogel Material Formation. *Biomacromolecules* **2009**, *10* (9), 2619–2625.
- (41) Valéry, C.; Artzner, F.; Paternostre, M. Peptide Nanotubes: Molecular Organisations, Self-Assembly Mechanisms and Applications. *Soft Matter* **2011**, *7* (20), 9583–9594.
- (42) Fu, I. W.; Markegard, C. B.; Nguyen, H. D. Solvent Effects on Kinetic Mechanisms of Self-Assembly by Peptide Amphiphiles via Molecular Dynamics Simulations. **2014**.
- (43) Ozkan, A. D.; Tekinay, A. B.; Guler, M. O.; Tekin, E. D. Effects of Temperature, PH and Counterions on the Stability of Peptide Amphiphile Nanofiber Structures. *RSC Adv.* **2016**, *6* (106), 104201–104214.
- (44) Lee, H.; Jeong, J. H.; Park, T. G. PEG Grafted Polylysine with Fusogenic Peptide for Gene Delivery: High Transfection Efficiency with Low Cytotoxicity. *J. Control. Release* **2002**, *79* (1–3), 283–291.
- (45) Meijer, J. T.; Henckens, M. J. A. G.; Minten, I. J.; Löwik, D. W. P. M.; Van Hest, J. C. M. Disassembling Peptide-Based Fibres by Switching the Hydrophobic-Hydrophilic Balance.

- Soft Matter* **2007**, 3 (9), 1135–1137.
- (46) Jeong, Y.; Joo, M. K.; Bahk, K. H.; Choi, Y. Y.; Kim, H. T.; Kim, W. K.; Jeong Lee, H.; Sohn, Y. S.; Jeong, B. Enzymatically Degradable Temperature-Sensitive Polypeptide as a New in-Situ Gelling Biomaterial. *J. Control. Release* **2009**, 137 (1), 25–30.
- (47) Christensen, T.; Hassouneh, W.; Trabbic-Carlson, K.; Chilkoti, A. Predicting Transition Temperatures of Elastin-like Polypeptide Fusion Proteins. *Biomacromolecules* **2013**, 14 (5), 1514–1519.
- (48) Hassouneh, W.; Fischer, K.; MacEwan, S. R.; Branscheid, R.; Fu, C. L.; Liu, R.; Schmidt, M.; Chilkoti, A. Unexpected Multivalent Display of Proteins by Temperature Triggered Self-Assembly of Elastin-like Polypeptide Block Copolymers. *Biomacromolecules* **2012**, 13 (5), 1598–1605.
- (49) Smits, F. C. M.; Buddingh, B. C.; Van Eldijk, M. B.; Van Hest, J. C. M. Elastin-like Polypeptide Based Nanoparticles: Design Rationale toward Nanomedicine. *Macromol. Biosci.* **2015**, 15 (1), 36–51.
- (50) Aluri, S.; Pastuszka, M. K.; Moses, A. S.; MacKay, J. A. Elastin-like Peptide Amphiphiles Form Nanofibers with Tunable Length. *Biomacromolecules* **2012**, 13 (9), 2645–2654.
- (51) Ribeiro, A.; Arias, F. J.; Reguera, J.; Alonso, M.; Rodríguez-Cabello, J. C. Influence of the Amino-Acid Sequence on the Inverse Temperature Transition of Elastin-like Polymers. *Biophys. J.* **2009**, 97 (1), 312–320.
- (52) Cho, Y.; Zhang, Y.; Christensen, T.; Sagle, L. B.; Chilkoti, A.; Cremer, P. S. Effects of Hofmeister Anions on the Phase Transition Temperature of Elastin-like Polypeptides. *J. Phys. Chem. B* **2008**, 112 (44), 13765–13771.
- (53) Wang, W.; Tetley, L.; Uchegbu, I. F. The Level of Hydrophobic Substitution and the

- Molecular Weight of Amphiphilic Poly-L-Lysine-Based Polymers Strongly Affects Their Assembly into Polymeric Bilayer Vesicles. *J. Colloid Interface Sci.* **2001**, *237* (2), 200–207.
- (54) Harada, A.; Cammas, S.; Kataoka, K. Stabilized R-Helix Structure of Poly ( L -Lysine ) - Block-Poly ( Ethylene Glycol ) in Aqueous Medium through Supramolecular Assembly. *Macromolecules* **1996**, *29* (96), 6183–6188.
- (55) FDA Board Decision Federal Alert- New Regulations. **1979**, *11*, 21730.
- (56) Bowerman, C. J.; Ryan, D. M.; Nissan, D. A.; Nilsson, B. L. The Effect of Increasing Hydrophobicity on the Self-Assembly of Amphipathic  $\beta$ -Sheet Peptides. *Mol. Biosyst.* **2009**, *5* (9), 1058–1069.
- (57) Mu, Y.; Yu, M. Effects of Hydrophobic Interaction Strength on the Self-Assembled Structures of Model Peptides. *Soft Matter* **2014**, *10* (27), 4956–4965.
- (58) Papadopoulos, P.; Floudas, G.; Klok, H.; Schnell, I.; Pakula, T. Self-Assembly and Dynamics of Poly(Gamma-Benzyl-L-Glutamate) Peptides. *Biomacromolecules* **2004**, *5* (1), 81–91.
- (59) Hamley, I. W. Self-Assembly of Amphiphilic Peptides. *Soft Matter* **2011**, *7* (9), 4122–4138.
- (60) Smith, A. M.; Williams, R. J.; Tang, C.; Coppo, P.; Collins, R. F.; Turner, M. L.; Saiani, A.; Ulijn, R. V. Fmoc-Diphenylalanine Self Assembles to a Hydrogel via a Novel Architecture Based on  $\pi$ - $\pi$  Interlocked  $\beta$ -Sheets. *Adv. Mater.* **2008**, *20* (1), 37–41.
- (61) Castelletto, V.; Moulton, C. M.; Cheng, G.; Hamley, I. W.; Hicks, M. R.; Rodger, A.; López-Pérez, D. E.; Revilla-López, G.; Alemán, C. Self-Assembly of Fmoc-Tetrapeptides Based on the RGDS Cell Adhesion Motif. *Soft Matter* **2011**, *7* (24), 11405–11415.
- (62) Hughes, M.; Frederix, P. W. J. M.; Raeburn, J.; Birchall, L. S.; Sadownik, J.; Coomer, F.

- C.; Lin, I. H.; Cussen, E. J.; Hunt, N. T.; Tuttle, T.; et al. Sequence/Structure Relationships in Aromatic Dipeptide Hydrogels Formed under Thermodynamic Control by Enzyme-Assisted Self-Assembly. *Soft Matter* **2012**, *8* (20), 5595–5602.
- (63) Fleming, S.; Ulijn, R. V. Design of Nanostructures Based on Aromatic Peptide Amphiphiles. *Chem. Soc. Rev.* **2014**, *43* (23), 8150–8177.
- (64) Chronopoulou, L.; Sennato, S.; Bordi, F.; Giannella, D.; Di Nitto, A.; Barbetta, A.; Dentini, M.; Togna, A. R.; Togna, G. I.; Moschini, S.; et al. Designing Unconventional Fmoc-Peptide-Based Biomaterials: Structure and Related Properties. *Soft Matter* **2014**, *10* (12), 1944–1952.
- (65) Javid, N.; Roy, S.; Zelzer, M.; Yang, Z.; Sefcik, J.; Ulijn, R. V. Cooperative Self-Assembly of Peptide Gelators and Proteins. *Biomacromolecules* **2013**, *14* (12), 4368–4376.
- (66) Huang, C. Y.; Klemke, J. W.; Getahun, Z.; DeGrado, W. F.; Gai, F. Temperature-Dependent Helix-Coil Transition of an Alanine Based Peptide. *J. Am. Chem. Soc.* **2001**, *123* (38), 9235–9238.
- (67) Cheng, G.; Castelletto, V.; Moulton, C. M.; Newby, G. E.; Hamley, I. W. Hydrogelation and Self-Assembly of Fmoc-Tripeptides: Unexpected Influence of Sequence on Self-Assembled Fibril Structure, and Hydrogel Modulus and Anisotropy. *Langmuir* **2010**, *26* (7), 4990–4998.
- (68) Trent, A.; Marullo, R.; Lin, B.; Black, M.; Tirrell, M. Structural Properties of Soluble Peptide Amphiphile Micelles. *Soft Matter* **2011**, *7* (20), 9572–9582.
- (69) Yoshidome, T.; Kinoshita, M. Hydrophobicity at Low Temperatures and Cold Denaturation of a Protein. *Phys. Rev. E - Stat. Nonlinear, Soft Matter Phys.* **2009**, *79* (3), 1–4.
- (70) Dias, C. L.; Ala-Nissila, T.; Wong-ekkabut, J.; Vattulainen, I.; Grant, M.; Karttunen, M.



- The Hydrophobic Effect and Its Role in Cold Denaturation. *Cryobiology* **2010**, *60* (1), 91–99.
- (71) Li, J.; Du, X.; Hashim, S.; Shy, A.; Xu, B. Aromatic-Aromatic Interactions Enable  $\alpha$ -Helix to  $\beta$ -Sheet Transition of Peptides to Form Supramolecular Hydrogels. *J. Am. Chem. Soc.* **2017**, *139* (1), 71–74.
- (72) Hughes, M.; Birchall, L. S.; Zuberi, K.; Aitken, L. A.; Debnath, S.; Javid, N.; Ulijn, R. V. Differential Supramolecular Organisation of Fmoc-Dipeptides with Hydrophilic Terminal Amino Acid Residues by Biocatalytic Self-Assembly. *Soft Matter* **2012**, *8* (45), 11565–11574.
- (73) Munkhbat, O.; Garzoni, M.; Raghupathi, K. R.; Pavan, G. M.; Thayumanavan, S. Role of Aromatic Interactions in Temperature-Sensitive Amphiphilic Supramolecular Assemblies. *Langmuir* **2016**, *32* (12), 2874–2881.
- (74) Chen, S. W.; Drakulic, S.; Deas, E.; Ouberai, M.; Aprile, F. A.; Arranz, R.; Ness, S.; Roodveldt, C.; Guilliams, T.; De-Genst, E. J.; et al. Structural Characterization of Toxic Oligomers That Are Kinetically Trapped during  $\alpha$ -Synuclein Fibril Formation. *Proc. Natl. Acad. Sci.* **2015**, *112* (16), E1994–E2003.
- (75) Yan, Y.; Huang, J.; Tang, B. Z. Kinetic Trapping – a Strategy for Directing the Self-Assembly of Unique Functional Nanostructures. *Chem. Commun.* **2016**, *52* (80), 11870–11884.
- (76) Mattia, E.; Otto, S. Supramolecular Systems Chemistry. *Nat. Nanotechnol.* **2015**, *10* (2), 111–119.
- (77) Jiwanich, S.; Ryu, J. H.; Bickerton, S.; Thayumanavan, S. Noncovalent Encapsulation Stabilities in Supramolecular Nanoassemblies. *J. Am. Chem. Soc.* **2010**, *132* (31), 10683–

10685.

## 2.6 NMR Spectrum of molecules

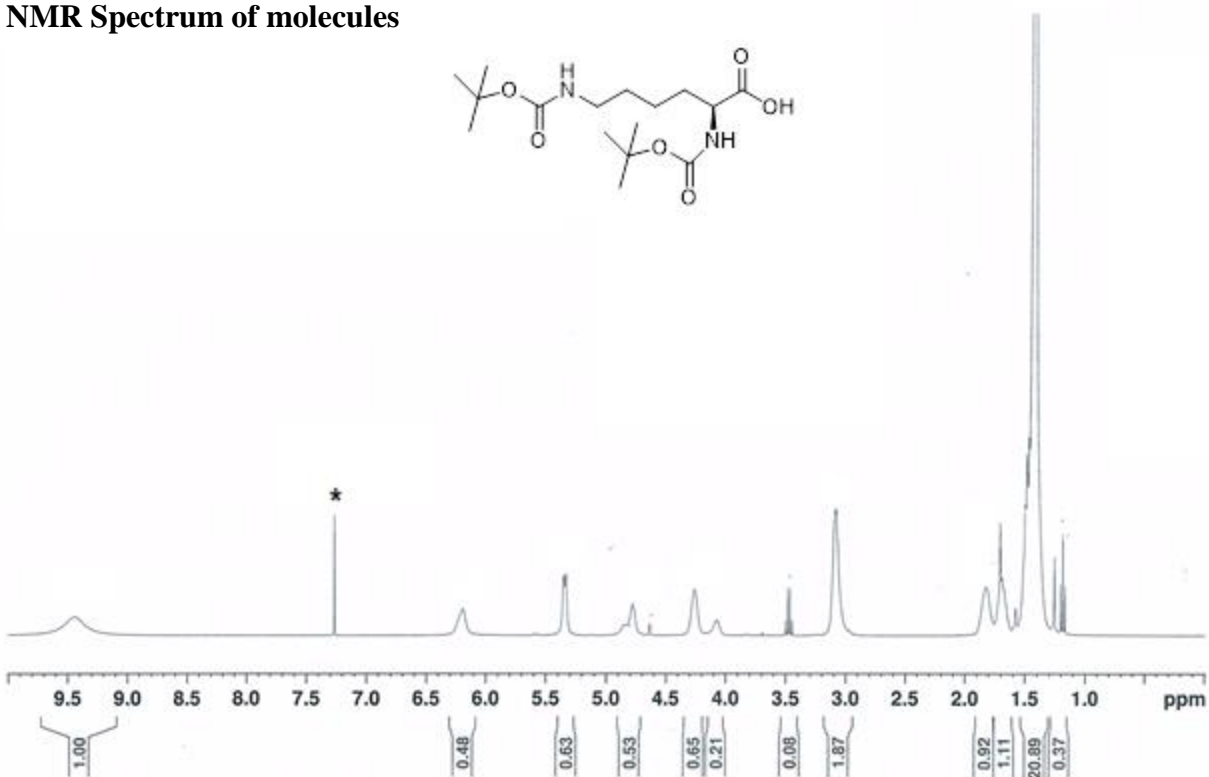


Figure 2.8: <sup>1</sup>H NMR spectrum of starting material (top) and molecule 2 (bottom)

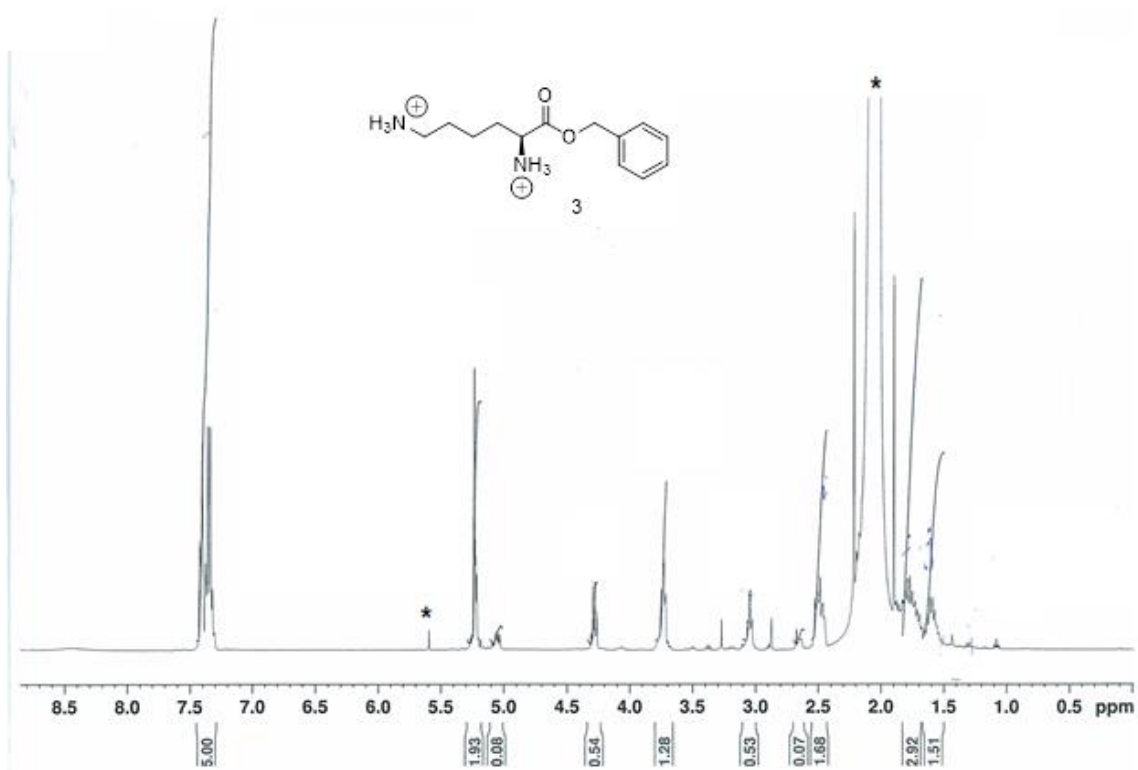
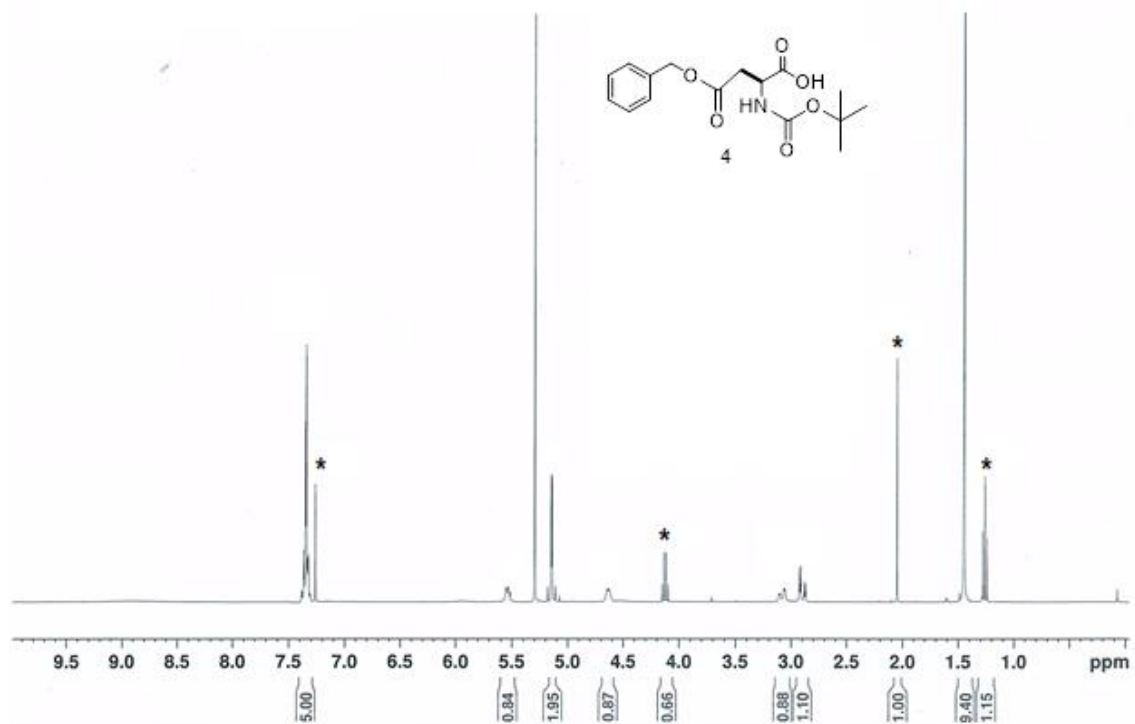


Figure 2.9: <sup>1</sup>H NMR spectrum of molecule 3 (top) and molecule 4 (bottom)



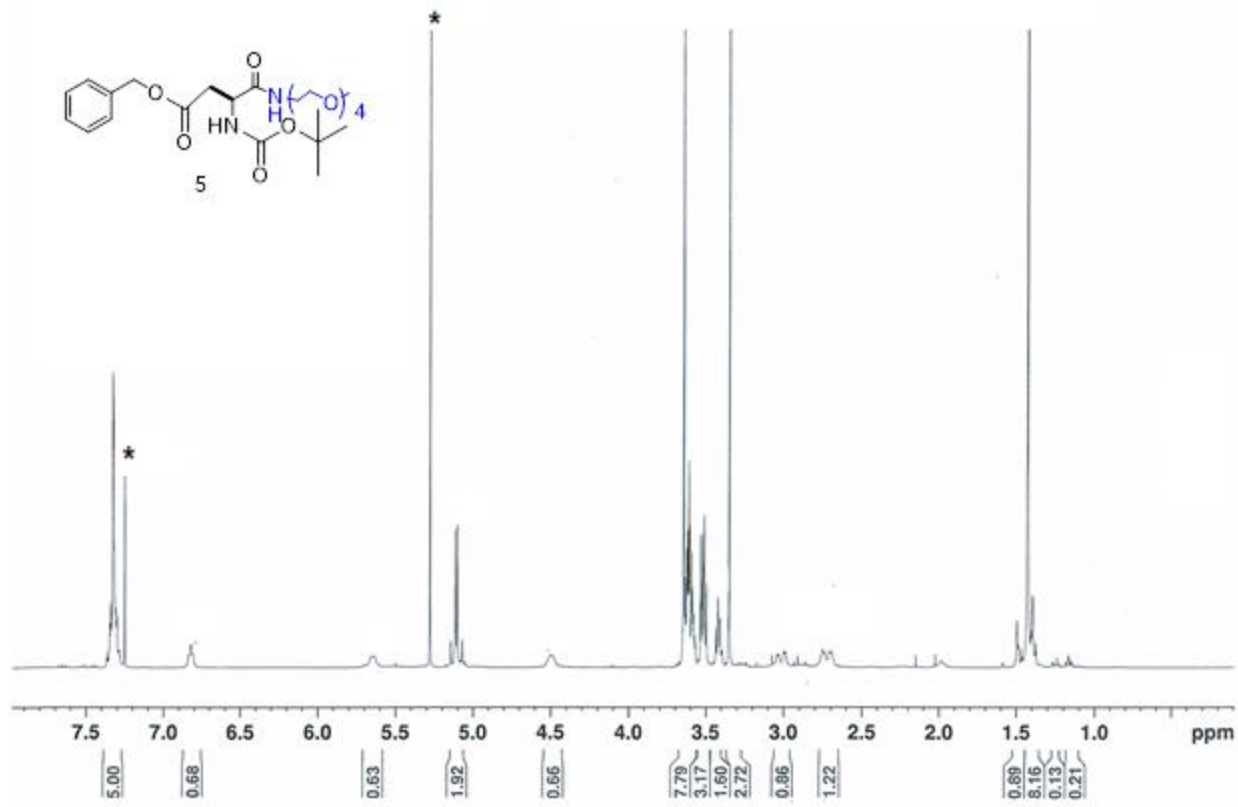
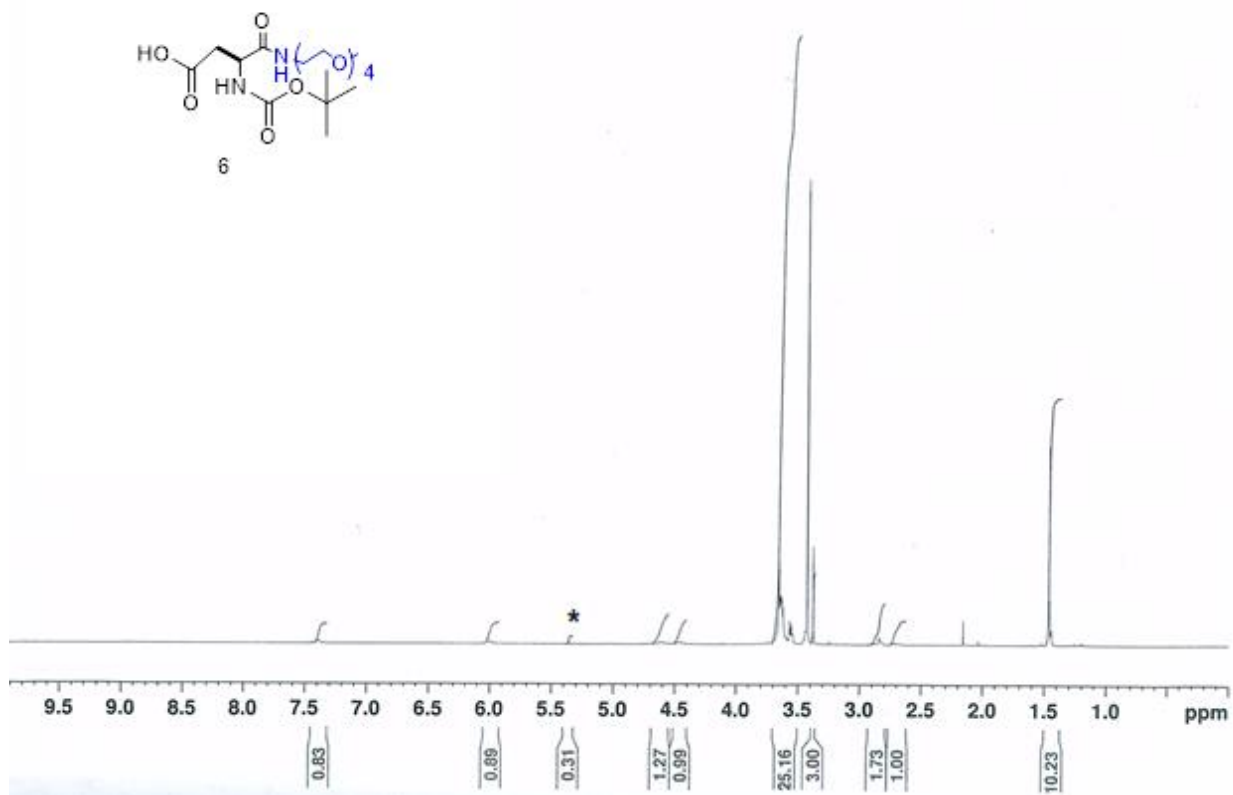


Figure 2.10 :  $^1\text{H}$  NMR spectrum of molecule 5 (top) and molecule 6 (bottom)



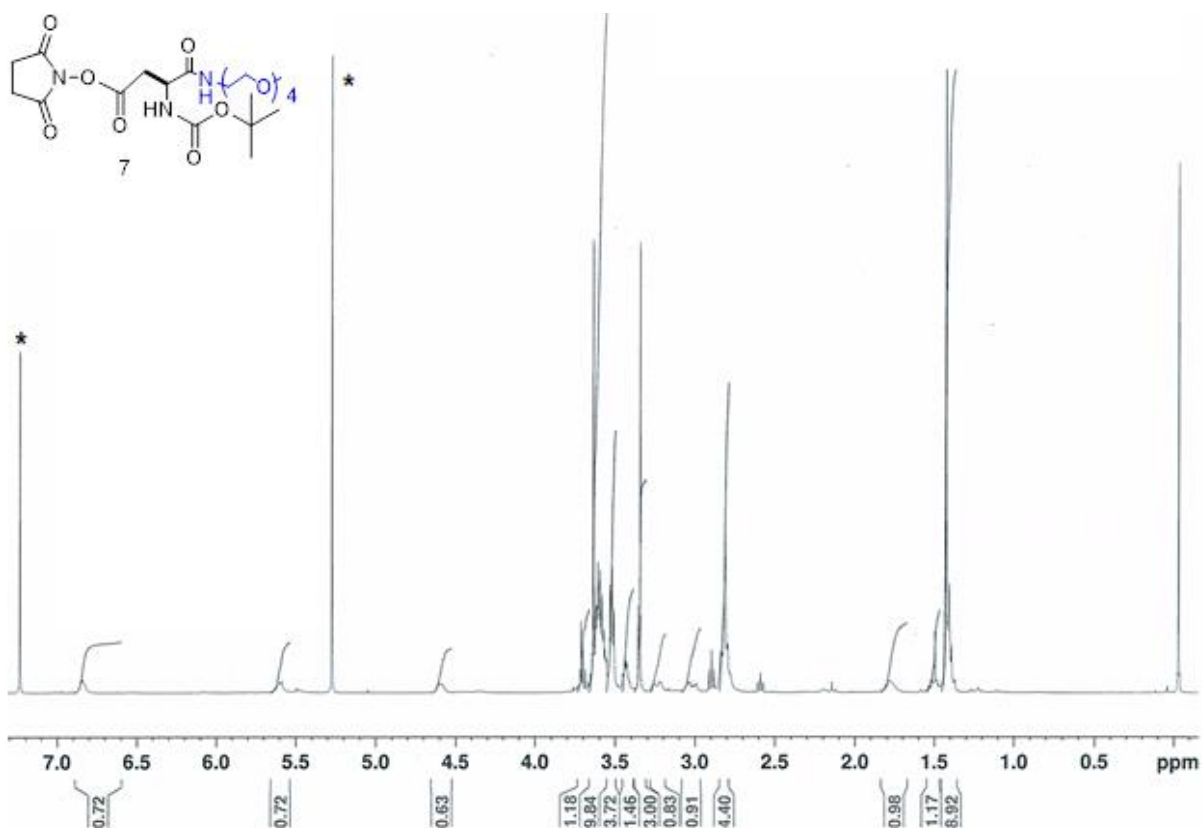
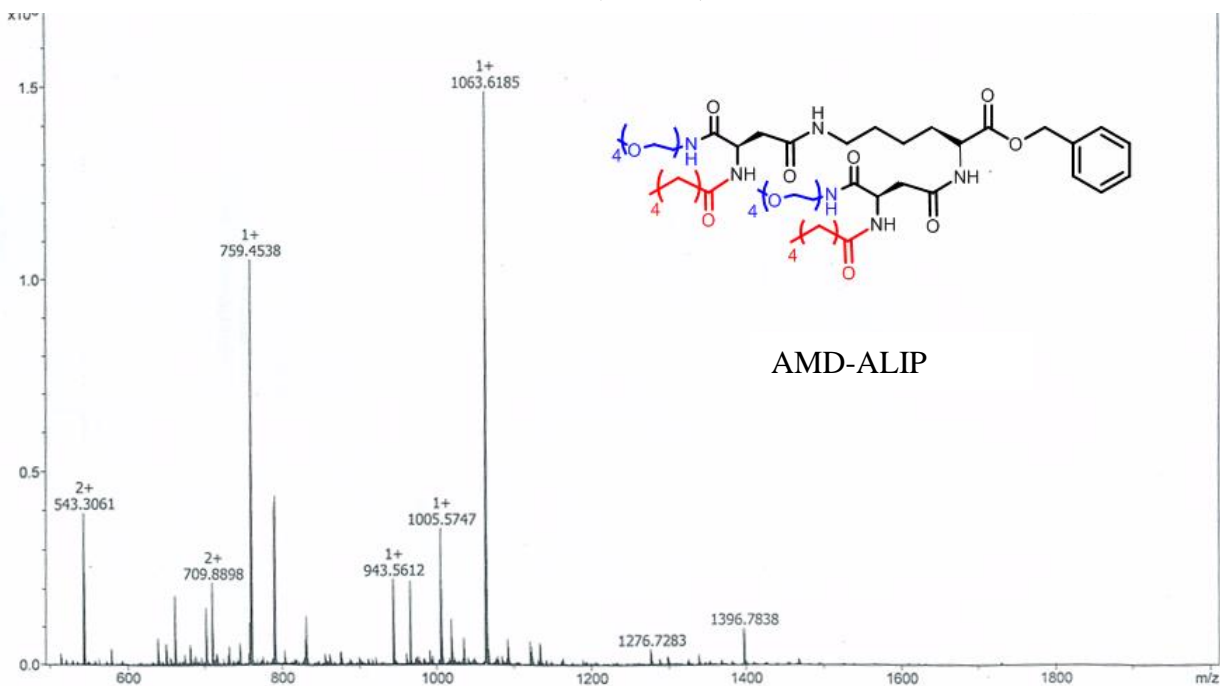
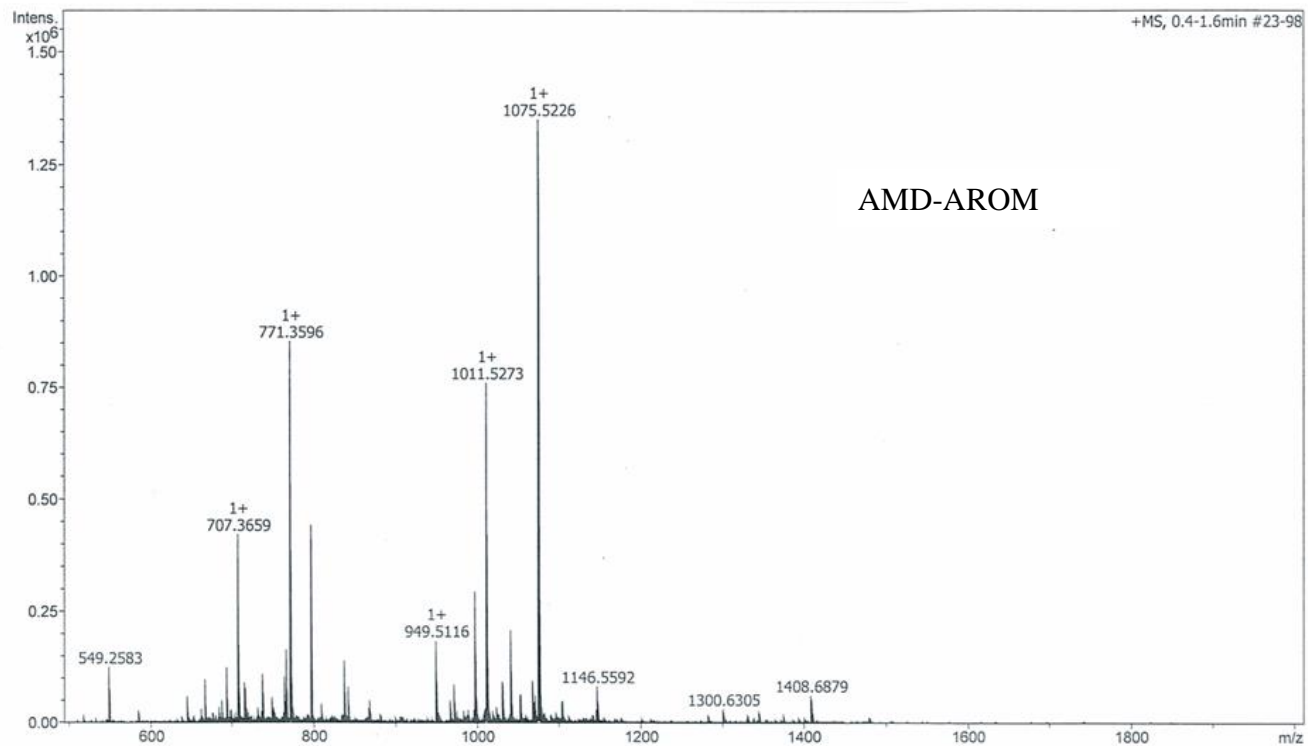


Figure 2.11 :  $^1\text{H}$  NMR spectrum of molecule 7 (top) and ESI-MS of molecule AMD-ALIP (bottom)





**Figure 2.12 : ESI-MS of molecule AMD-AROM**

## CHAPTER 3

### ALGINATE HYDROGELS FOR THE STABLE ENCAPSULATION AND RELEASE OF ARTIFICIAL SWEETENERS IN BEVERAGES

#### 3.1 Background and significance

Aspartame (N-L-aspartyl-L-phenylalanine-1-methyl ester) is a low-calorie sweetener obtained from two naturally occurring amino acids: L-phenylalanine and L-aspartic acid and is used widely in beverages and dietary products<sup>1-2</sup>. It does not have a bitter or metallic aftertaste and is about 180 times sweeter than sugar<sup>3</sup>. Hence, the quantity of aspartame required to impart the same amount of sweetness is minuscule in spite of the fact that it has the same caloric value of 4 kcal (17 kJ) per gram as that of cane sugar<sup>4</sup>. This makes it attractive as a low-calorie sweetener.

However, the stability of aspartame in solution is affected by pH, temperature and buffer over time and decomposition follows pseudo-first order kinetics<sup>5,6</sup>. Aspartame is reported to be most stable between pH 4-5 with a substantial decrease in stability under more acidic and neutral conditions. Below pH 3, which is typical of beverage formulations, the amide bond cleaves to form the methyl ester of phenyl alanine and aspartic acid (Figure 3.1)<sup>7,8,9</sup>. Moreover, it cannot be used in products that require baking or frying since aspartame degrades at higher temperatures<sup>10</sup>. However, the structure of aspartame is imperative for its sweetness to be perceived and this follows from the AH-B- $\gamma$  model proposed by Kier in 1972<sup>11</sup>. To circumvent this, industries resort to the addition of excess aspartame in food products to compensate for its degradation. However, this is not safe since several health issues such as headaches, migraines and memory loss have been implicated with an excess use of aspartame and this calls for decreased aspartame consumption<sup>4,12,13,14</sup>.



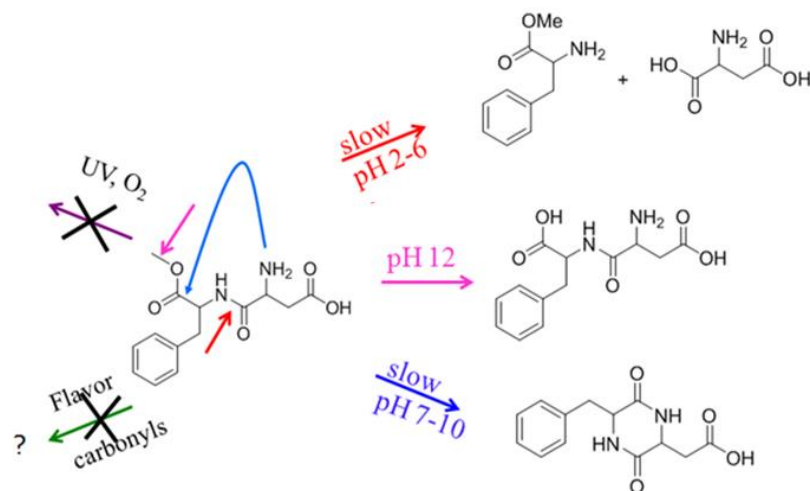


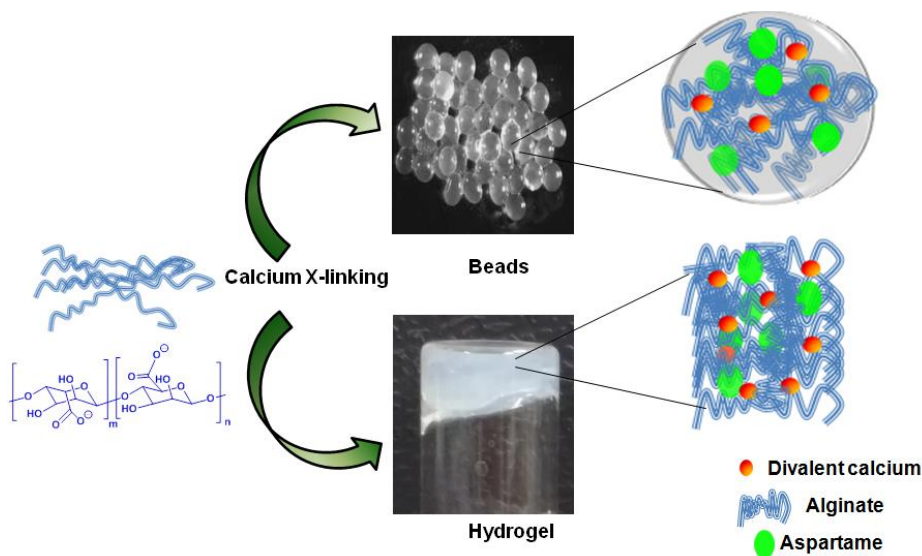
**Figure 3.1** Degradation pathways of aspartame at different pH

Encapsulation aims to preserve the stability of the active component during processing or storage conditions and serves as means to provide uniform taste, increased shelf-life, and protection from harsh conditions and in some cases, taste masking<sup>14</sup>. Schroeder et al. have shown that the stability of aspartame is enhanced in the presence of  $\beta$ -cyclodextrin ( $\beta$ -CD) to the formation of inclusion complexes between aspartame and  $\beta$ -CD<sup>15</sup>. However, the downfall with using cyclodextrins is that they can themselves be broken down into the body to yield glucose. The glucose released hence, has a caloric value which defeats the whole purpose of using a non-caloric sweetener such as aspartame. The microencapsulation of aspartame by double emulsion followed by complex coacervation was also found to enhance the stability of aspartame at 80 °C<sup>16</sup> however, the release profile could not be controlled. Therefore, there is a dire need for encapsulation systems that can release aspartame in a sustained manner so as to maintain a steady state concentration of aspartame in the beverage over time.

Biomolecules such as polysaccharides such as starch and its derivatives, plant extracts and marine extracts have been explored heavily in the recent past in the food industry and have been certified

as Generally Recognized as Safe (GRAS) materials<sup>17</sup>. Alginate is a naturally occurring anionic polysaccharide derived from brown seaweed. It contains blocks of (1-4) linked  $\beta$ -D-mannuronic acid (M) and  $\alpha$ -L-guluronic acid (L) monomers. The polymer is composed of three different forms of polymer segments: consecutive G, consecutive M and alternating G and M residues<sup>18</sup>. It is used extensively in tissue repair and regeneration due to its biocompatibility, biodegradability and non-antigenicity<sup>19</sup>. Owing to its anionic nature, it has a propensity to interact with cross-linking agents such as divalent metal ions like  $\text{Ca}^{2+}$  and also with cationic polyelectrolytes. The pH responsive behavior accounts for the high swelling ratios due to chain expansion from the presence of ionic carboxylate groups on the backbone and had been widely used in the form of alginate hydrogels and microspheres<sup>18, 20, 21, 22</sup>.

In this study, we aim to establish the critical differences between the release profiles of aspartame from microgels and bulk hydrogels of aspartame encapsulated calcium crosslinked alginate gels. We will, in particular, study the different parameters that dictate the gel architecture and hence, the morphology and the structure of the gels. We anticipate that the surface area characteristics



**Scheme 3.1** Schematic for alginate and calcium cross-linked microgel beads and hydrogels for aspartame encapsulation and release

arising out of the differences in the gel architecture will manifest in disparate release kinetics and mechanisms of release<sup>23,24</sup> between the microgels and bulk hydrogels (Scheme 3.1).

### 3.2 Materials and methods

All chemicals and reagents were purchased from commercial sources and were used as received, unless mentioned otherwise. Low viscosity sodium alginate (ALG) (CAS Number: 9005-38-3; Brookfield viscosity 4–12 cps (1% in H<sub>2</sub>O at 25 °C)) was purchased from Sigma-Aldrich (U.S.A.). Alginate solutions were prepared by adding 10mg of sodium alginate into HPLC grade water followed by sonication and then left to stir overnight until all the alginate dissolved. Aspartame stock solutions were prepared by dissolving a pre-determined amount of aspartame in HPLC water acidified with 1N HCl and then diluted to obtain the desired concentrations. Calcium chloride stock solutions were prepared by dissolving a measured amount of calcium chloride in HPLC grade water.

- **Fabrication of microgel beads:** For the preparation of microgel beads, alginate and aspartame solutions were mixed together in a 7 mL scintillation vial to afford various compositions of alginate and aspartame. This solution was then drawn into a syringe with different needle pore sizes (0.45 mm, 0.7 mm and 1 mm) and added into a bath of calcium chloride dropwise. The beads were then separated, freeze dried and stored at 5 °C. The amount of alginate, mode of addition, cross-linking time and concentration of cross-linker were varied to obtain microgel beads through I to V (Table 3.1).
- **Fabrication of bulk hydrogels:** For the preparation of bulk hydrogels, alginate and aspartame solutions were first mixed together in a 7 mL scintillation vial to afford various compositions of alginate and aspartame such that the total volume of the combined solution was 2 mL. To this solution, a predetermined amount of calcium chloride was added to afford a range of cross linking densities. The resultant solution was vortexed briefly to ensure mixing of the contents

and left to sit for 5-10 minutes upon which visible gelation was observed. The hydrogels so obtained were freeze dried and stored at 5 °C (Table 3.2)

- **Size determination of microgel beads:** The shape of the microgel beads was determined using an optical microscope, OM BX51. In a typical experiment the freeze dried microgel beads were subjected to imaging and the dimensions of one microgel bead was recorded. This was repeated for 10 other beads and the dimensions of the beads are reported using Image J software as the mean of 10 measurements.
- **Determination of encapsulation/loading efficiency for microgel beads and hydrogels:** For measuring the encapsulation efficiency of the beads, the absorbance of aspartame in the supernatant after isolating the beads was measured using a UV-Vis spectrometer ( $A_s$ ). This was then subtracted from the initial amount of aspartame  $A_{total}$  added to determine the amount of aspartame loaded ( $A_{load}$ ) in the beads to facilitate the calculation of loading in terms of weight % according the equation:

$$EE(bead) = \frac{A_{load} * 100}{A_{tot}}$$

Where  $A_{load} = A_{total} -$

$A_s$  where  $A_s$  is the concentration of aspartame in the supernatant.

The bulk hydrogels, on the other hand, encapsulated all the aspartame that was initially added.

Therefore, this too was converted to weight % loading according to the equation:

$$Loading\ efficiency(hydrogel)\ \% = \left( \frac{Amount\ of\ aspartame\ in\ microgel\ beads\ or\ bulk\ hydrogels}{Total\ amount\ of\ microgel\ beads\ or\ hydrogel} \right) *$$

100

- **Scanning electron microscopy analysis of hydrogels:** For Scanning electron microscopy (SEM) analysis, the freeze-dried hydrogels were sputtered with gold using Sputter coater CRX108 so as to afford a 5 nm layer for 10 minutes and then, imaged using FE-SEM Magellan 400.
- **Size exclusion chromatography (SEC) experiments:** SEC experiments were carried out on an Agilent Infinity 1260 with 100 mM pH 7 phosphate buffer as the mobile phase with a flow rate of 1mL/min with a 20  $\mu$ L injection loop equipped with a UV-Vis and RI detector. Bio SEC-5 column from Agilent Technologies with a molecular weight cut off of 100 Da was used as the stationary phase. The calibration curve was established for aspartame solutions in triplicate.
- **Statistical Analysis:** All experiments were carried out in triplicate using freshly prepared samples. The mean and standard deviations were calculated from these values and all measurements are reported as mean  $\pm$  SD.
- **Release experiments:** The effect of morphology on the loading and release kinetics of aspartame was studied in alginate-based microbeads and hydrogels. Size Exclusion Chromatography (SEC) was used to monitor the amount of aspartame released at 25  $^{\circ}$ C. Aspartame loaded microbead/hydrogel was placed in a 7 mL vial such that the total concentration of aspartame in a 7 mL solution was 5 mg. The vial was then gently filled with 6 mL of phosphate-citrate buffer at pH 2.3 and 4.3 and incubated in a ThermoScientific Precision incubator at 25  $^{\circ}$ C for 6 weeks.

The amount of aspartame released into the buffer at a given time was determined by measuring the absorbance intensity of aspartame in the aqueous solution surrounding the microbeads or hydrogel. A calibration curve prepared by measuring the intensities of known concentrations was

used to determine the concentration of released aspartame. The results reported here are normalized and converted to percent cumulative release.

### 3.3 Results and discussion

#### 3.3.1 Microgel beads: Influence of alginate composition, mode of addition, cross-linking time and concentration of cross-linker

The microgel beads I to V prepared (Table 3.1) were subjected to optical microscopy analysis to ascertain the effect of alginate, mode of addition, cross-linking time and concentration of cross-

	Aspartame (mmol)	Alginate (mmol)	Mode of addition	X-linking time	Amount of calcium chloride (mmoles)
I	0.034	0.050	1.2 mm syringe	30 min	2000
II	0.034	0.050	1.2 mm syringe	5 hours	2000
III	0.034	0.050	Pipette tip	30 min	2000
IV	0.034	0.050	1.2 mm syringe	30 min	500
V	0.034	0.151	1.2 mm syringe	30 min	2000

**Table 3.1** Fabrication of calcium cross linked alginate microgel beads I to V

linker on the size of the beads. The sizes of the beads were found to be in the range of 1.5 to 2mm depending on the fabrication conditions.

Increase in cross-linking time and increasing the concentration of alginate (II and V respectively) both had a negligible effect on the sizes of the beads when compared to I(control). However, the concentration of the cross-linker and the mode of addition i.e. the diameter of nozzle were both found to affect the bead size. In particular, the microgel beads with the lowest concentration of the cross linker had the largest sizes~2mm. This follows from the fact that the beads having a lower amount of cross linking would be loosely held as compared to the ones with a higher extent of cross linking and hence, the sizes observed. It is also understandable that the diameter of the nozzle



would dictate the sizes of the droplet formed and therefore, larger nozzles resulted in bigger beads (Figure 3.2).

We then, compared the aspartame loading efficiencies for microbeads I to V. While increasing the alginate composition had no effect on the aspartame encapsulation efficiency when compared to I, increasing the cross linking time and the size of the nozzle during addition into the cross linking solution resulted in substantial decrease in loading. A larger nozzle afforded beads with bigger sizes yet with a lower cross-linking density as compared to I since the volume change is significant (Figure 3.2). The ineffective cross linking network formed in this case paves way for aspartame molecules have a less tortuous path for diffusion during the time frame of the cross linking process explaining the decrease in loading efficiency<sup>25</sup>.

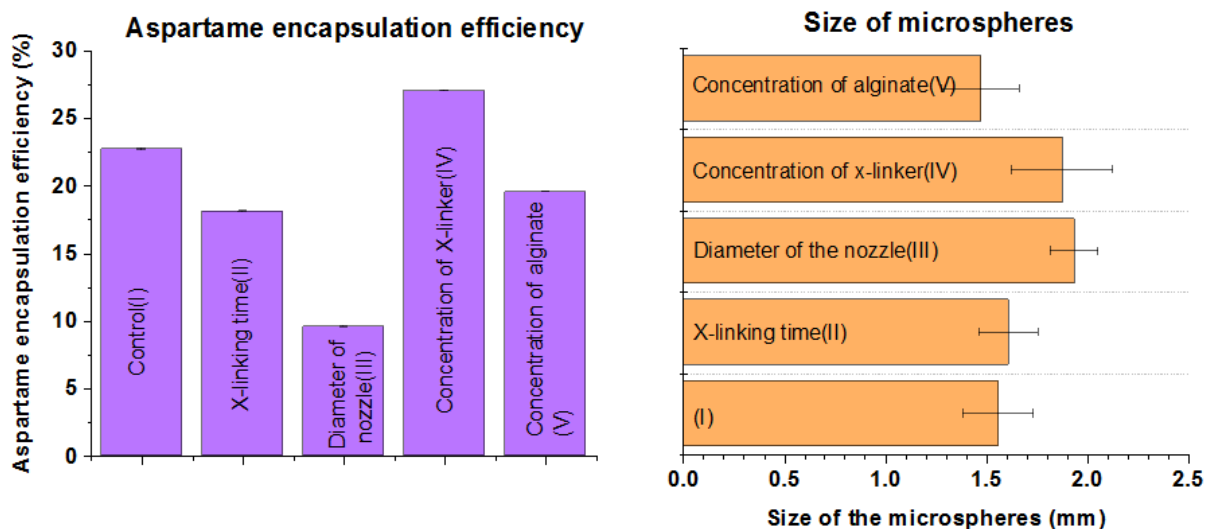


**Figure 3.2:** Loading efficiency and sizes of beads I to V as a function of alginate composition, mode of addition, cross-linking time and concentration of cross-linker

Increasing the cross-linking time results in a similar process where the loosely held aspartame molecules diffuse into the aqueous milieu leading to a drastic decrease in the encapsulation of

aspartame. However, decreasing the concentration of cross-linker resulted in an increase in aspartame loading. This can be attributed to the increase in the free volume inside the microgel beads owing to a lower degree of cross linking, facilitating the residence of more aspartame molecules<sup>23</sup>.

### 3.3.2 Bulk Hydrogels: Influence of alginate composition, mode of addition, cross-linking time and concentration of cross-linker

The hydrogels were found to have an aspartame loading of 100% by weight irrespective of the fabrication conditions (Figure 3.3) and the loading content was calculated to be between 30-60 wt%.

	Aspartame (mmoles)	Alginate (mmoles)	Amount of X-linker (mmoles)	Loading content (%)
B	0.136	0.050	100	60
C	0.084	0.050	100	36
D	0.034	0.050	100	30
F	0.084	0.050	250	48
H	0.084	0.050	5	52

**Table 3.2** Fabrication of calcium cross linked alginate hydrogels

They were, then, subjected to Scanning electron microscopy (SEM) analysis to ascertain the effect of alginate, mode of addition, cross-linking time and concentration of cross-linker on their morphology.

We first subjected alginate alone to SEM analysis and observed that alginate without any cross-linking was a porous polymer with a loose network structure with very large pore structures and hollow cavities. Gel F, on the other hand, had a denser yet non-homogeneous structure with organized and disorganized domains arising out of the high degree of cross linking (Figure 3.4).

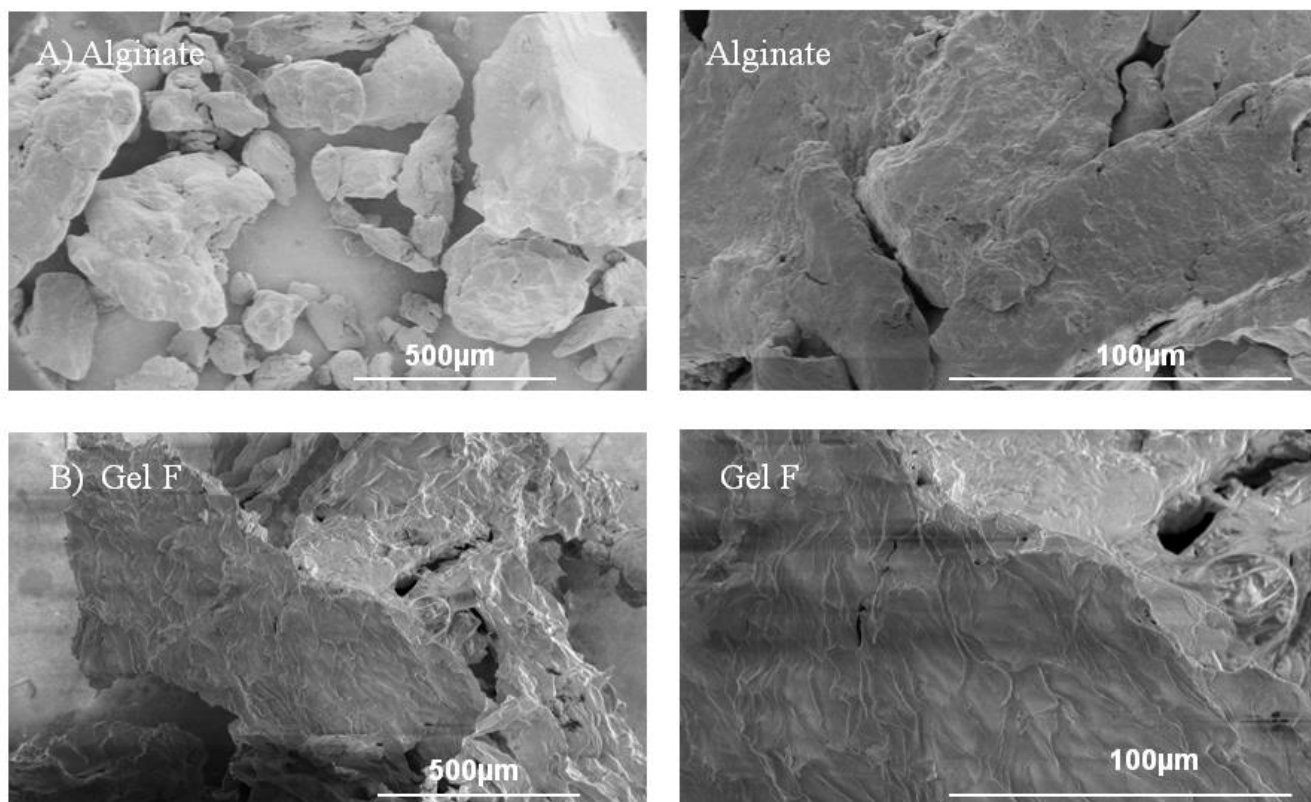


**Figure 3.3 :** SEM images of A) Alginate showing loose networks as compared to B) Gel F which exhibits ordered yet inhomogeneous networks

The gel is understood to be non-homogeneous owing to the kinetics of gelation with calcium chloride. The extent of cross linking and the morphology of the domains rely upon the diffusion of calcium ions to diffuse through the polymer matrix which is restricted upon cross linking of the outer layers resulting in dense layers on the outside and looser networks in the underlying layers of the bulk hydrogels<sup>26,27</sup>.

### 3.3.3 Resolution of aspartame and degradation products by size exclusion chromatography

To study the effect of morphology of the microgel and bulk hydrogels on the release kinetics of aspartame, we resorted to the technique size exclusion chromatography (SEC). However, it was

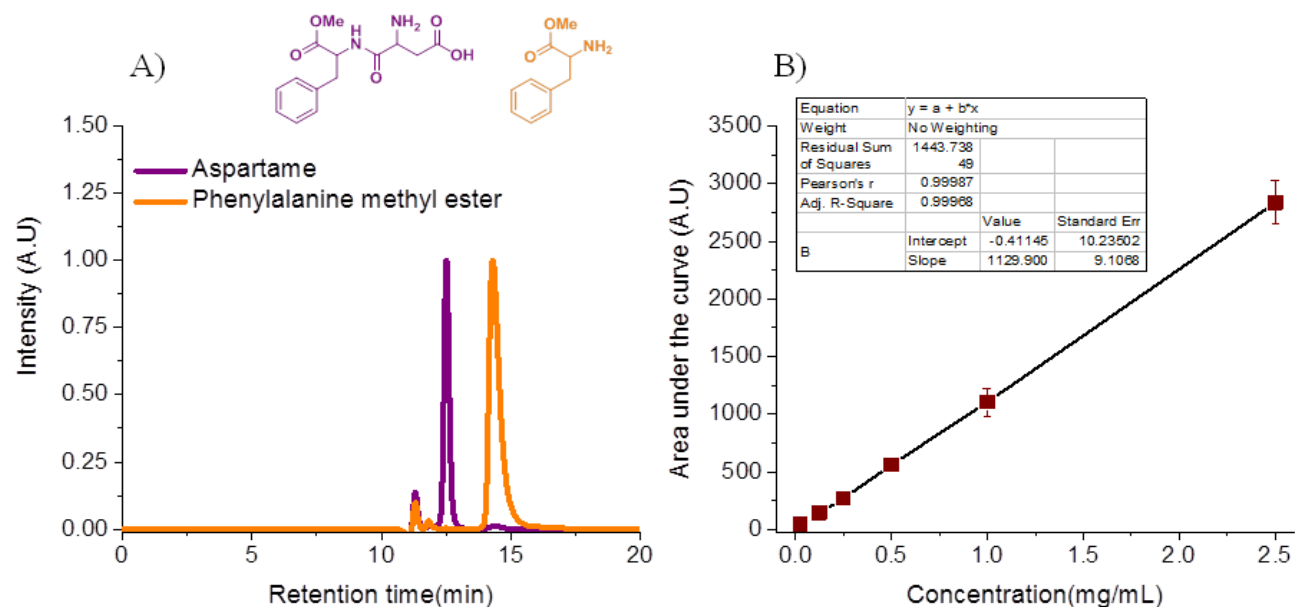


**Figure 3.4:** A) Resolution of aspartame and phenylalanine methyl ester using SEC B) Calibration curve for aspartame using SEC

necessary to establish this as a viable technique for the separation and quantification of aspartame from it by products, phenylalanine methyl ester and aspartic acid since SEC separates based on molecular weight and the molecular weight difference between aspartame and its degradation products is significantly small. Indeed, aspartame and phenylalanine methyl ester could be resolved by employing SEC (Figure 3.5). Further, a calibration curve for aspartame was established with a confidence value of 0.99. The limit of detection (LOD) and limit of quantification (LOQ) for this technique were calculated to be 0.035 mg/mL and 0.116 mg/mL respectively. The slope of the calibration curve was found to be 1129 with the intercept value as -0.41. The calibration curve so established has been used throughout to ascertain the extent of release or degradation of aspartame from either the microgel beads or the bulk hydrogels.

### 3.3.4 Release kinetics and release mechanism of microgel beads

The release of active agents from a hydrophilic matrix is understood to be brought about by wetting, penetration of solution into the matrix (swelling), polymer stress relaxation, diffusion through matrix, disintegration, dissolution, or erosion of matrix<sup>19,28</sup>. In that, the chemical composition, geometry, preparation technique and environmental conditions during release influence the modes of release<sup>20,29</sup>. To understand the parameters that affect the rate of release of aspartame from the microgel beads, the beads were incubated in a phosphate-citrate buffer and the amount of aspartame was assessed as a function of alginate composition, mode of addition, cross-linking time and concentration of cross-linker using the size exclusion chromatography method established in section 2.5.3 and is presented in Figure 6. The beads were also incubated at pH 4 as a control since aspartame is known to be the most stable at that pH and this could be used to understand the relative rates of aspartame degradation at pH 2 and 4.

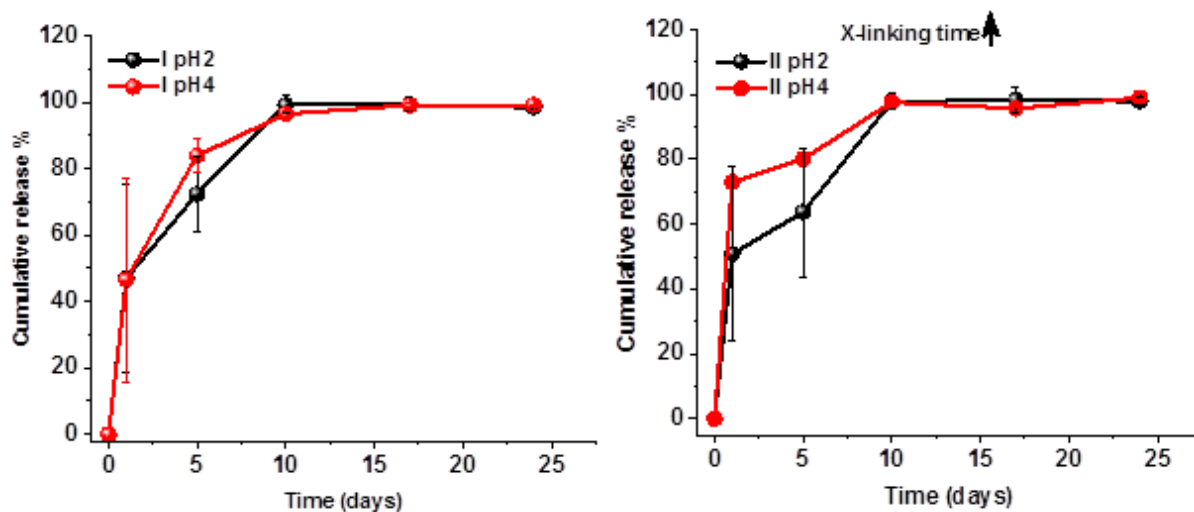


**Figure 3.5:** Release profiles of microgel beads I and II. Compared to control I, increase in cross-linking time results in a greatest burst release.

Regardless of the parameter that was varied, we observed that the microgel beads had a rapid initial release followed by a slower release very typical of a burst-release profile. Microgel beads with a greater time allowed for crosslinking i.e. II had a lower burst release at pH 2 compared to the control I, which had a comparable release at pH 2 and 4 (Figure 3.6). However, the burst release for II at pH 4 was found to be ~70% compared to ~50% in case on control I while the burst release at pH 2 for I and II were comparable. Therefore, it suffices to say that increase in cross-linking time does not reflect in the release profile at pH 2 while it affects the release profile at pH 4. This is understandable since the cross-links are active only at pH 4 and not at pH 2 owing to the loss of the negative charges on the carboxylate.

Increasing the concentration of alginate or decreasing the concentration of the cross-linker on the other hand, had no effect on the release rates at pH 2 and 4. This alludes to the presence of a threshold concentration of the cross-linker that is required to maintain the structural integrity of the microgel beads that translates into a difference in the kinetics of release. Upon increasing the size of the beads, we found that the burst release at pH 4 for III to decrease to 30% from 50% when compared to I (Figure 3.7). This follows from the fact that the beads owing to their bigger

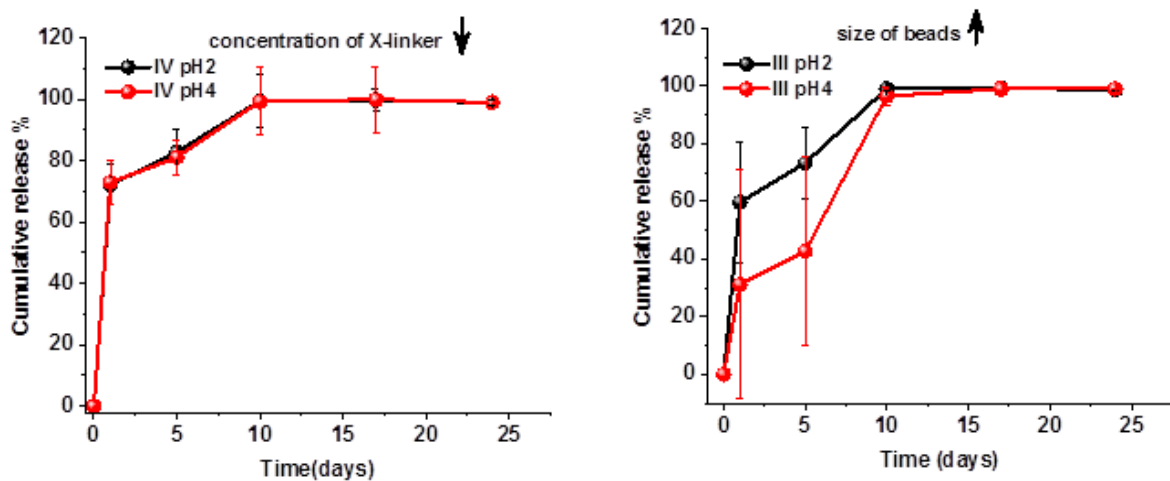


**Figure 3.6:** Release profiles for microgel beads IV and III. Increasing the size of the beads results in a higher burst release at pH 2 than at pH 4 while decreasing the concentration of the cross-linker has no effect on the release kinetics at pH 2 or 4.

size and the cross-links now provided a tortuous path for the encapsulated aspartame molecules resulting in a larger diffusivity path length accounting for the slower initial release rates<sup>30,31</sup>. However, at pH 2, the cross-linking density no longer plays a role and the release is dictated primarily by the diffusivity path length.

### **3.3.5 Mechanism of release of aspartame for microgel beads**

The burst release phenomenon observed in the microgel beads is understood to arise due to the loosely entrapped and surface-associated active agents. We then, wanted to elucidate the model and mechanism of aspartame release from the beads. This is exacerbated by the presence of solvent/polymer interactions, multidimensional diffusion resulting in changes in the free volume of the beads due to solvent transport i.e. polymer swelling/deswelling and multicomponent transport instead of single solute diffusion<sup>23,32</sup>. Therefore, we fitted the release of aspartame in 15mM phosphate-citrate buffer to several release models and obtained a correlation coefficient that was an accurate representation of the release model.

Through this exercise, we found that the microgel beads through I to V followed the Korsmeyer-Peppas model of release which is denoted by the equation:

$$\frac{M_t}{M_\infty} = kt(n), \text{ for } \frac{M_t}{M_\infty} < 0.6$$

Here,  $M_t$  is the cumulative amount of aspartame released at an arbitrary time  $t$ ,  $M_\infty$  is the cumulative amount of the substance released at an infinite time, and  $k$  is a constant incorporating structural and geometric characteristics of the device, and  $n$  is an exponent characterizing the

Model	I pH 2	I pH 4	II pH 2	II pH 4	III pH 2	III pH 4	IV pH 2	IV pH 4	V pH 2	V pH 4
Zero	0.627	0.586	0.644	0.463	0.569	0.765	0.462	0.466	0.427	0.446
First	0.643	0.561	0.710	0.738	0.694	0.726	0.685	0.700	0.660	0.743
Higuchi	0.697	0.652	0.644	0.463	0.569	0.841	0.503	0.500	0.465	0.479
Korsmeyer - Peppas	0.935	0.910	0.893	0.890	0.909	0.872	0.913	0.889	0.920	0.878

**Table 3.3:** Release models and corresponding correlation coefficients for the microgel beads. The release kinetics for the microgel beads I to V obey the Korsmeyer-Peppas model with a  $R^2$  value of  $> 0.88$ .

mechanism with which the release kinetics can be described<sup>21,33</sup>.

From Table 3.3, it can be inferred that the microgel beads obey the Korsmeyer-Peppas model irrespective of the pH and the regression analysis value ( $R^2$ ) was found to range from 0.87 to 0.93.

The Korsmeyer-Peppas model relates the values of  $n$  obtained upon fitting the release data to the above-mentioned equation. While a value of 0.45 for ‘ $n$ ’ indicates diffusion-controlled drug release that corresponds to diffusion-controlled drug release, a value of 0.89 indicates swelling controlled drug release that is reminiscent of Case II transport. For values of  $n$  that falls between



0.45 and 0.89, the mechanism of release is understood to be a juxtaposition of Fickian and Case II transport<sup>21,23</sup>. For the microgel beads I to V, we calculated the value of  $n$  to be  $\sim 0.1$  indicating that the release mechanism deviates from a Fickian trend given the complexity of the microstructure of the beads owing to the H-bonding interactions of alginate and aspartame and the cross-linking density arising out of the calcium ions (Figure 3.8 and 3.9).

This alludes to the fact that at values of  $n < 0.5$ , the rate of water penetration into the microgel

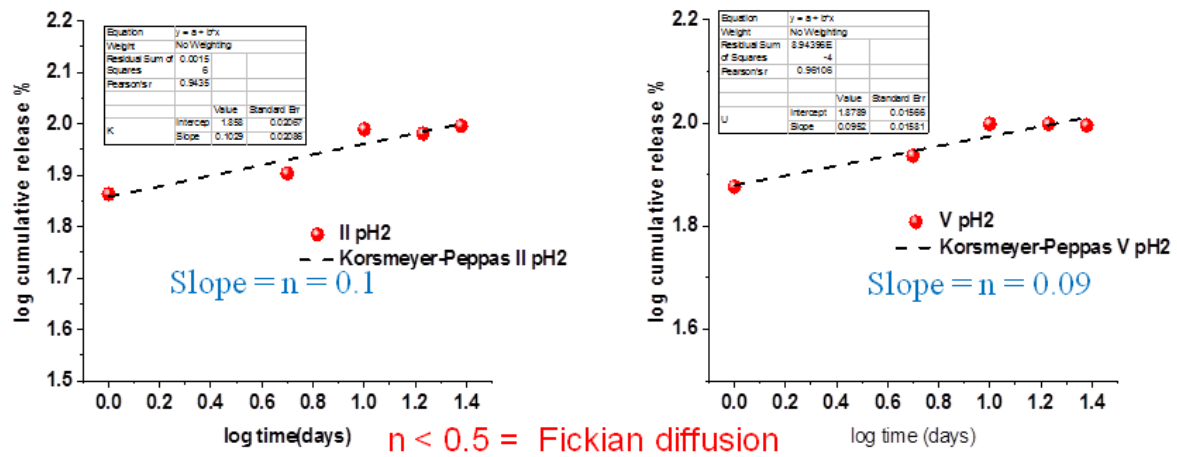


**Figure 3.7:** Kormsmeier-Peppas release model fitting for microspheres II and V. The slope of the graphs reveal the mechanism of aspartame release. Both gels II and V deviate from Fickian diffusion

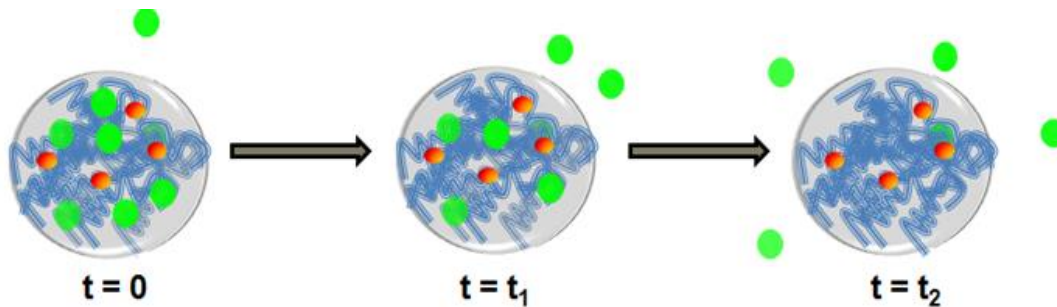


**Figure 3.8:** Mechanism of release of aspartame from microgel beads II and V

beads is less than the polymer chain relaxation rate<sup>34</sup>. Therefore, the diffusion of aspartame is

brought about by the relaxation of the polymer chains at pH 2 owing to the de-crosslinking and not by the swelling of the polymer matrix (Figure 3.10).

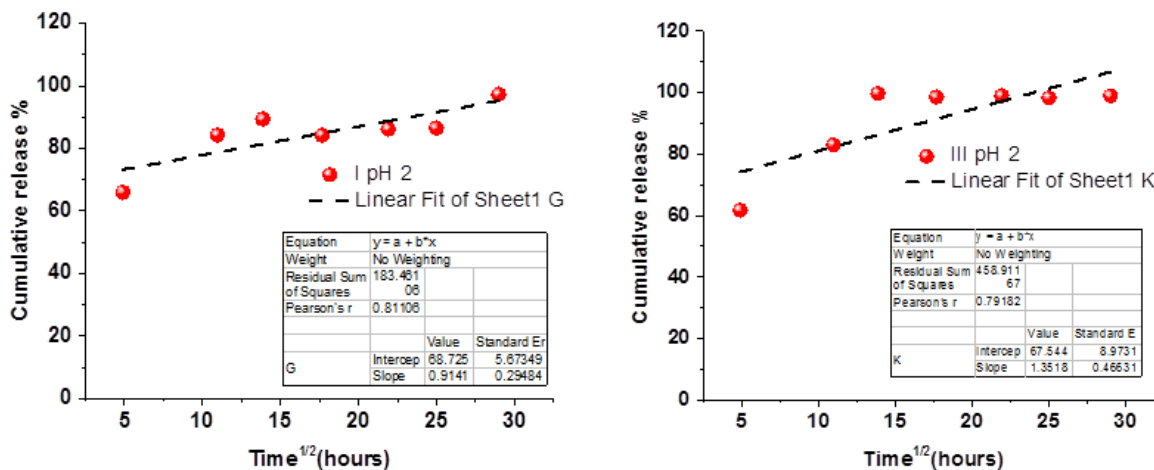


**Figure 3.9:** Higuchi release model for microspheres I and III

We next, fitted the release data to various models of release to understand the mechanism of release of aspartame.

### 3.3.6 Mechanism of release of aspartame for bulk hydrogels

Release of a guest from a polymer matrix is understood to depend on a plethora of processes such as drug-polymer affinity, cross link density, relative drug molecular weight and size, glass transition temperature and molecular relaxation of the hydrogels<sup>31,35</sup>. The release is brought about by interplay of factors such as diffusion, swelling and shrinkage and the morphology and the structure of the hydrogel are implicated in the release kinetics of a drug from a hydrogel matrix<sup>24,36,37</sup>.

We were therefore, interested in investigating the mechanism of release of aspartame from cross-linked alginate matrices in 15 mM phosphate-citrate buffer and fitted the release to several release

models to obtain a correlation coefficient that we believed to be an accurate representation of the release models.

Gels B, C and D differ only in the initial amount of aspartame loading and upon incubating them

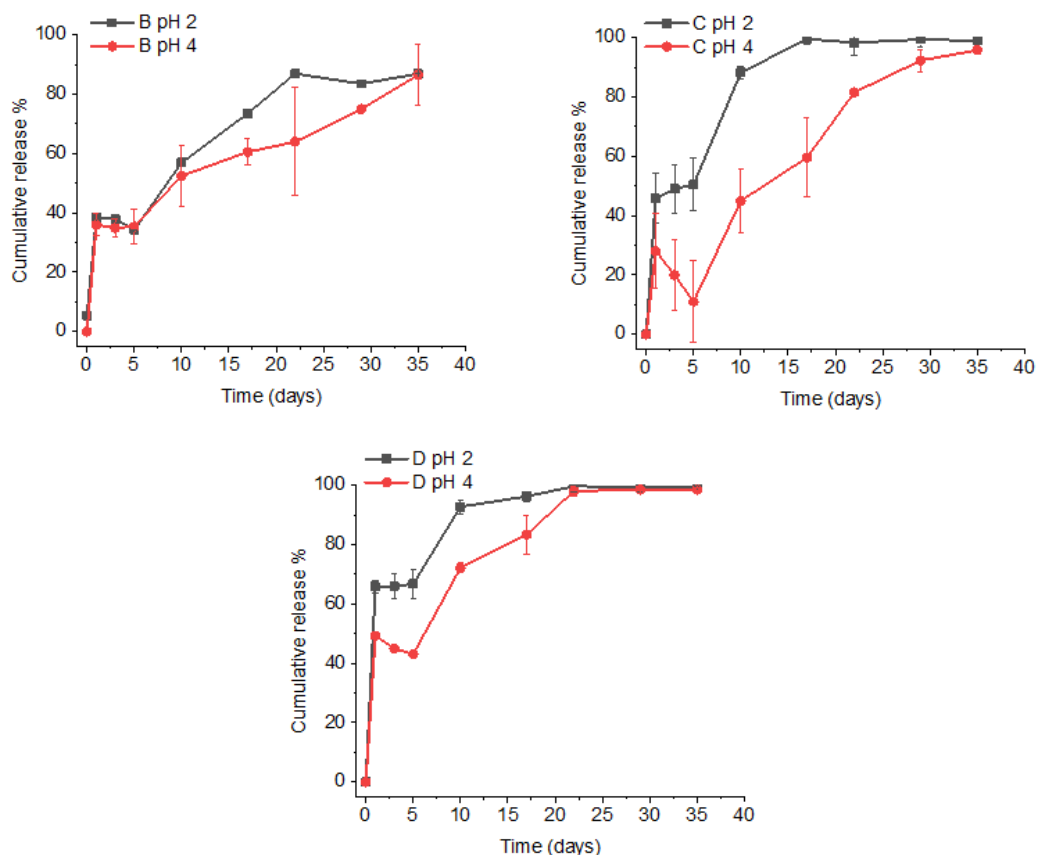


**Figure 3.10:** Cumulative release profiles of aspartame from gels B, C and D at pH 2 and 4 reveal two regimes of release: a burst release in the first five days and a sustained release over 5 weeks.

in 15 mM phosphate-citrate buffer, we found that the gels invariably have two regimes of release: a burst release in the first 5 days and then a sustained release profile over the next five weeks. While the release at pH 2 and pH 4 was found to be similar for Gel B, the release at pH was found to more than that at pH 4 for Gel C and D. Therefore, it can be concluded that at high aspartame loading, the release at pH 2 and pH 4 is comparable (Figure 3.11).

For the same initial aspartame loading, we expected that an increase in the cross-linking density would manifest in a slower burst release than a system with a higher degree of cross-linking since the network structure is understood to be stiffer resulting in a tortuous path for the guests. However,

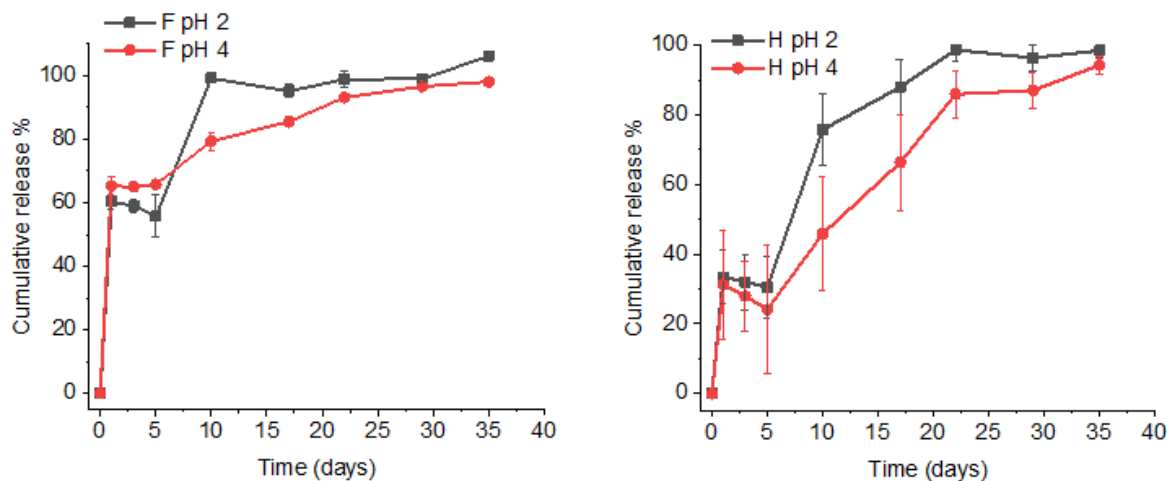


**Figure 3.11:** Cumulative release of aspartame from Gels F and H at pH 2 and pH 4. A faster release is observed for gel F as compared to gel H

upon incubating Gels F and H in buffer, we found the trend to be reversed. Gel F which had a higher degree of cross-linking was found to have a higher initial burst release compared to Gel H which had the lowest degree of cross-linking (Figure 3.12). We were intrigued by the observation that the rate of release of aspartame is the least amongst the hydrogels for the lowest cross linking. Therefore, we reasoned that this could arise out of a balance of interactions that serve to stabilize or destabilize the hydrogel matrix. At pH 4, the dipole-ion interactions arising out of the cross-linking between the carboxylates of the alginate and the calcium ions would contribute to stabilize the hydrogel matrix. However, it is worthwhile to mention that not all the carboxylates on the alginate are expected to be cross-linked owing to their occlusion because of the chain entanglements in the alginate network. The uncrosslinked carboxylates would now, serve to destabilize the hydrogel matrix because of electrostatic interactions. At pH 2, the crosslinking

between the carboxylates on the alginate and the calcium ions weakens owing to the protonation of the carboxylates that serve to weaken the matrix. However, this paves way for the carboxylic acid groups to be stabilized by intramolecular hydrogen bonding which is represented in Fig 3.14. Indeed, hydrogen bonding interactions in hydrogels have been reported to impart resilience and stiffness to hydrogels also resulting in segregated domains<sup>38</sup>.

We were, next interested in elucidating the model of release of aspartame from these hydrogel matrices. To this end, we fitted the release kinetics to several release models reported in literature and obtained the correlation coefficients or  $R^2$  values for the plots. We found that the hydrogel B obeyed the Higuchi's model of release with a  $R^2$  value of 0.94 and 0.96 at pH 2 and 4 respectively. Hydrogels C, D, F and H were found to follow the Korsmeyer-Peppas model of release with a  $R^2$  value~0.9 at both pH 2 and 4 (Table 3.4).

environment<sup>40,41</sup>. The slight deviation from Higuchi's model could be explained by the complexity of the heterogeneous system involved together with the capacity of the alginate to interact with the

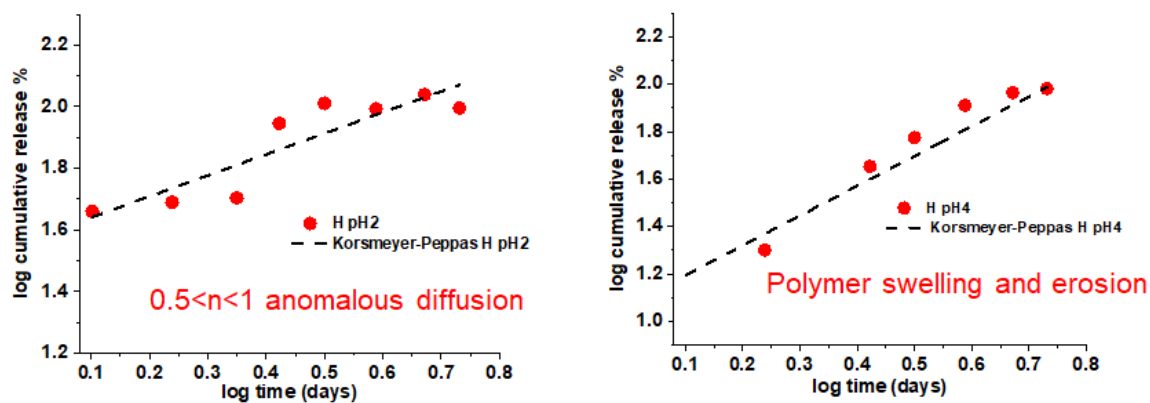


**Figure 3.12:** Release of aspartame from gel H at pH 2 and 4 when fitted to Korsmeyer-Peppas model

aspartame while the prime reason for the release is understood to be diffusion. That is the reason why in these special cases, diffusion is not the only factor to consider in the release process.

The model indicates that the release of aspartame is solely due to diffusion from the matrix and that the mode of diffusion is Fickian. This explains the two regimes of release in the kinetics plots. The burst release arises from the loosely bound aspartame to the matrix while the sustained release is brought about the release of aspartame upon slow erosion of the hydrogel matrix. The two populations of differentially bound aspartame are a result of the fast yet indiscriminate gelation kinetics of the cross-linking reaction between alginate and calcium that gives rise to disparate network structures in the hydrogel matrix (Figure 3.13).

For Gels C, D, F and H, the mode of release was found to be correlate with the Korsmeyer-Peppas model. Interestingly, the values of ‘n’ which are indicative of the drug release mechanism were found to be pH dependent in the case of Gel C.

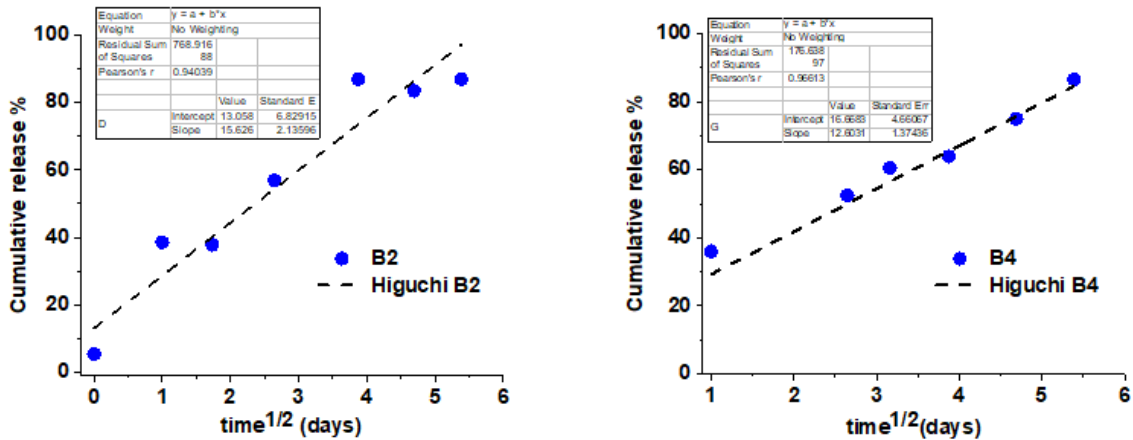


**Figure 3.13:** Release of aspartame from Gel B at pH 2 and 4 when fitted to Higuchi’s model

While the value of n was calculated to be 0.68 at pH 2, the same was found to be 1.2 at pH 4. This alludes to the presence of two different mechanisms of release depending on the pH.

At pH 2, the value of n falls between 0.45 and 0.89 which is indicative of an anomalous of non-fickian diffusion. This means that there is an interplay of diffusion and erosion-controlled release

of aspartame from the hydrogel matrix<sup>42</sup>. The diffusion and polymer relaxation rates are comparable and the effect of cross-linking here is understood to be negligible.

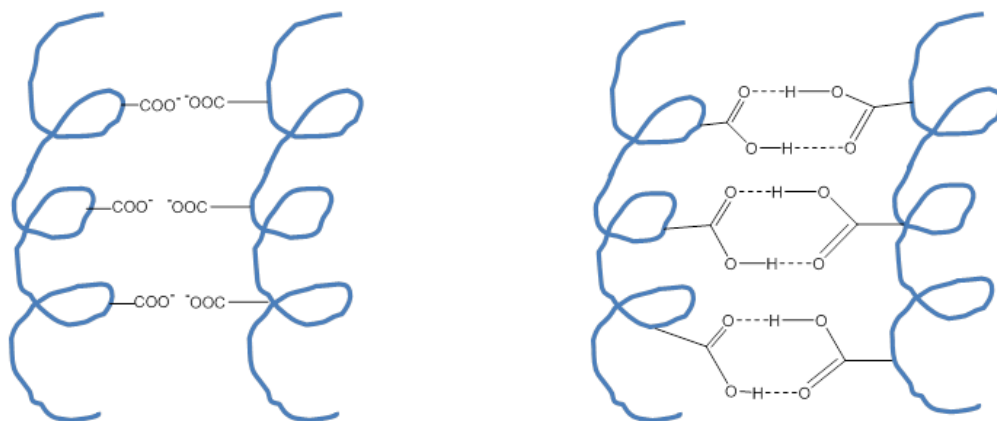


**Figure 3.14:** Schematic for the proposed H-bonding stabilization in Gel H

At pH 4, the value of  $n$  alludes to a mechanism referred to as Super Case 2 transport. This process is understood to be brought about by the erosion of the polymer chain and this paves way for the aspartame molecules to be released. Another mechanism could be a case where the aspartame release is zero-order such that release rate is constant and controlled by polymer relaxation. In the case of Gel C at pH 4, the cross-linking density dictates the release rate since the release of aspartame molecules is brought about solely due to polymer relaxation. Also, since the aspartame release is zero order and therefore, concentration dependent, the initial aspartame loading has been evaluated to play a major role in the release kinetics.

Model (R <sup>2</sup> )	B pH 2	B pH 4	C pH 2	C pH 4	D pH 2	D pH 4	F pH 2	F pH 4	H pH 2	H pH 4
Zero	0.69	0.78	0.54	0.84	0.36	0.64	0.47	0.45	0.67	0.75
First	0.83	0.93	0.59	0.64	0.49	0.70	0.58	0.81	0.63	0.72
Higuchi	0.89	0.96	0.80	0.86	0.65	0.85	0.73	0.73	0.84	0.85
Korsmeyer peppas	0.90	0.94	0.90	0.80	0.84	0.89	0.85	0.95	0.89	0.88

**Table 3.4:** Release models and corresponding correlation coefficients for the hydrogels. Bulk hydrogels obey the Korsmeyer-Peppas model of release with a R<sup>2</sup> value > 0.8

### 3.4 Conclusions

In conclusion, we have elucidated the critical differences in the release of an artificial sweetener, aspartame between microgels and bulk hydrogels of aspartame encapsulated calcium cross linked alginate gels. We have, in particular, studied the different parameters that dictate the gel architecture and hence, the morphology and the structure of the gels. Biopolymer hydrogels were prepared by ionotropic gelation and were investigated as systems that facilitate sustained release of aspartame. A Size Exclusion Chromatography (SEC) based method was developed to calculate the release of aspartame from cross-linked hydrogels. H-bonding stabilized hydrogels were found to increase the shelf-life of aspartame and the mechanism of release was found to be follow the Korsmeyer-Peppas model.



### 3.5 References

- (1) Tsakiris, S.; Giannoulia-Karantana, A.; Simintzi, I.; Schulpis, K. H. The Effect of Aspartame Metabolites on Human Erythrocyte Membrane Acetylcholinesterase Activity. *Pharmacol. Res.* **2006**, *53* (1), 1–5.
- (2) Lindeberg, G. A Convenient Synthesis of Aspartame. *J. Chem. Educ.* **1987**, *20* (c), 1062–1064.
- (3) Yuasa, Y.; Nagakura, a.; Tsuruta, H. Synthesis and Sweetness Characteristics of L-Aspartyl-D-Alanine Fenchyl Esters. *J. Agric. Food Chem.* **2001**, *49* (10), 5013–5018.
- (4) Marinovich, M.; Galli, C. L.; Bosetti, C.; Gallus, S.; La Vecchia, C. Aspartame, Low-Calorie Sweeteners and Disease: Regulatory Safety and Epidemiological Issues. *Food Chem. Toxicol.* **2013**, *60*, 109–115.
- (5) Bell, L. N.; Wetzel, C. R. Aspartame Degradation in Solution as Affected by Buffer Type and Concentration. *J. Agric. Food Chem.* **1995**, 2608–2612.
- (6) Chuy, S.; Bell, L. N. Kinetics of an Acid-Base Catalyzed Reaction (Aspartame Degradation) as Affected by Polyol-Induced Changes in Buffer pH and pKa Values. *J. Food Sci.* **2009**, *74* (1), 56–61.
- (7) Garbow, J. R.; Likos, J. J.; Schroeder, S. a. Structure, Dynamics, and Stability of Beta-Cyclodextrin Inclusion Complexes of Aspartame and Neotame. *J. Agric. Food Chem.* **2001**, *49* (4), 2053–2060.
- (8) Sohajda, T.; Béni, S.; Varga, E.; Iványi, R.; Rácz, Á.; Szente, L.; Noszál, B. Characterization of Aspartame-Cyclodextrin Complexation. *J. Pharm. Biomed. Anal.* **2009**, *50* (5), 737–745.
- (9) Bell, L. N.; Labuza, T. P. Aspartame Degradation Kinetics as Affected by pH in Intermediate and Low Moisture Food Systems. *J. Food Sci.* **1991**, *56* (1), 17–20.

- (10) Gaines, S. M.; Bada, J. L. Aspartame Decomposition and Epimerization in the Diketopiperazine and Dipeptide Products as a Function of pH and Temperature. *J. Org. Chem.* **1988**, *53* (12), 2757–2764.
- (11) Young Ju Kim; Seong Jun Han; Shi Choon Kim; Young Kee Kang. Conformation and Sweet Tastes of L-Aspartyl Dipeptide Methyl Esters. *Biopolymers* **1994**, *34* (8), 1037–1048.
- (12) Butchko, H. H.; Stargel, W. W.; Comer, C. P.; Mayhew, D. a; Benninger, C.; Blackburn, G. L.; de Sonneville, L. M. J.; Geha, R. S.; Hertelendy, Z.; Koestner, A.; et al. Aspartame: Review of Safety. *Regul. Toxicol. Pharmacol.* **2002**, *35*, S1–S93.
- (13) Oyama, Y.; Sakai, H.; Arata, T.; Okano, Y.; Akaike, N.; Sakai, K.; Noda, K. Cytotoxic Effects of Methanol, Formaldehyde, and Formate on Dissociated Rat Thymocytes: A Possibility of Aspartame Toxicity. *Cell Biol. Toxicol.* **2002**, *18* (1), 43–50.
- (14) Marques, H. M. C. A Review on Cyclodextrin Encapsulation of Essential Oils and Volatiles. *Flavour Fragr. J.* **2010**, *25* (5), 313–326.
- (15) Sohajda, T.; Béni, S.; Varga, E.; Iványi, R.; Rácz, Á.; Szente, L.; Noszál, B. Characterization of Aspartame-Cyclodextrin Complexation. *J. Pharm. Biomed. Anal.* **2009**, *50* (5), 737–745.
- (16) Rocha-Selmi, G. a.; Bozza, F. T.; Thomazini, M.; Bolini, H. M. a; Fávaro-Trindade, C. S. Microencapsulation of Aspartame by Double Emulsion Followed by Complex Coacervation to Provide Protection and Prolong Sweetness. *Food Chem.* **2013**, *139* (1–4), 72–78.
- (17) Xiao, Z.; Liu, W.; Zhu, G.; Zhou, R.; Niu, Y. A Review of the Preparation and Application of Flavour and Essential Oils Microcapsules Based on Complex Coacervation Technology. *J. Sci. Food Agric.* **2014**, *94* (8), 1482–1494.

- (18) Zhai, P.; Chen, X. B.; Schreyer, D. J. Preparation and Characterization of Alginate Microspheres for Sustained Protein Delivery within Tissue Scaffolds. *Biofabrication* **2013**, 5 (1),1-14.
- (19) Augst, A. D.; Kong, H. J.; Mooney, D. J. Alginate Hydrogels as Biomaterials. *Macromol. Biosci.* **2006**, 6 (8), 623–633.
- (20) Liao, J.; Wang, B.; Huang, Y.; Qu, Y.; Peng, J.; Qian, Z. Injectable Alginate Hydrogel Cross-Linked by Calcium Gluconate-Loaded Porous Microspheres for Cartilage Tissue Engineering. *ACS Omega* **2017**, 2 (2), 443–454.
- (21) Voo, W. P.; Ooi, C. W.; Islam, A.; Tey, B. T.; Chan, E. S. Calcium Alginate Hydrogel Beads with High Stiffness and Extended Dissolution Behaviour. *Eur. Polym. J.* **2016**, 75, 343–353.
- (22) Zhang, Z.; Zhang, R.; Zou, L.; McClements, D. J. Protein Encapsulation in Alginate Hydrogel Beads: Effect of PH on Microgel Stability, Protein Retention and Protein Release. *Food Hydrocoll.* **2016**, 58, 308–315.
- (23) Trongsatitkul, T.; Budhlall, B. M. Microgels or Microcapsules? Role of Morphology on the Release Kinetics of Thermoresponsive PNIPAm-Co-PEGMA Hydrogels. *Polym. Chem.* **2013**, 4 (5), 1502–1516.
- (24) Puguan, J. M. C.; Yu, X.; Kim, H. Journal of Colloid and Interface Science Characterization of Structure , Physico-Chemical Properties and Diffusion Behavior of Ca-Alginate Gel Beads Prepared by Different Gelation Methods. *J. Colloid Interface Sci.* **2014**, 432, 109–116.
- (25) Jang, J.; Seol, Y. J.; Kim, H. J.; Kundu, J.; Kim, S. W.; Cho, D. W. Effects of Alginate Hydrogel Cross-Linking Density on Mechanical and Biological Behaviors for Tissue

- Engineering. *J. Mech. Behav. Biomed. Mater.* **2014**, *37*, 69–77.
- (26) Smrdel, P.; Bogataj, M.; Mrhar, A. The Influence of Selected Parameters on the Size and Shape of Alginate Beads Prepared by Iontropic Gelation. *Sci. Pharm.* **2008**, *76* (1), 77–89.
- (27) Aslani, P.; Kennedy, R. A. Studies on Diffusion in Alginate Gels. I. Effect of Cross-Linking with Calcium or Zinc Ions on Diffusion of Acetaminophen. *J. Control. Release* **1996**, *42* (1), 75–82.
- (28) Hoffman, A. S. Hydrogels for Biomedical Applications. *Adv. Drug Deliv. Rev.* **2012**, *64*, 18–23.
- (29) Campbell, K. T.; Hadley, D. J.; Kukis, D. L.; Silva, E. A. Alginate Hydrogels Allow for Bioactive and Sustained Release of VEGF-C and VEGF-D for Lymphangiogenic Therapeutic Applications. *PLoS One* **2017**, *12* (7), 1-15.
- (30) Xu, Y.; Wang, L.; Tong, Y.; Xiang, S.; Guo, X.; Li, J.; Gao, H.; Wu, X. Study on the Preparation, Characterization, and Release Behavior of Carbosulfan/Polyurethane Microcapsules. *J. Appl. Polym. Sci.* **2016**, *133* (35), 1–9.
- (31) Lee, P. I.; Corporation, C. Interpretation of Drug-Release Kinetics from Hydrogel Matrices in Terms of Time-Dependent Diffusion Coefficients The Swelling Behavior and Drug Release Kinetics in Glassy Hydrogels Are Interpreted in Terms of Time- Dependent Diffusion Coefficients . *ACS Symposium Series* **1987**, *348*
- (32) Desai, S.; Perkins, J.; Harrison, B. S.; Sankar, J. Understanding Release Kinetics of Biopolymer Drug Delivery Microcapsules for Biomedical Applications. *Mater. Sci. Eng. B Solid-State Mater. Adv. Technol.* **2010**, *168* (1), 127–131.
- (33) Dash, V.; Mishra, S. K.; Singh, M.; Goyal, A. K.; Rath, G. Release Kinetic Studies of Aspirin Microcapsules from Ethyl Cellulose, Cellulose Acetate Phthalate and Their

- Mixtures by Emulsion Solvent Evaporation Method. *Sci. Pharm.* **2010**, 78 (1), 93–101.
- (34) Blandino, A.; Macias, M.; Cantero, D. Formation of Calcium Alginate Gel Capsules: Influence of Sodium Alginate and CaCl<sub>2</sub> Concentration on Gelation Kinetics. *J. Biosci. Bioeng.* **1999**, 88 (6), 686–689.
- (35) Cook, M. T.; Tzortzis, G.; Charalampopoulos, D.; Khutoryanskiy, V. V. Production and Evaluation of Dry Alginate-Chitosan Microcapsules as an Enteric Delivery Vehicle for Probiotic Bacteria. *Biomacromolecules* **2011**, 12 (7), 2834–2840.
- (36) Karbowiak, T.; Hervet, H.; Léger, L.; Champion, D.; Debeaufort, F.; Voilley, A. Effect of Plasticizers (Water and Glycerol) on the Diffusion of a Small Molecule in Iota-Carrageenan Biopolymer Films for Edible Coating Application. *Biomacromolecules* **2006**, 7 (6), 2011–2019.
- (37) Lehner, D.; Lindner, H.; Glatter, O. Determination of the Translational and Rotational Diffusion Coefficients of Rodlike Particles Using Depolarized Dynamic Light Scattering. *Langmuir* **2000**, 16 (4), 1689–1695.
- (38) Webber, M. J.; Appel, E. A.; Meijer, E. W.; Langer, R. Supramolecular Biomaterials. *Nat. Mater.* **2015**, 15 (1), 13–26.
- (39) Yu, W.; Jiang, Y. Y.; Sun, T. W.; Qi, C.; Zhao, H.; Chen, F.; Shi, Z.; Zhu, Y. J.; Chen, D.; He, Y. Design of a Novel Wound Dressing Consisting of Alginate Hydrogel and Simvastatin-Incorporated Mesoporous Hydroxyapatite Microspheres for Cutaneous Wound Healing. *RSC Adv.* **2016**, 6 (106), 104375–104387.
- (40) Chan, L. W.; Jin, Y.; Heng, P. W. S. Cross-Linking Mechanisms of Calcium and Zinc in Production of Alginate Microspheres. *Int. J. Pharm.* **2002**, 242 (1–2), 255–258.
- (41) Gorbunova, N.; Evteev, A.; Evdokimov, I.; Bannikova, A. Kinetics of Ascorbic Acid

Transport from Alginate Beads during in Vitro Digestion. **2016**, 55 (2), 148–158.

- (42) Katti, D. S.; Lakshmi, S.; Langer, R.; Laurencin, C. T. Toxicity, Biodegradation and Elimination of Polyanhydrides. *Adv. Drug Deliv. Rev.* **2002**, 54 (7), 933–961.

## CHAPTER 4

### AMPLIFICATION AND OPTICAL REPORTING OF INTERFACIAL MOLECULAR EVENTS USING LIQUID CRYSTALS

#### 4.1 Background and significance

Responsive or “smart” materials undergo changes in internal order and properties through their interactions with external influences such as, electrical and magnetic fields <sup>1-3</sup>, temperature <sup>4</sup>, pH <sup>5-7</sup>, electrolyte composition <sup>7-10</sup>, and UV irradiation <sup>11-14</sup>. These emerging classes of materials find potential applications as sensors <sup>9-14</sup>, actuators <sup>12-13</sup>, and for controlled release of active chemical agents <sup>6-8,14</sup>. Liquid crystals (LCs) present themselves as opportunities for the design of responsive materials due to their ability to amplify molecular-level events into the macroscopic scale <sup>27-28</sup>. In this context, the interactions of monomeric amphiphiles <sup>17-18, 24-26</sup> and polymeric amphiphiles <sup>18-24</sup> with the interfaces of LC films and droplets have been extensively studied in the past. These classes of amphiphiles have been reported to adsorb at the LC interfaces and trigger changes in ordering of the LCs that manifests in quantifiable optical signals.

LCs are anisotropic condensed phases that possess both the mobility of a fluid and the long-range order of crystalline solids <sup>17-20</sup>. The long range orientational order present in a nematic LC phase, where the constituent molecules align along a preferred direction called the director, gives rise to elasticity and tendency of the LC director to assume an unperturbed, homogeneously aligned state <sup>27-28</sup>. When amphiphilic adsorbates anchor at the LC interface, the elastic properties of the LC transmit and amplify this change in LC anchoring throughout the volume of the LC that lies within ~100 nm of the interface. Since LCs exhibit a phenomenon called ‘birefringence’ <sup>31-32</sup>, the optical appearance of the LC, as observed using polarized optical microscopy, changes with the director

profile within the LC <sup>39</sup>. Therefore, it is possible to interpret the presence and behavior of amphiphiles at a LC/aqueous interface by observing the optical appearance of the LC film.

Previous work in this context was motivated by the long-term goal of designing responsive LC systems based on stimuli-triggered changes in the degree of oligomerization of amphiphiles hosted at LC interfaces <sup>26-28</sup>. Most of the work in the field of stimuli-responsive assemblies is inspired by their implications in biological applications. Pathological imbalances are understood to be brought about by aberrations in protein activity and supramolecular scaffolds that can respond to variations in protein concentrations are of great significance <sup>42</sup>. In this context, non-covalent interaction-based changes in the assembly properties of amphiphiles presents greater opportunities since it encompasses a larger number of proteins that are implicated in signal transduction pathways <sup>43-45</sup>. However, a key barrier to the rationale design of such systems is, however, a gap in understanding of how oligomeric amphiphiles interact with LCs. Whereas, as noted above, the behaviors of amphiphilic polymers and monomers have been widely studied at LC interfaces, oligomers have been less investigated. Past studies have established, however, that the interactions of adsorbates/absorbates with nematic LCs are strongly dependent on the configurational degrees of freedom of the adsorbate/absorbate and the extent to which they are modified by the orientationally ordered environment of the LC <sup>33-37</sup>. For example, it is well known that flexible polymers segregate from nematic LCs because the structured environment of the LC reduces the configurational degrees of freedom of the polymer chain (entropic penalty) <sup>38-39</sup>. A recent study from our group has implicated that the degree of oligomerization impacts the anchoring of the amphiphiles with the LC. Herein, we study the interactions of oligomeric amphiphiles with nematic LC films, focusing on the hydrophilic-lipophilic balance (HLB) changes of the amphiphiles with the LC, upon introduction of a complementary enzyme. The hypothesis rests on the idea that the HLB of



an oligomer containing a small molecule ligand (complementary to a specific protein) would be significantly altered upon protein binding because a small molecule would be replaced by a rather large hydrophilic surface presented by the protein<sup>47-48</sup>. This nanoscopic event manifests itself as a disassembly event that can be leveraged to result in a macroscopic observable at the LC interface as an ordering transition.

#### 4.1.1 Design objectives

The molecular structures of the oligomers used in our study are shown in Scheme 4.1. Each amphiphilic unit is composed of a hydrophobic decyl side chain (red parts in Scheme 4.1) and a

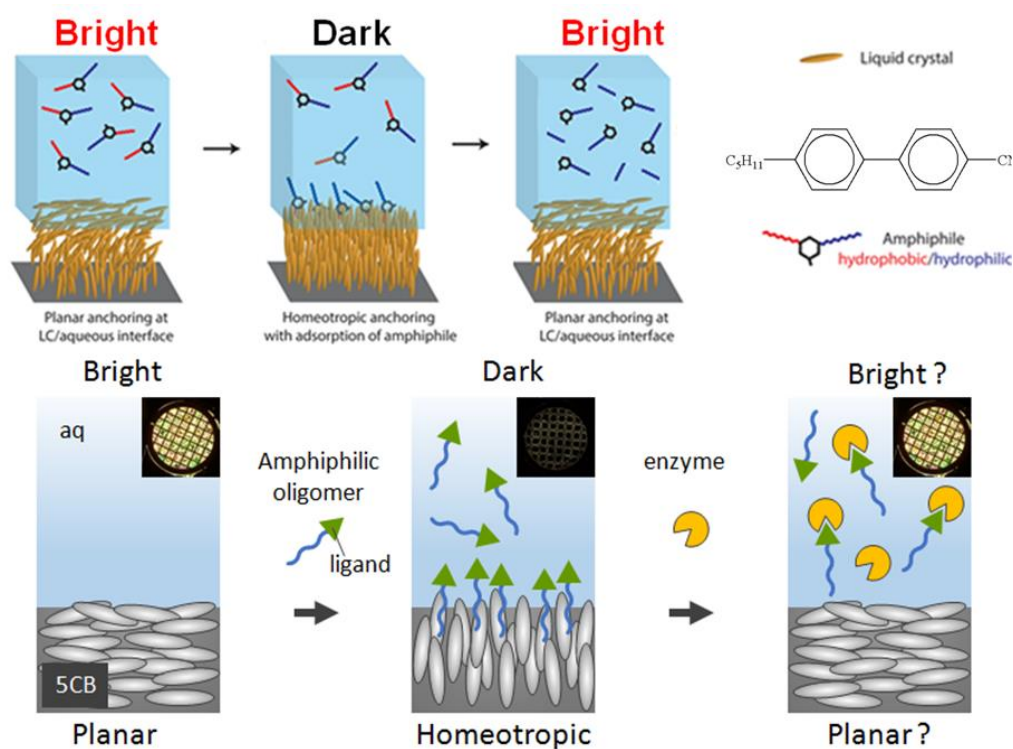
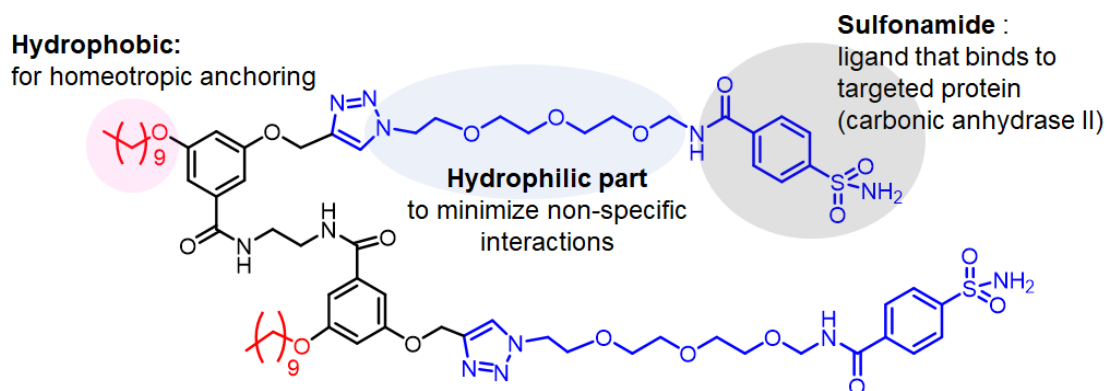


**Figure 4.1:** Illustration of the proposed mechanism for anchoring transition in the presence of oligomeric amphiphiles at the LC-water interface

hydrophilic pentaethylene glycol (PEG, blue parts in Scheme 4.1) side-chain linked via an aromatic core.

The monomer (O1), dimer (O2), and trimer (O3) are composed of these amphiphilic units, linked through an amide. In addition, the presence of side chain functionality confers responsiveness to this system as is chosen as a p-carboxy benzene sulfonamide that binds to an enzyme, carbonic anhydrase with a micromolar binding affinity<sup>49</sup>. In the Thayumanavan group, amphiphilic assemblies decorated with a ligand have been found to disassemble in response to a ligand-protein interaction. This, also known as binding induced disassembly is understood to be brought about by a change in the hydrophilic-lipophilic balance (HLB) of the amphiphilic assembly in response to the binding event and can be leveraged to bring about a molecular release event as well<sup>46-47</sup>.



**Scheme 4.1:** Molecular structure of the dimeric amphiphile with the hydrophobic, hydrophilic moieties along with the sulfonamide ligand (complementary to enzyme carbonic anhydrase)

In the experiments performed below, we compare the behaviors of the oligomers at the same concentration of amphiphilic repeat units, thus revealing the effects of degree of oligomerization

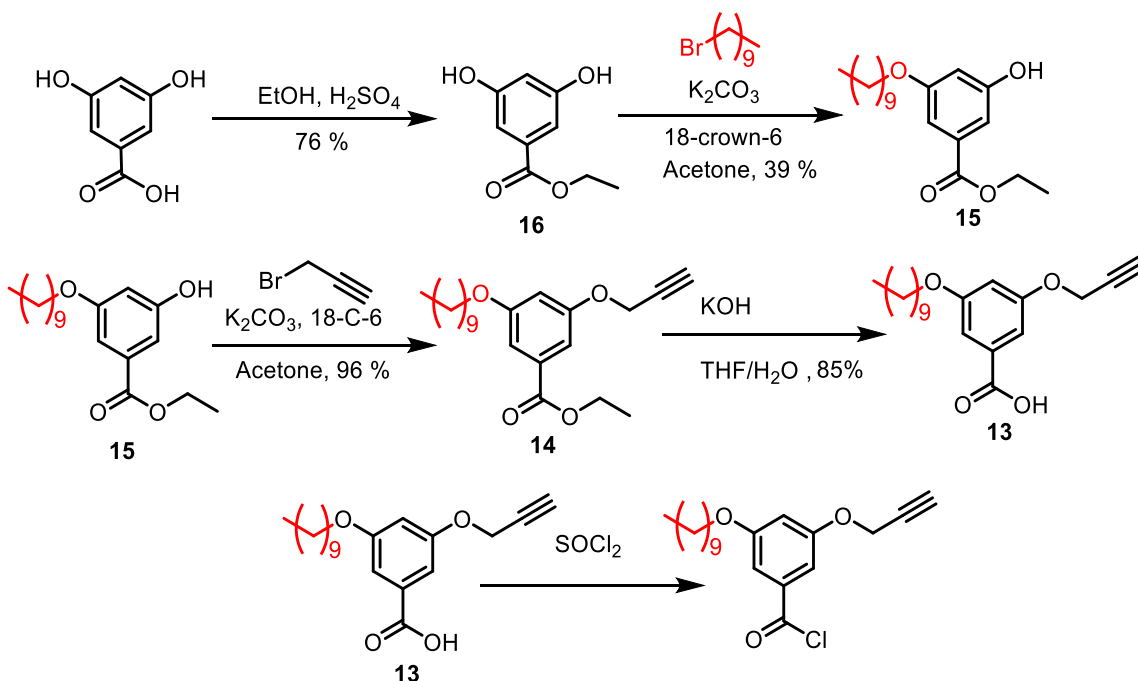
on the response of the LC. This amphiphilic scheme was chosen for its facile synthesis in addition to facilitating the easy inclusion of various responsive side-chain functionalities, which can be chosen depending on the desired external stimulus.

## 4.2 Materials and methods

All chemicals and reagents were purchased from commercial sources and were used as received, unless mentioned otherwise.  $^1\text{H}$  NMR spectra were recorded on 400 MHz NMR spectrometer using the residual proton resonance of the solvent as the internal standard. Chemical shifts are reported in parts per million (ppm). When peak multiplicities are given the following abbreviations are used: s, singlet; d, doublet; t, triplet; m, multiplet. Nematic liquid crystals, 4'-pentyl-cyanobiphenyl (5CB) was purchased from HCCH (Jiangsu Hecheng Display Technology Co., LTD). Dimethyloctadecyl[3-(trimethoxysilyl)propyl] ammonium chloride (DMOAP) was purchased from Sigma-Aldrich. Transmission electron microscopy (TEM) grids were purchased from Electron Microscopy Sciences. The polymeric alignment layer (PI2555) was purchased from HD Microsystems.

- **Synthesis of 16:** 20 g (0.150 mol) of 3,5 dihydroxy benzoic acid in a round bottom flask was dissolved in 500 mL ethanol under inert atmosphere. To this, 5 mL concentrated sulphuric acid ( $\text{H}_2\text{SO}_4$ ) and the resultant solution was left to reflux overnight. The reaction mixture was concentrated in vacuo, extracted using ethyl acetate and water. The combined extracts were dried over anhydrous  $\text{Na}_2\text{SO}_4$  and the crude product was obtained in 76 % yield.  $^1\text{H}$  NMR ( $\text{CDCl}_3$ , 400 MHz, TMS):  $\delta$  (ppm) = 7.25-7.37 (m, 2H), 6.75 (t, 1H), 5.2(broad s, 2 H), 4.35 (m, 2H), 1.41 (t, 3H). ( $\text{M}+\text{Na}^+$ ) from ESI spectroscopy: 203.06

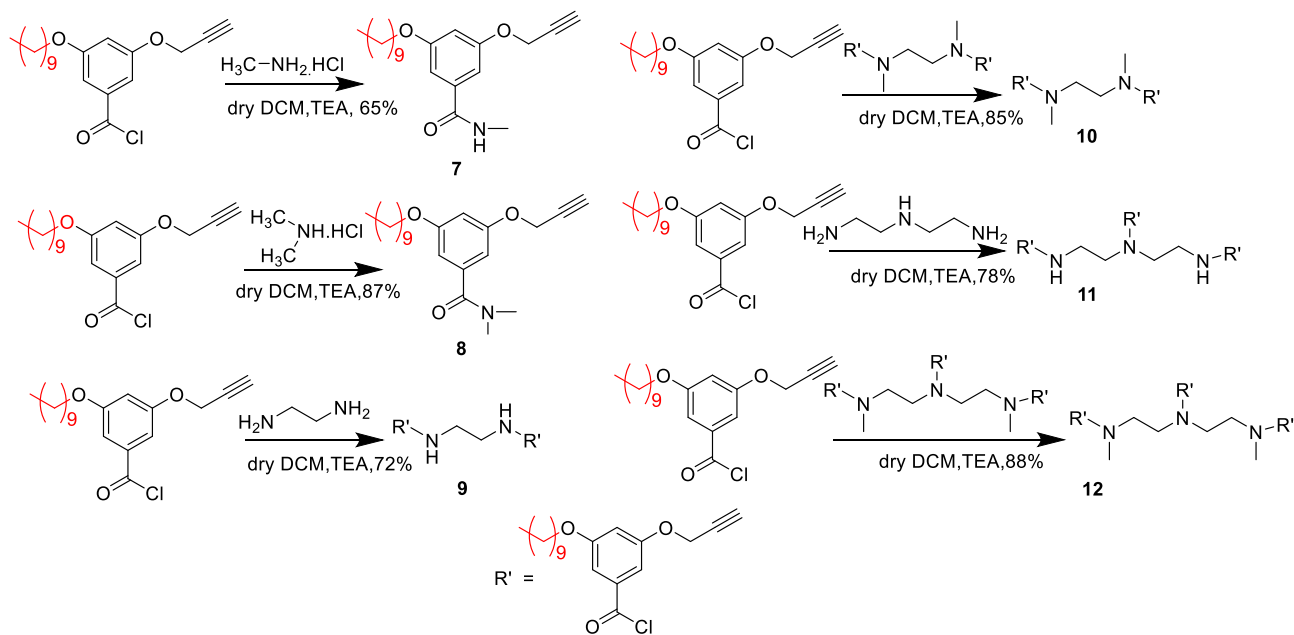
- Synthesis of 15:** 8 g (0.0439 mol) of **2** was taken in a round bottom flask and dissolved in 500 mL anhydrous acetone under inert atmosphere. To this, potassium carbonate ( $K_2CO_3$ ) ( 1.456g , 0.0105 mol) and 18-crown-6 (0.927g, 0.0035 mol) were added and the resultant solution was left to reflux. After 30 minutes, decyl bromide (1.8 mL, 0.0088 mol) was added dropwise to mixture which was then left to reflux overnight. The reaction mixture was concentrated in vacuo, extracted using ethyl acetate and water. The combined extracts were dried over anhydrous  $Na_2SO_4$  and the crude product was purified by silica gel chromatography using hexane and ethyl acetate as eluents to afford **3** in 40 % yield.  $^1H$  NMR ( $CDCl_3$ , 400 MHz, TMS):  $\delta$  (ppm) = 7.17-7.16 (m, 2H), 6.75 (t, 1H), 5.2 (broad s, 2 H), 4.35 (m, 2H), 4.04 (t, 2H), 1.8 (m, 2H), 1.41 (m, 12H), 0.89 (t, 3H). ( $M+Na^+$ ) from ESI spectroscopy: 345.21



**Scheme 4.2:** Synthesis of precursors 13-16

- **Synthesis of 14:** 2.1 g (0.0078 mol) of **3** was taken in a round bottom flask and dissolved in 200 mL anhydrous acetone under inert atmosphere. To this, potassium carbonate ( $K_2CO_3$ ) (1.16 g, 0.00843 mol) and 18-crown-6 (1.41 g, 0.0054 mol) were added and the resultant solution was left to reflux. After 30 minutes, propargyl bromide (1.38 mL, 0.00930 mol) was added dropwise to mixture which was then left to reflux overnight. The reaction mixture was concentrated in vacuo, extracted using ethyl acetate and water. The combined extracts were dried over anhydrous  $Na_2SO_4$  and the crude product was purified by silica gel chromatography using hexane and ethyl acetate as eluents to afford **4** in 95 % yield.  $^1H$  NMR ( $CDCl_3$ , 400 MHz, TMS):  $\delta$  (ppm) = 7.17-7.2 (m, 2H), 6.75 (t, 1H), 4.7(s, 2H), 4.35 (m, 2H), 3.98 (t, 2H), 2.5 (s, 1H), 1.41 (m, 12H), 1.8 (m, 2H), 0.89 (t, 3H). ( $M+Na^+$ ) from ESI spectroscopy: 383.23
- **Synthesis of 13:** 2 g (0.0056 mol) of **4** was taken in a round bottom flask and dissolved in 100 mL tetrahydrofuran under inert atmosphere. To this, potassium hydroxide pellets (0.93 g, 0.017 mol) dissolved in water (20 mL) was added and the reaction was left to reflux until completion which was monitored by TLC. The reaction mixture was concentrated in vacuo and extracted using ethyl acetate and 1N hydrochloric acid (HCl). The combined extracts were dried over anhydrous  $Na_2SO_4$  and concentrated to afford the crude product in 85 % yield.  $^1H$  NMR (Acetone- $d_6$ , 400 MHz, TMS):  $\delta$  (ppm) = 7.16 (m, 2H), 7.18 (m, 2H), 6.75 (t, 1H), 4.7(s, 2H), 4.04 (t, 2H), 2.5 (s, 1H), 1.41 (m, 9H), 1.8 (m, 2H), 0.89 (t, 3H). ( $M+Na^+$ ) from ESI spectroscopy: 355.20

- General procedure for synthesis of Oligomers (7-12):** To a solution of compound **13** in methylene chloride was added excess of thionyl chloride and the mixture was refluxed for 4 hours. The reaction mixture was then concentrated in vacuo to remove unreacted excess of thionyl chloride. The crude acid chloride product obtained was then dried for an additional 2 hours under vacuo and redispersed in methylene chloride. To this solution of acid chloride was then added appropriate equivalents of the corresponding amine and triethylamine and stirred at room temperature for 24 hours. The reaction mixture was then concentrated in vacuo and the residue was dissolved in water and extracted twice with ethyl acetate, the combined extracts were then dried over anhydrous  $\text{Na}_2\text{SO}_4$ . Upon evaporation of the solvent, the crude product was obtained in **7** (65 %), **8** (72 %), **9** (78 %), **10** (87 %), **11** (85 %) and **12**(88 %).



**Scheme 4.3:** Synthesis of oligomers 7-12

**7:**  $^1\text{H}$  NMR (DMSO- $d_6$ , 400 MHz, TMS):  $\delta$  (ppm) = 6.9 (s, 2H), 6.6 (m, 1H), 6.1(broad peak, 1H), 4.7 (s, 2H), 3.9 (t, 2H), 3.0 (s, 3H), 2.5 (s, 1H), 1.8 (m, 2H), 1.2-1.4 (m, 14 H), 0.89 (t, 3H) ( $\text{M}+\text{Na}^+$ ) from ESI spectroscopy: 368.48

**8:**  $^1\text{H}$  NMR ( $\text{CDCl}_3$ , 400 MHz, TMS):  $\delta$  (ppm) = 6.9 (s, 2H), 6.6 (m, 1H), 4.7 (s, 2H), 3.9 (t, 2H), 3.1 (s, 3H), 2.9 (s, 3H), 2.5 (s, 1H), 1.8 (m, 2H), 1.2-1.4 (m, 14 H), 0.89 (t, 3H) ( $\text{M}+\text{Na}^+$ ) from ESI spectroscopy: 382.51

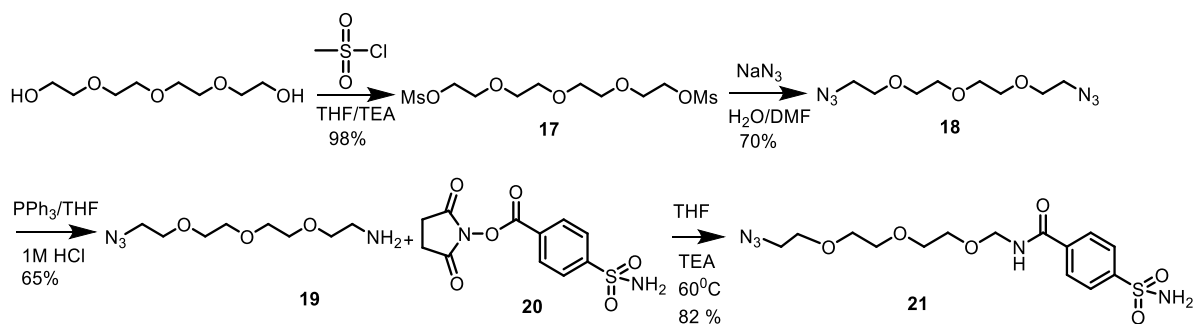
**9:**  $^1\text{H}$  NMR (DMSO- $d_6$ , 400 MHz, TMS):  $\delta$  (ppm) = 9.65(broad peak, 2H), 6.9 (s, 4H), 6.35 (s, 2H), 4.7(s, 4H), 3.95 (m, 4H), 3.5 (m, 4H), 2.5 (s, 2H), 1.65 (m, 4H), 1.2-1.4 (m, 28H), 0.89 (t, 6H) ( $\text{M}+\text{Na}^+$ ) from ESI spectroscopy: 711.45

**10:**  $^1\text{H}$  NMR ( $\text{CDCl}_3$ , 400 MHz, TMS):  $\delta$  (ppm) = 6.9 (m, 4H), 6.6 (t, 2H), 4.7(s, 4H) 3.95 (t, 4H), 3.5 (m, 4H), 2.5 (s, 3H), 1.8(m, 4H), 1.65 (m, 4H), 1.2-1.4( m, 28H), 0.89 (t, 6H) ( $\text{M}+\text{Na}^+$ ) from ESI spectroscopy: 739.48

**11:**  $^1\text{H}$  NMR ( $\text{CDCl}_3$ , 400 MHz, TMS):  $\delta$  (ppm) = 6.9 (s, 6H), 6.35 (s, 3H), 4.7(s, 6H), 3.95 (m, 6H), 3.1(m, 4H), 2.9 (m, 4H), 2.5 (s, 3H), 1.65 (m, 6H), 1.2-1.4 (m, 42H), 0.89 (t, 9H) ( $\text{M}+\text{Na}^+$ ) from ESI spectroscopy: 1068.68

**12:**  $^1\text{H}$  NMR ( $\text{CDCl}_3$ , 400 MHz, TMS):  $\delta$  (ppm) = 6.9 (s, 6H), 6.35 (s, 3H), 4.7(s, 6H), 3.95 (m, 6H), 3.2-3.4 (m, 7H), 2.9-3.1 (m, 7H), 2.5 (s, 3H), 1.65 (m, 6H), 1.2-1.4 (m, 42H), 0.89 (t, 9H) ( $\text{M}+\text{Na}^+$ ) from ESI spectroscopy: 1096.71

- Synthesis of 17:** 5g (0.0257 mol) of tetraethylene glycol was dissolved in anhydrous tetrahydrofuran in a round bottom flask and cooled to 0 °C. To this, triethylamine (7 mL, 0.0514 mol) was added and the reaction mixture was left to stir for 30 minutes. Mesityl chloride (4 mL, 0.0514 mol) was dissolved in 2 mL anhydrous tetrahydrofuran and added drop wise to the stirring solution. The mixture was left to stir overnight. The reaction mixture was then concentrated in vacuo and the residue was dissolved in water and extracted twice with ethyl acetate, the combined extracts were then dried over anhydrous Na<sub>2</sub>SO<sub>4</sub>. Upon evaporation of the solvent, the crude product was obtained in 89 % yield. <sup>1</sup>H NMR (CDCl<sub>3</sub>, 400 MHz, TMS): δ (ppm) = 4.35 (m, 4H), 3.5-3.8 (m, 12 H), 3.1 (s, 6H) (M+Na<sup>+</sup>) from ESI spectroscopy: 373.07
- Synthesis of 18:** To 10g (0.0285 mol) of **17** in 20 mL dimethylformamide, 80 mL water and sodium azide (9.26 g, 0.0142 mol) was added and the reaction was left to stir overnight. The reaction mixture was then extracted with 50 mL diethyl ether twice. The combined organic



**Scheme 4.4** Synthesis of sulfonamide-PEG ligand **21**

layer was washed with water, dried over anhydrous Na<sub>2</sub>SO<sub>4</sub> and concentrated under reduced pressure to obtain **18** as yellow oil in 73 % yield. <sup>1</sup>H NMR (CDCl<sub>3</sub>, 400 MHz, TMS): δ (ppm) = 3.5-3.8 (m, 12 H), 2.75 (t, 4H) (M+Na<sup>+</sup>) from ESI spectroscopy: 299.23



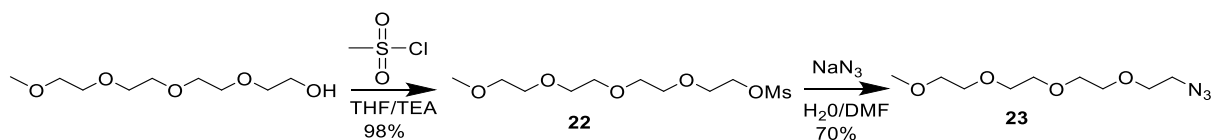
- Synthesis of 19:** To a solution of **18** (4g, 0.0144 mol) in diethylether: tetrahydrofuran: 1N HCl (50 mL: 10 mL: 50 mL) was added a solution of triphenylphosphine (4 g, 0.0144 mol) in diethyl ether using an addition funnel. The reaction was left to stir for 8 hours following which the organic layer was discarded. The aqueous layer was extracted twice with diethyl ether. The pH of the aqueous layer was adjusted to 12 using 1M NaOH and again extracted with dichloromethane. The combined organic layer was dried over anhydrous Na<sub>2</sub>SO<sub>4</sub> and concentrated under reduced pressure to obtain **19** as yellow oil in 52 % yield. <sup>1</sup>H NMR (CDCl<sub>3</sub>, 400 MHz, TMS): δ (ppm) = 3.5-3.8 (m, 14 H), 3.3 (t, 2H), 2.7 (t, 2H) (M+Na<sup>+</sup>) from ESI spectroscopy: 241.31
- Synthesis of 20:** To a solution of p-carboxy benzene sulfonamide (3g, 0.015 mol) in anhydrous tetrahydrofuran was added N-hydroxy succinimide (2.07 g, 0.018 mol) and left to stir for 30 minutes. The reaction mixture was then cooled to 0 °C and (3-dimethylaminopropyl)-N'-ethylcarbodiimide hydrochloride (3.7 g, 0.0195 mol) was added to the reaction mixture and was left to stir overnight. The reaction mixture was then concentrated in vacuo, the residue was dissolved in water and extracted twice with ethyl acetate. The combined extracts were washed with saturated sodium bicarbonate solution and brine and concentrated to afford **20** as a white solid in 92 % yield. <sup>1</sup>H NMR (CDCl<sub>3</sub>, 400 MHz, TMS): δ (ppm) = 7.75 (s, 2H) 7.9 (s, 2H), 2.8 (s, 4H). (M+Na<sup>+</sup>) from ESI spectroscopy: 321.37
- Synthesis of 21:** To a solution of **19** (0.88g, 0.004 mol) and **20** (1g, 0.003 mol) in anhydrous tetrahydrofuran was added triethylamine (0.52 mL, 0.004 mol) and the resultant mixture was left to reflux until completion of the reaction as indicated by TLC. The reaction mixture was

then concentrated in vacuo and the residue was dissolved in water and extracted twice with ethyl acetate. The combined extracts were then washed with 1N HCl, saturated sodium bicarbonate and dried over anhydrous Na<sub>2</sub>SO<sub>4</sub>. Upon evaporation of the solvent, the crude product was obtained in 89 % yield. <sup>1</sup>H NMR (CDCl<sub>3</sub>, 400 MHz, TMS): δ (ppm) = 7.75-7.9 (m, 4H), 5.8 (broad peak, 2H), 3.5-3.8 (m, 15 H), 3.35 (m, 2H) (M+Na<sup>+</sup>) from ESI spectroscopy: 424.14

- **General procedure for synthesis of Oligomers (1-6):** To a solution of compound 21 in a 7 mL vial in tetrahydrofuran was added the respective oligomers through 7-12. To this, 1 equivalent of copper sulphate pentahydrate and 1 equivalent of sodium ascorbate (with respect to the oligomers 7-12) dissolved in 1 mL water was added and the reaction mixture was left to stir overnight. The reaction mixture was extracted using ethyl acetate, water and the combined extracts were then dried over anhydrous Na<sub>2</sub>SO<sub>4</sub>. Upon evaporation of the solvent, the crude product was obtained in 1(81%), 2 (85%), 3 (72%), 4 (74%), 5 (53%), 6 (55%) yields respectively.
- **Synthesis of 22:** 5g (0.0257 mol) of tetraethylene glycol monomethyl ether was dissolved in anhydrous tetrahydrofuran in a round bottom flask and cooled to 0 °C. To this, triethylamine (7 mL, 0.0514 mol) was added and the reaction mixture was left to stir for 30 minutes. Mesyl chloride (4 mL, 0.0514 mol) was dissolved in 2 mL anhydrous tetrahydrofuran and added drop wise to the stirring solution. The mixture was left to stir overnight. The reaction mixture was then concentrated in vacuo and the residue was dissolved in water and extracted twice with ethyl acetate, the combined extracts were then dried over anhydrous Na<sub>2</sub>SO<sub>4</sub>. Upon evaporation of the solvent, the crude product was obtained in 89 % yield. <sup>1</sup>H NMR (CDCl<sub>3</sub>,

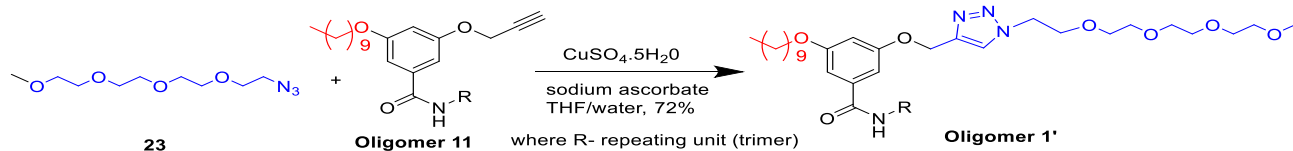
400 MHz, TMS):  $\delta$  (ppm) = 4.35 (m, 4H), 3.5-3.8 (m, 12 H), 3.3 (s, 3 H), 3.1 (s, 3H) ( $M+Na^+$ )  
 from ESI spectroscopy: 309.11

- **Synthesis of 23:** To 10g (0.0285 mol) of **22** in 20 mL dimethylformamide, 80 mL water and sodium azide (9.26 g, 0.0142 mol) was added and the reaction was left to stir overnight. The reaction mixture was then extracted with 50 mL diethyl ether twice. The combined organic layer was washed with water, dried over anhydrous  $Na_2SO_4$  and concentrated under reduced pressure to obtain **23** as yellow oil in 73 % yield.  $^1H$  NMR ( $CDCl_3$ , 400 MHz, TMS):  $\delta$  (ppm) = 3.5-3.8 (m, 12 H), 3.3 (s, 3 H), 2.75 (t, 2H) ( $M+Na^+$ ) from ESI spectroscopy: 256.14



**Scheme 4.5:** Synthesis of control PEG linker 23

- **General procedure for synthesis of Oligomers (1')**: To a solution of compound **23** in a 7 mL vial in tetrahydrofuran was added oligomer **11**. To this, 1 equivalent of copper sulphate pentahydrate and 1 equivalent of sodium ascorbate (with respect to the oligomer 11) dissolved in 1 mL water was added and the reaction mixture was left to stir overnight. The reaction mixture was extracted using ethyl acetate, water and the combined extracts were then dried over anhydrous  $Na_2SO_4$ . Upon evaporation of the solvent, the crude product was obtained in 1' (81%),



**Scheme 4.6:** Synthesis of oligomer with sulfonamide ligand 1'

Monomer:  $^1\text{H}$  NMR (Acetone  $d_6$ , 400 MHz, TMS):  $\delta$  (ppm) = 8.5 (m, 1H), 8.1 (d, 2H), 8.0 (d, 2H), 7.9 (s, 1H), 7.1 (m, 2H), 6.75 (m, 1H), 6.5 (s, 1H), 5.2 (s, 2H), 4.5 (t, 2H), 3.5- 4 (m, 16 H), 2.97 (d, 3H), 1.75 (m, 2H), 1.48(m, 2H), 1.18-1.32 (m, 12 H), 0.89 (t , 3H)  $^{13}\text{C}$  NMR (125 MHz; Acetone  $d_6$ ):  $\delta$  168.48, 168.09, 161.09, 142.57, 136. 27, 134.93, 128.15, 127. 05, 117.20, 109.83, 109.39, 106.09, 69.93, 68.75, 57.68, 50.11, 42.23, 31.87, 29.27, 25.73, 22.42, 13.52 ( $\text{M}+\text{Na}^+$ ) from ESI spectroscopy: 769.92

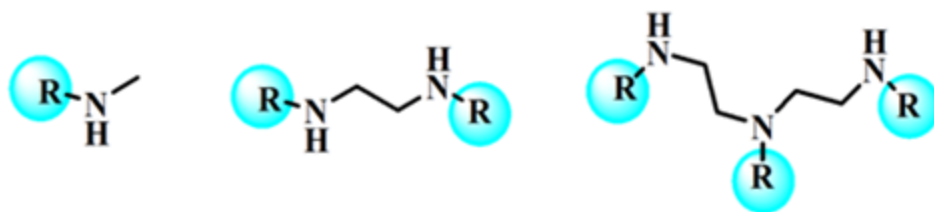
Me monomer:  $^1\text{H}$  NMR (Acetone  $d_6$ , 400 MHz, TMS):  $\delta$  (ppm) = 8.1 (d, 2H), 8.0 (d, 2H), 7.9 (s, 1H), 7.1 (m, 2H), 6.75 (m, 1H), 6.5 (s, 1H), 5.2 (s, 2H), 4.5 (t, 2H), 3.5- 4 (m, 16 H), 3.1 (s, 3H), 2.9 (s, 3H), 1.75 (m, 2H), 1.48(m, 2H), 1.18-1.32 (m, 12 H), 0.89 (t , 3H)  $^{13}\text{C}$  NMR (125 MHz; Acetone  $d_6$ ):  $\delta$  168.48, 168.09, 161.09, 142.57, 136. 27, 134.93, 128.15, 127. 05, 117.20, 109.83, 109.39, 106.09, 69.93, 68.75, 57.68, 50.11, 42.23, 35.94, 29.27, 25.73, 22.42, 13.52 ( $\text{M}+\text{Na}^+$ ) from ESI spectroscopy: 783.95

Dimer:  $^1\text{H}$  NMR (Acetone  $d_6$ , 400 MHz, TMS):  $\delta$  (ppm) = 8.5 (m, 2H), 8.21 (d, 4H), 7.98 (m, 2H), 7.89 (d,4H), 7.23 (s, 4H), 7.07 (m, 4H), 6.75 (s, 2H), 5.2 (s, 4H), 4.5 (t, 4H), 3.5- 4 (m, 32 H), 1.77 (m, 4H), 1.42 (m, 4H), 1.2-1.3 (m, 24 H), 0.89 (t , 6H)  $^{13}\text{C}$  NMR (125 MHz; Acetone  $d_6$ ):  $\delta$  168.48, 168.09, 161.09, 142.57, 136. 27, 134.93, 128.15, 127. 05, 117.20, 109.83, 109.39, 106.09, 69.93, 68.75, 57.68, 50.11, 42.23, 39.99, 29.27, 25.73, 22.42, 13.52 ( $\text{M}+\text{Na}^+$ ) from ESI spectroscopy: 1513.71

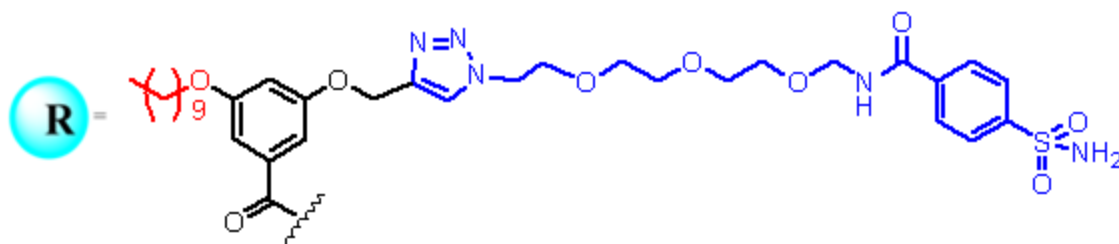
Me-dimer:  $^1\text{H}$  NMR (Acetone  $\text{d}_6$ , 400 MHz, TMS):  $\delta$  (ppm) = 8.21 (d, 4H), 7.89 (d,4H), 7.23 (s, 4H), 7.07 (m, 4H), 6.75 (s, 2H), 5.2 (s, 4H), 4.5 (t, 4H), 3.5- 4 (m, 32 H), 2.9 (s, 6H), 1.77 (m, 4H), 1.42 (m, 4H), 1.2-1.3 (m, 24 H), 0.89 (t , 6H)  $^{13}\text{C}$  NMR (125 MHz; Acetone  $\text{d}_6$ ):  $\delta$  168.48, 168.09, 161.09, 142.57, 136. 27, 134.93, 128.15, 127. 05, 117.20, 109.83, 109.39, 106.09, 69.93, 68.75, 57.68, 50.11, 45.90, 35.34, 29.27, 25.73, 22.42, 13.52 ( $\text{M}+\text{Na}^+$ ) from ESI spectroscopy: 1543.94

Trimer:  $^1\text{H}$  NMR (Acetone  $\text{d}_6$ , 400 MHz, TMS):  $\delta$  (ppm) 8.5 (m. 3H), 8.1 (d, 6H), 8.0 (d, 6H), 7.9 (s, 3H), 7.1 (m, 3H), 6.75 (m, 2H), 6.5 (s, 2H), 5.2 (s, 6H), 4.5 (t, 6H), 3.67 (t, 4H), 3.52 (m, 4H) 3.6- 4 (m, 48 H), 2.97 (d, 9H), 1.75 (m, 6H), 1.48(m, 6H), 1.18-1.32 (m, 36 H), 0.89 (t , 9H)  $^{13}\text{C}$  NMR (125 MHz; Acetone  $\text{d}_6$ ):  $\delta$  168.48, 168.09, 161.09, 142.57, 136. 27, 134.93, 128.15, 127. 05, 117.20, 109.83, 109.39, 106.09, 69.93, 68.75, 57.68, 50.11, 47.87, 38.33, 29.27, 25.73, 22.42, 13.52 ( $\text{M}+\text{Na}^+$ ) from ESI spectroscopy: 2404.14

Me-trimer:  $^1\text{H}$  NMR (Acetone  $\text{d}_6$ , 400 MHz, TMS):  $\delta$  (ppm) = 8.1 (d, 6H), 8.0 (d, 6H), 7.9 (m, 3H), 7.1 (m, 3H), 6.75 (m, 2H), 6.5 (s, 2H), 5.2 (s, 6H), 4.5 (t, 6H), 3.71 (m, 4H), 3.6- 4 (m, 48 H), 2.87 (s, 6H), 1.75 (m, 6H), 1.48(m, 6H), 1.18-1.32 (m, 36 H), 0.89 (t , 9H)  $^{13}\text{C}$  NMR (125 MHz; Acetone  $\text{d}_6$ ):  $\delta$  168.48, 168.09, 161.09, 142.57, 136. 27, 134.93, 128.15, 127. 05, 117.20, 109.83, 109.39, 106.09, 69.93, 68.75, 57.68, 50.11, 47.87, 46.21, 34.39, 29.27, 25.73, 22.42, 13.52 ( $\text{M}+\text{Na}^+$ ) from ESI spectroscopy: 2446.06

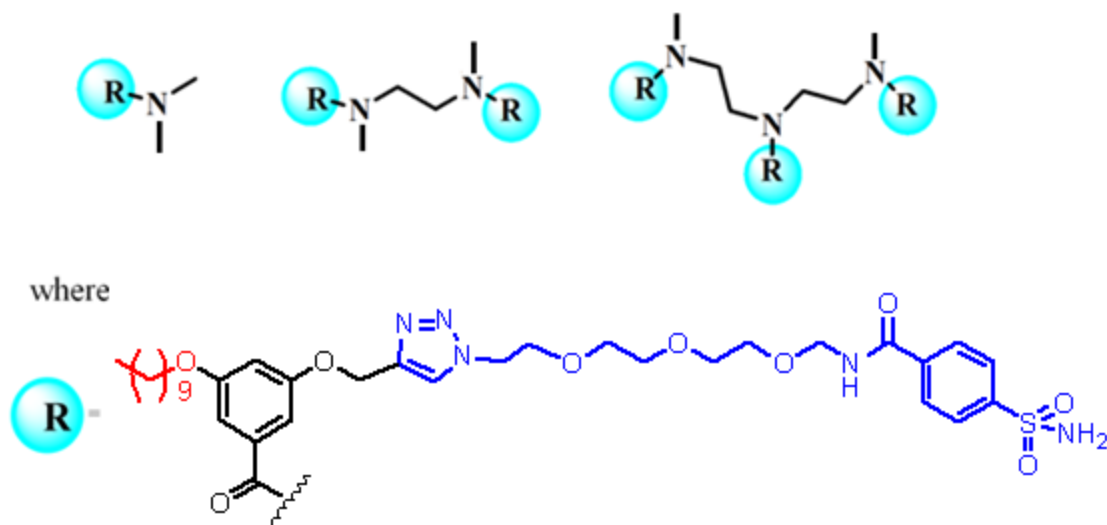


where



**Scheme 4.7:** Structures of oligomers with sulfonamide ligand

- General procedure for critical aggregation concentration (CAC) determination:** The stock solutions of oligomers 1-6 respectively, were made by a standard method of dispersing the weighed compound in 100 $\mu$ L acetone and then adding a predetermined amount of HPLC grade water in a scintillation vial with a stir bar. 40  $\mu$ L of Nile Red stock (1mM in acetone) was then added to the vial in a dropwise manner. The contents were sonicated for 5 minutes and vortexed for 2 minutes, following which they were left to stir for 8 hours at room temperature uncapped to facilitate the evaporation of acetone. The excess insoluble Nile Red was removed by filtration using a membrane with a pore size of 0.450 $\mu$ m. The intensity at the maxima was plotted as a function of concentration of the amphiphiles and the inflexion point was noted to be the critical aggregation concentration or CAC.



**Scheme 4.8:** Structures of methylated oligomers with sulfonamide ligand

- Size determination using Dynamic light scattering study (DLS):** The stock solutions of oligomers 1-6 respectively, were made by a standard method of dispersing the weighed compound in 100 $\mu$ L acetone and then adding a predetermined amount of HPLC grade water in a scintillation vial with a stir bar. The contents were sonicated for 5 minutes and vortexed for 2 minutes, following which they were left to stir for 8 hours at room temperature uncapped to facilitate the evaporation of acetone. DLS was performed on a Malvern Nano-Zetasizer instrument with a 637 nm laser with non-invasive backscattering technology detected at 173°. All sizes are reported as the hydrodynamic diameter ( $D_H$ ) and were repeated in triplicate. The reported sizes are an average of three individual DLS measurements.

- CAC and DLS profiles for molecules 1-6

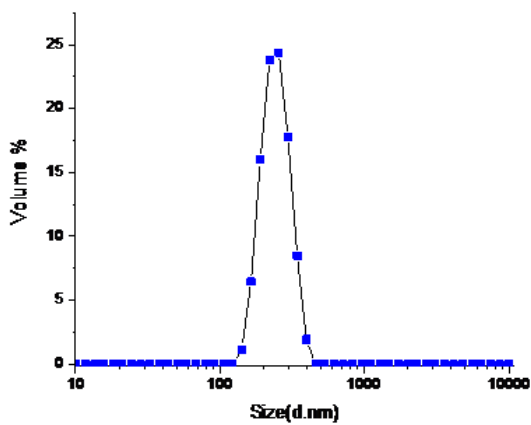
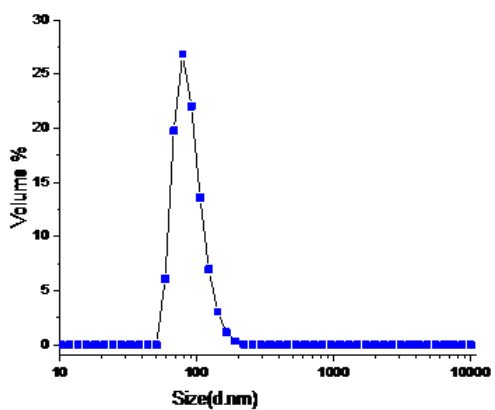
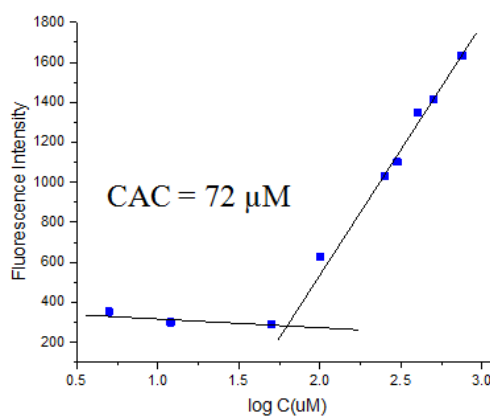
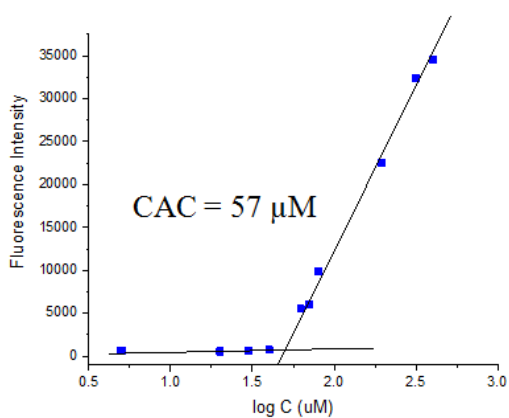
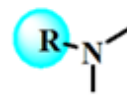
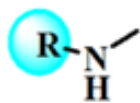


Figure 4.2 a : CAC(top) and DLS(bottom) profiles for molecule 1(left) and 2(right)



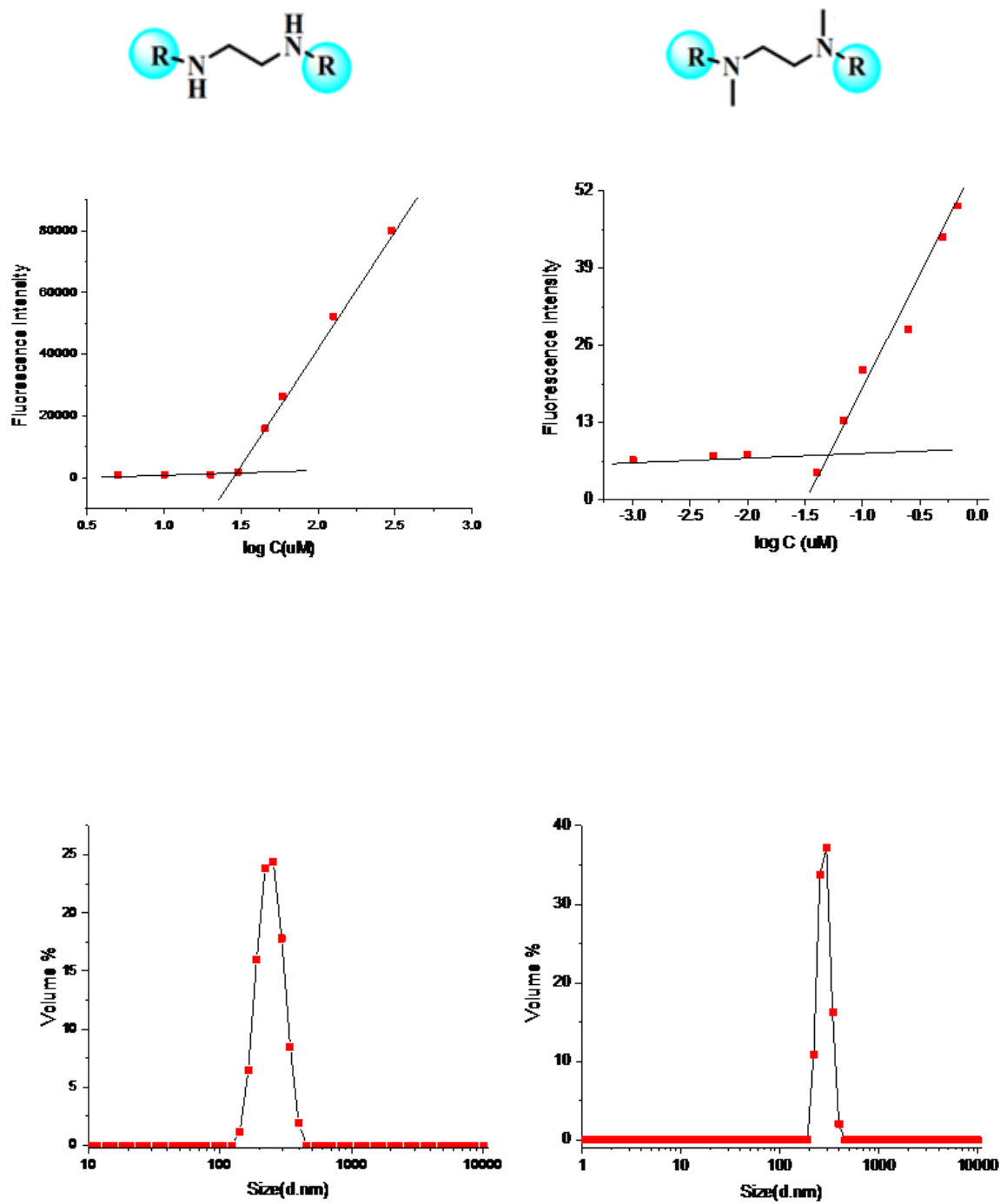


Figure 4.2 b : CAC(top) and DLS(bottom) profiles for molecule 3(left) and 4(right)

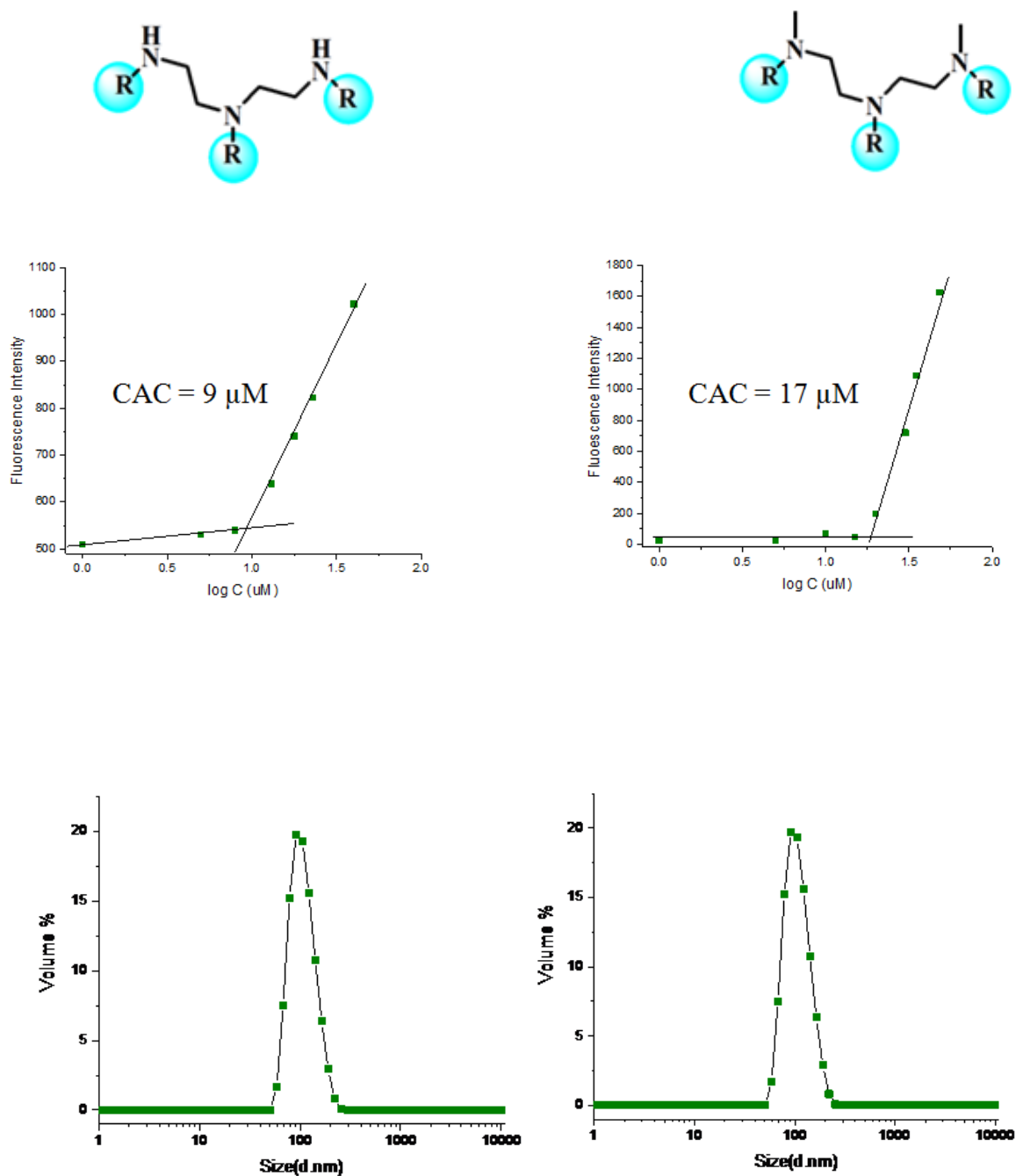


Figure 4.2 c : CAC(top) and DLS(bottom) profiles for molecule 5(left) and 6(right)

- **Monitoring disassembly using Dynamic light scattering study (DLS):** The solution of oligomers was diluted to the required concentration using pH 7.4 phosphate buffer (PBS) so

that the concentration of the buffer was 50 mM in the resultant solution. For the dimer, to a 0.4 mL solution of oligomer in PBS buffer was added 0.6 mL of a 50 $\mu$ M bovine carbonic anhydrase (bCA) solution such that final concentration of the dimer and bCA in the solution was 10  $\mu$ M and 20  $\mu$ M respectively (Aldrich, 7.5 mg/mL pH 7.4 PBS buffer) and mixed well. The DLS experiment was performed as a function of time and the disassembly was monitored by the change in size of aggregates over time. Prior to the DLS experiment, the dust in the oligomers solution was removed by passing it through a syringe filter (0.22  $\mu$ m). The temperature was maintained at 25 °C throughout the experiment.

- **Preparation of LC films.** LC films were prepared by depositing nematic 4'-pentyl-4-biphenylcarbonitrile (5CB) into a gold TEM grid (10  $\mu$ m in thickness) placed on glass substrates that were coated with either DMOAP or a polyimide (PI) that was rubbed to achieve unidirectional planar alignment. Subsequently, the LC film was immersed into an aqueous bath containing 10 mM phosphate buffered saline (PBS) at pH 7.4 and the relevant amphiphilic oligomer. To prevent evaporation of the aqueous solutions and keep the concentration of oligomers in the solution during the experiments, a glass slide was used to cap off the bath and we seal the bath with Dow Corning 748 Sealant. After the well is capped and sealed, the well is placed onto the microscope and a time lapse is taken to observe the state of the LC film over time.

### 4.3 Result and discussion

The oligomers synthesized according to Scheme 1-5 were characterized using  $^1\text{H}$  and  $^{13}\text{C}$  NMR and mass spectroscopy.

#### 4.3.1 Characterization of self-assembly and binding-induced disassembly (BID)

To study the aggregation properties of the oligomers, they were dispersed in water at different concentrations and the critical aggregation concentrations (CAC) were calculated using Nile Red, a hydrophobic dye as a spectroscopic probe. We, then, investigated the size of these assemblies above the CAC using dynamic light scattering (DLS). The amphiphiles were found to self-assemble into aggregates and the critical aggregation concentrations and the sizes of the aggregates formed by these assemblies are listed in Table 4.A.

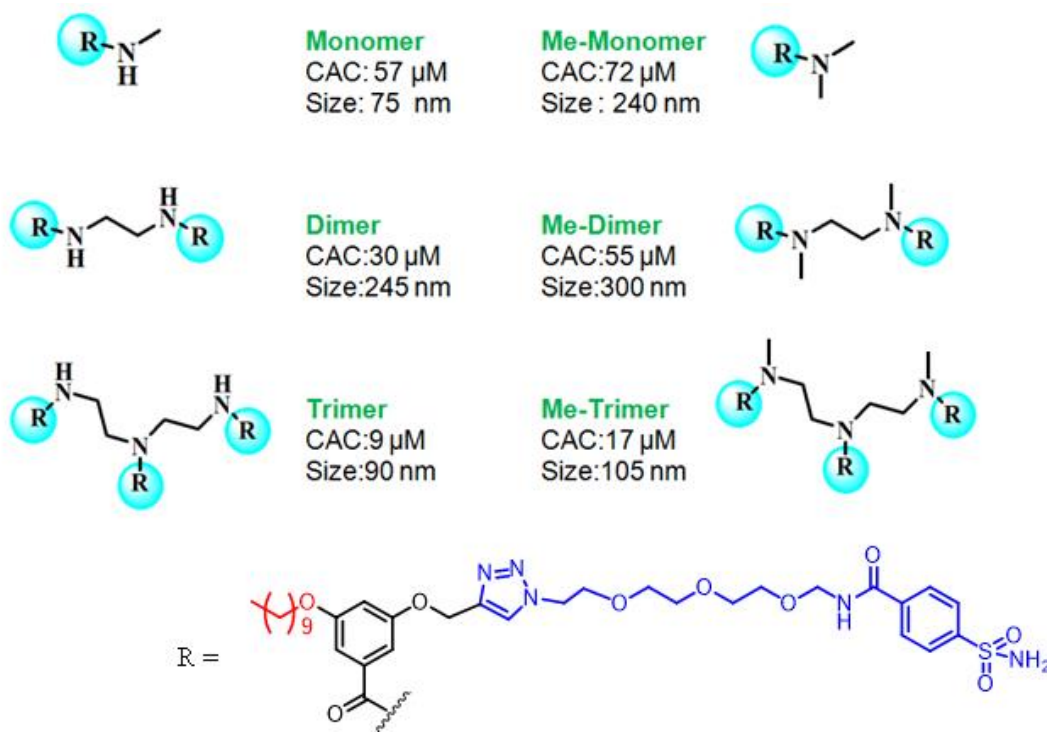


**Table 4.1:** CACs and sizes of aggregates from oligomers 1-6

Next, we investigated the behavior of the aggregates formed by the dimer in the presence of a complementary protein, carbonic anhydrase. To this end, we subjected aqueous solutions of these aggregates above critical aggregation concentration to the enzyme carbonic anhydrase such that the molar ratio of the ligand: protein was maintained at 1:1. We then, monitored the change in the aggregation properties using dynamic light scattering. It was found that the amphiphilic assemblies disassembled in the presence of bovine carbonic anhydrase and the disassembly occurred in a period of 4 hours as observed from DLS (Fig 4.2).

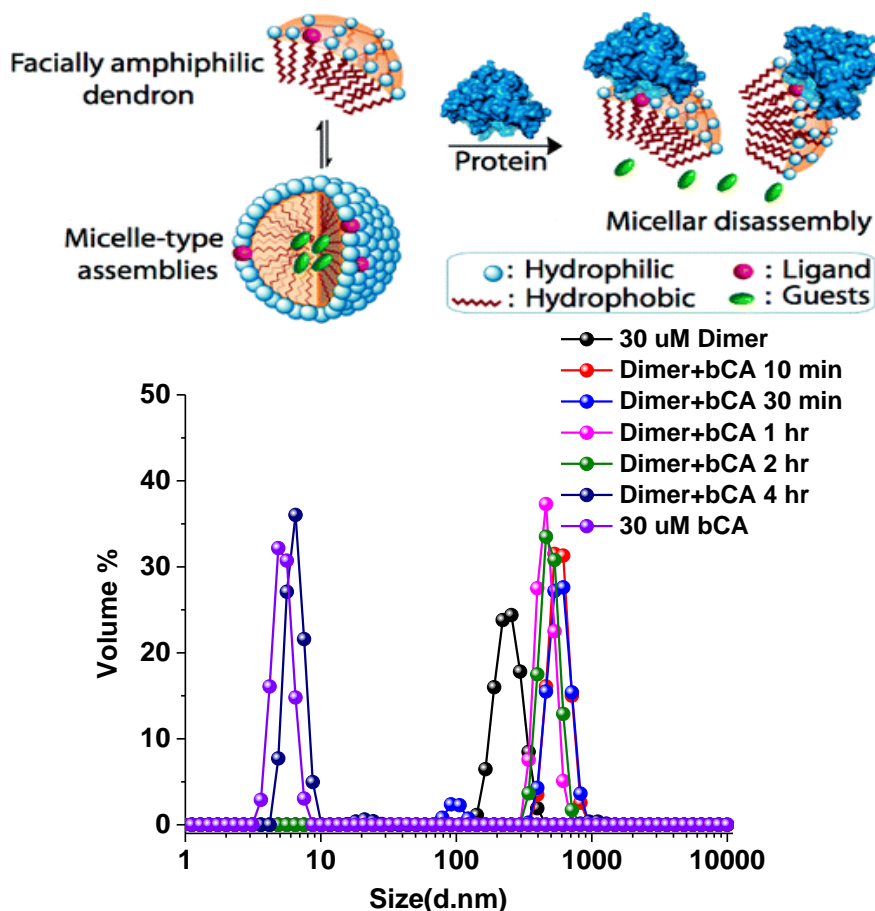


**Figure 4.3:** Principle of binding-induced disassembly (BID) and disassembly of dimer with complementary protein bovine carbonic anhydrase as monitored by DLS

### 4.3.2 Anchoring transition in the presence of the oligomers at the aqueous-LC interface

We then, performed experiments to determine if the amphiphilic oligomers would partition to LC interfaces and influence the ordering of LCs. To this end, LC films (10  $\mu\text{m}$  in thickness) were prepared by depositing nematic 4'-pentyl-4-biphenylcarbonitrile (5CB) into a gold TEM grid placed on a glass substrate functionalized with dimethyloctadecyl[3-(trimethoxysilyl)propyl] ammonium chloride (DMOAP). The DMOAP functionalization was performed to impose a homeotropic orientation of 5CB at the treated substrate<sup>40-41</sup>. Subsequently, the LC film was immersed into a bath containing 10 mM phosphate buffered saline (PBS) at pH 7.4 and the dimeric amphiphilic oligomer (Fig 4.3). We first investigated the influence of the dimeric oligomer dispersed in an aqueous solution on the orientation of 5CB at the LC/aqueous interface by characterizing optical appearance of the LC films using polarizing optical microscopy (POM)<sup>18-20</sup>. The LC film, when immersed under aqueous PBS (no oligomer), exhibited a Schlieren texture with dark brushes (Fig 4.3) that correspond to regions of the LC where the director is either parallel or perpendicular to one of the crossed polarizer<sup>20</sup>.

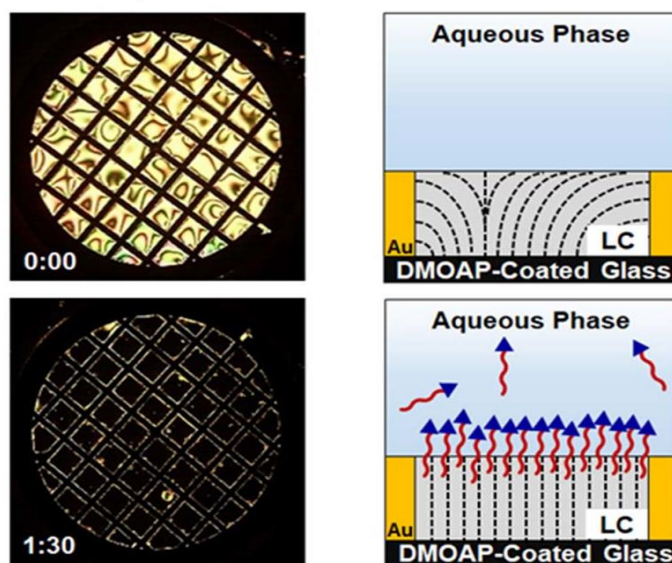


**Figure 4.4:** Polarized light microscopy images of aqueous-LC interface decorated with dimeric oligomers exhibiting a homeotropic anchoring transition

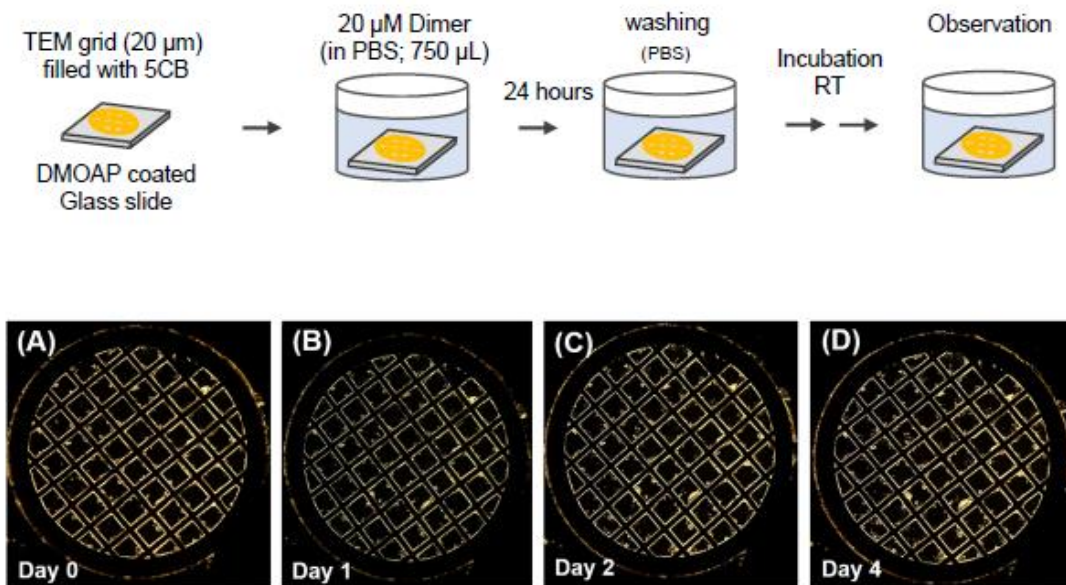


**Figure 4.5 :** Stability of aqueous-LC interface decorated with dimer (A) 0 day, (B) 1 day, (C) 2 day, and (D) 4 day.

Because 5C B anchors with a perpendicular orientation (homeotropic) at the DMOAP-coated glass substrate, the bright optical appearance of the LC film is consistent with past reports of planar anchoring of nematic 5CB at the interface to the bulk aqueous phases with neutral pH and low ionic strength<sup>7-10</sup>.

Next, we wanted to investigate the stability of the homeotropic anchoring. This was achieved by introducing the LC coated TEM into an aqueous solution of the dimeric amphiphile and observing the homeotropic anchoring over several days. It was found that the homeotropic anchoring so observed was stable up to four days. The resultant homeotropic anchoring was maintained for several days without showing evidence of birefringent domains (Fig 4.4).

#### **4.3.3 Binding-induced transition at the aqueous-LC interface in the presence of carbonic anhydrase and dimer**

We then, explored how the binding of a complementary protein, carbonic anhydrase would affect the anchoring transition of a film of 5CB. Our hypothesis was that the binding of the protein to the dimeric would result in desorption of the amphiphiles and would give rise to birefringent domains

typical of a planar anchoring. To test this, 5 CB coated TEM grids were incubated in an aqueous solution of the dimeric amphiphile. After attaining homeotropic anchoring, carbonic anhydrase was introduced into the system such that the moles of the ligand (sulfonamide) to the protein was 1: 1 and the anchoring transition resulting thereof, was monitored. It was found that the interface changed to bright from dark indicative of desorption of amphiphiles and thereby, binding of the dimeric amphiphile to the complementary ligand.

To test whether the desorption of the dimer from the LC interface was indeed due to the sulfonamide-bCA binding, we imaged the response of the aqueous- LC interface decorated with the dimer with non-complementary proteins, Bovine Serum Albumin (BSA) and Lysozyme at the same concentrations as bCA. The responses of the aqueous-LC interface to these non-complementary enzymes is shown in Fig 4.5. It was interesting to note that while lysozyme did not evoke a response in terms of an anchoring transition, BSA was found to induce a change in the LC ordering and this manifested in a bright field image of the LC film that was absent in case of lysozyme.

We reasoned that such an observation could arise due to the non-specific nature of the protein-ligand interaction and one important factor that needs to be accounted for is the electrostatic interaction between the non-specific enzymes and the sulfonamide<sup>48-49</sup>. The pI values of the proteins used in this study are given in Table 4.1. It is interesting to observe that both BSA and bCA that induce an ordering transition at the aqueous-LC interface have a pI of 5.4 and 5.3 respectively, while lysozyme that doesn't induce an ordering transition has a pI of 11.35



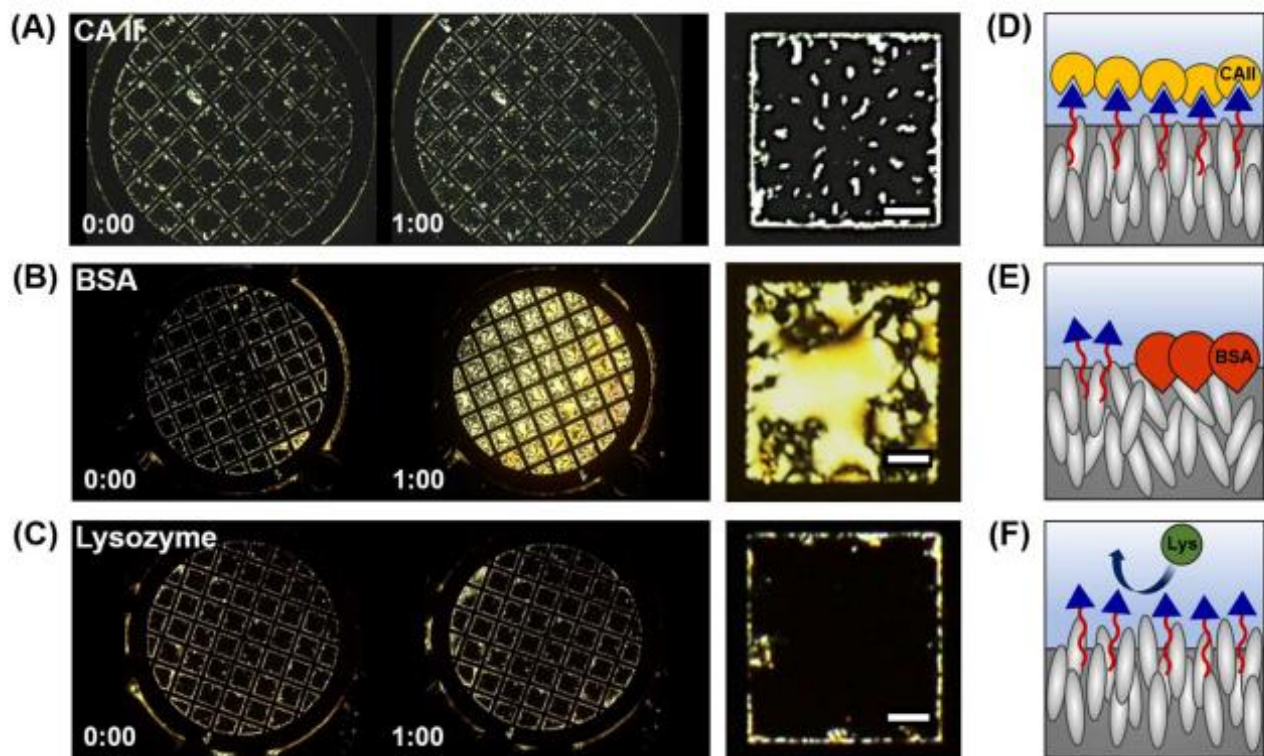


**Figure 4.6:** The images of the response of aqueous-LC interface decorated from H-dimer ( $20 \mu\text{M}$ ) with (A) Carbonic anhydrase II ( $4 \mu\text{M}$ ), (B) BSA ( $4 \mu\text{M}$ ), and (C) lysozyme ( $4 \mu\text{M}$ ). The schematic illustrations of the response of aqueous-LC interface to (D) Carbonic anhydrase II ( $4 \mu\text{M}$ ), (E) BSA ( $4 \mu\text{M}$ ), and (F) lysozyme ( $4 \mu\text{M}$ ). All magnified images were represented on the middle and white bar in the magnified images represented  $100 \mu\text{m}$ .

At pH 7.4, which is the pH at which the experiments are performed, BSA and bCA will have a net negative charge while lysozyme would have a net positive charge. If BSA and bCA did evoke a response at the aqueous-LC interface, this would mean that the LC itself should have a net positive charge for the non-specific interaction to occur.

To test if the LC response was indeed because of the electrostatic interactions between the LC interface and the proteins of interest, we recorded the zeta potential of 5 CB droplets in milliQ water, PBS at pH 7.4 and when incubated with 20  $\mu$ M dimer and found that the zeta potential values were -70, -37 and -40 mV respectively. In other words, the LC interface contains a net

**Table 1. Properties of Proteins Used in This Study**

	CA II	BSA	lysozyme
Origin	bovine	bovin	chicken
M.W. [kDa]	29	66	14
pI	5.4	5.3	11.35

**Table 2. Zeta Potential Measurement of Aqueous-LC Interfaces**

sample	Zeta potential [mV]*
5CB droplets in milliQ	-69.9 $\pm$ 0.8
5CB droplets in PBS	-37.1 $\pm$ 1.9
5CB droplets in 20 $\mu$ M Dimer	-40.0 $\pm$ 1.4

\*: mean  $\pm$  SD

**Table 4.2:** Molecular weights and pI values of proteins CA II, BSA and lysozyme (Table 1) and Zeta potential measurements of the LC-aqueous interface (Table 2)

negative charge when incubated with the dimer and this, rules out the possibility of there being electrostatics driven complex formation at the aqueous-LC interface. We further wanted to investigate if the non-specific binding of BSA on the aqueous-LC interface is blocked due to the binding between bCA and sulfonamide. To this end, we performed an experiment wherein we first decorated the LC interfaces with the dimeric amphiphiles and incubated it with bCA (0.4  $\mu$ M) for 2 hours. We then, introduced 1  $\mu$ M BSA into the system and observed the appearance of an

anchoring transition using Polarized Light Microscopy (PLM). Interestingly, we found that the non-specific response from BSA was completely suppressed suggesting that interfaces that are pre-saturated with bCA blocked any non-specific response from BSA. To test this hypothesis further, we performed a control experiment wherein the dimer decorated LC interfaces were treated with a premixed solution of bCA (1  $\mu\text{M}$ ) and BSA (1  $\mu\text{M}$ ). It was observed that even in this case, the non-specific response from BSA was indeed suppressed (Fig 4.6). Finally, we incubated the dimer decorated LC interfaces with a premixed solution lysozyme (1  $\mu\text{M}$ ) and BSA (1  $\mu\text{M}$ ) and found the appearance of bright domains corresponding to the non-specific binding of BSA with the dimer.

These experiments indeed, reveal that saturating the LC interface with a complementary binding

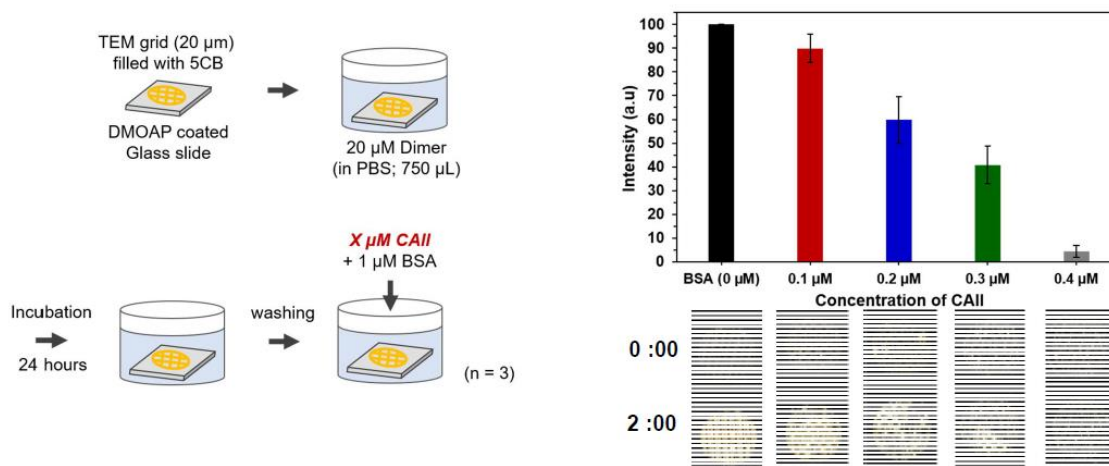


**Figure 4.7:** (A) The relative intensities of aqueous-LC interface decorated with dimer with different concentration of CA II and BSA

protein i.e. bCA suppresses the non-specific binding with other proteins. This is brought about because bCA binds faster to the dimer than BSA and hence, pre-saturates the LC interface. If this were to be true, then there would exist a threshold concentration of bCA below which the binding of BSA would not be suppressed.

To investigate this possibility, we incubated the dimer decorated LC interfaces with a premixed solution of bCA and BSA such that the concentrations of bCA were varied from 0-0.4  $\mu\text{M}$  while the concentration of BSA was fixed to be 1  $\mu\text{M}$ . We then, recorded the relative intensities of the aqueous-LC interfaces decorated with different concentrations of bCA and found that the threshold concentration of bCA required to block the non-specific binding with BSA was 0.4  $\mu\text{M}$  (Fig 4.7).

#### 4.3.4 Competitive inhibition experiment to determine kinetics of binding of complementary vs non-complementary proteins

To gain more insight into the specific binding between the sulfonamide-containing dimer and the protein bCA, we designed a competitive inhibition experiment. We use two commercially

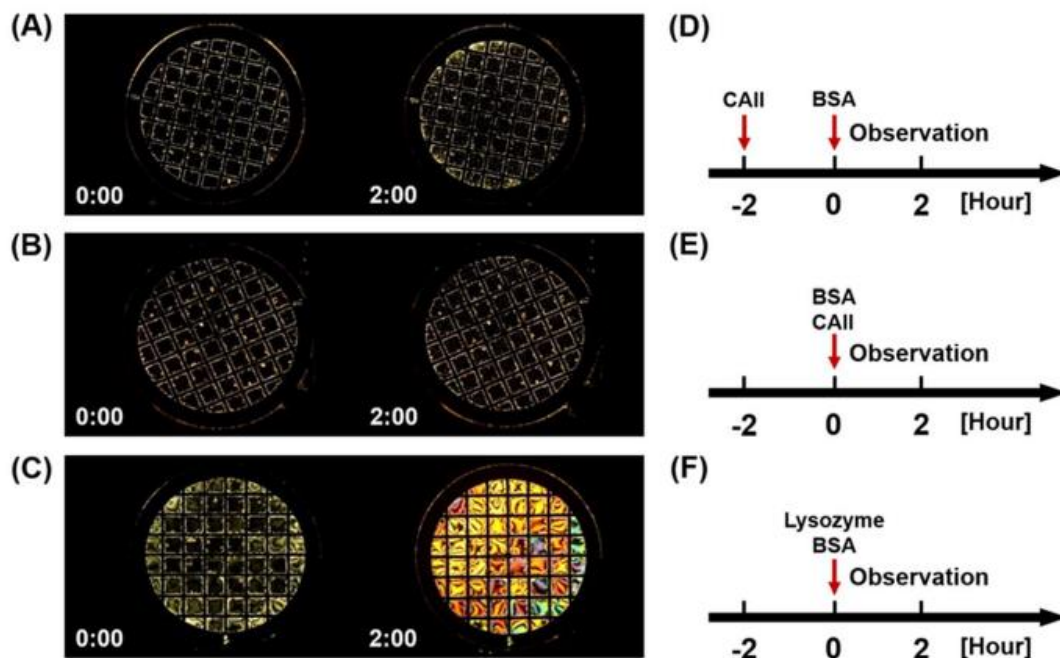


**Figure 4.8:** The polarized light microscopy images of anchoring transition of aqueous-LC interface decorated from dimer (20  $\mu\text{M}$ ) with (A) Carbonic anhydrase II (0.4  $\mu\text{M}$ ) – Dimer complex after contacting with BSA (1  $\mu\text{M}$ ), (B) Carbonic anhydrase II (1  $\mu\text{M}$ ) and BSA (1  $\mu\text{M}$ ) simultaneously, and (C) lysozyme (1  $\mu\text{M}$ ) and BSA (1  $\mu\text{M}$ ) simultaneously. Time interval to add CA II (0.4  $\mu\text{M}$ ), BSA (1  $\mu\text{M}$ ), and lysozyme (1  $\mu\text{M}$ ) onto the well. All samples were incubated for 2 hour and observed by polarized light microscopy.

available inhibitors ethoxzolamide and benzenesulfonamide that have  $K_D$  (dissociation constant) values of 0.1 nM and 970 nM respectively and the  $K_D$  values indicate that both these molecules

bind strongly to bCA compared to the sulfonamide moiety on the dimer which has a higher  $K_D$  value than the inhibitor molecules<sup>50</sup>.

We hypothesize that if the anchoring transition at the LC interface is brought about indeed by the specificity in binding between the dimer molecule and bCA, then an inhibitor molecule that has a higher propensity of binding should be able to replace the dimer molecules from binding to bCA. To investigate this possibility, we performed an experiment wherein we incubated the dimer decorated aqueous-LC interfaces with bCA (0.4  $\mu\text{M}$ ) and then subjected them to a sequential addition of the non-specific protein, BSA (1  $\mu\text{M}$ ) followed by 4  $\mu\text{M}$  ethoxzolamide or benzenesulfonamide.

We then, monitored the relative intensities of the interfaces with time with the inhibitors. If our hypothesis above were to be true, we should observe a bright domain at the LC interface since the inhibitors would deplete the interface of any bCA and that would then, facilitate the non-specific binding of BSA to the dimer at the aqueous-LC interface. We indeed, found that the release of bCA was enhanced in the presence of inhibitors such as ethoxzolamide and benzenesulfonamide which manifested as a bright domain in the LC film corresponding to the non-specific binding of BSA as was revealed by PLM.

### 4.3.5 Digestion of carbonic anhydrase using Thermolysin to probe non-specific binding

Finally, we used an enzyme Thermolysin (TLN) that could preferentially digest bCA and would allow BSA to bind non-specifically to the dimer at the aqueous-LC interface. Thermolysin is an

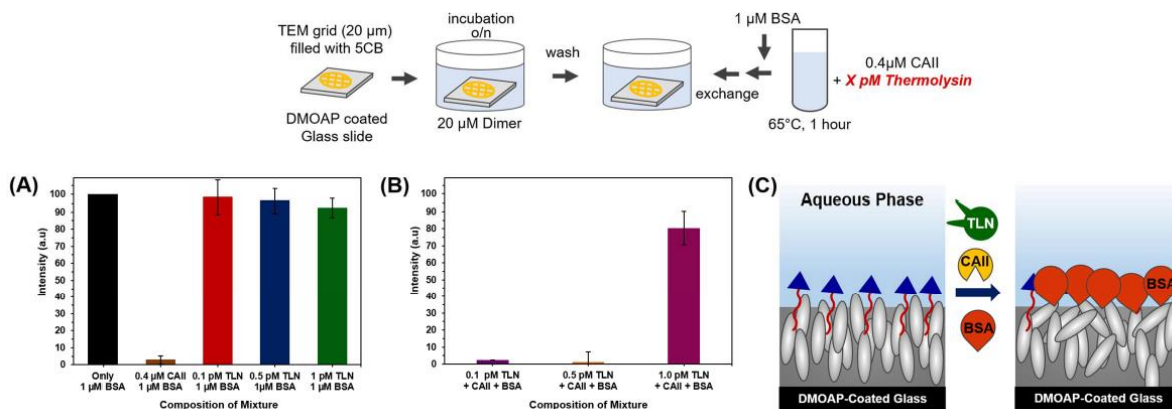


**Figure 4.9:** The relative intensity of aqueous-LC interface of (A) All control samples, (B) The relative intensity of aqueous-LC interface with different concentration of TLN, (C) the schematic illustration of experimental system with TLN, CA II, and BSA, (D) the schematic illustration of role of TLN in the mixture of CA II (0.4  $\mu$ M) and BSA (1  $\mu$ M)

extracellular metalloendopeptidase containing four calcium ions and uses Zinc and Calcium as cofactors<sup>50</sup>. The enzyme hydrolyzes peptide bonds on the N-terminal side of hydrophobic amino acid residues and is quite stable up to 80  $^{\circ}$ C<sup>51</sup>.

A solution of bCA and Thermolysin was obtained by mixing 0.4  $\mu$ M bCA and 0.1, 0.5 and 1 pM TLN respectively and this solution was incubated at 65  $^{\circ}$ C for one hour. To this, 1  $\mu$ M BSA was added and the resulting solution was added to the dimer decorated aqueous-LC interface. Following this, the relative intensity of aqueous-LC interface was monitored with different concentrations of TLN (Fig 4.8). It was observed that upon increasing TLN concentration, the intensity of the bright domain increased suggesting that TLN indeed digests bCA to allow for the non-specific binding of BSA and the threshold concentration of TLN required to digest bCA was found to be 0.1 pM. This mechanism of degradation was also corroborated using gel

electrophoresis experiments. We found that similar concentrations of TLN (as the experiment mentioned above) when incubated with 0.4  $\mu\text{M}$  bCA at 65 °C for one hour resulted in lighter bands in gel electrophoresis whose intensity could then be extrapolated to relate to the extent of degradation.

#### **4.4 Conclusions**

In conclusion, dimer was the only amphiphilic oligomer that was found to adsorb at the aqueous-LC interface to trigger a homeotropic anchoring transition. Tiny particles appeared on the interface in response to the addition of bCA and in case of BSA, the interface changed to bright. The specific binding between CA II and sulfonamide on aqueous-LC interface was found to prevent the non-specific binding of BSA, and the threshold concentration of CA II was calculated to be 0.4  $\mu\text{M}$ . In addition, CA II was found to bind to sulfonamide on the interface stronger than BSA resulting in the blocking of non-specific binding of BSA on aqueous-LC interface. This mechanism was corroborated using addition of inhibitor which enhanced the release of CA II from aqueous-LC interface by modulating the strength of binding. Digestion of bCA by an enzyme Thermolysin was found to induce an anchoring transition from homeotropic to planar owing to the non-specific binding with BSA. The design rules established here provide insight into the rational design of oligomers that can be used as triggers to create responsive LCs wherein microscopic events could be translated into macroscopic observables.

## 4.5 References

- (1) A) Yang, D.-K.; Wu, S.-T., *Fundamentals of Liquid Crystal Devices*. John Wiley & Sons, Ltd.: Chichester, 2006. B) Zhuang, J.; Gordon, M.; Ventura, J.; Li, L. Thayumanavan, S. "Multi-Stimuli Responsive Macromolecules and Their Assemblies" *Chem. Soc. Rev.* **2013**, *42*, 7421-7435.
- (2) Yeh, P.; Gu, C., *Optics of liquid crystal displays*. John Wiley & Sons, Inc.: New York, 1999.
- (3) Gwag, J. S.; Kim, Y. K.; Lee, C. H.; Kim, J. H., Realization of Multi-Stable Ground States in a Nematic Liquid Crystal by Surface and Electric Field Modification. *Sci. Rep.* **2015**, *5*, 11368.
- (4) Kim, Y.-K.; Senyuk, B.; Lavrentovich, O. D., Molecular reorientation of a nematic liquid crystal by thermal expansion. *Nat Commun* **2012**, *3*, 1133.
- (5) Ohm, C.; Brehmer, M.; Zentel, R., Liquid Crystalline Elastomers as Actuators and Sensors. *Adv. Mater.* **2010**, *22* (31), 3366-3387.
- (6) Fong, W. K.; Hanley, T.; Boyd, B. J., Stimuli responsive liquid crystals provide 'on-demand' drug delivery in vitro and in vivo. *J. Control. Release* **2009**, *135* (3), 218-226.
- (7) Kim, Y.-K.; Wang, X.; Mondkar, P.; Bukusoglu, E.; Abbott, N. L., Self-reporting and self-regulating responsive liquid crystals. *Nature* **2018**, DOI: 10.1038/s41586-018-0098-y.
- (8) Nazaruk, E.; Miszta, P.; Filipek, S.; Gorecka, E.; Landau, E. M.; Bilewicz, R., Lyotropic Cubic Phases for Drug Delivery: Diffusion and Sustained Release from the Mesophase Evaluated by Electrochemical Methods. *Langmuir* **2015**, *31* (46), 12753-12761.
- (9) Kwon, J.-Y.; Khan, M.; Park, S.-Y., pH-Responsive liquid crystal double emulsion droplets prepared using microfluidics. *RSC Adv.* **2016**, *6* (61), 55976-55983.



- (10) Bi, X. Y.; Hartono, D.; Yang, K. L., Real-Time Liquid Crystal pH Sensor for Monitoring Enzymatic Activities of Penicillinase. *Adv. Funct. Mater.* **2009**, *19* (23), 3760-3765.
- (11) Kim, Y.-K.; Huang, Y.; Tsuei, M.; Wang, X.; Gianneschi, N. C.; Abbott, N. L., Multi-Scale Responses of Liquid Crystals Triggered by Interfacial Assemblies of Cleavable Homopolymers. *ChemPhysChem.* **2018**, *19*, 1-10
- (12) Gelebart, A. H.; Mulder, D. J.; Varga, M.; Konya, A.; Vantomme, G.; Meijer, E. W.; Selinger, R. L. B.; Broer, D. J., Making waves in a photoactive polymer film. *Nature* **2017**, *546* (7660), 632-636.
- (13) Yamada, M.; Kondo, M.; Mamiya, J. I.; Yu, Y. L.; Kinoshita, M.; Barrett, C. J.; Ikeda, T., Photomobile polymer materials: Towards light-driven plastic motors. *Angew. Chem.-Int. Edit.* **2008**, *47* (27), 4986-4988.
- (14) Barhoumi, A.; Liu, Q.; Kohane, D. S., Ultraviolet light-mediated drug delivery: Principles, applications, and challenges. *J. Control. Release* **2015**, *219*, 31-42.
- (15) Carlton, R. J.; Gupta, J. K.; Swift, C. L.; Abbott, N. L., Influence of Simple Electrolytes on the Orientational Ordering of Thermotropic Liquid Crystals at Aqueous Interfaces. *Langmuir* **2012**, *28*, 31-36.
- (16) Zou, J.; Bera, T.; Davis, A. A.; Liang, W.; Fang, J., Director Configuration Transitions of Polyelectrolyte Coated Liquid-Crystal Droplets. *J. Phys. Chem. B* **2011**, *115* (29), 8970-8974.
- (17) Popov, P.; Mann, E. K.; Jakli, A., Thermotropic liquid crystal films for biosensors and beyond. *J. Mat. Chem. B* **2017**, *5* (26), 5061-5078.
- (18) Bukusoglu, E.; Pantoja, M. B.; Mushenheim, P. C.; Wang, X.; Abbott, N. L., Design of responsive and active (soft) materials using liquid crystals. *Annual Review of Chemical and Biomolecular Engineering* **2016**, *7*, 163-196.

- (19) Miller, D. S.; Wang, X. G.; Abbott, N. L., Design of Functional Materials Based on Liquid Crystalline Droplets. *Chem. Mater.* **2014**, *26* (1), 496-506.
- (20) Carlton, R. J.; Hunter, J. T.; Miller, D. S.; Abbasi, R.; Mushenheim, P. C.; Tan, L. N.; Abbott, N. L., Chemical and biological sensing using liquid crystals. *Liq. Cryst. Rev.* **2013**, *1* (1), 29-51.
- (21) Sidiq, S.; Prasad, G.; Mukhopadhaya, A.; Pal, S. K., Poly(L-lysine)-Coated Liquid Crystal Droplets for Cell-Based Sensing Applications. *J. Phys. Chem. B* **2017**, *121* (16), 4247-4256.
- (22) Bera, T.; Deng, J.; Fang, J., Protein-Induced Configuration Transitions of Polyelectrolyte-Modified Liquid Crystal Droplets. *J. Phys. Chem. B* **2014**, *118* (18), 4970-4975.
- (23) Kinsinger, M. I.; Sun, B.; Abbott, N. L.; Lynn, D. M., Reversible control of ordering transitions at aqueous/liquid crystal interfaces using functional amphiphilic polymers. *Adv. Mater.* **2007**, *19* (23), 4208-4212.
- (24) Lockwood, N. A.; Gupta, J. K.; Abbott, N. L., Self-assembly of amphiphiles, polymers and proteins at interfaces between thermotropic liquid crystals and aqueous phases. *Surf. Sci. Rep.* **2008**, *63* (6), 255-293.
- (25) Alino, V. J.; Pang, J.; Yang, K. L., Liquid Crystal Droplets as a Hosting and Sensing Platform for Developing Immunoassays. *Langmuir* **2011**, *27* (19), 11784-11789.
- (26) Fletcher, P. D. I.; Kang, N.-G.; Paunov, V. N., UV Polymerisation of Surfactants Adsorbed at the Nematic Liquid Crystal-Water Interface Produces an Optical Response. *ChemPhysChem* **2009**, *10* (17), 3046-3053.
- (27) Kleman, M.; Lavrentovich, O. D., *Soft Matter Physics: An Introduction*. Springer: New York, 2003.
- (28) de Gennes, P. G.; Prost, J., *The Physics of Liquid Crystals*. Clarendon Press: Oxford, 1993.

- (29) Kim, Y.-K.; Shiyonovskii, S. V.; Lavrentovich, O. D., Morphogenesis of defects and tactoids during isotropic nematic phase transition in self assembled lyotropic chromonic liquid crystals. *J. Phys.: Condens. Matter* **2013**, *25*, 404202.
- (30) Wood, T. A.; Lintuvuori, J. S.; Schofield, A. B.; Marenduzzo, D.; Poon, W. C. K., A self-quenched defect glass in a colloid-nematic liquid crystal composite. *Science* **2011**, *334*, 79-83.
- (31) Dierking, I., *Textures of Liquid Crystals*. Wiley-VCH Verlag GmbH & Co. KGaA: New York, 2004.
- (32) Demus, D.; Goodby, J.; Gray, G. W.; Spiess, H.-W.; Vill, V., *Handbook of Liquid Crystals*. Wiley-VCH Verlag GmbH: New York, 1998; Vol. Vol. 2
- (33) Omer, M.; Khan, M.; Kim, Y. K.; Lee, J. H.; Kang, I.-K.; Park, S.-Y., Biosensor utilizing a liquid crystal/water interface functionalized with poly(4-cyanobiphenyl-4'-oxyundecylacrylate-b-((2-dimethyl amino) ethyl methacrylate)). *Colloid Surf. B-Biointerfaces* **2014**, *121*, 400-408.
- (34) Kim, J.; Khan, M.; Park, S.-Y., Glucose Sensor using Liquid-Crystal Droplets Made by Microfluidics. *ACS Appl. Mater. Interfaces* **2013**, *5* (24), 13135-13139.
- (35) Seo, J.-M.; Khan, W.; Park, S.-Y., Protein detection using aqueous/LC interfaces decorated with a novel polyacrylic acid block liquid crystalline polymer. *Soft Matter* **2012**, *8* (1), 198-203.
- (36) Khan, W.; Choi, J. H.; Kim, G. M.; Park, S. Y., Microfluidic formation of pH responsive 5CB droplets decorated with PAA-b-LCP. *Lab Chip* **2011**, *11* (20), 3493-3498.
- (37) Lee, D.-Y.; Seo, J.-M.; Khan, W.; Kornfield, J. A.; Kurji, Z.; Park, S.-Y., pH-responsive aqueous/LC interfaces using SGLCP-b-polyacrylic acid block copolymers. *Soft Matter* **2010**, *6* (9), 1964-1970.
- (38) Utracki, L. A.; Jamieson, A. M., *Polymer Physics: From Suspensions to Nanocomposites and Beyond*. John Wiley & Sons, INC.: Hoboken, New Jersey, 2010.

- (39) Scruggs, N. R.; Kornfield, J. A., Synergistic ordering of side-group liquid crystal polymer and small molecule liquid crystal: Order and phase Behavior of nematic polymer solutions. *Macromol. Chem. Phys.* **2007**, *208* (19-20), 2242-2253.
- (40) Ryzhkova, A. V.; Musevic, I., Particle size effects on nanocolloidal interactions in nematic liquid crystals. *Phys Rev E* **2013**, *87* (3), 032501.
- (41) Conradi, M.; Ravnik, M.; Bele, M.; Zorko, M.; Zumer, S.; Musevic, I., Janus nematic colloids. *Soft Matter* **2009**, *5* (20), 3905-3912.
- (42) Raghupathi, K. R.; Guo, J.; Munkhbat, O.; Rangadurai, P.; Thayumanavan, S. Supramolecular Disassembly of Facially Amphiphilic Dendrimer Assemblies in Response to Physical, Chemical, and Biological Stimuli. *Acc. Chem. Res.* **2014**, *47*, 2200–2211.
- (43) Israelachvili, J. N.; Mitchell, D. J.; Ninham, B. W. Theory of self-assembly of hydrocarbon amphiphiles into micelles and bilayers. *J. Chem. Soc., Faraday Trans II.* **1976**, *72*, 1525–1568.
- (44) Evans, D. F.; Ninham, B. W. Molecular forces in the self-organization of amphiphiles. *J. Phys. Chem.* **1986**, *90*, 226–234.
- (45) Nagarajan, R. Molecular packing parameter and surfactant self-assembly: The neglected role of the surfactant tail. *Langmuir.* **2002**, *18*, 31–38
- (46) Azagarsamy, M. A.; Yesilyurt, V.; Thayumanavan, S. Disassembly of dendritic micellar containers due to protein binding. *J. Am. Chem. Soc.* **2010**, *132*, 4550–4551.
- (47) Yesilyurt, V.; Ramireddy, R.; Azagarsamy, M. A.; Thayumanavan, S. Accessing lipophilic ligands in dendrimer-based amphiphilic supramolecular assemblies for protein-induced disassembly. *Chem. Eur. J.* **2012**, *18*, 223–229.
- (48) (a) Amado Torres, D.; Garzoni, M.; Subrahmanyam, A.; Pavan, G. M.; Thayumanavan, S. Protein-Triggered Supramolecular Disassembly: Insights Based on Variations in Ligand Location

- in Amphiphilic Dendrons *J. Am. Chem. Soc.* 2014, 136, 5385–5399. (b) Azagarsamy, M. A.; Yesilyurt, V.; Thayumanavan, S. Disassembly of Dendritic Micellar Containers Due to Protein Binding *J. Am. Chem. Soc.* **2010**, 132, 4550–4551.
- (49) Krishnamurthy, V. M.; Kaufman, G. K.; Urbach, A. R.; Gitlin, I.; Gudiksen, K. L.; Weibel, D. B.; Whitesides, G. M. Intrinsic thermodynamics of sulfonamide inhibitor binding to human carbonic anhydrases I and II *Chem. Rev.* **2008**, 108, 946–1051.
- (50) Holmes MA, Matthews BW Structure of thermolysin refined at 1.6 Å resolution. *J. Mol. Biol.* **1982**, 160 (4), 623–639.
- (51) Matthews BW, Weaver LH, Kester WR (1974). "The conformation of thermolysin". *J. Biol. Chem.* **1974**, 249 (24), 8030–8044.

4.6 NMR spectrum of molecules

15

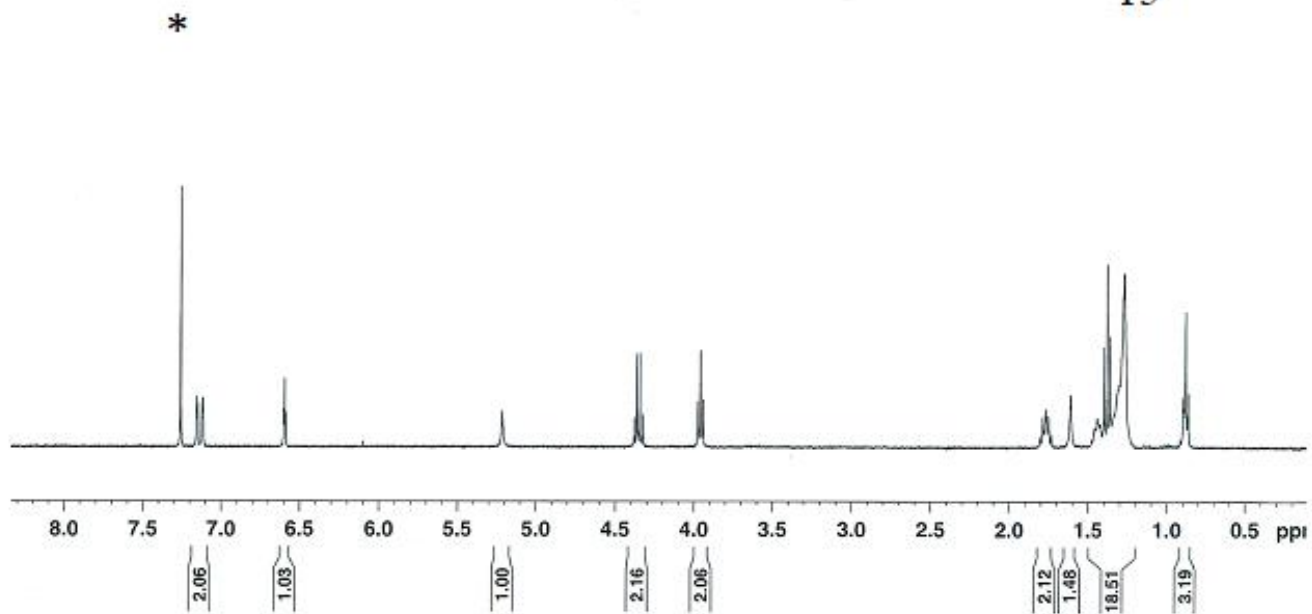
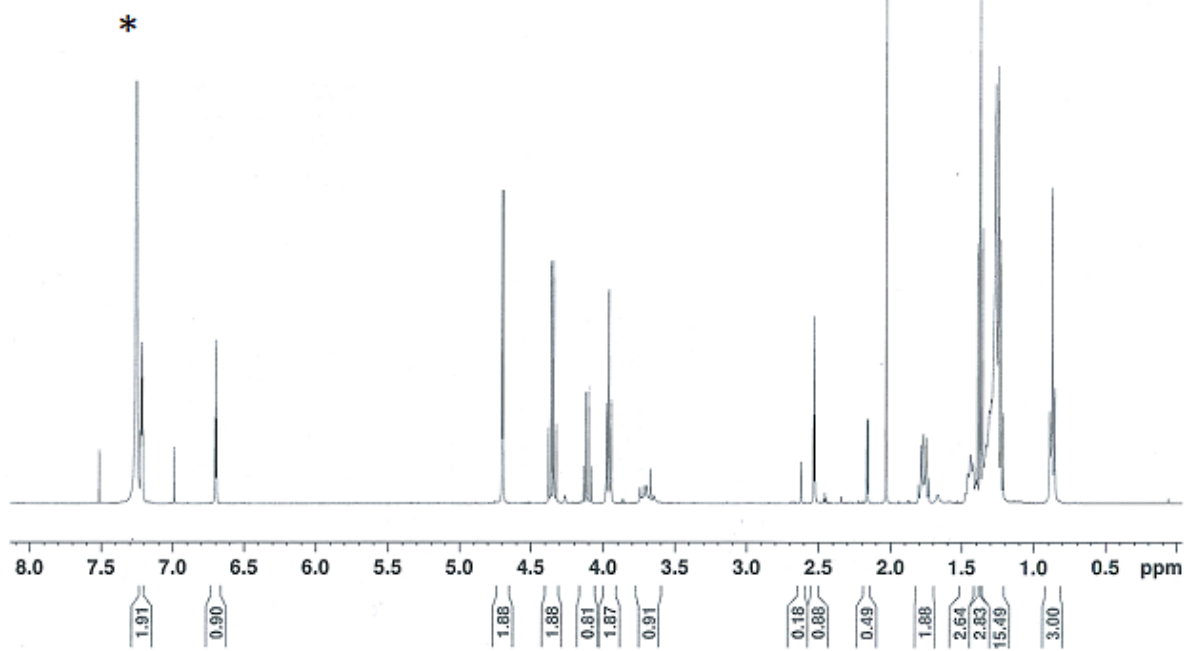


Figure 4.10:  $^1\text{H}$  NMR of molecules 15(top) and 14(bottom)

14



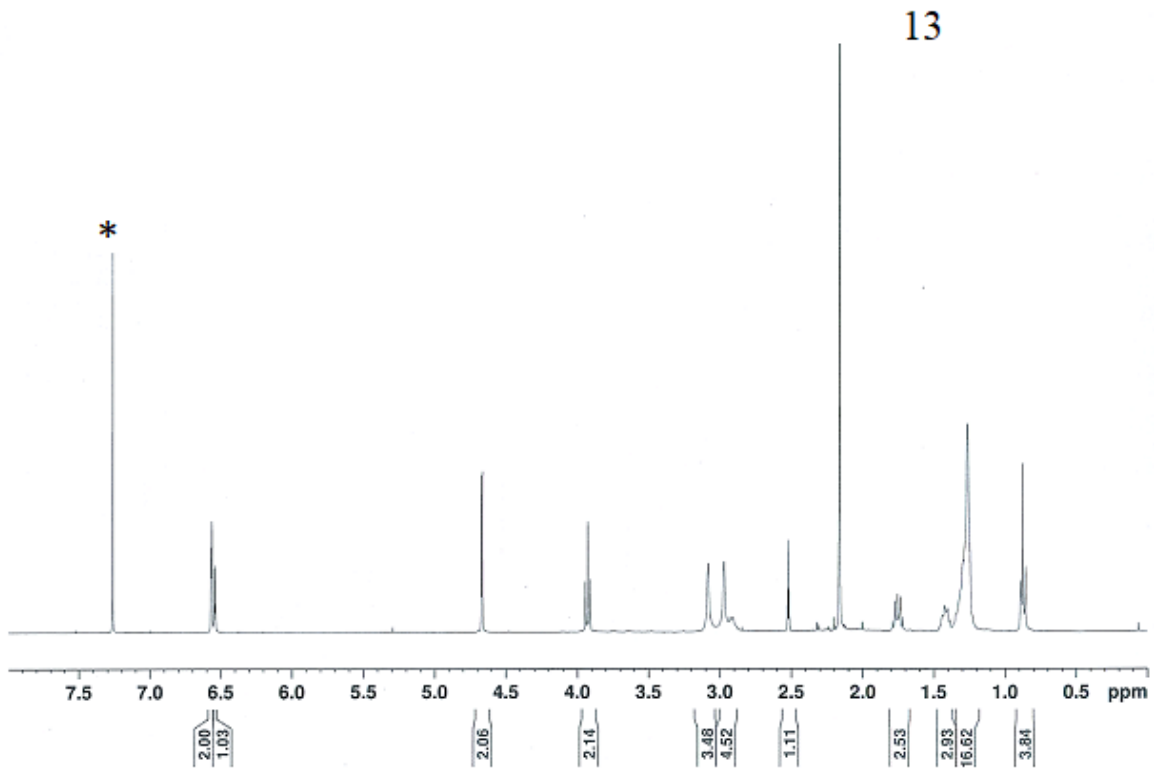
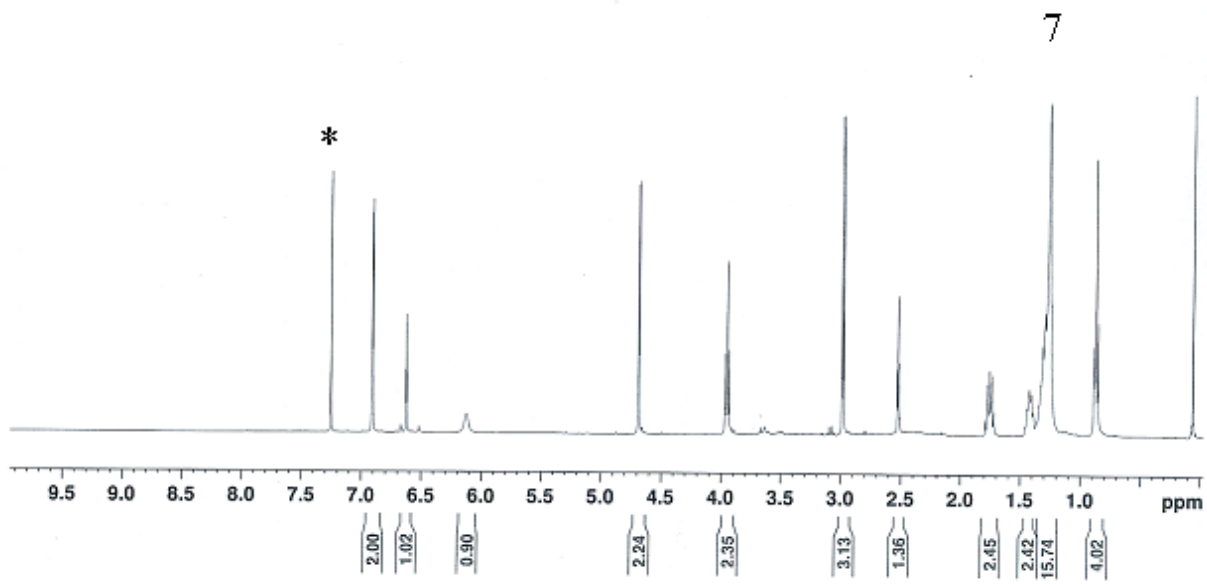


Figure 4.11:  $^1\text{H}$  NMR of molecules 13(top) and 7(bottom)



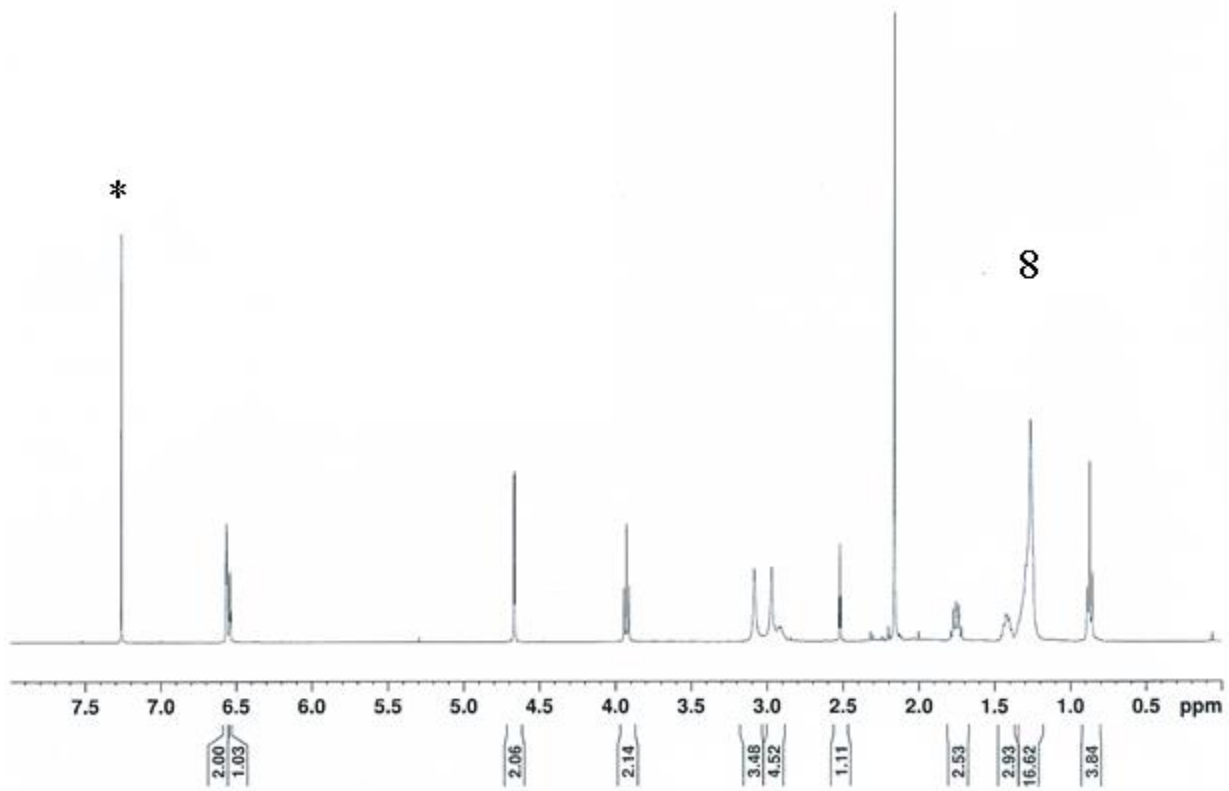
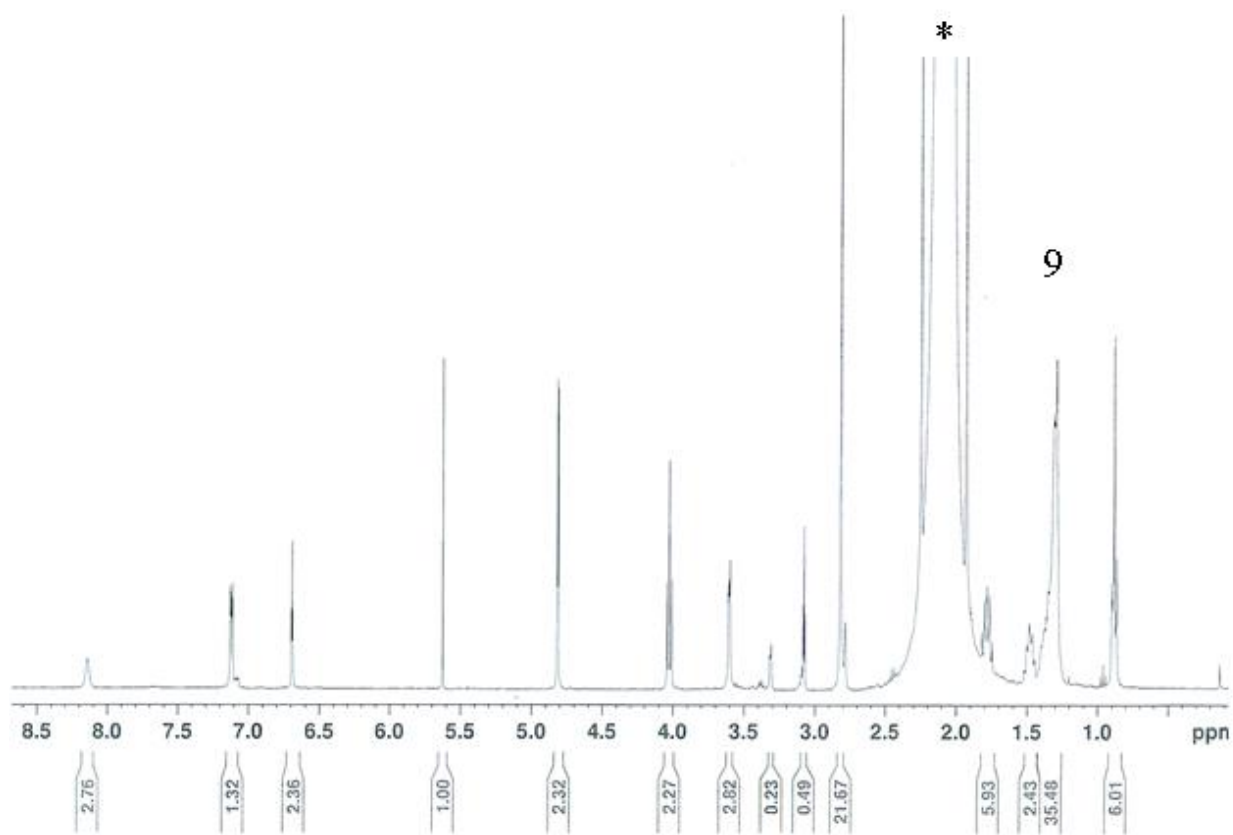


Figure 4.12:  $^1\text{H}$  NMR of molecules 8(top) and 9(bottom)





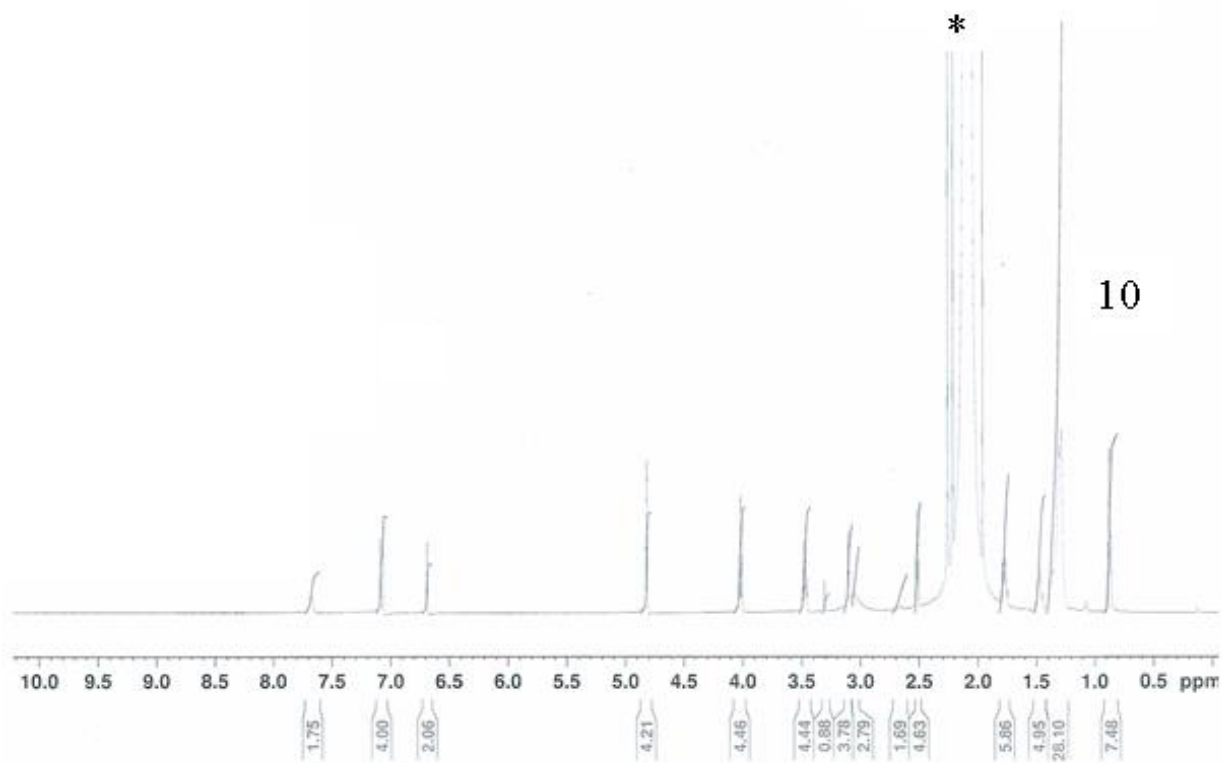
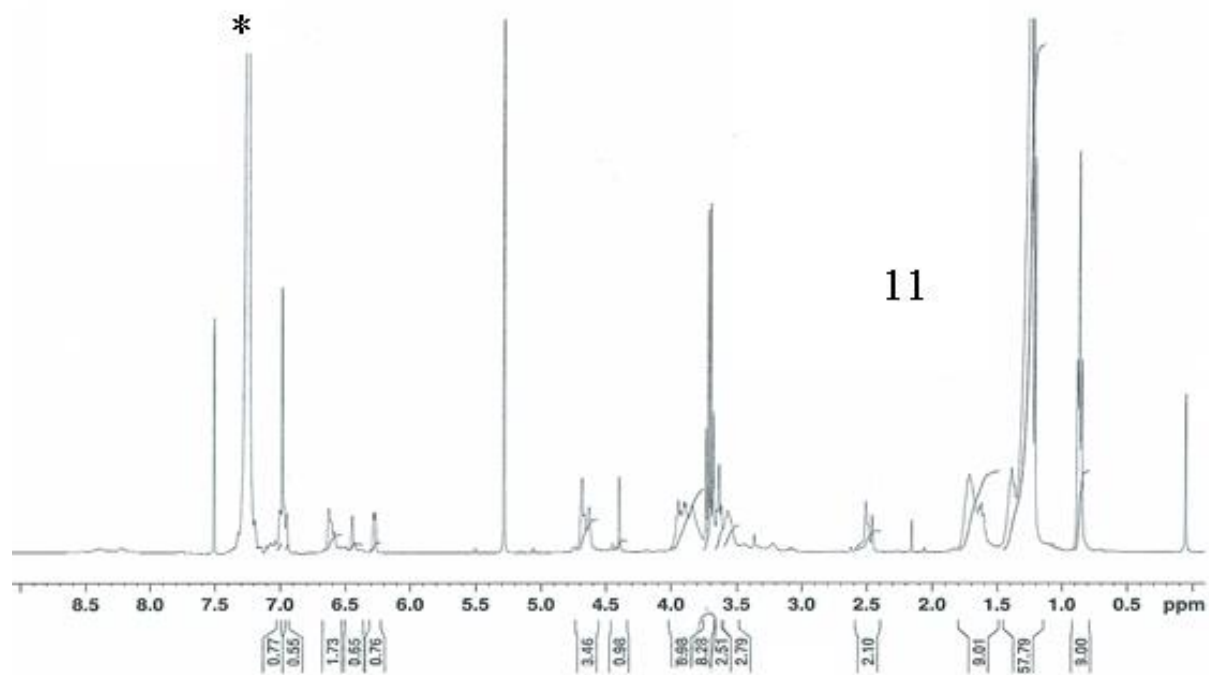


Figure 4.13:  $^1\text{H}$  NMR of molecules 10(top) and 11(bottom)



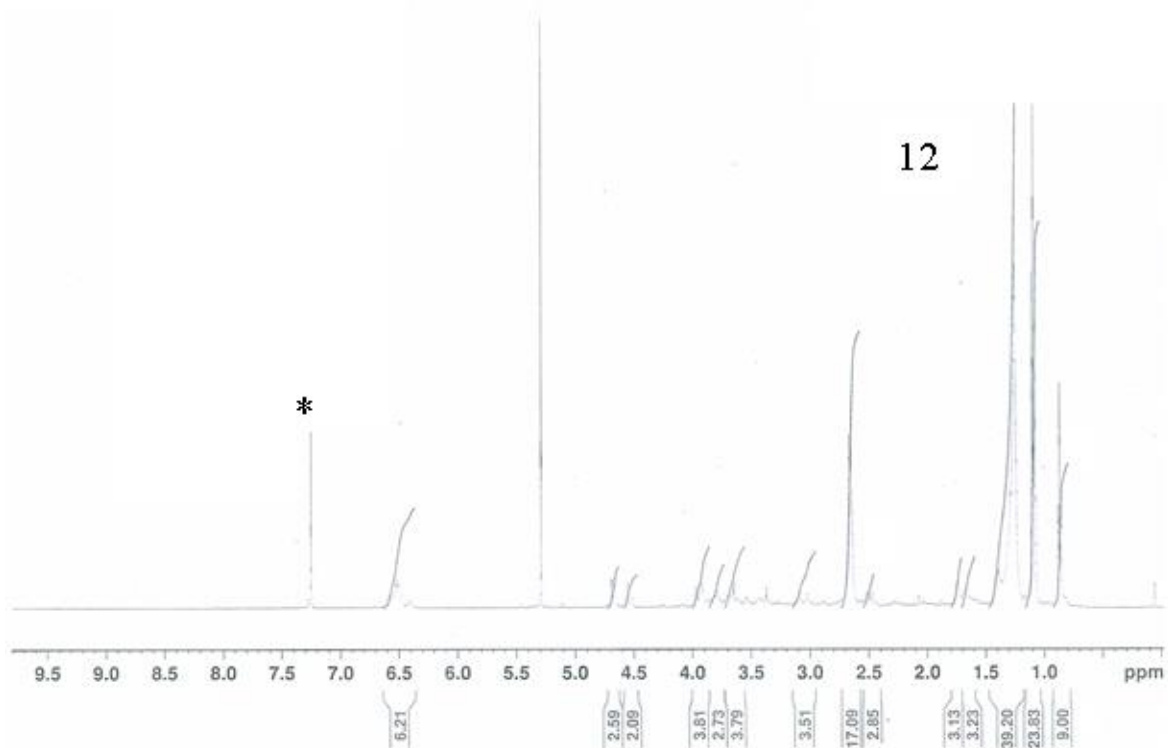
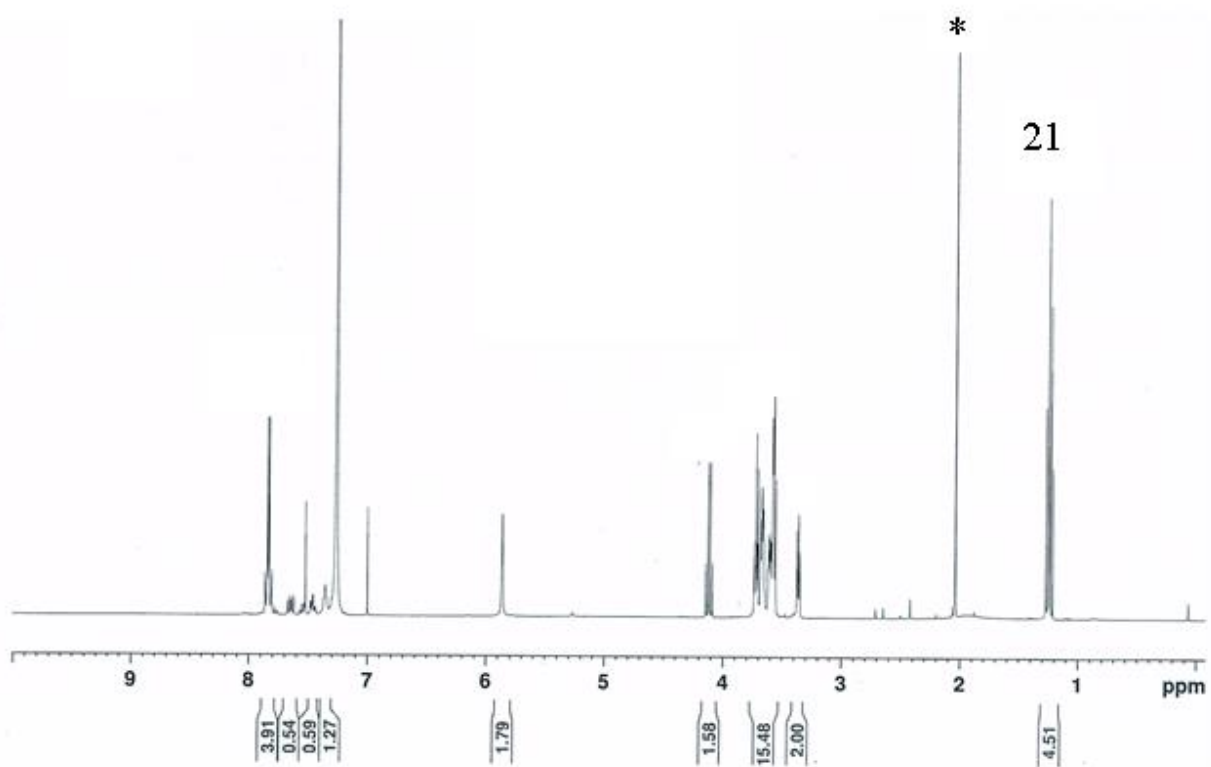


Figure 4.14:  $^1\text{H}$  NMR of molecules 12(top) and 21(bottom)



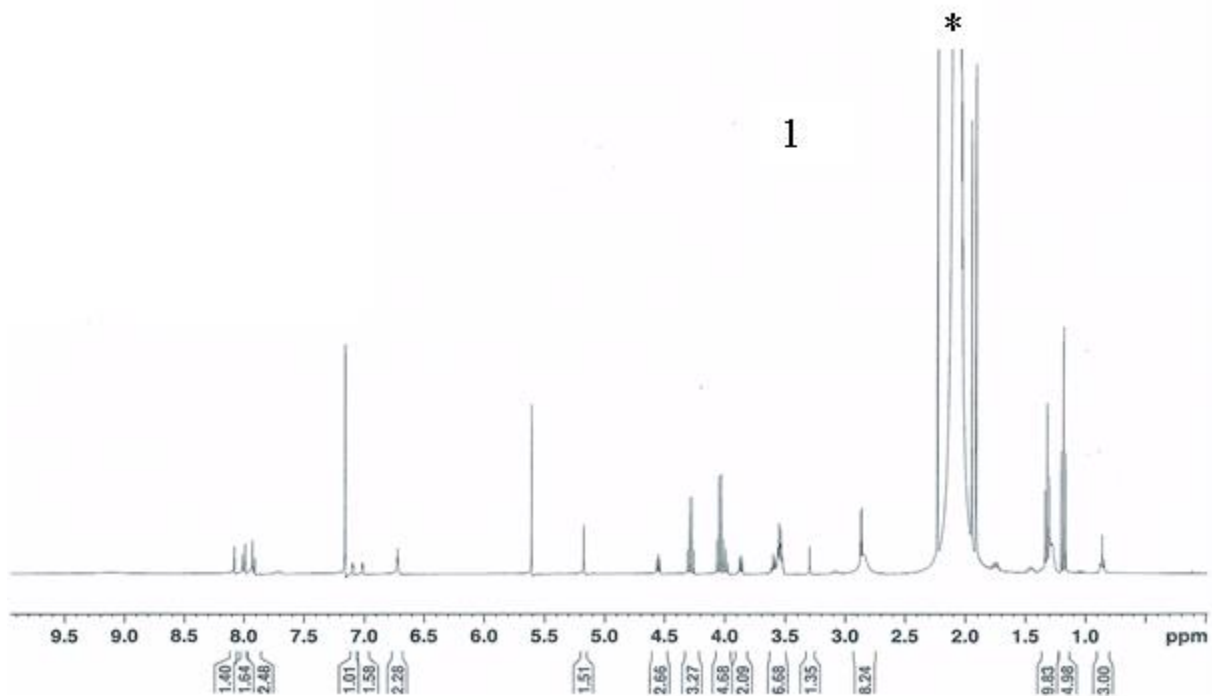
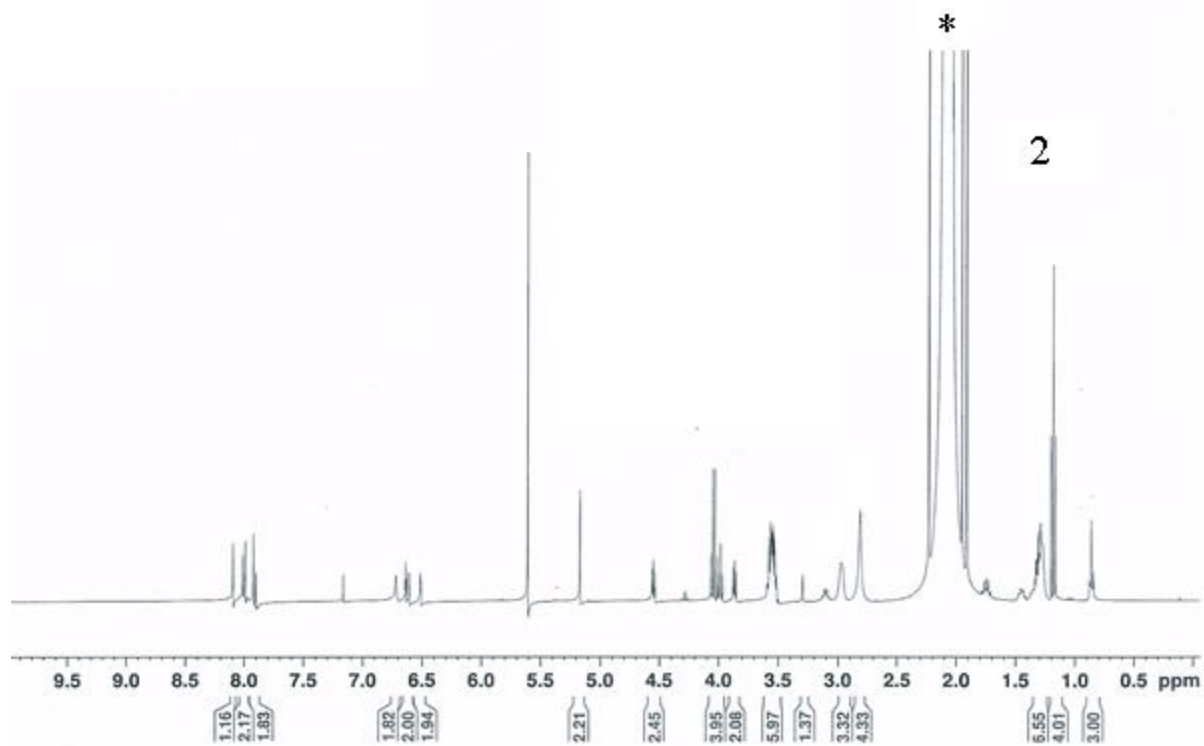


Figure 4.15:  $^1\text{H}$  NMR of molecules 1(top) and 2(bottom)



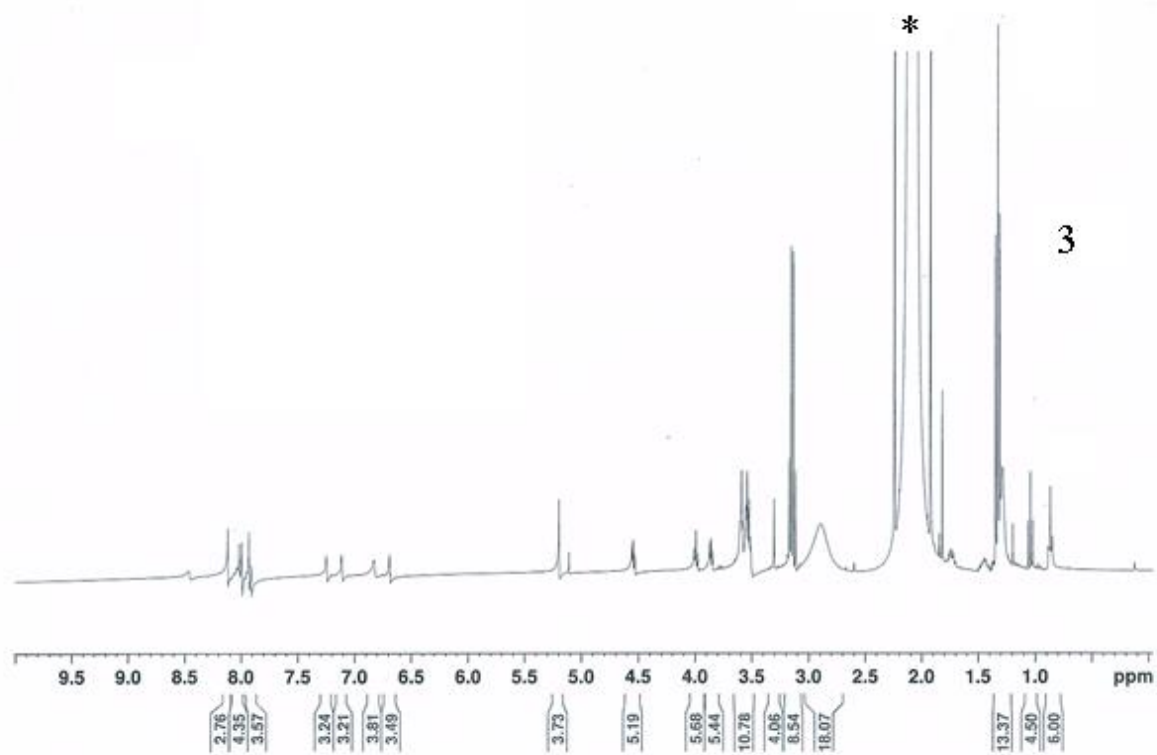
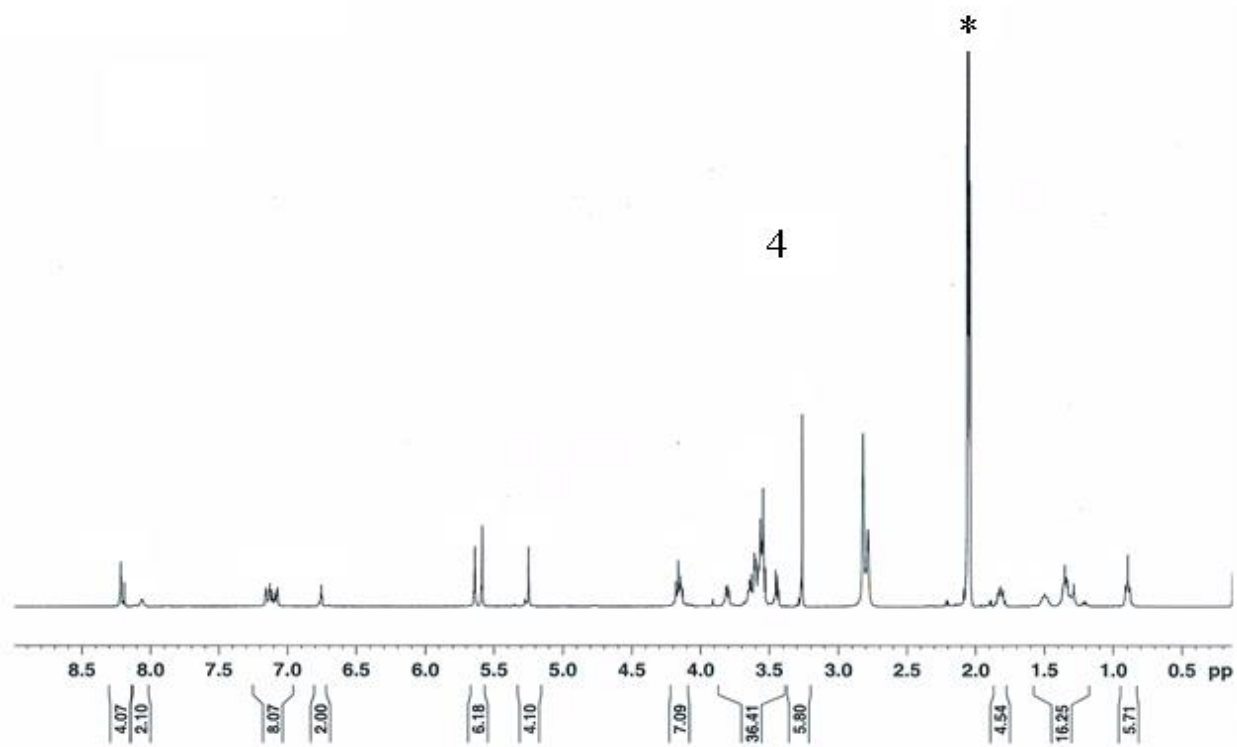


Figure 4.16:  $^1\text{H}$  NMR of molecules 3(top) and 4(bottom)



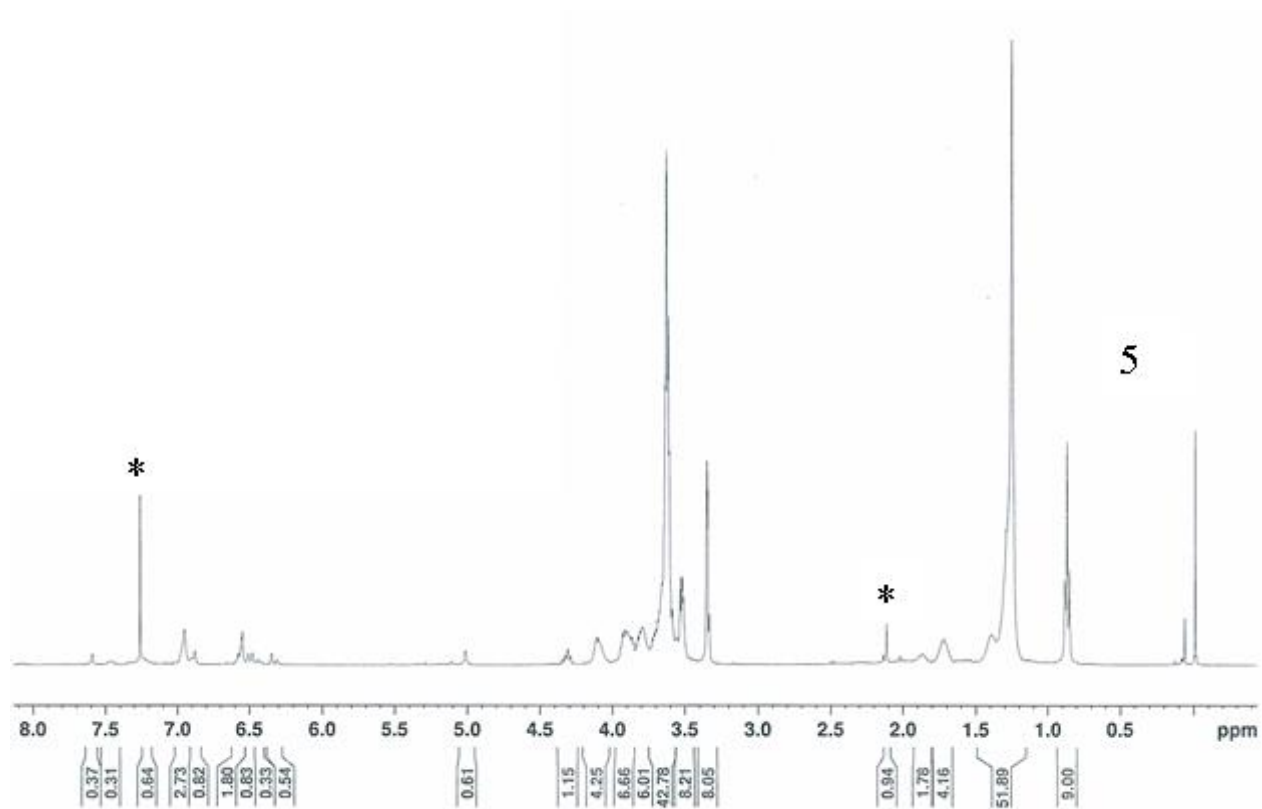
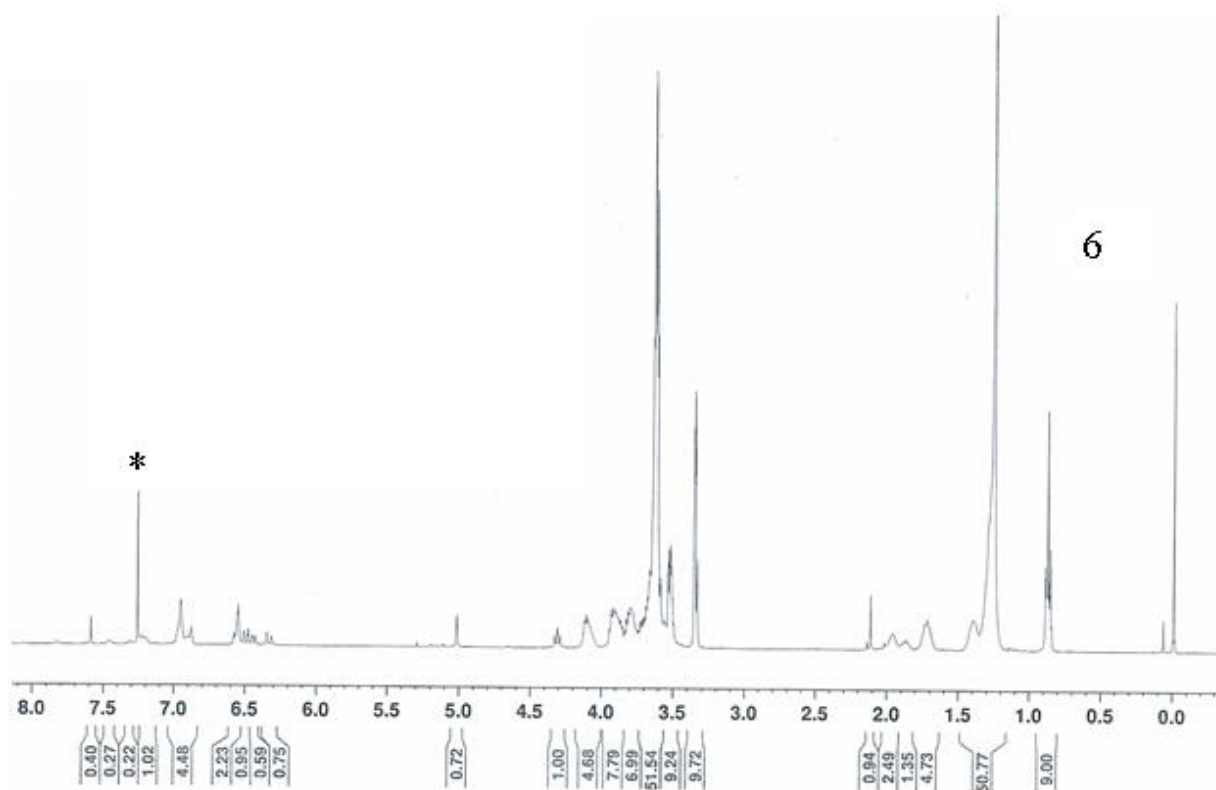


Figure 4.17:  $^1\text{H}$  NMR of molecules 5(top) and 6(bottom)



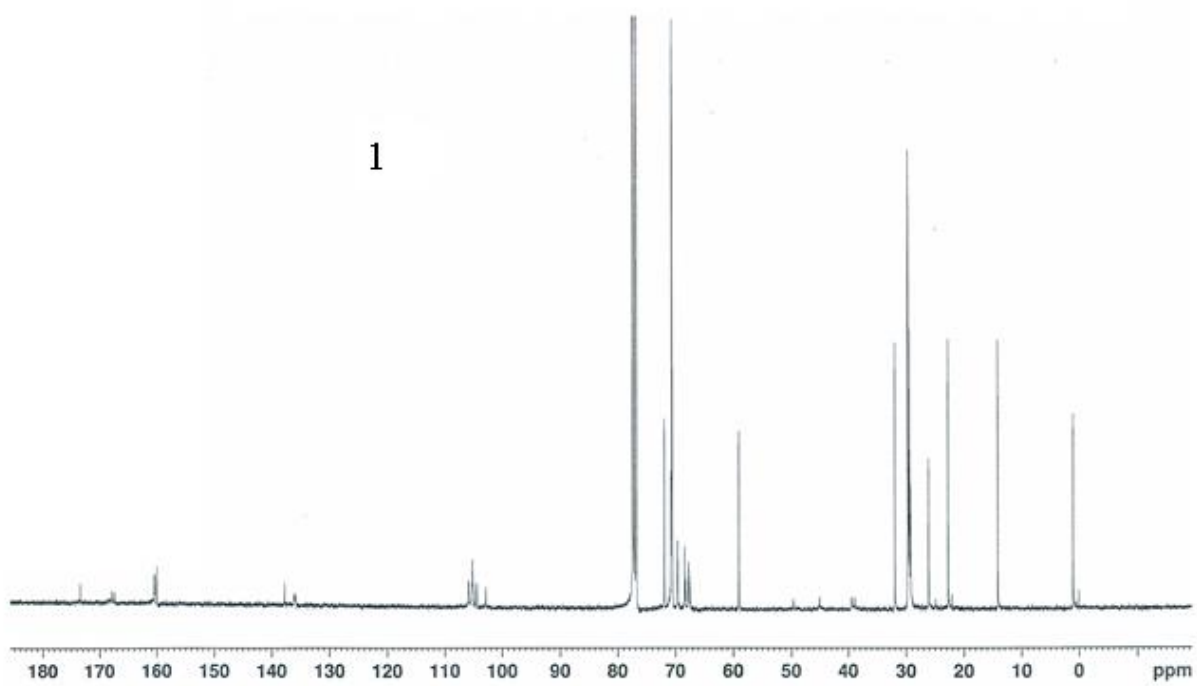
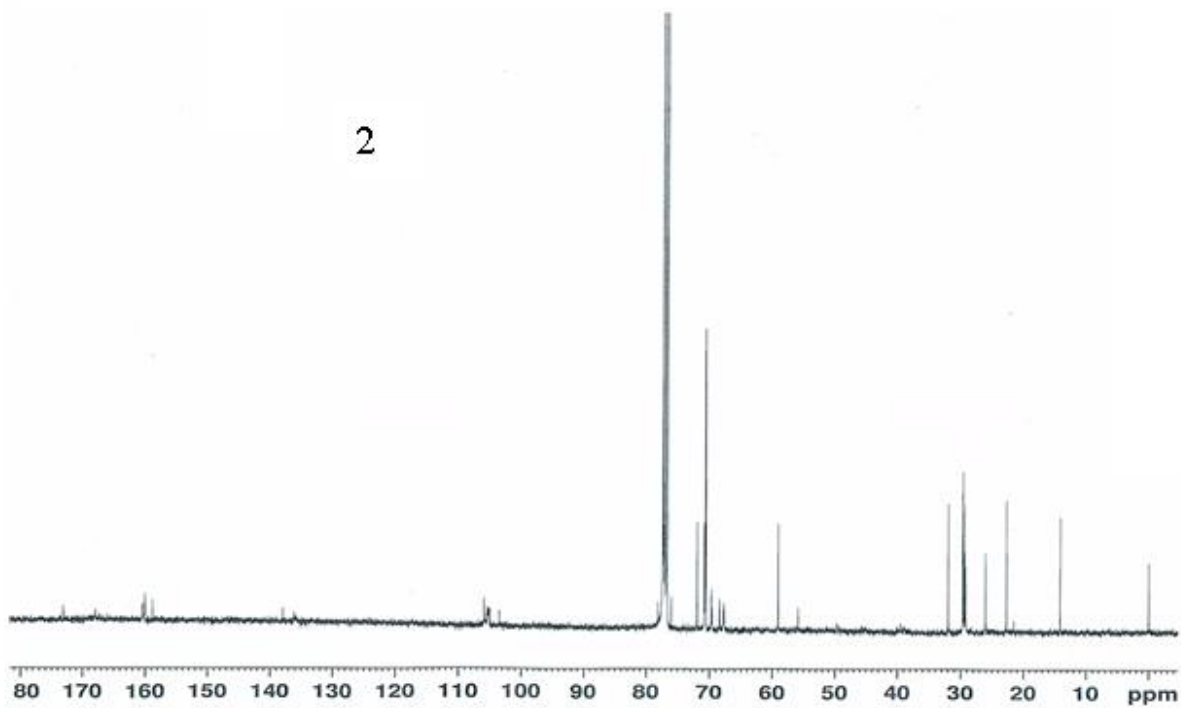


Figure 4.18: <sup>13</sup>C NMR of molecules 1(top) and 2(bottom)



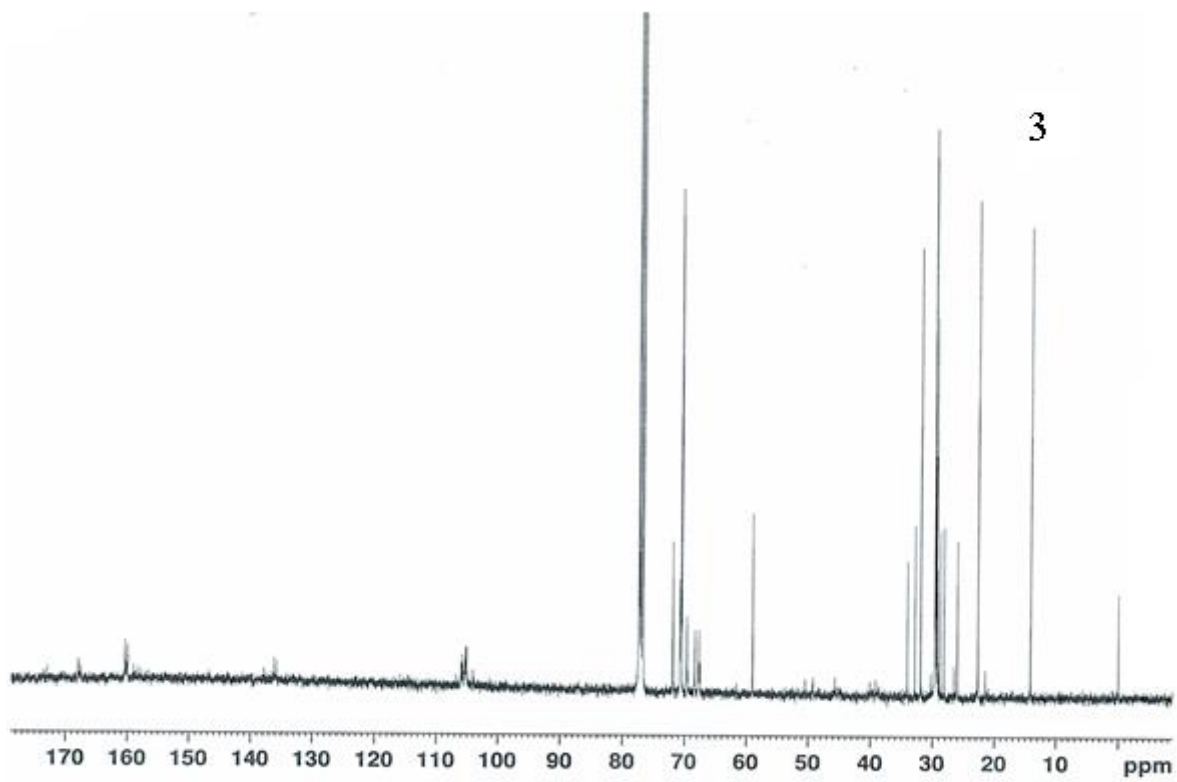
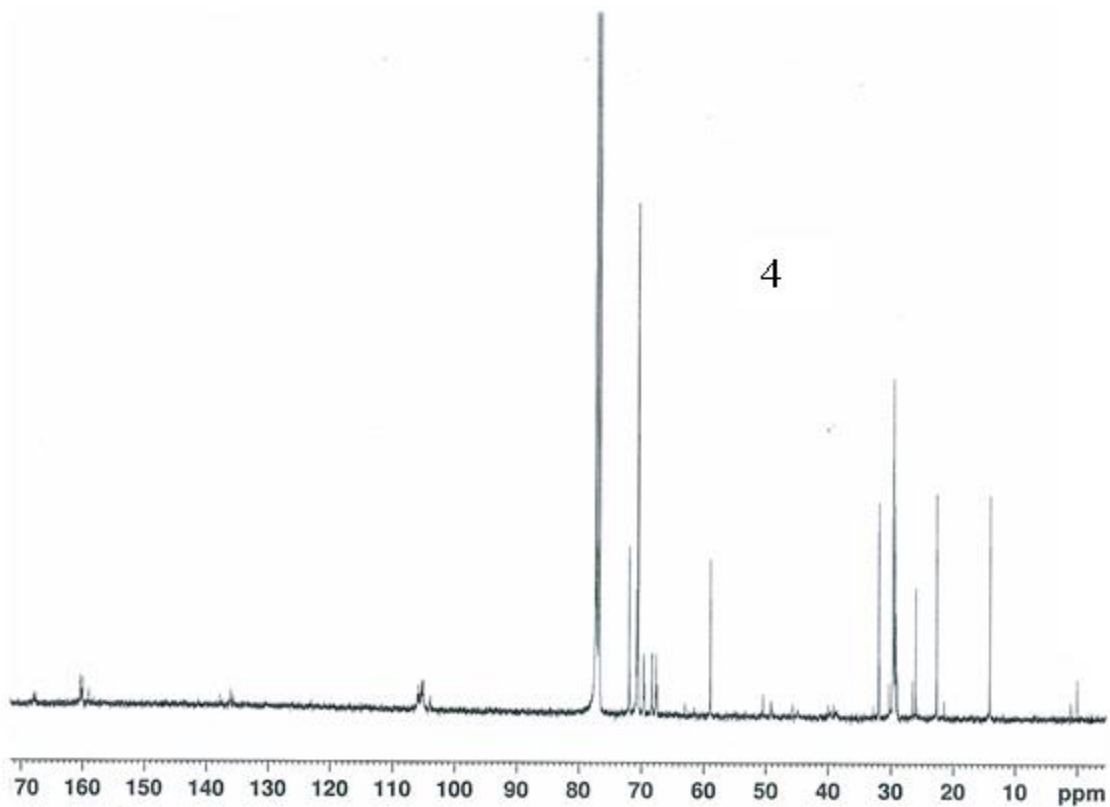


Figure 4.19:  $^{13}\text{C}$  NMR of molecules 3(top) and 4(bottom)



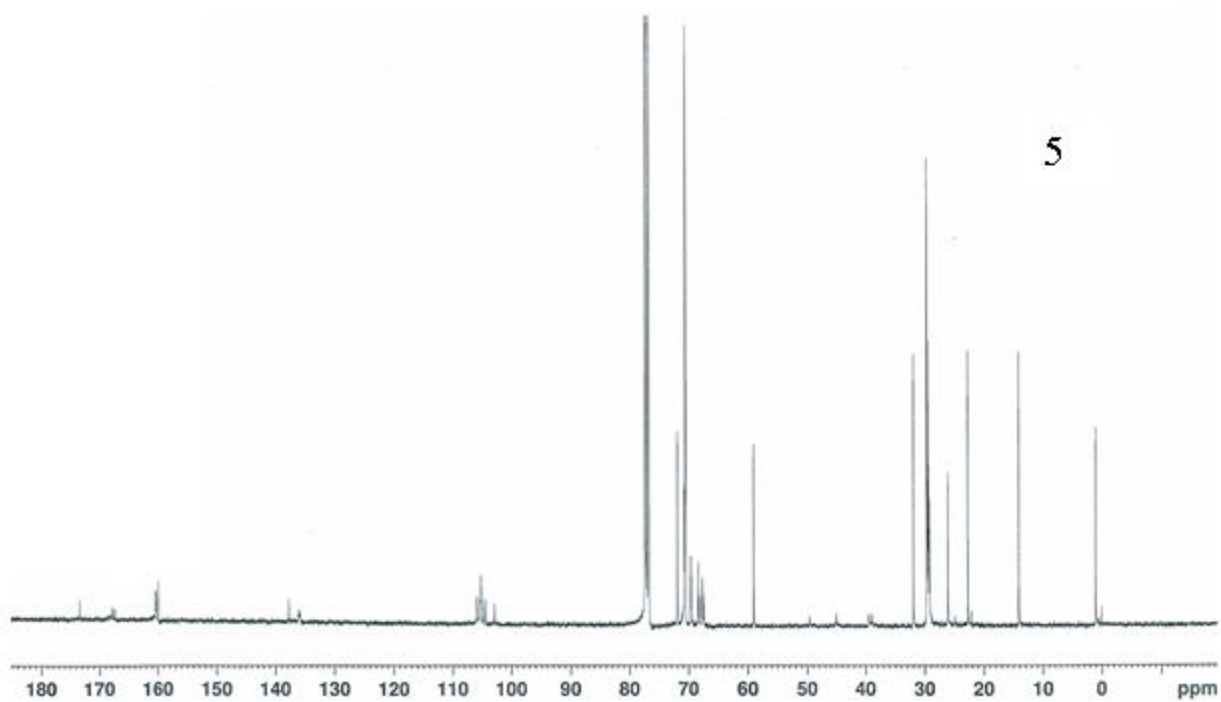
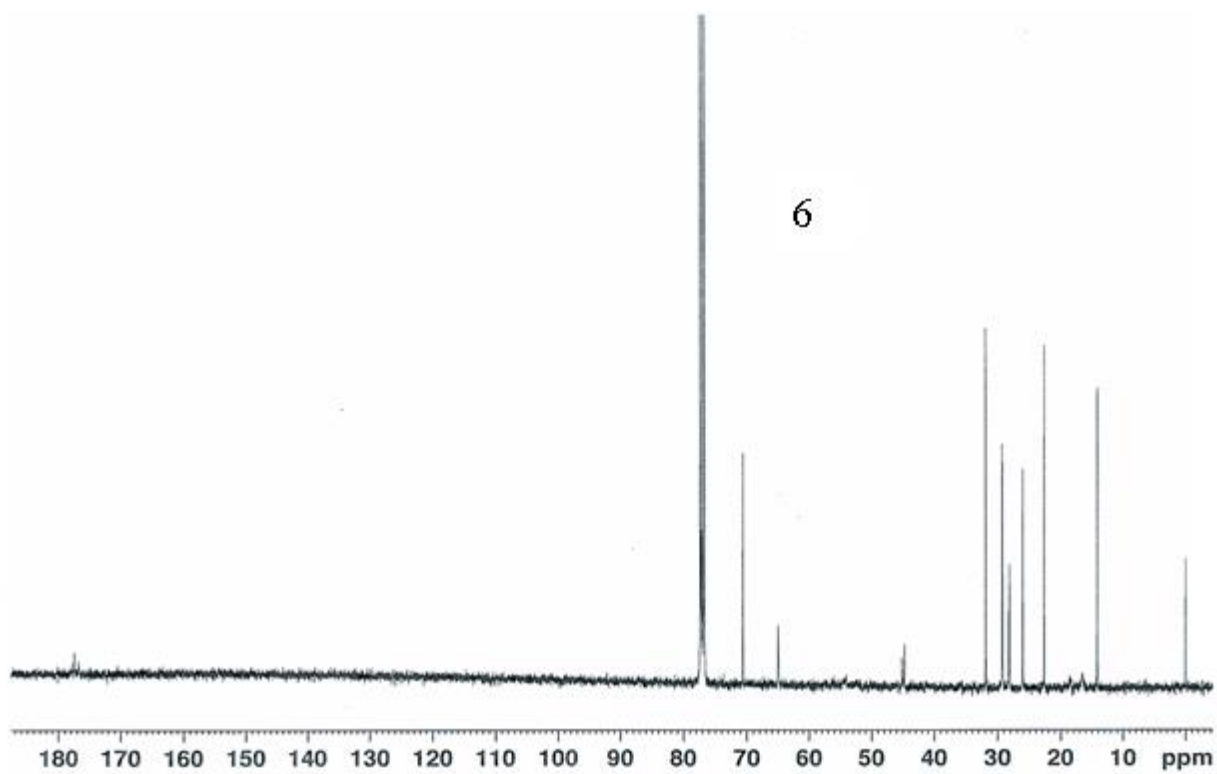


Figure 4.20:  $^{13}\text{C}$  NMR of molecules 5(top) and 6(bottom)





## CHAPTER 5

### SUMMARY AND FUTURE DIRECTIONS

#### 5.1 Summary

The self-assembly of stimuli-responsive scaffolds based on micelles, liposomes, hydrogels and thin films has been of considerable interest in areas such as diagnostics, sensing, drug delivery and cryptic catalysis<sup>1,2,3</sup>. These systems need to be endowed with certain design features which influence the self-assembly and the responsiveness of the scaffold when subjected to external stimuli which could be physical, chemical or biological in nature<sup>4,5</sup>. This kind of insight is still lacking in our understanding of how these systems respond to various stimuli. In this thesis, our objective is to establish structure-property relationships between the influence of structural design and the target material properties. Of interest to us are pH, temperature (chemical) and enzyme/proteins (biological) as stimuli and we have performed experiments to validate the responsive features of these systems.

In Chapter 2, we have established the design principles for oligomeric peptides to exhibit a unique size transition well below the LCST. We have found that incorporation of aromatic hydrophobic groups diminishes the thermo-sensitivity of the peptide nanoassemblies. The size transition is brought about by a loss of secondary structures at low temperatures and the temperature-dependent aggregation properties also gave rise to disparity in terms of guest encapsulation ability upon changing temperature. Since these molecules are designed to incorporate FDA approved components and the assembly is biodegradable, this system has interesting applications in the food industry and in cryptic catalysis.

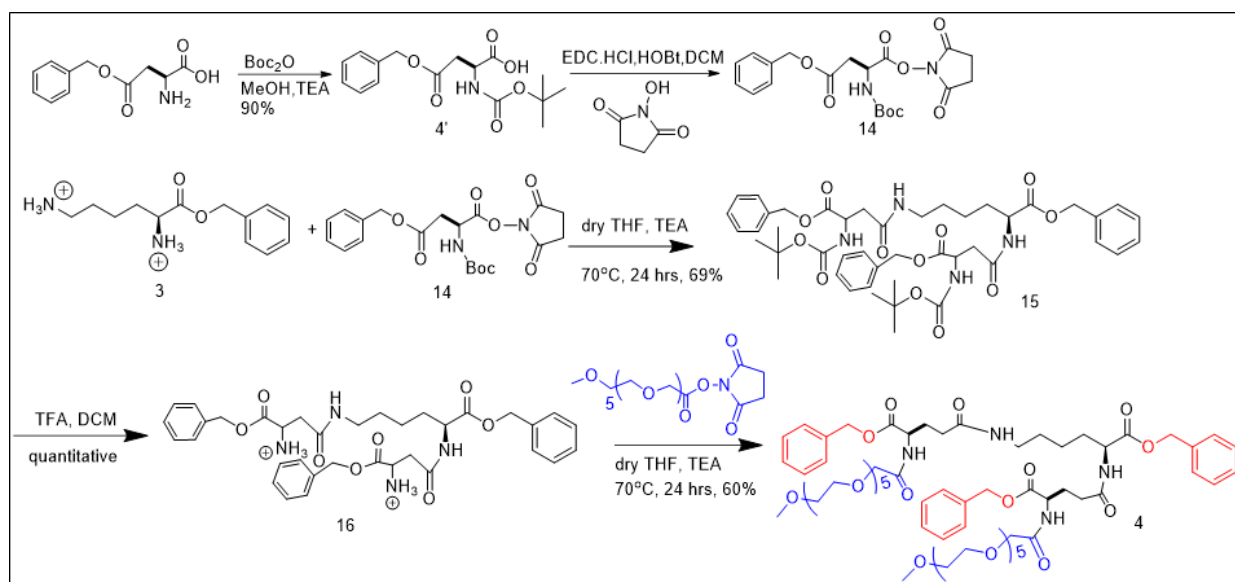
In Chapter 3, we have established structure-property relationships pertaining to the release of an artificial sweetener, aspartame from microgels and bulk hydrogels of aspartame encapsulated calcium cross linked alginate gels. We have, in particular, studied the different parameters that dictate the gel architecture and hence, the morphology and the structure of the gels. We have validated the effect of cross link densities and sizes on the release kinetics of the microgel spheres and bulk hydrogels. The release data was fitted to kinetic models available from literature to elucidate the pathway constraints dictated the release pathway.

In Chapter 4, structure-property relationships were developed using libraries of polymeric and oligomer amphiphiles to make possible rational design of triggers for amplification via LC response. To this end, we synthesized a wide range of stimuli-responsive amphiphilic oligomers that responded to a protein, carbonic anhydrase (CA II). Dimer was the only amphiphilic oligomer that was found to adsorb at the aqueous-LC interface to trigger a homeotropic anchoring transition. Moreover, CA II was found to bind to sulfonamide on the interface stronger than BSA resulting in the blocking of non-specific binding of bovine serum albumin (BSA) on aqueous-LC interface. This mechanism was corroborated using addition of inhibitor which enhanced the release of CA II from aqueous-LC interface by modulating the strength of binding. The design rules established here provide insight into the rational design of oligomers with triggers that can couple specific molecular events to LCs to achieve highly amplified responses. This paves way to develop principles based on LCs that permit incorporation of feedback for massive amplification that can be leveraged for targeting and triggering.

## 5.2 Future directions

### 5.2.1 Role of linker in thermo responsive behavior

In Chapter 2, we found that incorporation of a hydrophobic aromatic unit diminishes temperature sensitivity. From the observations so far in Chapter 2, we were interested in incorporating an ester linkage in the peptide backbone and examining the thermo-responsive behavior of those



**Scheme 5.1:** Synthesis of amphiphilic peptide 4

assemblies. This is because the amide bond is known to be planar and hence, rigid owing to the partial double bond character arising out of the delocalization of the lone pair of electrons of the nitrogen atom of the amide group<sup>6,7,8,9</sup>. Considering this, we designed and synthesized molecule 4 (Scheme 1) with similar amphiphilic functionalities.

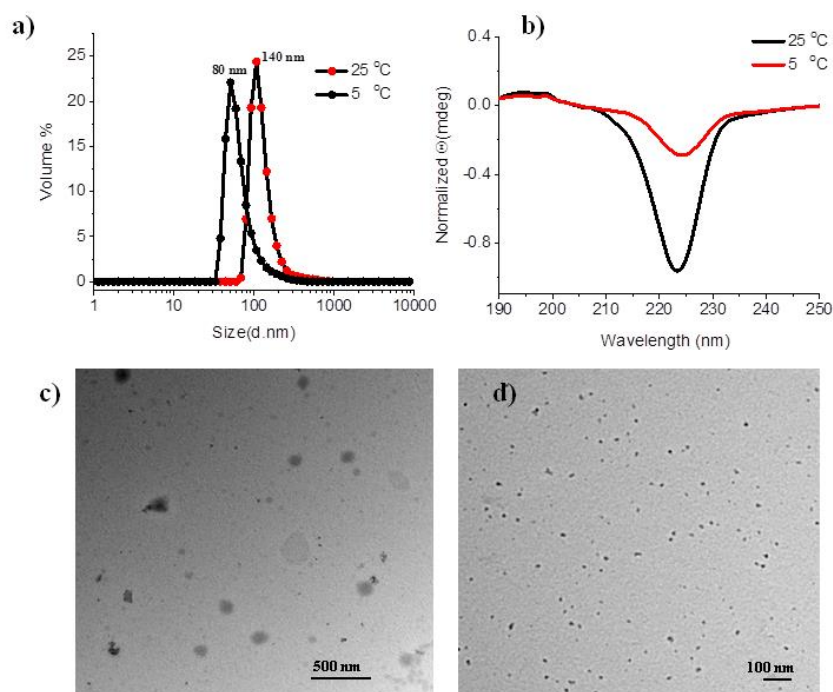


**Figure 5.1:**a) Temperature-dependent size variation for molecule 4 from DLS b) CD spectrum for molecule 4 indicates higher ordered structures at 25 °C with a substantial loss at 5 °C. TEM images for molecule 17 at c) 25 °C and d) 5 °C support the data obtained

A benzyl alcohol group was chosen as the hydrophobic group since it is GRAS and used widely in food products and a pentaethylene glycol was used as the hydrophilic functionality.

Molecule 4 differs from molecule 1 in the fact that the hydrophobic functionality (benzyl alcohol) is tethered to the peptide backbone solely by means of an ester linkage which is biodegradable.

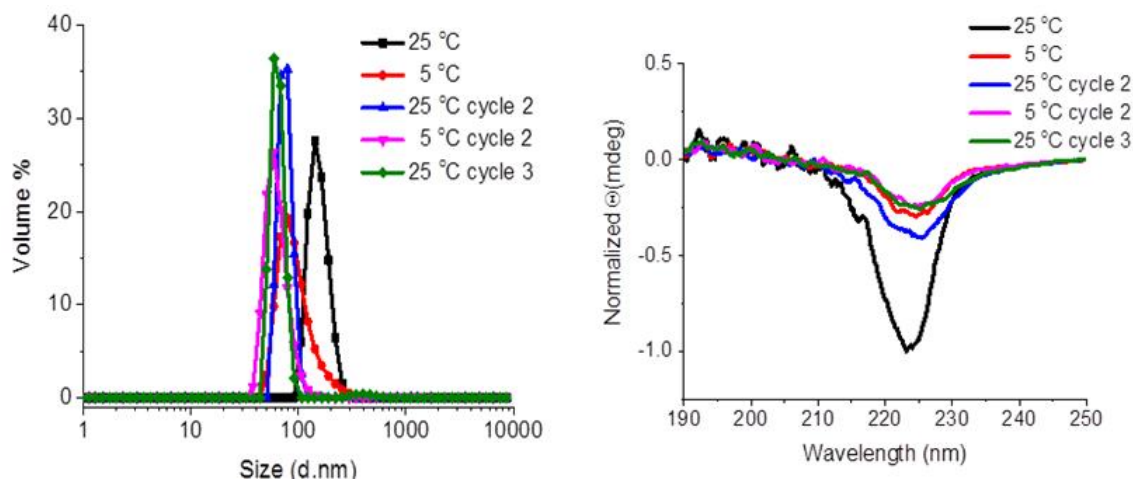
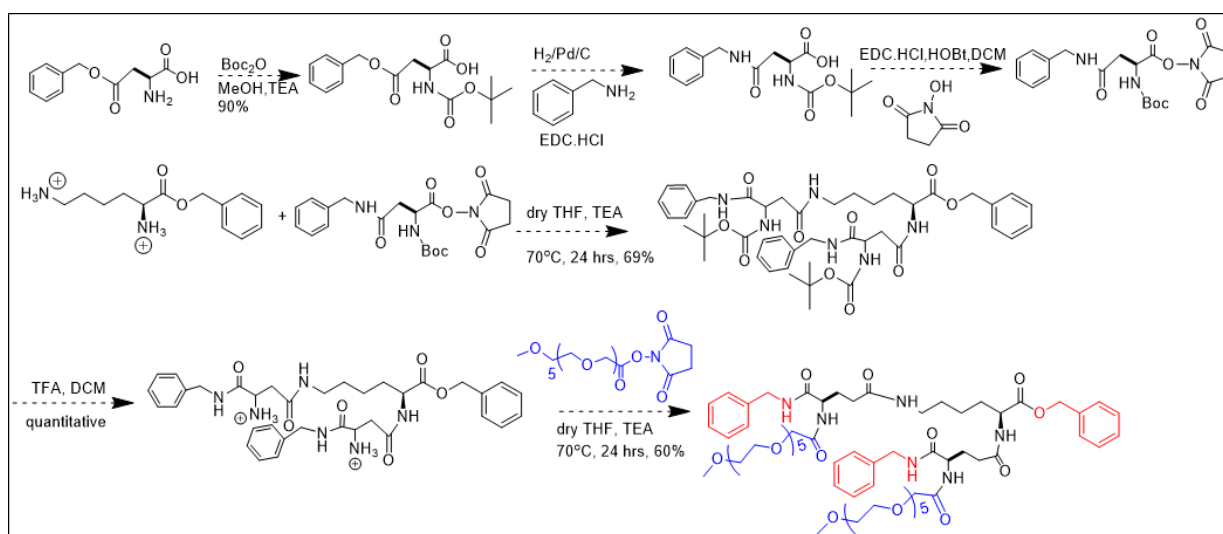


**Figure 5.2:** DLS sizes for molecule 4 indicate that the size transition is irreversible over several heating and cooling cycles and that the peptide nanoassemblies are kinetically trapped at 25 °C

We, then, dispersed molecule 4 in water and studied the temperature-dependent aggregation properties using light scattering. Molecule 4 too, was found to self-assemble into aggregates ~140 nm at 25 °C which corroborated with the transmission electron microscopy (TEM) data as well.

Upon decreasing temperature, molecule 4 was found to exhibit a sharp size transition at 5 °C akin to molecule 12 with the size at 5 °C being ~80 nm. Circular dichroism studies suggest the presence



**Scheme 5.2:** Synthesis of control molecule 5

of ordered structures typical of oligo-esters i.e. 225 nm for  $\pi$ - $\pi^*$  transition<sup>10-11</sup> and a significant loss of secondary structure was observed at low temperatures (Figure 1). Therefore, one could say that the rigidity of the hydrophobic unit and the linker structure both, dictate the overall rigidity of the peptide nanoassemblies in addition of the presence of the oligoethylene glycol and therefore, the aggregation properties at low temperatures. If our hypothesis were to be true, we should be able to validate the same using the control molecule 5 shown in Scheme 2. We will perform temperature dependent DLS and CD experiments to notice if there is any change in the aggregation properties of the control amphiphile upon change in temperature.

### 5.2.2 pH dependent degradation of peptide nanoassemblies

We anticipated that the peptide nanoassemblies would hydrolyze and degrade owing to the choice of biodegradable ester and amide linkages in the backbone<sup>12,13</sup>.

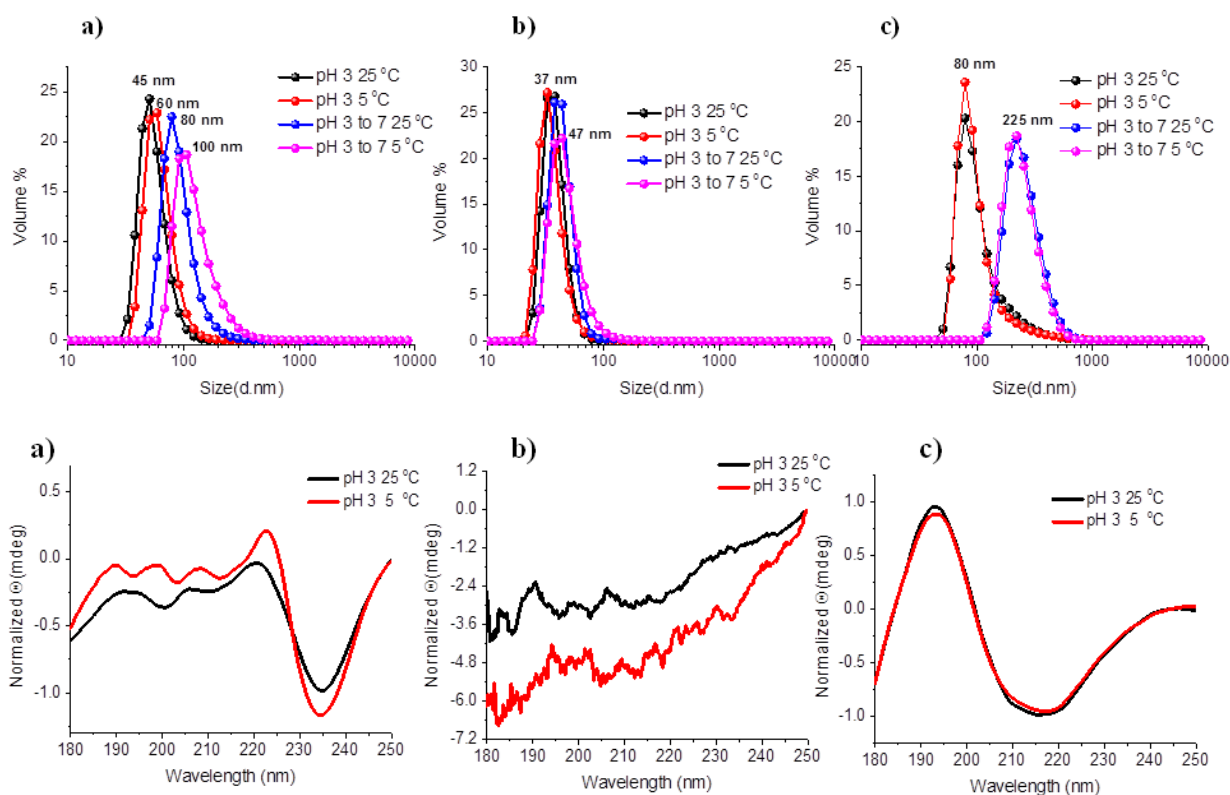


**Figure 5.3:** CD spectra of a) molecule 12, b) molecule 13 and c) molecule 17 upon incubation in acidic medium show that the nanoassemblies adopt a different secondary structure than their native conformation

It is worthwhile to note that acid-catalyzed hydrolysis of the peptide nanoassemblies gives rise to different secondary structures for molecules 1, 2 and 4 (Figure 3) than that previously observed and hence, different aggregation properties (Figure 3). If our hypothesis were to be true, we should observe peaks corresponding to the degraded oligomers when subjected to mass spectroscopy analysis. Mass spectroscopy needs to be performed to observe if the hydrolysis of the peptide nanoassemblies proposes the formation of charged by-products and introducing a charge on a peptide backbone<sup>14,15</sup> which might explain the sudden change in the nature of secondary structures formed upon hydrolysis.

### 5.2.3 Triggerable Multi-Scale Responses via Liquid Crystallinity

In Chapter 4, we have developed structure-properties relationships for the design of oligomeric and polymeric amphiphiles that couple a range of stimuli to LC responses and LC-based principles that permit incorporation of feedback for massive amplification. We now, intend to leverage

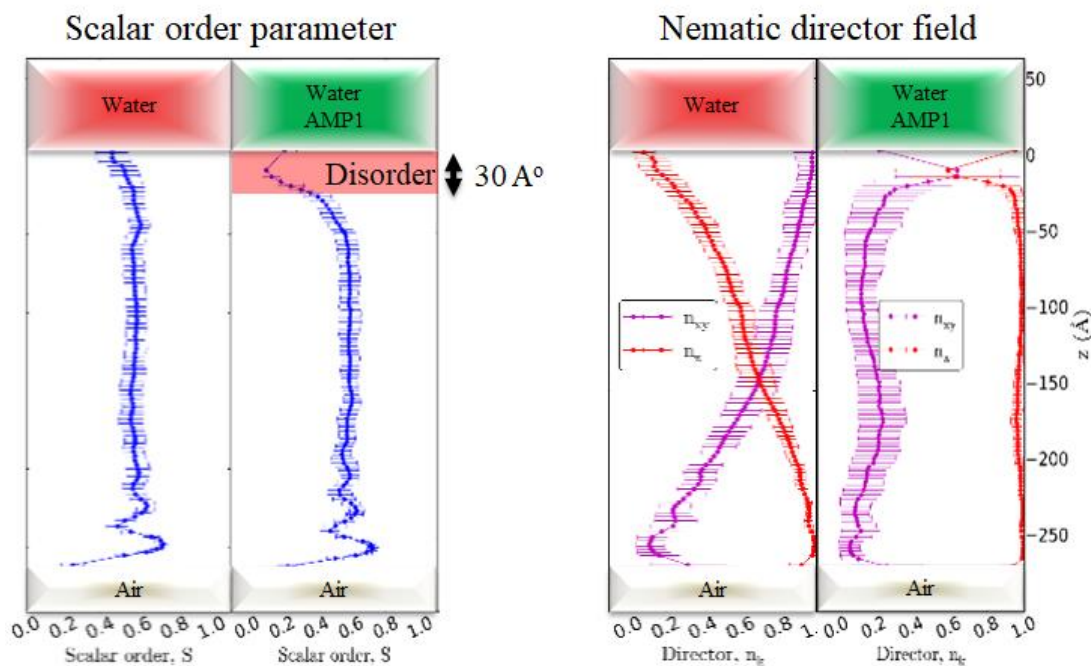


**Figure 5.4:** Simulations indicate that oligomeric dimer disrupts ordering of LC interface

structure-property relationships for oligomeric and polymer amphiphiles to rationally design LCs systems that respond to a range of stimuli to combine designs of triggerable oligomeric and polymeric amphiphiles with amplification schemes based on release of microcargo (e.g., release of initiator of polymerization). Exploration of non-equilibrium states of LCs for amplification with a particular focus on mechanical triggers (e.g., foot of an insect, acoustic event) is also of interest to us. Moving forward our objective is to design oligomeric and polymeric amphiphiles that integrate multiple stimuli-responsive groups.

#### **5.2.4 Understanding the mechanism for the dimer to cause the LC homeotropic anchoring**

Our group has always been interested in understanding structure-property relationships at the molecular level, and we were intrigued by the fact that the dimeric amphiphilic oligomer was the only amphiphile that cause a homeotropic anchoring transition at the LC-aqueous interface. To understand this, we have initiated MD simulation experiments in collaboration. Preliminary studies suggest that the dimer disrupts the ordering of the LC interface through a change in easy axis (Figure 5.4) and this is a new mechanism that has never been reported before.



### 5.3 Materials and methods

All chemicals and reagents were purchased from commercial sources and were used as received, unless mentioned otherwise. <sup>1</sup>H NMR spectra were recorded on 400 MHz NMR spectrometer using the residual proton resonance of the solvent as the internal standard. Chemical shifts are reported in parts per million (ppm). When peak multiplicities are given the following abbreviations are used: s, singlet; d, doublet; t, triplet; m, multiplet

- **Synthesis of 4'**: 5 g (0.0223 mol) of L-Aspartic acid β-benzyl ester was dissolved in anhydrous methanol in a round bottom flask and cooled to 0 °C under inert atmosphere. To this solution, triethylamine (4 mL, 0.025 mol) and di-tert-butyl-dicarbonate (5.38 g, 0.025 mol) were added and the solution was left to stir overnight. The reaction mixture was concentrated in vacuo, extracted using ethyl acetate and water, followed by washing with saturated NaHCO<sub>3</sub>. The combined extracts were dried over anhydrous Na<sub>2</sub>SO<sub>4</sub> to afford **4** in 90% yield and was used as it is. <sup>1</sup>H NMR (CDCl<sub>3</sub>, 400 MHz, TMS): δ (ppm) = 7.35(m, 5H), 5.5(broad d, 1H), 5.1(d,2H), 4.5(broad m, 1H), 3.1(broad m, 1H), 2.9(dd, 1H), 1.5(s,9H) (M+Na<sup>+</sup>) from ESI spectroscopy: 346.14
- **Synthesis of 14**: Same procedure as compound **7**. Yield:78% <sup>1</sup>H NMR(CDCl<sub>3</sub>, 400 MHz, TMS): δ (ppm) = 7.35(m, 5H), 6.2(broad peak, 1H), 5.1(d,2H), 4.5(broad m, 1H), 3.65(broad m, 1H), 2.9(dd, 1H), 2.8(m,4H), 1.5(s,9H) (M+Na<sup>+</sup>) from ESI spectroscopy: 443.15
- **Synthesis of 15**: Same procedure as compound **8**. Yield:69% <sup>1</sup>H NMR was attempted by dissolving the compound in various solvents. However, it was found to be sparingly soluble. <sup>1</sup>H NMR in acetone denotes all the characteristic peaks for the product but the integration does

not come out as expected owing to low solubility of the compound. (M+Na<sup>+</sup>) from ESI spectroscopy: 869.35

- **Synthesis of 4:** Same procedure as compound **1 and 2**. Yield: 60% (M+Na<sup>+</sup>) from ESI spectroscopy: 1253.60

To study the aggregation properties of 12 and 13, the peptides were dispersed in water at different concentrations and the critical aggregation concentrations (CAC) were calculated using DiI, a hydrophobic dye as a spectroscopic probe. The stock solutions of 12(1.23 mM), 13(1.86 mM) and 17(1.38 mM) respectively, were made by a standard method of dispersing the weighed compound in required amount of HPLC grade water in a scintillation vial with a stir bar followed by sonication and vortex for 5 minutes. The required concentrations were prepared by a serial dilution of this stock with water, sonicated for 30 minutes and left to equilibrate at ambient temperature for 1 hour. 40  $\mu$ L of DiI stock (1mM in acetone) was then added to the vial in a drop wise manner. The contents were sonicated for 5 minutes and vortexed for 2 minutes, following which they were left to stir for 8 hours at room temperature uncapped to facilitate the evaporation of acetone. The excess insoluble DiI was removed by filtration using a membrane with a pore size of 0.450 $\mu$ m.

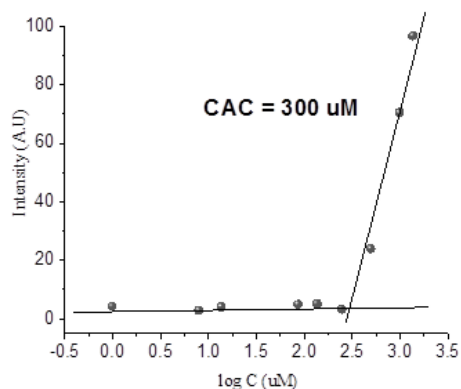


**Figure 5.5:** Critical aggregation concentrations of peptide 4

The intensity at the maxima (589 nm) were plotted as a function of concentration of the peptide

amphiphiles and the inflexion point was noted to be the critical aggregation concentration or CAC (Figure 5).

- **Temperature dependent Dynamic light scattering study (DLS):** The stock solution of 4 (1.38 mM) respectively, were made by a standard method of dispersing the weighed compound in required amount of HPLC grade water in a scintillation vial with a stir bar followed by sonication and vortex for 5 minutes. DLS was performed on a Malvern nano-zeta sizer instrument with a 637 nm laser with non-invasive backscattering technology detected at 173°. All sizes are reported as the hydrodynamic diameter ( $D_H$ ) and were repeated in triplicate. Variable temperature DLS experiments were performed by equilibrating the aqueous solutions for 5 minutes at the respective temperature before the size measurements.
- **Temperature dependent Transmission electron microscopy (TEM) study:** For TEM studies, concentrations same as that for DLS measurements were used. Briefly, one drop (10 $\mu$ L) of each sample was drop casted on carbon coated Cu grid and allowed to dry for 24 hours (at ambient temperature) before imaging them. For the size measurement at low temperature, the same sample was incubated at 5°C following which it was drop casted and allowed to dry before imaging. TEM images were recorded on a JEOL-2000FX machine operating at an accelerating voltage of 100 kV.
- **Temperature dependent Circular Dichroism (CD) studies:** CD spectra of the peptide nano assemblies were recorded on JASCO J-1500 spectrophotometer. In a typical experiment, 200  $\mu$ L of the peptide amphiphiles solution (concentrations same as that in DLS and TEM measurements) was injected into a quartz cuvette of 1-mm path length, equilibrated at 25 °C and 5 °C for 5 min and scanned from 180 to 250 nm (scan rate: 20 nm/min, interval: 0.2 nm, average of three spectra).

### 5.4 NMR spectrum of molecules

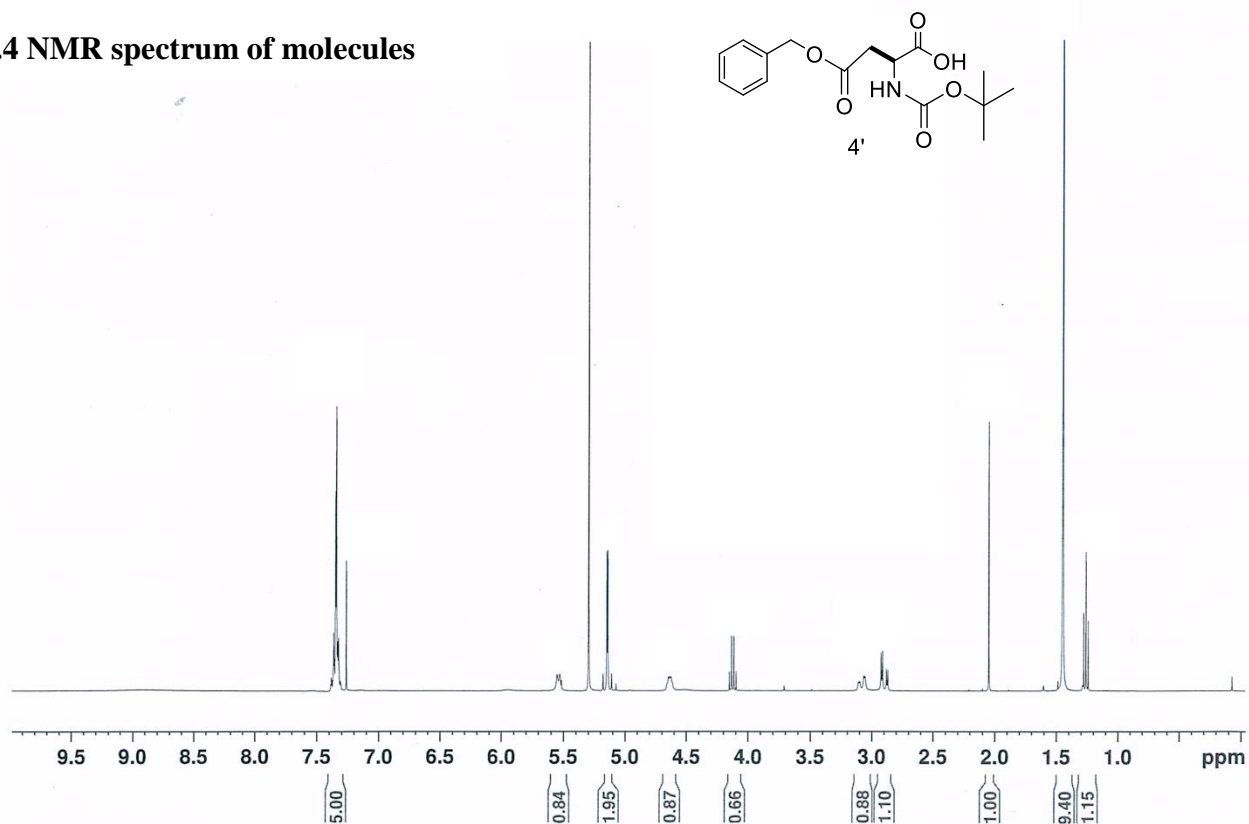
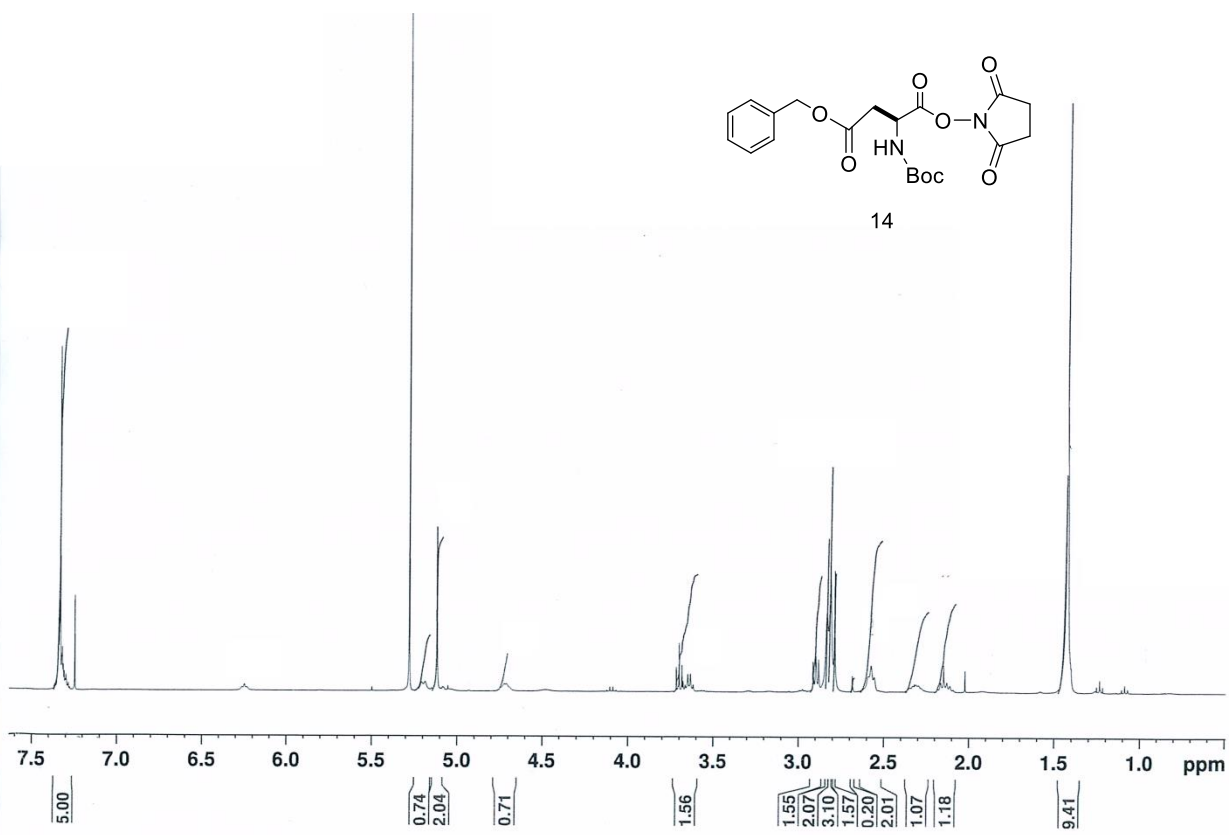
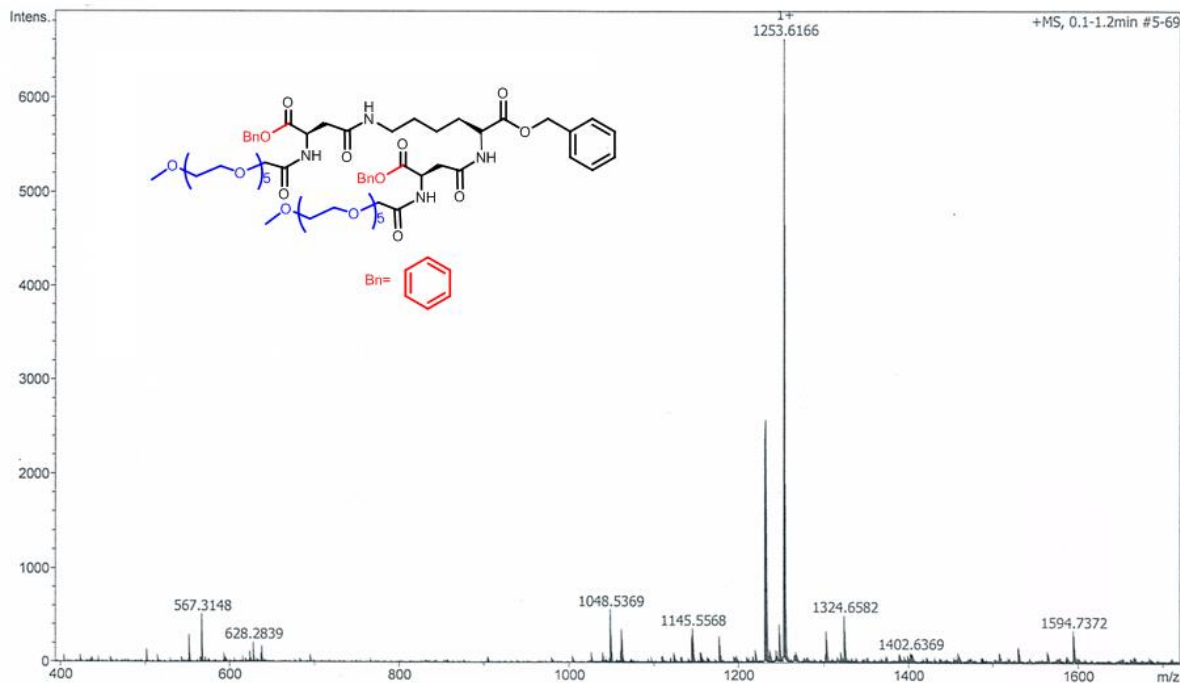


Figure 5.6 : <sup>1</sup>H NMR of molecules 4'(top) and 14(bottom)





**Figure 5.7: ESI-MS of molecule EST-AROM(4')**

## 5.5 References

- (1) Lee, J. H.; Yigit, M. V.; Mazumdar, D.; Lu, Y. Molecular Diagnostic and Drug Delivery Agents Based on Aptamer-Nanomaterial Conjugates. *Adv. Drug Deliv. Rev.* **2010**, *62* (6), 592–605.
- (2) Raghupathi, K. R.; Guo, J.; Munkhbat, O.; Rangadurai, P.; Thayumanavan, S. Supramolecular Disassembly of Facially Amphiphilic Dendrimer Assemblies in Response to Physical, Chemical, and Biological Stimuli. *Acc. Chem. Res.* **2014**, *47* (7), 2200–2211.
- (3) Schmaljohann, D. Thermo- and PH-Responsive Polymers in Drug Delivery. *Adv. Drug Deliv. Rev.* **2006**, *58* (15), 1655–1670.
- (4) Jun, H. W.; Paramonov, S. E.; Hartgerink, J. D. Biomimetic Self-Assembled Nanofibers. *Soft Matter* **2006**, *2* (3), 177–181.
- (5) de Las Heras Alarcon, C.; Pennadam, S.; Alexander, C. Stimuli Responsive Polymers for Biomedical Applications. *Chem. Soc. Rev.* **2005**, *34* (3), 276–285.
- (6) Mujika, J. I.; Matxain, J. M.; Eriksson, L. A.; Lopez, X. Resonance Structures of the Amide Bond: The Advantages of Planarity. *Chem. - A Eur. J.* **2006**, *12* (27), 7215–7224.
- (7) Li, Z. T.; Hou, J. L.; Li, C.; Yi, H. P. Shape-Persistent Aromatic Amide Oligomers: New Tools for Supramolecular Chemistry. *Chem. - An Asian J.* **2006**, *1* (6), 766–778.
- (8) Zhang, Y.; Zheng, Y.; Xiong, W.; Peng, C.; Zhang, Y.; Duan, R.; Che, Y.; Zhao, J. Morphological Transformation between Nanocoils and Nanoribbons via Defragmentation Structural Rearrangement or Fragmentation-Recombination Mechanism. *Sci. Rep.* **2016**, *6* (June), 1–8.
- (9) Hughes, M.; Frederix, P. W. J. M.; Raeburn, J.; Birchall, L. S.; Sadownik, J.; Coomer, F. C.; Lin, I. H.; Cussen, E. J.; Hunt, N. T.; Tuttle, T.; et al. Sequence/Structure Relationships

- in Aromatic Dipeptide Hydrogels Formed under Thermodynamic Control by Enzyme-Assisted Self-Assembly. *Soft Matter* **2012**, 8 (20), 5595–5602.
- (10) Breedveld, V.; Nowak, A. P.; Sato, J.; Deming, T. J.; Pine, D. J. Rheology of Block Copolypeptide Solutions: Hydrogels with Tunable Properties. *Macromolecules* **2004**, 37 (10), 3943–3953.
- (11) Hatip Koc, M.; Cinar Ciftci, G.; Baday, S.; Castelletto, V.; Hamley, I. W.; Guler, M. O. Hierarchical Self-Assembly of Histidine-Functionalized Peptide Amphiphiles into Supramolecular Chiral Nanostructures. *Langmuir* **2017**, 33 (32), 7947–7956.
- (12) Katti, D. S.; Lakshmi, S.; Langer, R.; Laurencin, C. T. Toxicity, Biodegradation and Elimination of Polyanhydrides. *Adv. Drug Deliv. Rev.* **2002**, 54 (7), 933–961.
- (13) Middleton, J. C.; Tipton, A. J. Synthetic Biodegradable Polymers as Orthopedic Devices. *Biomaterials* **2000**, 21 (23), 2335–2346.
- (14) Ganesan, S. J.; Matysiak, S. Role of Backbone Dipole Interactions in the Formation of Secondary and Supersecondary Structures of Proteins. *J. Chem. Theory Comput.* **2014**, 10 (6), 2569–2576.
- (15) Sali, D.; Bycroft, M.; Fersht, a R. Stabilization of Protein Structure by Interaction of Alpha-Helix Dipole with a Charged Side Chain. *Nature*. **1988**, 335,740–743.

## APPENDIX

### EFFECT OF HOFMEISTER IONS ON THE SIZE, SUB-LCST AND ENCAPSULATION STABILITY OF TRIMERIC OLIGOMERS

#### A.1 Background and significance

##### A1.1 Hofmeister effect

The effects of salts and osmolytes on the folding of proteins and colloidal structures in aqueous solutions have been long studied<sup>1</sup>. In as early as 1888, the identity and concentration of anions present in solution has been found to induce a plethora of macromolecular phase transition. This ability of an anion to affect this macromolecular phase transition in aqueous solution generally

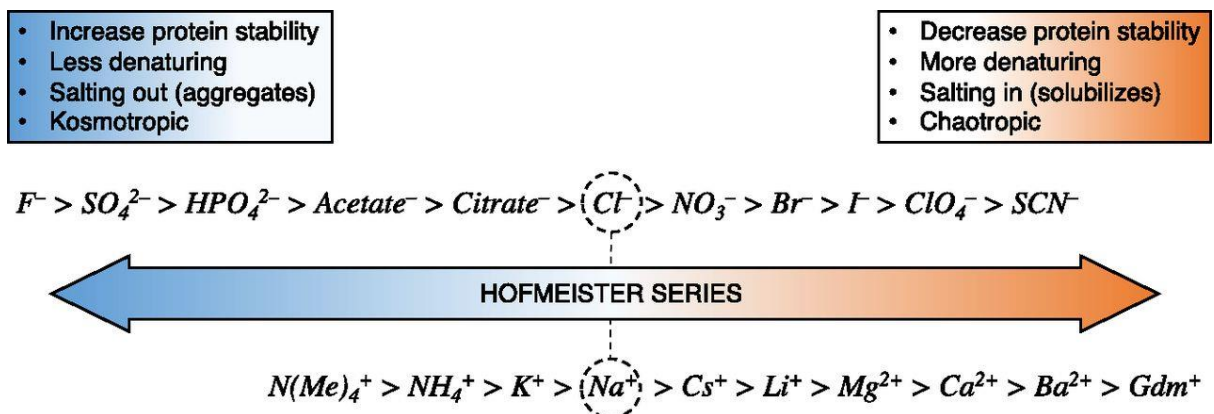


**Figure A.1:** The Hofmeister series showing Kosmotropes and Chaotropes

follows a trend which is commonly referred to as the Hofmeister series. This series has been implicated in protein crystallization, ion exchange, surface tension of electrolytes or bubble coalescence<sup>2</sup>. The series ranks the relative influence of ions on the physical behavior of a wide variety of aqueous processes. This behavior is more pronounced for anions than cations. Ions on the left are called 'Kosmotropes', which tend to precipitate proteins and prevent unfolding of



proteins. Ions on the right are called ‘Chaotropes’, which increase the solubility and promote the denaturation of proteins<sup>3</sup>.

Kosmotropes are referred to as water structure makers because they have the propensity to strengthen hydrogen-bonding network of bulk water owing to their large hydration energies. Chaotropes on the other hand, break the hydrogen bonding network owing to their small hydration energies. While the molecular origin is not fully understood, the Hofmeister series is associated with ion hydration in homogeneous and heterogeneous environments while its molecular origin has not been completely understood.

### **A1.2 Effect of Hofmeister ions on water soluble polymers**

The implications of the findings of the Hofmeister series have been well-established in the biological realm. However, the chemical explorations have been vastly unexplored. For example, addition of salts has been demonstrated to lower the Lower Critical Solution Temperature (LCST) of water soluble polymers such as poly ethylene glycol (PEG) and poly n-isopropyl acrylamide (PNIPAM) and the effect is in accordance with the findings of the Hofmeister series. LCST is understood to be brought about due to the hydrophobic collapse of the PEG and PNIPAM polymer chains owing to their reduced hydrogen-bonding interaction with water<sup>3,4</sup>. While variations in macroscopic phase transitions or LCST have been extensively studied, changes in the aggregation properties of polymeric aggregates upon addition of salts has not been well established. In the Thayumanavan research group, studies have demonstrated that the size and the core density of a polymeric aggregate containing oligoethylene glycol (OEG) and pyridyl sulfide (PDS) units as side chain functionalities can be fine-tuned by an appropriate choice of chaotropes or kosmotropes<sup>5</sup>. Further, the encapsulation stability of hydrophobic guest molecules

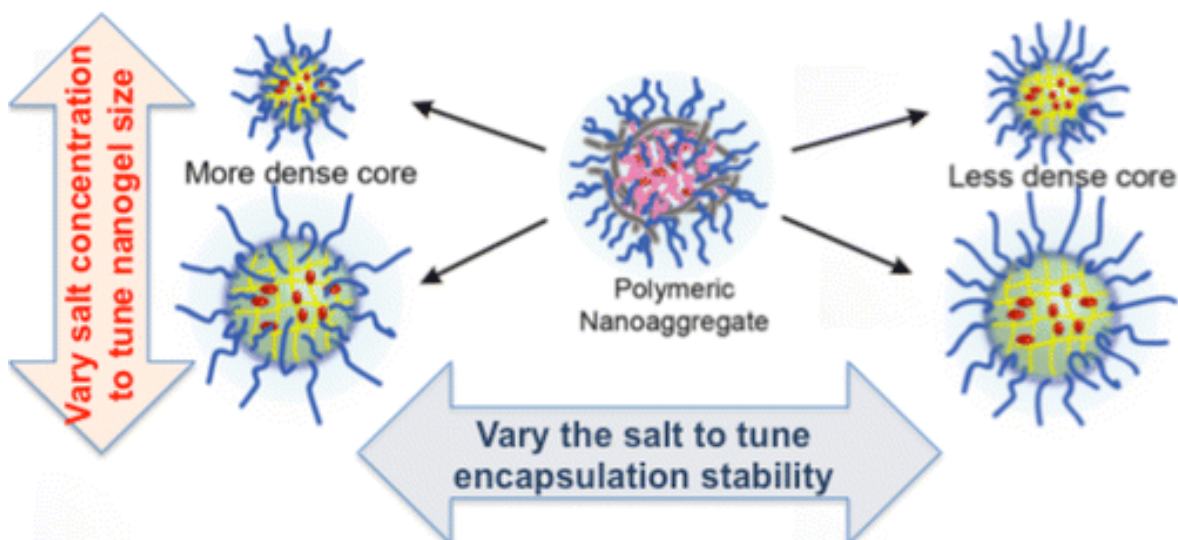


**Figure A.2:** Effect of Hofmeister Ions on the Size and Encapsulation Stability of Polymer Nanogels

were found to depend on the salts used during preparation of the polymeric aggregates. While chaotropic anions afforded aggregates with higher encapsulation stability, the reverse was found to be the case for Kosmotropes. Salt-dependent hydration of the OEG groups was attributed to be the cause for changes in the core density of the polymeric aggregate giving rise to the leaky character of the polymeric aggregate.

### A1.3 Hypothesis and design principle

Oligo and Poly ethylene glycol based hydrophilic functional groups are renowned for exhibiting LCST behavior. In our group, we were interested in determining the factors that account for the temperature sensitivity of PEG groups and embarked in a study to investigate the thermosensitive properties of oligo ethylene based supramolecular assemblies below the LCST. A sub-LCST was observed well below the LCST of oligo ethylene glycol based dendrons which was accompanied by a change in size of these supramolecular assemblies<sup>6,7</sup>. It was interesting to note that the host-guest properties were significantly altered at low temperature that affected the guest encapsulation stability indicating that the assemblies became a lot more dynamic at low temperatures. This was

hypothesized to arise due to increased hydration of PEG chains at lower temperatures. While the effect of Hofmeister series on LCST has been studied extensively, there is a dearth of studies that relate the effects of the Hofmeister series to sub-LCST. In this study, we embark on a study to reveal the same.

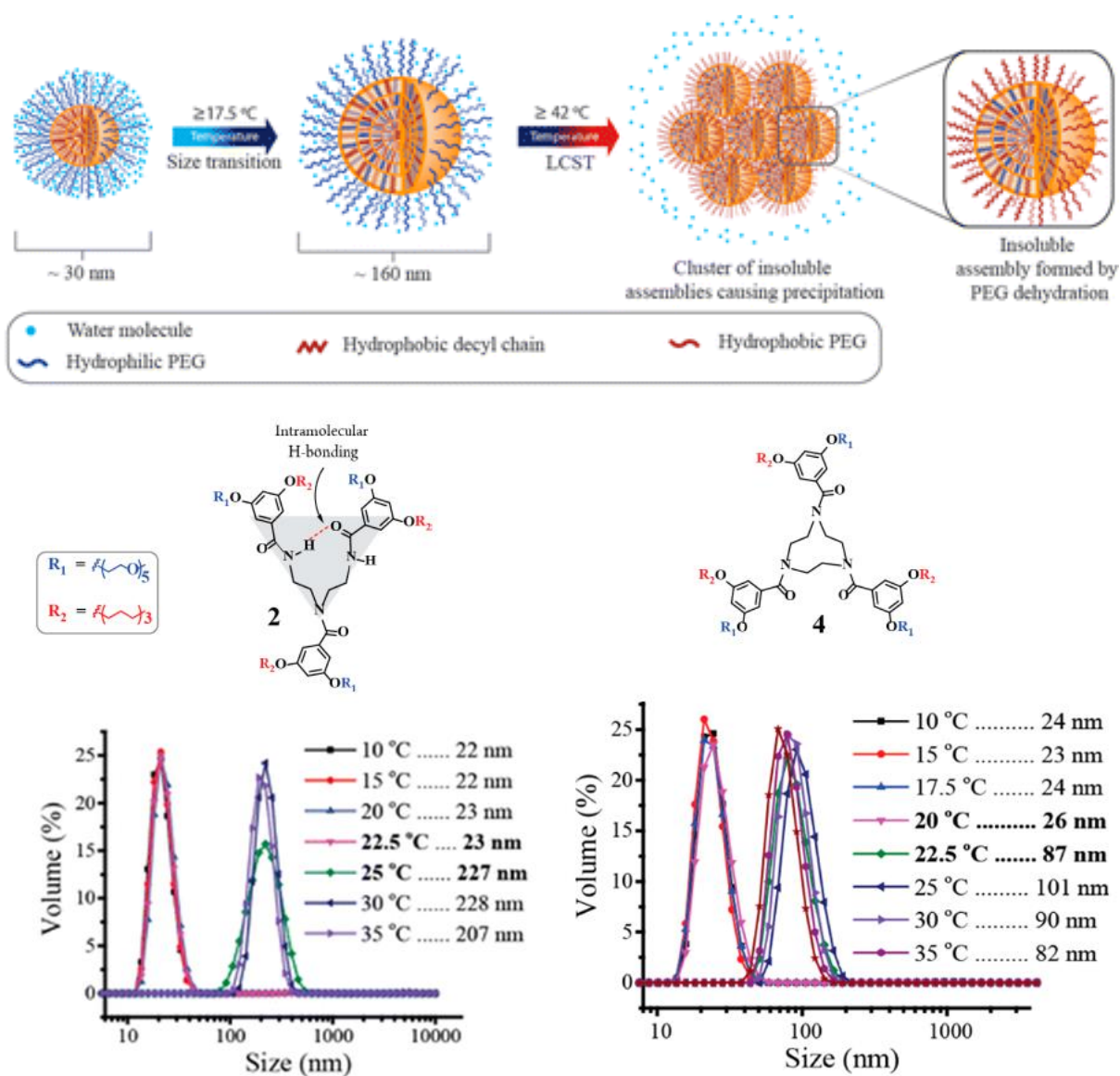


**Figure A.3:** Sub-LCST and trimers exhibiting a change in aggregation properties below sub-LCST

## **A.2 Materials and methods**

### **A2.1 Synthesis and Characterization**

All chemicals and reagents were purchased from commercial sources and were used as received, unless otherwise mentioned. <sup>1</sup>H-NMR spectra were recorded on 400 MHz Bruker NMR spectrometer using the residual proton resonance of the solvent as the internal standard. Chemical shifts are reported in parts per million (ppm). When peak multiplicities are given the following abbreviations are used: s, singlet; d, doublet; t, triplet; m, multiplet. <sup>13</sup>C-NMR spectra were proton decoupled and measured on a 500 MHz Bruker spectrometer with 125 MHz frequency by using carbon signal of the deuterated solvent as the internal standard. <sup>1</sup>H NMR of the methylated amphiphiles showed incorrect integrations and were rounded to the expected values. To clearly confirm the formation and purity of those products mass spectrometry was performed and reported. Molecules 1, 2 and 3 were synthesized following the previously reported procedure<sup>7</sup>.

### **A2.2 Dynamic Light Scattering**

DLS was performed on a Malvern nano-zeta sizer instrument with a 637 nm laser source with non-invasive backscattering technology detected at 173°. All sizes are reported as the hydrodynamic diameter (DH) and were repeated in triplicate. All samples were prepared in water at pH 7 by brief sonication and vortexing at room temperature. Variable temperature DLS experiments were performed by equilibrating the aqueous solutions for 6 minutes at the respective temperature before the size measurements. Salt dependent DLS was performed by making a 1M stock solution of Na<sub>2</sub>SO<sub>4</sub>, NaCl, NaSCN and diluting it with the amphiphile solution to acquire the desired concentration.

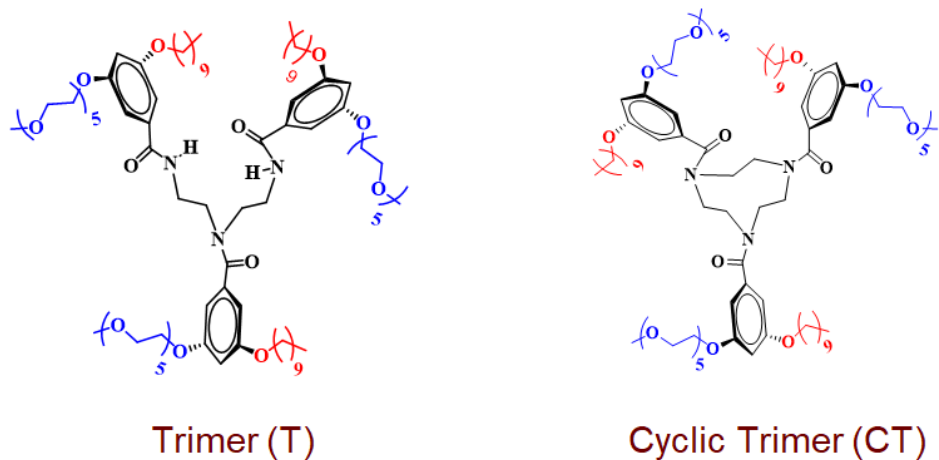
For cloud point measurement, the polymer (10 mg/mL) in water or salt solution was used. The temperature was increased from 10 to 60 °C in 2 °C increments. Equilibration time at each temperature was 10 min. Above the LCST, the polymer chains collapse into a globule and produce a more compressed particle with a higher refractive index, so scattering intensity was monitored as a function of temperature to determine the LCST behavior of polymer solution. For size distribution measurement, we used the polymer (10 mg/mL) or nanogel (1 mg/mL) solution in water or each salt solution, which contains a specific salt concentration. The measurement was kept constant at 25 °C throughout the experiment. Dust was eliminated by filtering the solution through 0.45 µm membrane filter.

### **A2.3 Guest Exchange experiments using FRET**

FRET studies were performed on a PTI spectrofluorometer with a XenoFlash power supply and Quantum TC125 temperature control. Dye loading (DiI and DiO) in the micelles was always done at 1 wt % of the corresponding amphiphile as follows: 20 µL of 0.5 mg/mL dye (DiO or DiI) in acetone was added to a 20 mL glass vial containing 1 mg of amphiphile, to this mixture was added additional 40 µL of acetone to homogeneously mix all the components. The acetone was then evaporated using a mild argon flow, followed by addition of calculated amount of water to make 25 µM amphiphile solutions.

Temperature dependent guest exchange experiments were done as follows: 25 µM amphiphile solution loaded with DiO was equilibrated at corresponding temperature in the fluorimeter cell for 6 minutes, similarly 25 µM amphiphile solution containing DiI was equilibrated at the same

temperature outside using an ice bath or hot water bath for 6 minutes, upon equilibration DiI containing solution was briskly transferred into a 1 mL syringe and added to DiO containing solution. DiO was excited at 440 nm, and DiI emission was monitored at 567 nm at different time points.



**Scheme A.1:** Structures of the trimeric amphiphiles used in the study

### A.3 Results and discussion

#### A.3.1 Effect of Hofmeister ions on the aggregation properties of trimers

The oligomers were synthesized and characterized in accordance with the procedure mentioned in section A.2. We, then, investigated the size of these assemblies in the presence of three salts at 25 °C namely kosmotropic (sodium sulfate), weakly kosmotropic (sodium chloride) and chaotropic (sodium thiocyanate) using dynamic light scattering (DLS). Kosmotropes namely, sodium sulfate

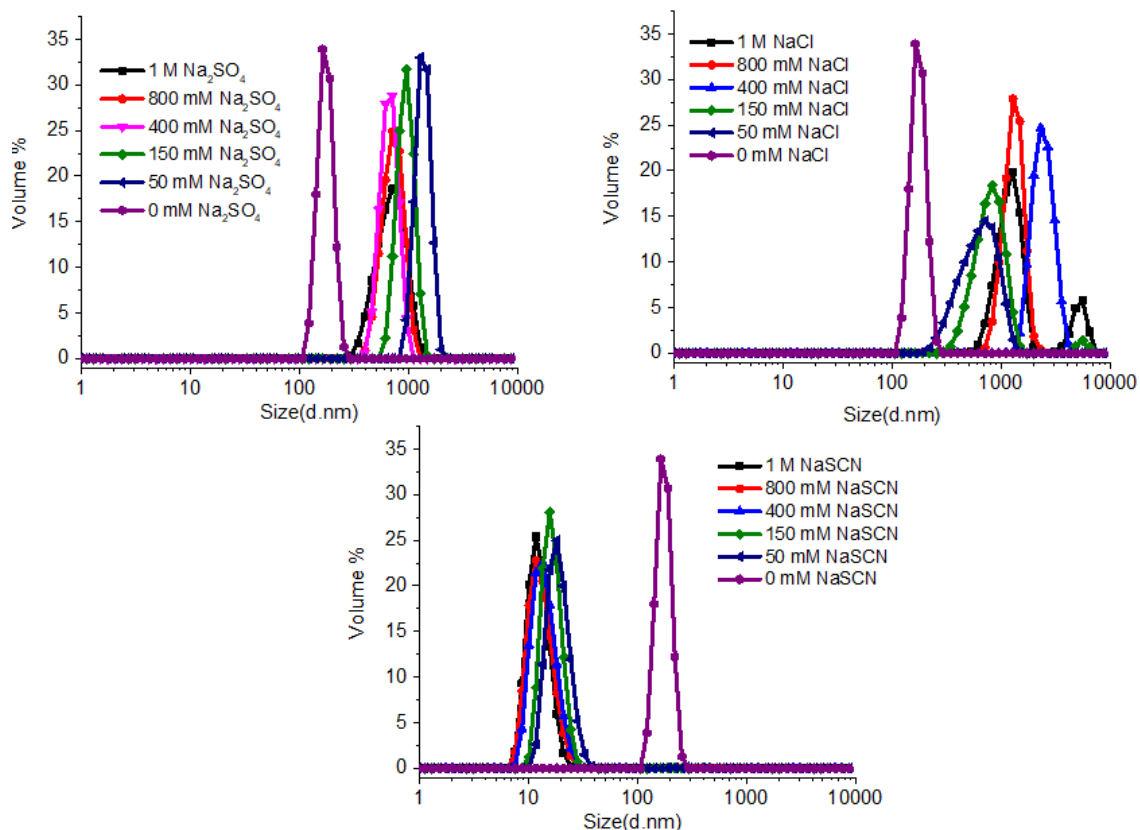


**Figure A.4:** Dynamic light scattering (DLS) of trimer (T) in the presence of kosmotropic (sodium sulfate), weakly kosmotropic (sodium chloride) and chaotropic salts (sodium thiocyanate)

and sodium chloride were found to induce aggregation of these assemblies and gave rise to assemblies which were about 1  $\mu\text{m}$  in size from DLS. On the other hand, sodium

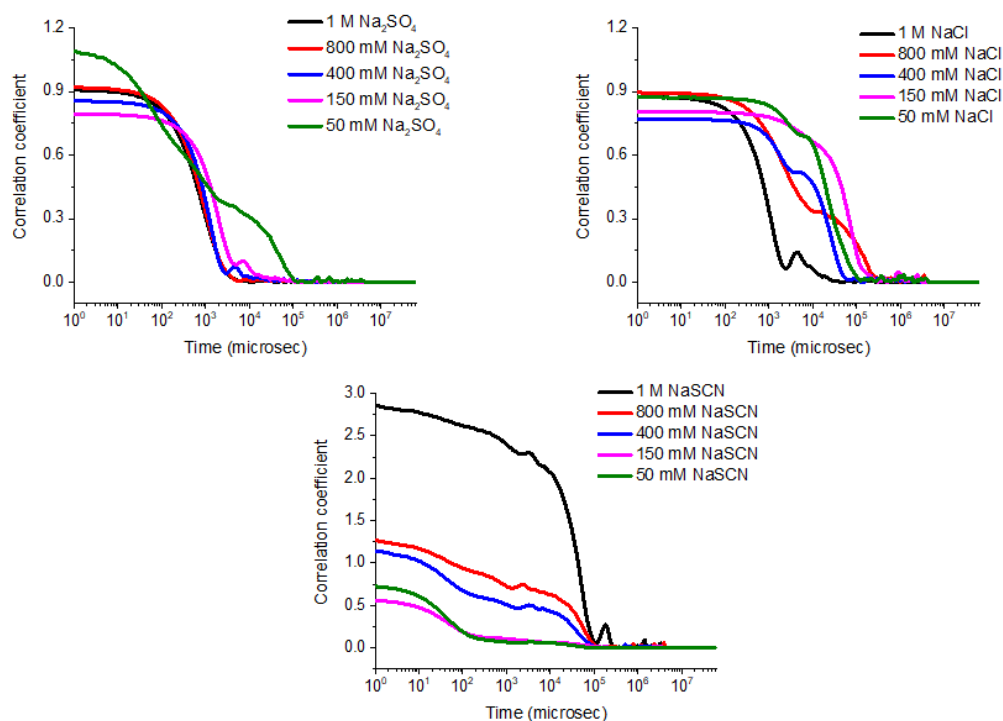


**Figure A.5:** Correlation coefficients as given by Dynamic light scattering (DLS) of trimer (T) in the presence of kosmotropic (sodium sulfate), weakly kosmotropic (sodium chloride) and chaotropic salts (sodium thiocyanate)

thiocyanate which is a chaotrope was found to reduce the size of these assemblies to about 10 nm in size.

This result interestingly coincides with a previous finding wherein the OEG chains in these oligomeric assemblies were hypothesized to be hydrated better at lower temperatures and chaotropic anions are understood to bring about a similar effect<sup>5</sup>. This is taken to be because of better hydration of OEG chains upon introduction of chaotropic ions and a subsequent change in the hydrophilic-lipophilic balance (HLB) resulting in the change in the aggregation properties of the oligomeric trimers. On the other hand, kosmotropes which are understood to dehydrate OEG



chains induce inter-aggregate crosslinking resulting in larger assemblies. Also, the threshold concentration required to induce aggregation of these assemblies is found to be  $\sim 50$  mM.

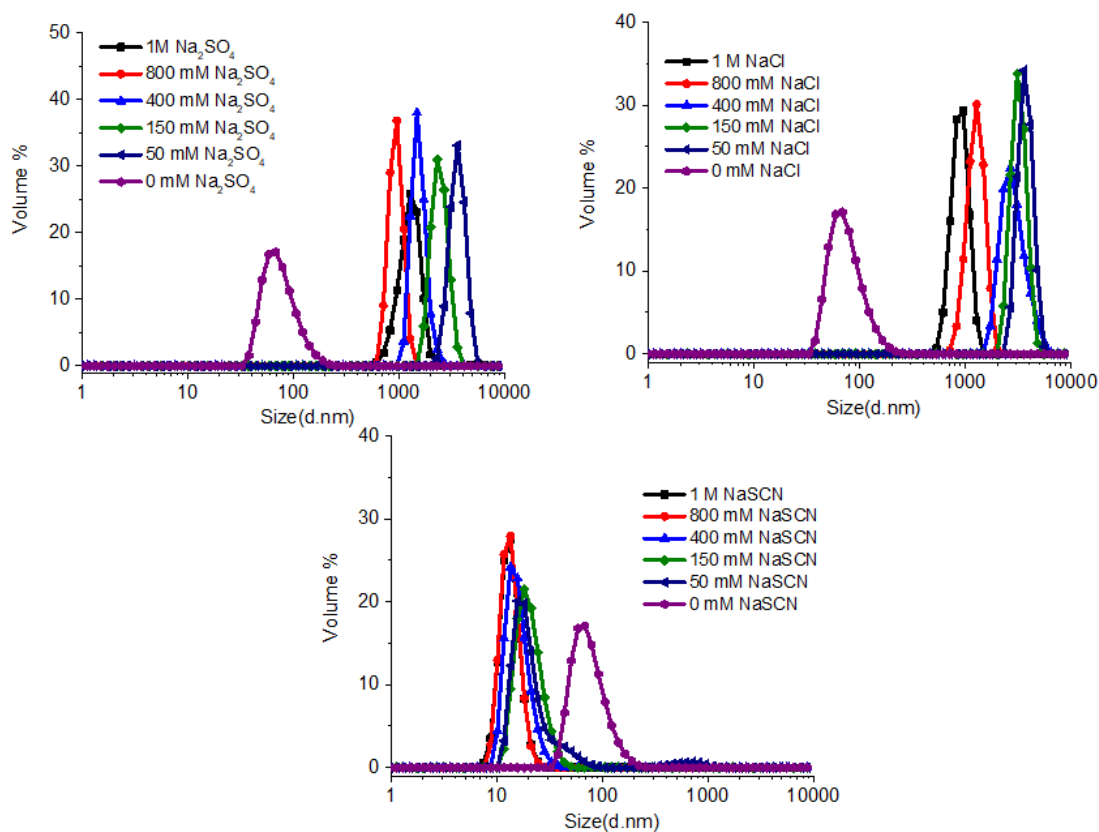


**Figure A.6:** Dynamic light scattering (DLS) of cyclic trimer (CT) in the presence of kosmotropic (sodium sulfate), weakly kosmotropic (sodium chloride) and chaotropic salts (sodium thiocyanate)

### A.3.2 Effect of Hofmeister ions of the sub-LCST of trimers

Because the Hofmeister ions change the LCST of these OEG containing amphiphiles, we hypothesized that the behavior so observed would hold true even for the sub-LCST behavior for the trimers. To test this hypothesis, we subjected these trimer solutions containing 500 mM sodium sulfate/sodium chloride/sodium thiocyanate to different temperatures and recorded the sizes of these aggregates at different temperatures.

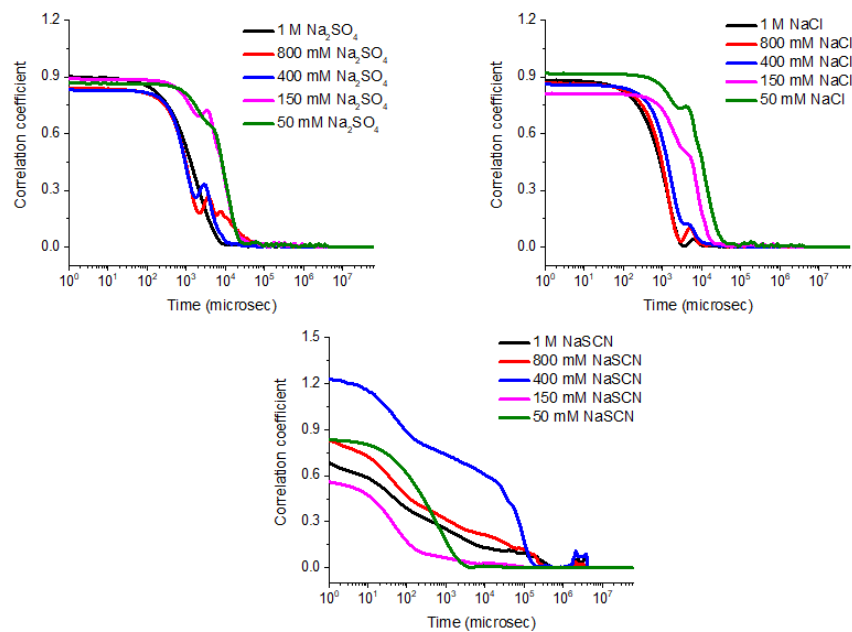


**Figure A.7:** Correlation coefficients as determined by dynamic light scattering (DLS) of cyclic trimer (CT) in the presence of kosmotropic (sodium sulfate), weakly kosmotropic (sodium chloride) and chaotropic salts (sodium thiocyanate)

We found that the sizes of the aggregates at different temperatures could not be determined because

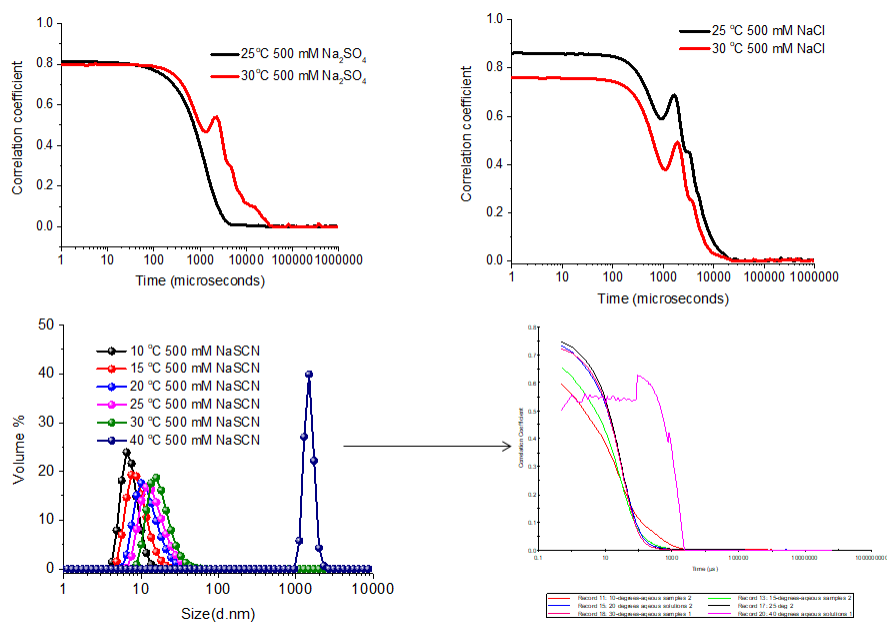


**Figure A.8:** Correlation coefficients as determined by dynamic light scattering (DLS) of trimer (T) in the presence of 500 mM kosmotropic (sodium sulfate), weakly kosmotropic (sodium chloride) and chaotropic salts (sodium thiocyanate) at different temperatures

the correlation coefficients obtained from DLS measurements were not reliable and this suggests that the size measurement is not possible for the trimer. As for the cyclic trimer, the sizes could be obtained reproducibly however, the correlation coefficient were still not reliable. Hence, the results obtained herewith are not conclusive.

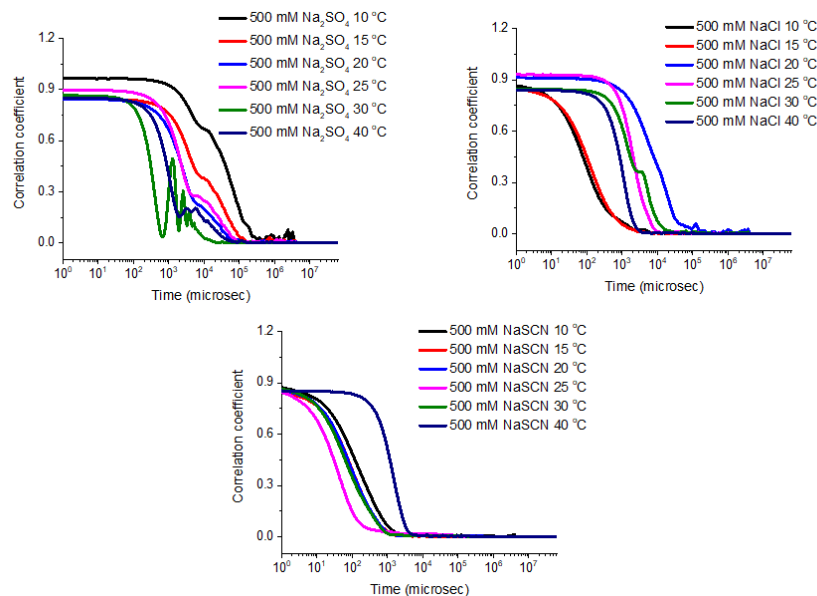


**Figure A.9:** Correlation coefficients as determined by dynamic light scattering (DLS) of cyclic trimer (CT) in the presence of 500 mM kosmotropic (sodium sulfate), weakly kosmotropic (sodium chloride) and chaotropic salts (sodium thiocyanate) at different temperatures

Our explanation for the observed discrepancies in the correlation coefficients stems from an earlier research wherein several research groups have reported a change in viscosity upon addition of salts<sup>8</sup>. It is important to note that the principle of dynamic light scattering rests on the Stokes-Einstein equation and the hydrodynamic radius is calculated assuming the solution viscosity to be the same. If the solution viscosity were to change based on the concentration of salts involved, then approximating the viscosity to be the same for all the salt concentrations and that too at

different temperatures would lead to erroneous results. This explains the trends seen in the correlation coefficients observed in the above DLS measurements.

### A.3.3 Dynamics of exchange using Foster Resonance Energy Transfer (FRET)

Considering the salt-dependent aggregation behavior, we were interested in investigating the implications of this behavior in guest exchange. While we did not anticipate any difference in the encapsulation of guest molecules based on minor salt dependent variations in the assembly, we expected such changes to affect the dynamics of guest exchange between the host and the bulk solvent which is referred to as the encapsulation stability. We hypothesize that if the solvation of the host were to differ upon addition of salts, then the encapsulation stability should follow suit since guest encapsulation are governed by solvophobic interactions.

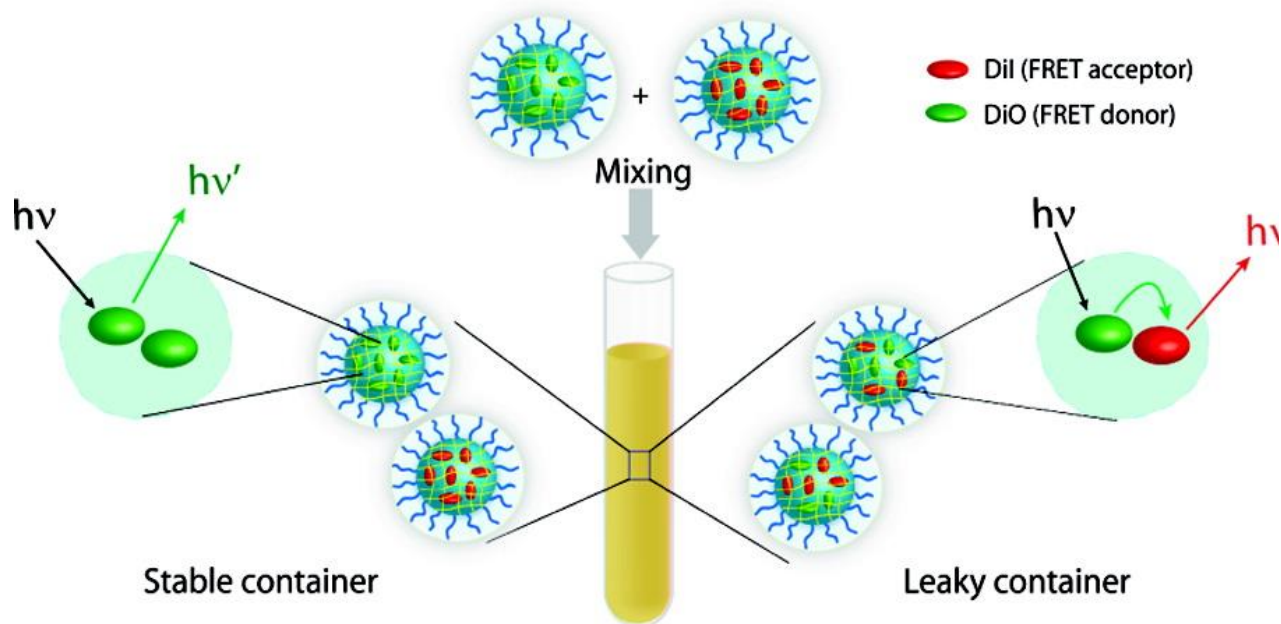


**Figure A.10:** Working principle of the FRET-based method to determine the dynamics of exchange in supramolecular assemblies

If the oligomer were to be more hydrophilic upon addition of chaotropes, then the dynamics of exchange should be faster than in case of weakly kosmotropic or kosmotropic salts. The dynamics of guest exchange and thus, the leakage coefficient can be measured using a Foster Resonance Energy Transfer (FRET)-based method<sup>9</sup>. Here, two separate solutions of the host-guest assembly are mixed: one comprising of a FRET donor dye (DiO) and the other container containing an

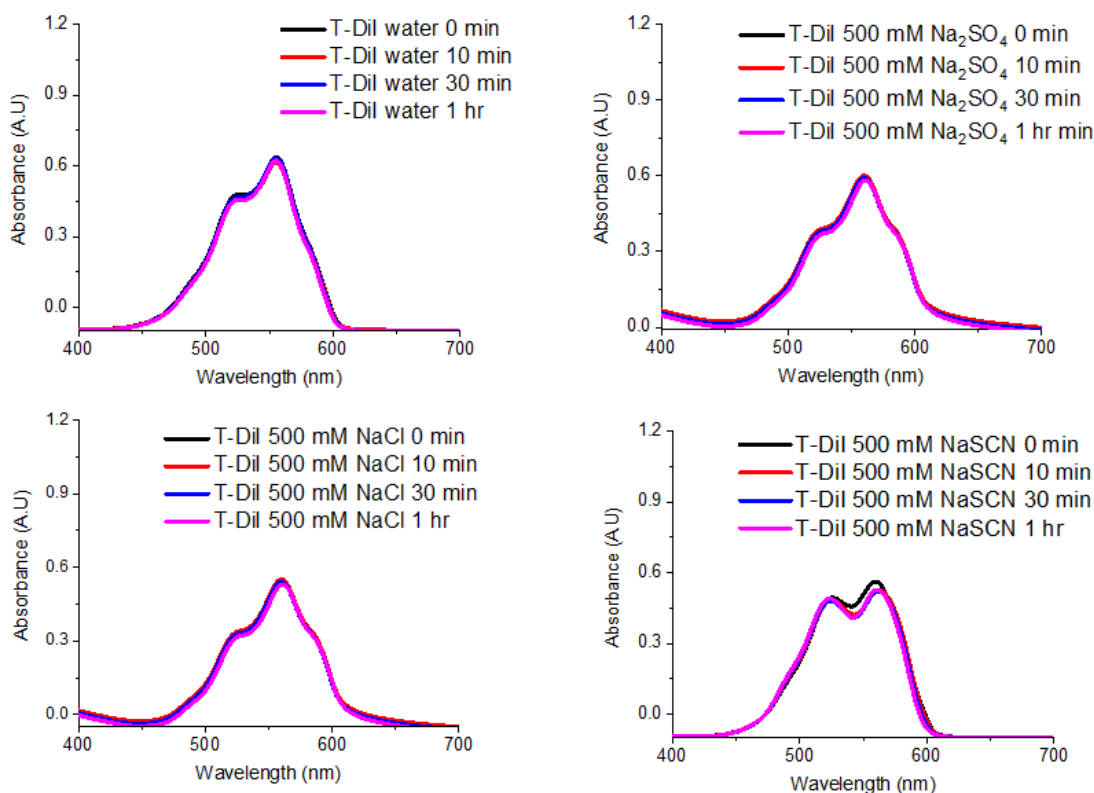


**Figure A.11:** Absorbance of DiI in dye-loaded trimer (T) upon addition of kosmotrope (Na<sub>2</sub>SO<sub>4</sub> and NaCl) and chaotropes (NaSCN)

acceptor dye (DiI). If there were to be a rapid exchange of these dye molecules upon mixing such that the donor and acceptor would result in the same supramolecular assembly, this would lead to

a decrease in the donor emission and a concomitant increase in the acceptor emission when the donor molecule is excited. On the other hand, when there is no guest exchange, there will be no

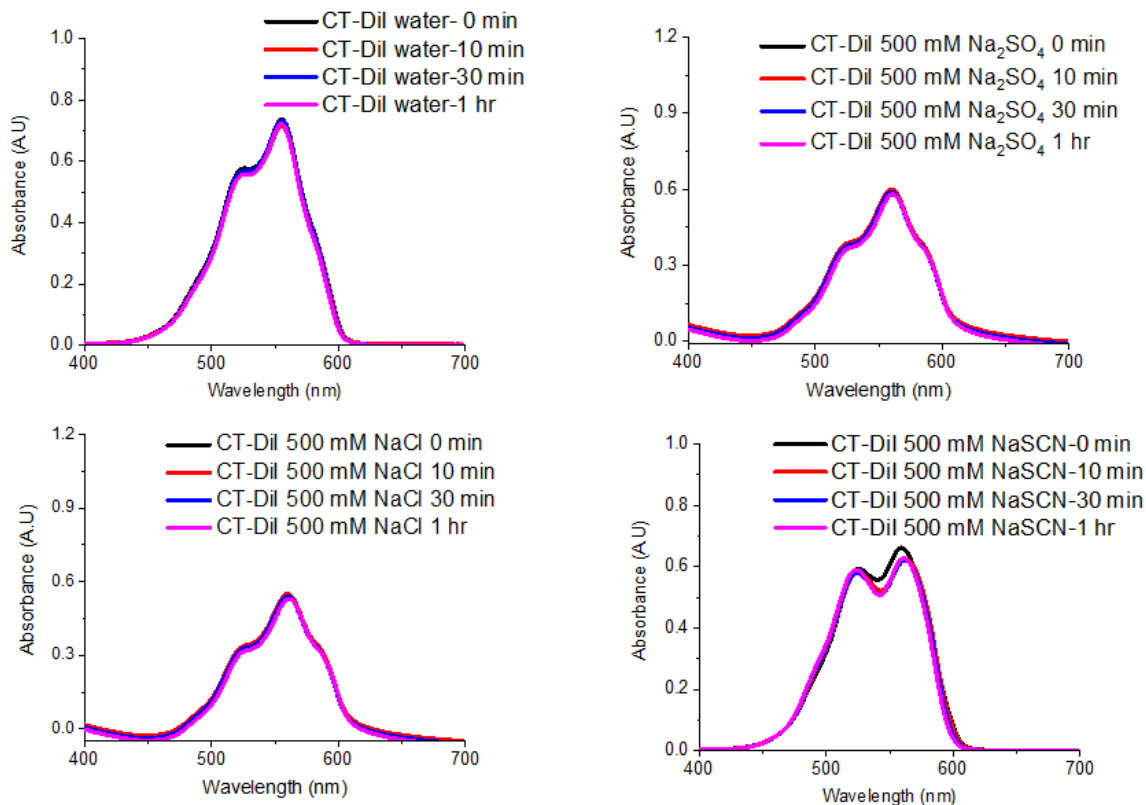


**Figure A.12:** Absorbance of DiI in dye-loaded cyclic trimer (CT) upon addition of kosmotrope (Na<sub>2</sub>SO<sub>4</sub> and NaCl) and chaotropes (NaSCN)

evolution of the relative emission intensities of the donor and acceptor over time.

To test this hypothesis, we first tested the encapsulation stability of the trimers by monitoring the absorption spectrum of the guest molecule (DiI). We measured the leakage and precipitation of the dye molecule.

The solution that contains kosmotropes such as sodium sulfate and sodium chloride should dehydrate the exposed OEG groups thus, rendering the nanogels less leaky. Chaotropes on the other hand, would render the assembly leakier because more OEG groups would be hydrated.

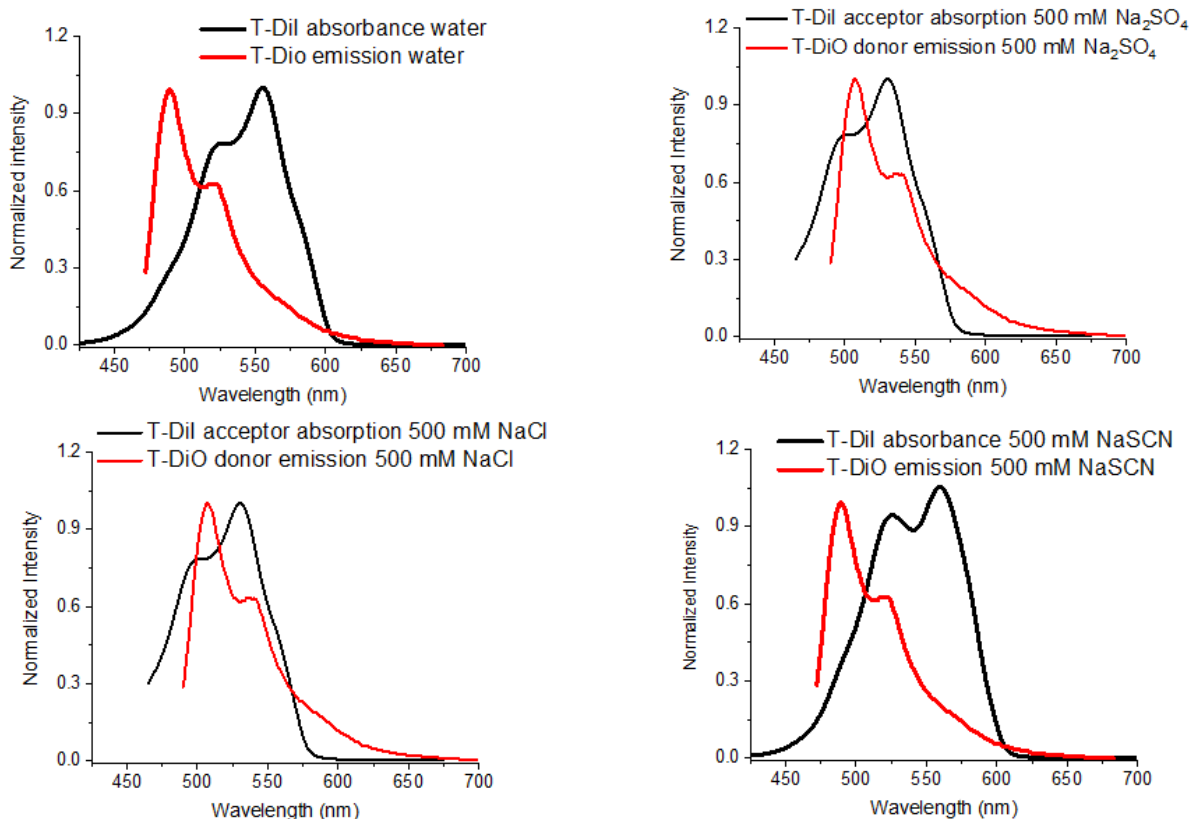


**Figure A.13:** Overlap integral for DiO and DiI in dye-loaded trimer (T) upon addition of kosmotrope (Na<sub>2</sub>SO<sub>4</sub> and NaCl) and chaotropes (NaSCN)

Indeed, we found this to be the case (Fig 11 and 12). In both the trimer and the cyclic trimer, there is little or no dye leakage in the presence of only kosmotropes. Therefore, the encapsulation stability of guest molecules is dependent on the nature of the salt used for the preparation of the nanogels.

FRET or Forster Resonance Energy transfer is based on the principle of transfer of excitation energy of a donor to a nearby acceptor in a non-radiative manner through dipole-dipole interactions

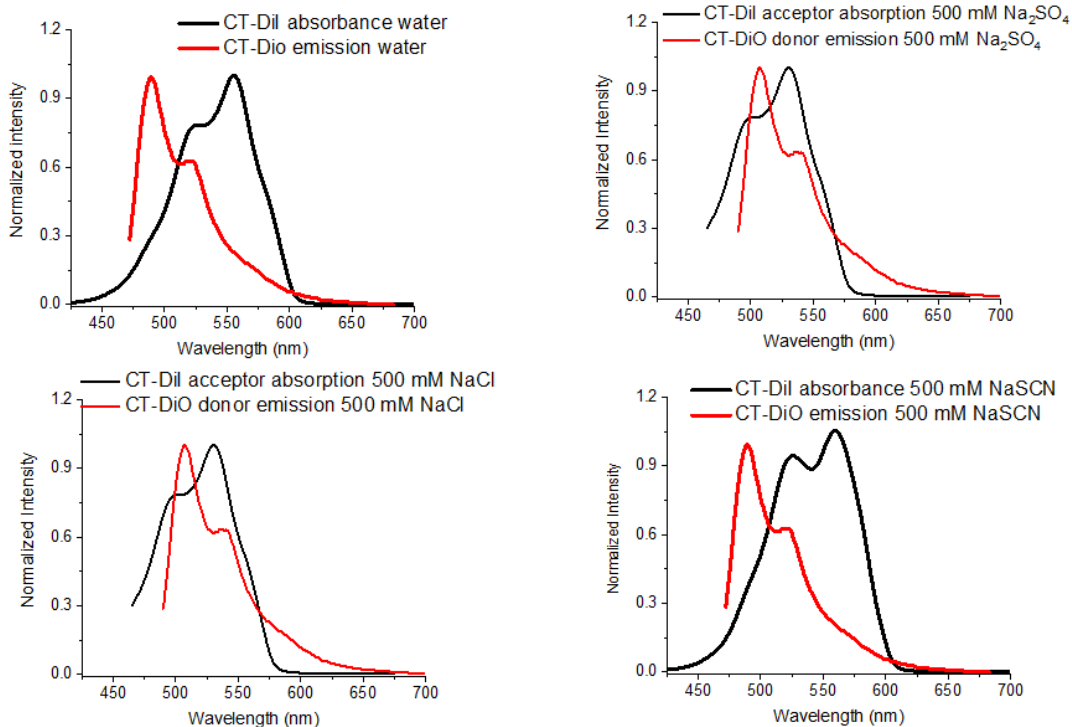


**Figure A.14:** Overlap integral for DiO and DiI in dye-loaded cyclic trimer (CT) upon addition of kosmotrope (Na<sub>2</sub>SO<sub>4</sub> and NaCl) and chaotropes (NaSCN)

and the resonance frequencies of the donor-acceptor need to be similar<sup>10</sup>. We next, investigated if this FRET-based method could indeed be used for the system of interest to us. To this end, we tested if the basic prerequisites of FRET were met by the dye-loaded oligomeric system that we are using here. One of the most important prerequisites for FRET to be conclusive is the overlap integral between the donor emission and the acceptor absorbance spectrum<sup>11</sup>. Because the salts change the hydrophilicity of the interior of the assembly, we anticipated shifts in the emission spectrum of the dyes DiO and DiI due to the change in the microenvironment of the interior of the assembly<sup>12</sup>. We measured the emission spectrum of the donor (DiO) and the absorbance spectrum



of the acceptor (DiI) in the presence of different salts and extrapolated the overlap integral (Figure 13 and 14).

Note that there are no shifts observed in the acceptor absorbance spectrum and it remains the same irrespective of the choice of salt. However, there is a drastic shift in the emission spectrum of the donor (DiO) in various salts and this alludes to the change in the extent of the overlap integral. There is a bathochromic shift observed for the donor (DiO) in case of kosmotropic salts while that is absent in case of water and chaotropes (NaSCN). Therefore, the extent of overlap is more for kosmotropes than chaotropes and that would result in a faster FRET for the kosmotropes. Note that this defies our previous hypothesis in which chaotropes were thought to make the assemblies more leaky and result in the faster exchange of the hydrophobic guest molecules. Therefore, it suffices to say that this technique is not viable to study the dynamics of exchange of the trimeric oligomers.

#### **A.4 Conclusions**

We observed that there are subtle differences in the aggregation states of OEG-functionalized amphiphilic oligomers in aqueous phase, endowed by the presence of various salts. Salt-dependent hydration of the OEG units in the nanogel was hypothesized to cause variations in dynamics of monomer aggregate equilibrium, which then determine the leaky character of the aggregates. A FRET-based method was evaluated to study the dynamics of monomer-aggregate equilibrium and needs to be assessed further.

## A.5 References

- (1) Zhang, Y.; Cremer, P. S. The Inverse and Direct Hofmeister Series for Lysozyme. *Proc. Natl. Acad. Sci.* **2009**, *106* (36), 15249–15253.
- (2) Bloksma, M. M.; Bakker, D. J.; Weber, C.; Hoogenboom, R.; Schubert, U. S. The Effect of Hofmeister Salts on the LCST Transition of Poly(2-Oxazoline)s with Varying Hydrophilicity. *Macromol. Rapid Commun.* **2010**, *31* (8), 724–728.
- (3) Cho, Y.; Zhang, Y.; Christensen, T.; Sagle, L. B.; Chilkoti, A.; Cremer, P. S. Effects of Hofmeister Anions on the Phase Transition Temperature of Elastin-like Polypeptides. *J. Phys. Chem. B* **2008**, *112* (44), 13765–13771.
- (4) Kashyap, S.; Jayakannan, M. Super LCST Thermo-Responsive Nanoparticle Assembly for ATP Binding through the Hofmeister Effect. *J. Mater. Chem. B* **2015**, *00*, 1–11.
- (5) Li, L.; Ryu, J. H.; Thayumanavan, S. Effect of Hofmeister Ions on the Size and Encapsulation Stability of Polymer Nanogels. *Langmuir* **2013**, *29* (1), 50–55.
- (6) Fuller, J. M.; Raghupathi, K. R.; Ramireddy, R. R.; Subrahmanyam, A. V.; Yesilyurt, V.; Thayumanavan, S. Temperature-Sensitive Transitions below LCST in Amphiphilic Dendritic Assemblies: Host-Guest Implications. *J. Am. Chem. Soc.* **2013**, *135* (24), 8947–8954.
- (7) Raghupathi, K. R.; Sridhar, U.; Byrne, K.; Raghupathi, K.; Thayumanavan, S. Influence of Backbone Conformational Rigidity in Temperature-Sensitive Amphiphilic Supramolecular Assemblies.
- (8) Sedláč, M. What Can Be Seen by Static and Dynamic Light Scattering in Polyelectrolyte Solutions and Mixtures? *Langmuir* **1999**, *15* (12), 4045–4051.
- (9) Jiwanich, S.; Ryu, J. H.; Bickerton, S.; Thayumanavan, S. Noncovalent Encapsulation

- Stabilities in Supramolecular Nanoassemblies. *J. Am. Chem. Soc.* **2010**, *132* (31), 10683–10685.
- (10) Yefimova, S. L.; Tkacheva, T. N.; Kurilchenko, I. Y.; Sorokin, A. V.; Malyukin, Y. V. Spectroscopic Study of Interactions between Dye Molecules in Micelle and Liposome Nanovolumes. *J. Appl. Spectrosc.* **2013**, *79* (6), 914–921.
- (11) Xie, M.; Wang, S.; Singh, A.; Cooksey, T. J.; Marquez, M. D.; Bhattarai, A.; Kourentzi, K.; Robertson, M. L. Fluorophore Exchange Kinetics in Block Copolymer Micelles with Varying Solvent-Fluorophore and Solvent-Polymer Interactions. *Soft Matter* **2016**, *12* (29), 6196–6205.
- (12) Raghupathi, K. R.; Guo, J.; Munkhbat, O.; Rangadurai, P.; Thayumanavan, S. Supramolecular Disassembly of Facially Amphiphilic Dendrimer Assemblies in Response to Physical, Chemical, and Biological Stimuli. *Acc. Chem. Res.* **2014**, *47* (7), 2200–2211.

## BIBLIOGRAPHY

Aathimanikandan, S. V.; Savariar, E. N.; Thayumanavan, S. Temperature-Sensitive Dendritic Micelles. *J. Am. Chem. Soc.* **2005**, *127* (42), 14922–14929.

Alino, V. J.; Pang, J.; Yang, K. L., Liquid Crystal Droplets as a Hosting and Sensing Platform for Developing Immunoassays. *Langmuir* **2011**, *27* (19), 11784–11789.

Aluri, S.; Pastuszka, M. K.; Moses, A. S.; MacKay, J. A. Elastin-like Peptide Amphiphiles Form Nanofibers with Tunable Length. *Biomacromolecules* **2012**, *13* (9), 2645–2654.

Amado Torres, D.; Azagarsamy, M. A.; Thayumanavan, S. Supramolecular Displacement-Mediated Activation of a Silent Fluorescence Probe for Label-Free Ligand Screening. *J. Am. Chem. Soc.* **2012**, *134* (17), 7235–7237.

Amado Torres, D.; Garzoni, M.; Subrahmanyam, A. V.; Pavan, G. M.; Thayumanavan, S. Protein-Triggered Supramolecular Disassembly: Insights Based on Variations in Ligand Location in Amphiphilic Dendrons. *J. Am. Chem. Soc.* **2014**, *136* (14), 5385–5399.

Aslani, P.; Kennedy, R. A. Studies on Diffusion in Alginate Gels. I. Effect of Cross-Linking with Calcium or Zinc Ions on Diffusion of Acetaminophen. *J. Control. Release* **1996**, *42* (1), 75–82.

Augst, A. D.; Kong, H. J.; Mooney, D. J. Alginate Hydrogels as Biomaterials. *Macromol. Biosci.* **2006**, *6* (8), 623–633.

Azagarsamy, M. A.; Sokkalingam, P.; Thayumanavan, S. Enzyme-Triggered Disassembly of Dendrimer-Based Amphiphilic Nanocontainers. *J. Am. Chem. Soc.* **2009**, *131* (40), 14184–14185.

Azagarsamy, M. A.; Yesilyurt, V.; Thayumanavan, S. Disassembly of Dendritic Micellar Containers Due to Protein Binding. *J. Am. Chem. Soc.* **2010**, *132* (13), 4550–4551.

Azagarsamy, M. A.; Yesilyurt, V.; Thayumanavan, S. Disassembly of dendritic micellar containers due to protein binding. *J. Am. Chem. Soc.* **2010**, *132*, 4550–4551.

Bai, W.; Jiang, Z.; Ribbe, A. E.; Thayumanavan, S. Smart Organic Two-Dimensional Materials Based on a Rational Combination of Non-Covalent Interactions. *Angew. Chemie - Int. Ed.* **2016**, *55* (36), 10707–10711.

Balce, D. R.; Yates, R. M. Redox-Sensitive Probes for the Measurement of Redox Chemistries within Phagosomes of Macrophages and Dendritic Cells. *Redox Biol.* **2013**, *1* (1), 467–474.

Barhoumi, A.; Liu, Q.; Kohane, D. S., Ultraviolet light-mediated drug delivery: Principles, applications, and challenges. *J. Control. Release* **2015**, *219*, 31-42.

Bell, L. N.; Labuza, T. P. Aspartame Degradation Kinetics as Affected by pH in Intermediate and Low Moisture Food Systems. *J. Food Sci.* **1991**, *56* (1), 17–20.

Bell, L. N.; Wetzel, C. R. Aspartame Degradation in Solution as Affected by Buffer Type and Concentration. *J. Agric. Food Chem.* **1995**, 2608–2612.

Bera, T.; Deng, J.; Fang, J., Protein-Induced Configuration Transitions of Polyelectrolyte-Modified Liquid Crystal Droplets. *J. Phys. Chem. B* **2014**, *118* (18), 4970-4975.

Bi, X. Y.; Hartono, D.; Yang, K. L., Real-Time Liquid Crystal pH Sensor for Monitoring Enzymatic Activities of Penicillinase. *Adv. Funct. Mater.* **2009**, *19* (23), 3760-3765.

Blandino, A.; Macias, M.; Cantero, D. Formation of Calcium Alginate Gel Capsules: Influence of Sodium Alginate and CaCl<sub>2</sub> Concentration on Gelation Kinetics. *J. Biosci. Bioeng.* **1999**, *88* (6), 686–689.

Bloksma, M. M.; Bakker, D. J.; Weber, C.; Hoogenboom, R.; Schubert, U. S. The Effect of Hofmeister Salts on the LCST Transition of Poly(2-Oxazoline)s with Varying Hydrophilicity. *Macromol. Rapid Commun.* **2010**, *31* (8), 724–728.

Bowerman, C. J.; Ryan, D. M.; Nissan, D. A.; Nilsson, B. L. The Effect of Increasing Hydrophobicity on the Self-Assembly of Amphipathic Beta-Sheet Peptides. *Mol. Biosyst.* **2009**, *5* (9), 1058–1069.

Breedveld, V.; Nowak, A. P.; Sato, J.; Deming, T. J.; Pine, D. J. Rheology of Block Copolyptide Solutions: Hydrogels with Tunable Properties. *Macromolecules* **2004**, *37* (10), 3943–3953.

Bukusoglu, E.; Pantoja, M. B.; Mushenheim, P. C.; Wang, X.; Abbott, N. L., Design of responsive and active (soft) materials using liquid crystals. *Annual Review of Chemical and Biomolecular Engineering* **2016**, *7*, 163-196.

Butchko, H. H.; Stargel, W. W.; Comer, C. P.; Mayhew, D. a; Benninger, C.; Blackburn, G. L.; de Sonnevile, L. M. J.; Geha, R. S.; Hertelendy, Z.; Koestner, A.; et al. Aspartame: Review of Safety. *Regul. Toxicol. Pharmacol.* **2002**, *35*, S1–S93.

Cabral, H.; Nishiyama, N.; Kataoka, K. Supramolecular Nanodevices: From Design Validation to Theranostic Nanomedicine. *Acc. Chem. Res.* **2011**, *44* (10), 999–1008.

Campbell, K. T.; Hadley, D. J.; Kukis, D. L.; Silva, E. A. Alginate Hydrogels Allow for Bioactive and Sustained Release of VEGF-C and VEGF-D for Lymphangiogenic Therapeutic Applications. *PLoS One* **2017**, *12* (7), 1-15.

Carlton, R. J.; Gupta, J. K.; Swift, C. L.; Abbott, N. L., Influence of Simple Electrolytes on the Orientational Ordering of Thermotropic Liquid Crystals at Aqueous Interfaces. *Langmuir* **2012**, *28*, 31-36.

Carlton, R. J.; Hunter, J. T.; Miller, D. S.; Abbasi, R.; Mushenheim, P. C.; Tan, L. N.; Abbott, N. L., Chemical and biological sensing using liquid crystals. *Liq. Cryst. Rev.* **2013**, *1* (1), 29-51.

Castelletto, V.; Moulton, C. M.; Cheng, G.; Hamley, I. W.; Hicks, M. R.; Rodger, A.; López-Pérez, D. E.; Revilla-López, G.; Alemán, C. Self-Assembly of Fmoc-Tetrapeptides Based on the RGDS Cell Adhesion Motif. *Soft Matter* **2011**, *7* (24), 11405–11415.

Chan, L. W.; Jin, Y.; Heng, P. W. S. Cross-Linking Mechanisms of Calcium and Zinc in Production of Alginate Microspheres. *Int. J. Pharm.* **2002**, *242* (1–2), 255–258.

Chen, C.; Wang, Z.; Li, Z. Thermoresponsive Polypeptides from Pegylated Poly-l-Glutamates. *Biomacromolecules* **2011**, *12* (8), 2859–2863.

Chen, S. W.; Drakulic, S.; Deas, E.; Ouberai, M.; Aprile, F. A.; Arranz, R.; Ness, S.; Roodveldt, C.; Guilliams, T.; De-Genst, E. J.; et al. Structural Characterization of Toxic Oligomers That Are Kinetically Trapped during  $\alpha$ -Synuclein Fibril Formation. *Proc. Natl. Acad. Sci.* **2015**, *112* (16), E1994–E2003.

Cheng, C.-C.; Wang, J.-H.; Chuang, W.-T.; Liao, Z.-S.; Huang, J.-J.; Huang, S.-Y.; Fan, W.-L.; Lee, D.-J. Dynamic Supramolecular Self-Assembly: Hydrogen Bonding-Induced Contraction and Extension of Functional Polymers. *Polym. Chem.* **2017**, *8* (21), 3294–3299.

Cheng, G.; Castelletto, V.; Moulton, C. M.; Newby, G. E.; Hamley, I. W. Hydrogelation and Self-Assembly of Fmoc-Triptides: Unexpected Influence of Sequence on Self-Assembled Fibril Structure, and Hydrogel Modulus and Anisotropy. *Langmuir* **2010**, *26* (7), 4990–4998.

Cheng, W.; Gu, L.; Ren, W.; Liu, Y. Stimuli-Responsive Polymers for Anti-Cancer Drug Delivery. *Mater. Sci. Eng. C* **2015**, *45*, 600–608.

Cho, Y.; Zhang, Y.; Christensen, T.; Sagle, L. B.; Chilkoti, A.; Cremer, P. S. Effects of Hofmeister Anions on the Phase Transition Temperature of Elastin-like Polypeptides. *J. Phys. Chem. B* **2008**, *112* (44), 13765–13771.

Cho, Y.; Zhang, Y.; Christensen, T.; Sagle, L. B.; Chilkoti, A.; Cremer, P. S. Effects of Hofmeister Anions on the Phase Transition Temperature of Elastin-like Polypeptides. *J. Phys. Chem. B* **2008**, *112* (44), 13765–13771.

Christensen, T.; Hassouneh, W.; Trabbic-Carlson, K.; Chilkoti, A. Predicting Transition Temperatures of Elastin-like Polypeptide Fusion Proteins. *Biomacromolecules* **2013**, *14* (5), 1514–1519.

Chronopoulou, L.; Sennato, S.; Bordi, F.; Giannella, D.; Di Nitto, A.; Barbetta, A.; Dentini, M.; Togna, A. R.; Togna, G. I.; Moschini, S.; et al. Designing Unconventional Fmoc-Peptide-Based Biomaterials: Structure and Related Properties. *Soft Matter* **2014**, *10* (12), 1944–1952.

Chuy, S.; Bell, L. N. Kinetics of an Acid-Base Catalyzed Reaction (Aspartame Degradation) as Affected by Polyol-Induced Changes in Buffer pH and pKa Values. *J. Food Sci.* **2009**, *74* (1), 56–61.

Colombo, G.; Soto, P.; Gazit, E. Peptide Self-Assembly at the Nanoscale: A Challenging Target for Computational and Experimental Biotechnology. *Trends Biotechnol.* **2007**, *25* (5), 211–218.

Conradi, M.; Ravnik, M.; Bele, M.; Zorko, M.; Zumer, S.; Musevic, I., Janus nematic colloids. *Soft Matter* **2009**, *5* (20), 3905–3912.

Cook, M. T.; Tzortzis, G.; Charalampopoulos, D.; Khutoryanskiy, V. V. Production and Evaluation of Dry Alginate-Chitosan Microcapsules as an Enteric Delivery Vehicle for Probiotic Bacteria. *Biomacromolecules* **2011**, *12* (7), 2834–2840.

Dan, K.; Bose, N.; Ghosh, S. Vesicular Assembly and Thermo-Responsive Vesicle-to-Micelle Transition from an Amphiphilic Random Copolymer. *Chem. Commun.* **2011**, *47* (46), 12491.

Dash, V.; Mishra, S. K.; Singh, M.; Goyal, A. K.; Rath, G. Release Kinetic Studies of Aspirin Microcapsules from Ethyl Cellulose, Cellulose Acetate Phthalate and Their Mixtures by Emulsion Solvent Evaporation Method. *Sci. Pharm.* **2010**, *78* (1), 93–101.

de Gennes, P. G.; Prost, J., *The Physics of Liquid Crystals*. Clarendon Press: Oxford, 1993.

de Las Heras Alarcon, C.; Pennadam, S.; Alexander, C. Stimuli Responsive Polymers for Biomedical Applications. *Chem. Soc. Rev.* **2005**, *34* (3), 276–285.

Demus, D.; Goodby, J.; Gray, G. W.; Spiess, H.-W.; Vill, V., *Handbook of Liquid Crystals*. Wiley-VCH Verlag GmbH: New York, 1998; Vol. Vol. 2

Desai, S.; Perkins, J.; Harrison, B. S.; Sankar, J. Understanding Release Kinetics of Biopolymer Drug Delivery Microcapsules for Biomedical Applications. *Mater. Sci. Eng. B Solid-State Mater. Adv. Technol.* **2010**, *168* (1), 127–131.

Dias, C. L.; Ala-Nissila, T.; Wong-ekkabut, J.; Vattulainen, I.; Grant, M.; Karttunen, M. The Hydrophobic Effect and Its Role in Cold Denaturation. *Cryobiology* **2010**, *60* (1), 91–99.  
Dierking, I., *Textures of Liquid Crystals*. Wiley-VCH Verlag GmbH & Co. KGaA: New York, 2004.

Dutta, K.; Hu, D.; Zhao, B.; Ribbe, A. E.; Zhuang, J.; Thayumanavan, S. Templated Self-Assembly of a Covalent Polymer Network for Intracellular Protein Delivery and Traceless Release. *J. Am. Chem. Soc.* **2017**, *139* (16), 5676–5679.

Evans, D. F.; Ninham, B. W. Molecular forces in the self-organization of amphiphiles. *J. Phys. Chem.* **1986**, *90*, 226–234.

FDA Board Decision Federal Alert- New Regulations. **1979**, *11*, 21730.

Feil, H.; Bae, Y. H.; Feijen, J.; Kim, S. W. Effect of Comonomer Hydrophilicity and Ionization on the Lower Critical Solution Temperature of N-Isopropylacrylamide Copolymers. *Macromolecules* **1993**, *26* (10), 2496–2500.

Fleming, S.; Ulijn, R. V. Design of Nanostructures Based on Aromatic Peptide Amphiphiles. *Chem. Soc. Rev.* **2014**, *43* (23), 8150–8177.

Fletcher, P. D. I.; Kang, N.-G.; Paunov, V. N., UV Polymerisation of Surfactants Adsorbed at the Nematic Liquid Crystal-Water Interface Produces an Optical Response. *ChemPhysChem* **2009**, *10* (17), 3046-3053.

Fong, W. K.; Hanley, T.; Boyd, B. J., Stimuli responsive liquid crystals provide 'on-demand' drug delivery in vitro and in vivo. *J. Control. Release* **2009**, *135* (3), 218-226.

Fu, I. W.; Markegard, C. B.; Nguyen, H. D. Solvent Effects on Kinetic Mechanisms of Self-Assembly by Peptide Amphiphiles via Molecular Dynamics Simulations. **2014**.



Fuller, J. M.; Raghupathi, K. R.; Ramireddy, R. R.; Subrahmanyam, A. V.; Yesilyurt, V.; Thayumanavan, S. Temperature-Sensitive Transitions below LCST in Amphiphilic Dendritic Assemblies: Host-Guest Implications. *J. Am. Chem. Soc.* **2013**, *135* (24), 8947–8954.

Gaines, S. M.; Bada, J. L. Aspartame Decomposition and Epimerization in the Diketopiperazine and Dipeptide Products as a Function of pH and Temperature. *J. Org. Chem.* **1988**, *53* (12), 2757–2764.

Ganesan, S. J.; Matysiak, S. Role of Backbone Dipole Interactions in the Formation of Secondary and Supersecondary Structures of Proteins. *J. Chem. Theory Comput.* **2014**, *10* (6), 2569–2576.

Gao, J.; Liu, X.; Secinti, H.; Jiang, Z.; Munkhbat, O.; Xu, Y.; Guo, X.; Thayumanavan, S. Photoactivation of Ligands for Extrinsically and Intrinsically Triggered Disassembly of Amphiphilic Nanoassemblies. *Chem. - A Eur. J.* **2018**, *24* (8), 1789–1794.

Gaplovsky, M.; Il'ichev, Y. V.; Kamdzhilov, Y.; Kombarova, S. V.; Mac, M.; Schwörer, M. A.; Wirz, J. Photochemical Reaction Mechanisms of 2-Nitrobenzyl Compounds: 2-Nitrobenzyl Alcohols Form 2-Nitroso Hydrates by Dual Proton Transfer. *Photochem. Photobiol. Sci.* **2005**, *4* (1), 33–42.

Garbow, J. R.; Likos, J. J.; Schroeder, S. a. Structure, Dynamics, and Stability of Beta-Cyclodextrin Inclusion Complexes of Aspartame and Neotame. *J. Agric. Food Chem.* **2001**, *49* (4), 2053–2060.

Gazit, E. Self-Assembled Peptide Nanostructures: The Design of Molecular Building Blocks and Their Technological Utilization. *Chem. Soc. Rev.* **2007**, *36* (8), 1263–1269.

Gelebart, A. H.; Mulder, D. J.; Varga, M.; Konya, A.; Vantomme, G.; Meijer, E. W.; Selinger, R. L. B.; Broer, D. J., Making waves in a photoactive polymer film. *Nature* **2017**, *546* (7660), 632-636.

Ghosh, S.; Irvin, K.; Thayumanavan, S. Tunable Disassembly of Micelles Using a Redox Trigger. *Langmuir* **2007**, *23* (15), 7916–7919.

González, D. C.; Savariar, E. N.; Thayumanavan, S. Fluorescence Patterns from Supramolecular Polymer Assembly and Disassembly for Sensing Metallo- and Nonmetalloproteins. *J. Am. Chem. Soc.* **2009**, *131* (22), 7708–7716.

Gorbunova, N.; Evteev, A.; Evdokimov, I.; Bannikova, A. Kinetics of Ascorbic Acid Transport from Alginate Beads during in Vitro Digestion. **2016**, *55* (2), 148–158.

Gordon, M. R.; Zhao, B.; Anson, F.; Fernandez, A.; Singh, K.; Homyak, C.; Canakci, M.; Vachet, R. W.; Thayumanavan, S. Matrix Metalloproteinase-9-Responsive Nanogels for Proximal Surface Conversion and Activated Cellular Uptake. *Biomacromolecules* **2018**, *19* (3), 860–871.

Guo, J.; Zhuang, J.; Wang, F.; Raghupathi, K. R.; Thayumanavan, S. Protein and Enzyme Gated Supramolecular Disassembly. *J. Am. Chem. Soc.* **2014**, *136* (6), 2220–2223.

Gwag, J. S.; Kim, Y. K.; Lee, C. H.; Kim, J. H., Realization of Multi-Stable Ground States in a Nematic Liquid Crystal by Surface and Electric Field Modification. *Sci. Rep.* **2015**, *5*, 11368.

Hamley, I. W. Self-Assembly of Amphiphilic Peptides. *Soft Matter* **2011**, *7* (9), 4122–4138.

Harada, A.; Cammas, S.; Kataoka, K. Stabilized R-Helix Structure of Poly ( L -Lysine ) - Block-Poly ( Ethylene Glycol ) in Aqueous Medium through Supramolecular Assembly. *Macromolecules* **1996**, *29* (96), 6183–6188.

Hassouneh, W.; Fischer, K.; MacEwan, S. R.; Branscheid, R.; Fu, C. L.; Liu, R.; Schmidt, M.; Chilkoti, A. Unexpected Multivalent Display of Proteins by Temperature Triggered Self-Assembly of Elastin-like Polypeptide Block Copolymers. *Biomacromolecules* **2012**, *13* (5), 1598–1605.

Hatakeyama, H. Recent Advances in Endogenous and Exogenous Stimuli-Responsive Nanocarriers for Drug Delivery and Therapeutics. *Chem. Pharm. Bull* **2017**, *65* (7), 612–617.

Hatip Koc, M.; Cinar Ciftci, G.; Baday, S.; Castelletto, V.; Hamley, I. W.; Guler, M. O. Hierarchical Self-Assembly of Histidine-Functionalized Peptide Amphiphiles into Supramolecular Chiral Nanostructures. *Langmuir* **2017**, *33* (32), 7947–7956.

Hatip Koc, M.; Cinar Ciftci, G.; Baday, S.; Castelletto, V.; Hamley, I. W.; Guler, M. O. Hierarchical Self-Assembly of Histidine-Functionalized Peptide Amphiphiles into Supramolecular Chiral Nanostructures. *Langmuir* **2017**, *33* (32), 7947–7956.

Hocine, S.; Li, M.-H. Thermoresponsive Self-Assembled Polymer Colloids in Water. *Soft Matter* **2013**, *9* (25), 5839.

Hoffman, A. S. Hydrogels for Biomedical Applications. *Adv. Drug Deliv. Rev.* **2012**, *64*, 18–23.

Holmes MA, Matthews BW Structure of thermolysin refined at 1.6 Å resolution. *J. Mol. Biol.* **1982**, *160* (4), 623–639.

Hu, X.; Tian, J.; Liu, T.; Zhang, G.; Liu, S. Photo-Triggered Release of Caged Camptothecin Prodrugs from Dually Responsive Shell Cross-Linked Micelles. *Macromolecules* **2013**, *46* (15), 6243–6256.

Huang, C. Y.; Klemke, J. W.; Getahun, Z.; DeGrado, W. F.; Gai, F. Temperature-Dependent Helix-Coil Transition of an Alanine Based Peptide. *J. Am. Chem. Soc.* **2001**, *123* (38), 9235–9238.

Hughes, M.; Birchall, L. S.; Zuberi, K.; Aitken, L. A.; Debnath, S.; Javid, N.; Ulijn, R. V. Differential Supramolecular Organisation of Fmoc-Dipeptides with Hydrophilic Terminal Amino Acid Residues by Biocatalytic Self-Assembly. *Soft Matter* **2012**, *8* (45), 11565–11574.

Hughes, M.; Frederix, P. W. J. M.; Raeburn, J.; Birchall, L. S.; Sadownik, J.; Coomer, F. C.; Lin, I. H.; Cussen, E. J.; Hunt, N. T.; Tuttle, T.; et al. Sequence/Structure Relationships in Aromatic Dipeptide Hydrogels Formed under Thermodynamic Control by Enzyme-Assisted Self-Assembly. *Soft Matter* **2012**, *8* (20), 5595–5602.

Hyun, J.; Lee, W. K.; Nath, N.; Chilkoti, A.; Zauscher, S. Capture and Release of Proteins on the Nanoscale by Stimuli-Responsive Elastin-like Polypeptide “Switches.” *J. Am. Chem. Soc.* **2004**, *126* (23), 7330–7335.

Israelachvili, J. N.; Mitchell, D. J.; Ninham, B. W. Theory of Self-Assembly of Hydrocarbon Amphiphiles into Micelles and Bilayers. *J. Chem. Soc. Faraday Trans. 2* **1976**, *72*, 1525.

Jain, K.; Vedarajan, R.; Watanabe, M.; Ishikiriya, M.; Matsumi, N. Tunable LCST Behavior of Poly(N-Isopropylacrylamide/Ionic Liquid) Copolymers. *Polym. Chem.* **2015**, *6* (38), 6819–6825.

Jang, J.; Seol, Y. J.; Kim, H. J.; Kundu, J.; Kim, S. W.; Cho, D. W. Effects of Alginate Hydrogel Cross-Linking Density on Mechanical and Biological Behaviors for Tissue Engineering. *J. Mech. Behav. Biomed. Mater.* **2014**, *37*, 69–77.

Javid, N.; Roy, S.; Zelzer, M.; Yang, Z.; Sefcik, J.; Ulijn, R. V. Cooperative Self-Assembly of Peptide Gelators and Proteins. *Biomacromolecules* **2013**, *14* (12), 4368–4376.

Jeong, B.; Gutowska, A. Lessons from Nature : Stimuli- Responsive Polymers and Their Biomedical Applications. *TRENDS Biotechnol.* **2002**, *20* (7), 305–311.

Jeong, Y.; Joo, M. K.; Bahk, K. H.; Choi, Y. Y.; Kim, H. T.; Kim, W. K.; Jeong Lee, H.; Sohn, Y. S.; Jeong, B. Enzymatically Degradable Temperature-Sensitive Polypeptide as a New in-Situ Gelling Biomaterial. *J. Control. Release* **2009**, *137* (1), 25–30.

Jiang, L.; Yan, Y.; Drechsler, M.; Huang, J. Enzyme-Triggered Model Self-Assembly in Surfactant-Cyclodextrin Systems. *Chem. Commun.* **2012**, *48* (59), 7347–7349.

Jiwanich, S.; Ryu, J. H.; Bickerton, S.; Thayumanavan, S. Noncovalent Encapsulation Stabilities in Supramolecular Nanoassemblies. *J. Am. Chem. Soc.* **2010**, *132* (31), 10683–10685.

Jones, S. T.; Walsh-Korb, Z.; Barrow, S. J.; Henderson, S. L.; Del Barrio, J.; Scherman, O. A. The Importance of Excess Poly(N-Isopropylacrylamide) for the Aggregation of Poly(N-Isopropylacrylamide)-Coated Gold Nanoparticles. *ACS Nano* **2016**, *10* (3), 3158–3165.

Jonker, A. M.; Löwik, D. W. P. M.; Van Hest, J. C. M. Peptide- and Protein-Based Hydrogels. *Chem. Mater.* **2012**, *24* (5), 759–773.

Jun, H. W.; Paramonov, S. E.; Hartgerink, J. D. Biomimetic Self-Assembled Nanofibers. *Soft Matter* **2006**, *2* (3), 177–181.

Karbowiak, T.; Hervet, H.; Léger, L.; Champion, D.; Debeaufort, F.; Voilley, A. Effect of Plasticizers (Water and Glycerol) on the Diffusion of a Small Molecule in Iota-Carrageenan Biopolymer Films for Edible Coating Application. *Biomacromolecules* **2006**, *7* (6), 2011–2019.

Kashyap, S.; Jayakannan, M. Super LCST Thermo-Responsive Nanoparticle Assembly for ATP Binding through the Hofmeister Effect. *J. Mater. Chem. B* **2015**, *00*, 1–11.

Katti, D. S.; Lakshmi, S.; Langer, R.; Laurencin, C. T. Toxicity, Biodegradation and Elimination of Polyanhydrides. *Adv. Drug Deliv. Rev.* **2002**, *54* (7), 933–961.

Khan, W.; Choi, J. H.; Kim, G. M.; Park, S. Y., Microfluidic formation of pH responsive 5CB droplets decorated with PAA-b-LCP. *Lab Chip* **2011**, *11* (20), 3493-3498.

Kim, J.; Khan, M.; Park, S.-Y., Glucose Sensor using Liquid-Crystal Droplets Made by Microfluidics. *ACS Appl. Mater. Interfaces* **2013**, *5* (24), 13135-13139.

Kim, Y.-K.; Huang, Y.; Tsuei, M.; Wang, X.; Gianneschi, N. C.; Abbott, N. L., Multi-Scale Responses of Liquid Crystals Triggered by Interfacial Assemblies of Cleavable Homopolymers. *ChemPhysChem* **2018**, *19*, 1-10

Kim, Y.-K.; Senyuk, B.; Lavrentovich, O. D., Molecular reorientation of a nematic liquid crystal by thermal expansion. *Nat Commun* **2012**, *3*, 1133.

Kim, Y.-K.; Shiyonovskii, S. V.; Lavrentovich, O. D., Morphogenesis of defects and tactoids during isotropic nematic phase transition in self assembled lyotropic chromonic liquid crystals. *J. Phys.: Condens. Matter* **2013**, *25*, 404202.

Kim, Y.-K.; Wang, X.; Mondkar, P.; Bukusoglu, E.; Abbott, N. L., Self-reporting and self-regulating responsive liquid crystals. *Nature* **2018**, DOI: 10.1038/s41586-018-0098-y.

Kinsinger, M. I.; Sun, B.; Abbott, N. L.; Lynn, D. M., Reversible control of ordering transitions at aqueous/liquid crystal interfaces using functional amphiphilic polymers. *Adv. Mater.* **2007**, *19* (23), 4208-4212.

Klaikherd, A.; Nagamani, C.; Thayumanavan, S. Multi-Stimuli Sensitive Amphiphilic Block Copolymer Assemblies. *J. Am. Chem. Soc.* **2009**, *131* (13), 4830–4838.

Kleman, M.; Lavrentovich, O. D., *Soft Matter Physics: An Introduction*. Springer: New York, 2003.

Krishna, O. D.; Kiick, K. L. Protein- and Peptide-Modified Synthetic Polymeric Biomaterials. *Biopolymers* **2010**, *94* (1), 32–48.

Krishnamurthy, V. M.; Kaufman, G. K.; Urbach, A. R.; Gitlin, I.; Gudixsen, K. L.; Weibel, D. B.; Whitesides, G. M. Intrinsic thermodynamics of sulfonamide inhibitor binding to human carbonic anhydrases I and II *Chem. Rev.* 2008, *108*, 946–1051.

Kumar, S.; Dory, Y. L.; Lepage, M.; Zhao, Y. Surface-Grafted Stimuli-Responsive Block Copolymer Brushes for the Thermo-, Photo- and pH-Sensitive Release of Dye Molecules. *Macromolecules* **2011**, *44* (18), 7385–7393.

Kunz, W.; Testard, F.; Zemb, T. Correspondence between Curvature, Packing Parameter, and Hydrophilic-Lipophilic Deviation Scales around the Phase-Inversion Temperature. *Langmuir* **2009**, *25* (1), 112–115.

Kwon, J.-Y.; Khan, M.; Park, S.-Y., pH-Responsive liquid crystal double emulsion droplets prepared using microfluidics. *RSC Adv.* **2016**, *6* (61), 55976-55983.

Lee, D.-Y.; Seo, J.-M.; Khan, W.; Kornfield, J. A.; Kurji, Z.; Park, S.-Y., pH-responsive aqueous/LC interfaces using SGLCP-b-polyacrylic acid block copolymers. *Soft Matter* **2010**, *6* (9), 1964-1970.

Lee, H.; Jeong, J. H.; Park, T. G. PEG Grafted Polylysine with Fusogenic Peptide for Gene Delivery: High Transfection Efficiency with Low Cytotoxicity. *J. Control. Release* **2002**, *79* (1–3), 283–291.

Lee, J. H.; Yigit, M. V.; Mazumdar, D.; Lu, Y. Molecular Diagnostic and Drug Delivery Agents Based on Aptamer-Nanomaterial Conjugates. *Adv. Drug Deliv. Rev.* **2010**, *62* (6), 592–605.

Lee, J. H.; Yigit, M. V.; Mazumdar, D.; Lu, Y. Molecular Diagnostic and Drug Delivery Agents Based on Aptamer-Nanomaterial Conjugates. *Adv. Drug Deliv. Rev.* **2010**, *62* (6), 592–605.

Lee, P. I.; Corporation, C. Interpretation of Drug-Release Kinetics from Hydrogel Matrices in Terms of Time-Dependent Diffusion Coefficients The Swelling Behavior and Drug Release Kinetics in Glassy Hydrogels Are Interpreted in Terms of Time-Dependent Diffusion Coefficients. *ACS Symposium Series* **1987**, *348*

Lehner, D.; Lindner, H.; Glatter, O. Determination of the Translational and Rotational Diffusion Coefficients of Rodlike Particles Using Depolarized Dynamic Light Scattering. *Langmuir* **2000**, *16* (4), 1689–1695.

Li, J.; Du, X.; Hashim, S.; Shy, A.; Xu, B. Aromatic-Aromatic Interactions Enable  $\alpha$ -Helix to  $\beta$ -Sheet Transition of Peptides to Form Supramolecular Hydrogels. *J. Am. Chem. Soc.* **2017**, *139* (1), 71–74.

Li, L.; Raghupathi, K.; Yuan, C.; Thayumanavan, S. Surface Charge Generation in Nanogels for Activated Cellular Uptake at Tumor-Relevant pH. *Chem. Sci.* **2013**, *4* (9), 3654–3660.

Li, L.; Ryu, J. H.; Thayumanavan, S. Effect of Hofmeister Ions on the Size and Encapsulation Stability of Polymer Nanogels. *Langmuir* **2013**, *29* (1), 50–55.

Li, M.-H.; Keller, P. Stimuli-Responsive Polymer Vesicles. *Soft Matter* **2009**, *5* (5), 927–937.

Li, Z. T.; Hou, J. L.; Li, C.; Yi, H. P. Shape-Persistent Aromatic Amide Oligomers: New Tools for Supramolecular Chemistry. *Chem. - An Asian J.* **2006**, *1* (6), 766–778.

Liao, J.; Wang, B.; Huang, Y.; Qu, Y.; Peng, J.; Qian, Z. Injectable Alginate Hydrogel Cross-Linked by Calcium Gluconate-Loaded Porous Microspheres for Cartilage Tissue Engineering. *ACS Omega* **2017**, *2* (2), 443–454.

Lindeberg, G. A Convenient Synthesis of Aspartame. *J. Chem. Educ.* **1987**, *20* (c), 1062–1064.

Lindhoud, S.; de Vries, R.; Norde, W.; Stuart, M. a C. Structure and Stability of Complex Coacervate Core Micelles with Lysozyme. *Biomacromolecules* **2007**, *8* (7), 2219–2227.

Liu, B.; Thayumanavan, S. Substituent Effects on the pH Sensitivity of Acetals and Ketals and Their Correlation with Encapsulation Stability in Polymeric Nanogels. *J. Am. Chem. Soc.* **2017**, *139* (6), 2306–2317.

Liu, C. W.; Su, M.; Li, X. L.; Xue, T.; Liu, N.; Yin, J.; Zhu, Y. Y.; Wu, Z. Q. Multi-Stimuli-Responsive Chiral Organogels Based on Peptide Derivatives. *Soft Matter* **2015**, *11* (28), 5727–5737.

Liu, X.; Hu, D.; Jiang, Z.; Zhuang, J.; Xu, Y.; Guo, X.; Thayumanavan, S. Multi-Stimuli-Responsive Amphiphilic Assemblies through Simple Postpolymerization Modifications. *Macromolecules* **2016**, *49* (17), 6186–6192.

Liu, Y.; Terrell, J. L.; Tsao, C. Y.; Wu, H. C.; Javvaji, V.; Kim, E.; Cheng, Y.; Wang, Y.; Ulijn, R. V.; Raghavan, S. R.; et al. Biofabricating Multifunctional Soft Matter with Enzymes and Stimuli-Responsive Materials. *Adv. Funct. Mater.* **2012**, *22* (14), 3004–3012.

Lockwood, N. A.; Gupta, J. K.; Abbott, N. L., Self-assembly of amphiphiles, polymers and proteins at interfaces between thermotropic liquid crystals and aqueous phases. *Surf. Sci. Rep.* **2008**, *63* (6), 255–293.

Luo, T.; Kiick, K. L. Noncovalent Modulation of the Inverse Temperature Transition and Self-Assembly of Elastin-b-Collagen-like Peptide Bioconjugates. *J. Am. Chem. Soc.* **2015**, *137* (49), 15362–15365.

Marine, J. E.; Song, S.; Liang, X.; Watson, M. D.; Rudick, J. G. Bundle-Forming  $\alpha$ -Helical Peptide–dendron Hybrid. *Chem. Commun.* **2015**, *51* (76), 14314–14317.

Marinovich, M.; Galli, C. L.; Bosetti, C.; Gallus, S.; La Vecchia, C. Aspartame, Low-Calorie Sweeteners and Disease: Regulatory Safety and Epidemiological Issues. *Food Chem. Toxicol.* **2013**, *60*, 109–115.

Marques, H. M. C. A Review on Cyclodextrin Encapsulation of Essential Oils and Volatiles. *Flavour Fragr. J.* **2010**, *25* (5), 313–326.

Mart, R. J.; Osborne, R. D.; Stevens, M. M.; Ulijn, R. V. Peptide-Based Stimuli-Responsive Biomaterials. *Soft Matter* **2006**, *2* (10), 822.

Matthews BW, Weaver LH, Kester WR (1974). "The conformation of thermolysin". *J. Biol. Chem.* **1974**, *249* (24), 8030–8044.

Mattia, E.; Otto, S. Supramolecular Systems Chemistry. *Nat. Nanotechnol.* **2015**, *10* (2), 111–119.

Meijer, J. T.; Henckens, M. J. A. G.; Minten, I. J.; Löwik, D. W. P. M.; Van Hest, J. C. M. Disassembling Peptide-Based Fibres by Switching the Hydrophobic-Hydrophilic Balance. *Soft Matter* **2007**, *3* (9), 1135–1137.

Middleton, J. C.; Tipton, A. J. Synthetic Biodegradable Polymers as Orthopedic Devices. *Biomaterials* **2000**, *21* (23), 2335–2346.

Miller, D. S.; Wang, X. G.; Abbott, N. L., Design of Functional Materials Based on Liquid Crystalline Droplets. *Chem. Mater.* **2014**, *26* (1), 496–506.

Miravet, J. F.; Escuder, B.; Segarra-Maset, M. D.; Tena-Solsona, M.; Hamley, I. W.; Dehsorkhi, A.; Castelletto, V. Self-Assembly of a Peptide Amphiphile: Transition from Nanotape Fibrils to Micelles. *Soft Matter* **2013**, *9* (13), 3558.

Molla, M. R.; Marcinko, T.; Prasad, P.; Deming, D.; Garman, S. C.; Thayumanavan, S. Unlocking a Caged Lysosomal Protein from a Polymeric Nanogel with a pH Trigger. *Biomacromolecules* **2014**, *15* (11), 4046–4053.

Molla, M. R.; Prasad, P.; Thayumanavan, S. Protein-Induced Supramolecular Disassembly of Amphiphilic Polypeptide Nanoassemblies. *J. Am. Chem. Soc.* **2015**, *137* (23), 7286–7289.

Molla, M. R.; Rangadurai, P.; Pavan, G. M.; Thayumanavan, S. Experimental and Theoretical Investigations in Stimuli Responsive Dendrimer-Based Assemblies. *Nanoscale* **2015**, *7* (9), 3817–3837.

Mu, Y.; Yu, M. Effects of Hydrophobic Interaction Strength on the Self-Assembled Structures of Model Peptides. *Soft Matter* **2014**, *10* (27), 4956–4965.

Mujika, J. I.; Matxain, J. M.; Eriksson, L. A.; Lopez, X. Resonance Structures of the Amide Bond: The Advantages of Planarity. *Chem. - A Eur. J.* **2006**, *12* (27), 7215–7224.

Munkhbat, O.; Garzoni, M.; Raghupathi, K. R.; Pavan, G. M.; Thayumanavan, S. Role of Aromatic Interactions in Temperature-Sensitive Amphiphilic Supramolecular Assemblies. *Langmuir* **2016**, *32* (12), 2874–2881.

Nagarajan, R. Molecular packing parameter and surfactant self-assembly: The neglected role of the surfactant tail. *Langmuir.* **2002**, *18*, 31–38



Nazaruk, E.; Miszta, P.; Filipek, S.; Gorecka, E.; Landau, E. M.; Bilewicz, R., Lyotropic Cubic Phases for Drug Delivery: Diffusion and Sustained Release from the Mesophase Evaluated by Electrochemical Methods. *Langmuir* **2015**, *31* (46), 12753-12761.

Nuhn, H.; Klok, H. A. Secondary Structure Formation and LCST Behavior of Short Elastin-like Peptides. *Biomacromolecules* **2008**, *9* (10), 2755–2763.

Ohm, C.; Brehmer, M.; Zentel, R., Liquid Crystalline Elastomers as Actuators and Sensors. *Adv. Mater.* **2010**, *22* (31), 3366-3387.

Omer, M.; Khan, M.; Kim, Y. K.; Lee, J. H.; Kang, I.-K.; Park, S.-Y., Biosensor utilizing a liquid crystal/water interface functionalized with poly(4-cyanobiphenyl-4'-oxyundecylacrylate-b-((2-dimethyl amino) ethyl methacrylate)). *Colloid Surf. B-Biointerfaces* **2014**, *121*, 400-408.

Oyama, Y.; Sakai, H.; Arata, T.; Okano, Y.; Akaike, N.; Sakai, K.; Noda, K. Cytotoxic Effects of Methanol, Formaldehyde, and Formate on Dissociated Rat Thymocytes: A Possibility of Aspartame Toxicity. *Cell Biol. Toxicol.* **2002**, *18* (1), 43–50.

Ozkan, A. D.; Tekinay, A. B.; Guler, M. O.; Tekin, E. D. Effects of Temperature, pH and Counterions on the Stability of Peptide Amphiphile Nanofiber Structures. *RSC Adv.* **2016**, *6* (106), 104201–104214.

Papadopoulos, P.; Floudas, G.; Klok, H.; Schnell, I.; Pakula, T. Self-Assembly and Dynamics of Poly(Gamma-Benzyl-L-Glutamate) Peptides. *Biomacromolecules* **2004**, *5* (1), 81–91.

Pennakalathil, J.; Jahja, E. Red Emitting, Cucurbituril-Capped, pH-Responsive Conjugated Oligomer-Based Nanoparticles for Drug Delivery and Cellular Imaging. **2014**.

Popov, P.; Mann, E. K.; Jakli, A., Thermotropic liquid crystal films for biosensors and beyond. *J. Mat. Chem. B* **2017**, *5* (26), 5061-5078.

Puguan, J. M. C.; Yu, X.; Kim, H. Journal of Colloid and Interface Science Characterization of Structure, Physico-Chemical Properties and Diffusion Behavior of Ca-Alginate Gel Beads Prepared by Different Gelation Methods. *J. Colloid Interface Sci.* **2014**, *432*, 109–116.

Raghupathi, K. R.; Azagarsamy, M. A.; Thayumanavan, S. Guest-Release Control in Enzyme-Sensitive, Amphiphilic-Dendrimer-Based Nanoparticles through Photochemical Crosslinking. *Chem. - A Eur. J.* **2011**, *17* (42), 11752–11760.

Raghupathi, K. R.; Guo, J.; Munkhbat, O.; Rangadurai, P.; Thayumanavan, S. Supramolecular Disassembly of Facially Amphiphilic Dendrimer Assemblies in Response to Physical, Chemical, and Biological Stimuli. *Acc. Chem. Res.* **2014**, *47* (7), 2200–2211.

Raghupathi, K. R.; Sridhar, U.; Byrne, K.; Raghupathi, K.; Thayumanavan, S. Influence of Backbone Conformational Rigidity in Temperature-Sensitive Amphiphilic Supramolecular Assemblies. *J. Am. Chem. Soc.* **2015**, 150420131555003.

Raghupathi, K.; Li, L.; Ventura, J.; Jennings, M.; Thayumanavan, S. PH Responsive Soft Nanoclusters with Size and Charge Variation Features. *Polym. Chem.* **2014**, *5* (5), 1737–1742.

Rajagopal, K.; Lamm, M. S.; Haines-Butterick, L. a.; Pochan, D. J.; Schneider, J. P. Tuning the pH Responsiveness of  $\beta$ -Hairpin Peptide Folding, Self-Assembly, and Hydrogel Material Formation. *Biomacromolecules* **2009**, *10* (9), 2619–2625.

Rajdev, P.; Molla, M. R.; Ghosh, S. Understanding the Role of H-Bonding in Aqueous Self-Assembly of Two Naphthalene Diimide (NDI)-Conjugated Amphiphiles. *Langmuir* **2014**, *30* (8), 1969–1976.

Ramireddy, R. R.; Raghupathi, K. R.; Torres, D. A.; Thayumanavan, S. Stimuli Sensitive Amphiphilic Dendrimers. *New J. Chem.* **2012**, *36* (2), 340–349.

Ramström, O.; Mosbach, K. Synthesis and Catalysis by Molecularly Imprinted Materials. *Curr. Opin. Chem. Biol.* **1999**, *3* (6), 759–764.

Rangadurai, P.; Molla, M. R.; Prasad, P.; Caissy, M.; Thayumanavan, S. Temporal and Triggered Evolution of Host-Guest Characteristics in Amphiphilic Polymer Assemblies. *J. Am. Chem. Soc.* **2016**, *138* (24), 7508–7511.

Ribeiro, A.; Arias, F. J.; Reguera, J.; Alonso, M.; Rodríguez-Cabello, J. C. Influence of the Amino-Acid Sequence on the Inverse Temperature Transition of Elastin-like Polymers. *Biophys. J.* **2009**, *97* (1), 312–320.

Rocha-Selmi, G. a.; Bozza, F. T.; Thomazini, M.; Bolini, H. M. a; Fávoro-Trindade, C. S. Microencapsulation of Aspartame by Double Emulsion Followed by Complex Coacervation to Provide Protection and Prolong Sweetness. *Food Chem.* **2013**, *139* (1–4), 72–78.

Roy, D.; Cambre, J. N.; Sumerlin, B. S. Future Perspectives and Recent Advances in Stimuli-Responsive Materials. *Prog. Polym. Sci.* **2010**, *35* (1–2), 278–301.

Rudolph, T.; Kumar Allampally, N.; Fernández, G.; Schacher, F. H. Controlling Aqueous Self-Assembly Mechanisms by Hydrophobic Interactions. *Chem. - A Eur. J.* **2014**, *20* (43), 13871–13875.

Ryu, J. H.; Roy, R.; Ventura, J.; Thayumanavan, S. Redox-Sensitive Disassembly of Amphiphilic Copolymer Based Micelles. *Langmuir* **2010**, *26* (10), 7086–7092.

Ryu, J.-H.; Chacko, R. T.; Jiwanich, S.; Bickerton, S.; Babu, R. P.; Thayumanavan, S. Self-Cross-Linked Polymer Nanogels: A Versatile Nanoscopic Drug Delivery Platform Supporting Info. *J. Am. Chem. Soc.* **2010**, *3* (c), 2–10.

Ryzhkova, A. V.; Musevic, I., Particle size effects on nanocolloidal interactions in nematic liquid crystals. *Phys Rev E* **2013**, *87* (3), 032501.

Saito, N.; Kobayashi, H.; Yamaguchi, M. “Inverse” Thermoresponse: Heat-Induced Double-Helix Formation of an Ethynylhelicene Oligomer with Tri(Ethylene Glycol) Termini. *Chem. Sci.* **2016**, *7* (6), 3574–3580.

Sali, D.; Bycroft, M.; Fersht, a R. Stabilization of Protein Structure by Interaction of Alpha-Helix Dipole with a Charged Side Chain. *Nature.* **1988**, *335*,740–743.

Salim, M.; Minamikawa, H.; Sugimura, A.; Hashim, R. Amphiphilic Designer Nano-Carriers for Controlled Release: From Drug Delivery to Diagnostics. *Med. Chem. Commun.* **2014**, *5* (11), 1602–1618.

Savariar, E. N.; Ghosh, S.; González, D. C.; Thayumanavan, S. Disassembly of Noncovalent Amphiphilic Polymers with Proteins and Utility in Pattern Sensing. *J. Am. Chem. Soc.* **2008**, *130* (16), 5416–5417.

Schmaljohann, D. Thermo- and pH-Responsive Polymers in Drug Delivery. *Adv. Drug Deliv. Rev.* **2006**, *58* (15), 1655–1670.

Scruggs, N. R.; Kornfield, J. A., Synergistic ordering of side-group liquid crystal polymer and small molecule liquid crystal: Order and phase Behavior of nematic polymer solutions. *Macromol. Chem. Phys.* **2007**, *208* (19-20), 2242-2253.

Sedláč, M. What Can Be Seen by Static and Dynamic Light Scattering in Polyelectrolyte Solutions and Mixtures? *Langmuir* **1999**, *15* (12), 4045–4051.

Seo, J.-M.; Khan, W.; Park, S.-Y., Protein detection using aqueous/LC interfaces decorated with a novel polyacrylic acid block liquid crystalline polymer. *Soft Matter* **2012**, *8* (1), 198-203.

Settanni, G.; Zhou, J.; Suo, T.; Schöttler, S.; Landfester, K.; Schmid, F.; Mailänder, V. Protein Corona Composition of PEGylated Nanoparticles Correlates Strongly with Amino Acid Composition of Protein Surface. **2016**.

Sidiq, S.; Prasad, G.; Mukhopadhaya, A.; Pal, S. K., Poly(L-lysine)-Coated Liquid Crystal Droplets for Cell-Based Sensing Applications. *J. Phys. Chem. B* **2017**, *121* (16), 4247-4256.

Smith, A. M.; Williams, R. J.; Tang, C.; Coppo, P.; Collins, R. F.; Turner, M. L.; Saiani, A.; Ulijn, R. V. Fmoc-Diphenylalanine Self Assembles to a Hydrogel via a Novel Architecture Based on  $\pi$ - $\pi$  Interlocked  $\beta$ -Sheets. *Adv. Mater.* **2008**, *20* (1), 37–41.

Smits, F. C. M.; Buddingh, B. C.; Van Eldijk, M. B.; Van Hest, J. C. M. Elastin-like Polypeptide Based Nanoparticles: Design Rationale toward Nanomedicine. *Macromol. Biosci.* **2015**, *15* (1), 36–51.

Smrdel, P.; Bogataj, M.; Mrhar, A. The Influence of Selected Parameters on the Size and Shape of Alginate Beads Prepared by Iontropic Gelation. *Sci. Pharm.* **2008**, *76* (1), 77–89.

Sohajda, T.; Béni, S.; Varga, E.; Iványi, R.; Rácz, Á.; Szente, L.; Noszál, B. Characterization of Aspartame-Cyclodextrin Complexation. *J. Pharm. Biomed. Anal.* **2009**, *50* (5), 737–745.

Stasko, N. A.; Fischer, T. H.; Schoenfisch, M. H. S-Nitrosothiol-Modified Dendrimers as Nitric Oxide Delivery Vehicles. *Biomacromolecules* **2008**, *9* (3), 834–841.

Stuart, M. A. C.; Huck, W. T. S.; Genzer, J.; Müller, M.; Ober, C.; Stamm, M.; Sukhorukov, G. B.; Szleifer, I.; Tsukruk, V. V.; Urban, M.; et al. Emerging Applications of Stimuli-Responsive Polymer Materials. *Nat. Mater.* **2010**, *9* (2), 101–113.

Stupp, S. I.; Palmer, L. C. Supramolecular Chemistry and Self-Assembly in Organic Materials Design. *Chem. Mater.* **2014**, *26* (1), 507–518.

Tamura, A.; Ikeda, G.; Seo, J. H.; Tsuchiya, K.; Yajima, H.; Sasaki, Y.; Akiyoshi, K.; Yui, N. Molecular Logistics Using Cytocleavable Polyrotaxanes for the Reactivation of Enzymes Delivered in Living Cells. *Sci. Rep.* **2013**, *3*, 22–24.

Torchilin, V. P. Structure and Design of Polymeric Surfactant-Based Drug Delivery Systems. *J. Control. Release* **2001**, *73* (2–3), 137–172.

Trent, A.; Marullo, R.; Lin, B.; Black, M.; Tirrell, M. Structural Properties of Soluble Peptide Amphiphile Micelles. *Soft Matter* **2011**, *7* (20), 9572–9582.

Trongsatitkul, T.; Budhlall, B. M. Microgels or Microcapsules? Role of Morphology on the Release Kinetics of Thermoresponsive PNIPAm-Co-PEGMA Hydrogels. *Polym. Chem.* **2013**, *4* (5), 1502–1516.

Tsakiris, S.; Giannoulia-Karantana, A.; Simintzi, I.; Schulpis, K. H. The Effect of Aspartame Metabolites on Human Erythrocyte Membrane Acetylcholinesterase Activity. *Pharmacol. Res.* **2006**, *53* (1), 1–5.

Ukpebor, O. T.; Shah, A.; Bazov, E.; Boutis, G. S. Inverse Temperature Transition of Elastin like Motifs in Major Ampullate Dragline Silk: MD Simulations of Short Peptides and NMR Studies of Water Dynamics. *Soft Matter* **2014**, *10* (5), 773–785.

Ulijn, R. V. Enzyme-Responsive Materials: A New Class of Smart Biomaterials. *J. Mater. Chem.* **2006**, *16* (23), 2217–2225.

Ulijn, R. V.; Smith, A. M. Designing Peptide Based Nanomaterials. *Chem. Soc. Rev.* **2008**, *37* (4), 664–675.

Utracki, L. A.; Jamieson, A. M., *Polymer Physics: From Suspensions to Nanocomposites and Beyond*. John Wiley & Sons, INC.: Hoboken, New Jersey, 2010.

Valéry, C.; Artzner, F.; Paternostre, M. Peptide Nanotubes: Molecular Organisations, Self-Assembly Mechanisms and Applications. *Soft Matter* **2011**, *7* (20), 9583–9594.

Ventura, J.; Eron, S. J.; González-Toro, D. C.; Raghupathi, K.; Wang, F.; Hardy, J. A.; Thayumanavan, S. Reactive Self-Assembly of Polymers and Proteins to Reversibly Silence a Killer Protein. *Biomacromolecules* **2015**, *16* (10), 3161–3171.

Voo, W. P.; Ooi, C. W.; Islam, A.; Tey, B. T.; Chan, E. S. Calcium Alginate Hydrogel Beads with High Stiffness and Extended Dissolution Behaviour. *Eur. Polym. J.* **2016**, *75*, 343–353.

Wang, F.; Klaikherd, A.; Thayumanavan, S. Temperature Sensitivity Trends and Multi-Stimuli Sensitive Behavior in Amphiphilic Oligomers. *J. Am. Chem. Soc.* **2011**, *133* (34), 13496–13503.

Wang, H.; Raghupathi, K. R.; Zhuang, J.; Thayumanavan, S. Activatable Dendritic <sup>19</sup>F Probes for Enzyme Detection. *ACS Macro Lett.* **2015**, *4* (4), 422–425.

Wang, H.; Yang, Z. Short-Peptide-Based Molecular Hydrogels: Novel Gelation Strategies and Applications for Tissue Engineering and Drug Delivery. *Nanoscale* **2012**, *4* (17), 5259–5267.

Wang, H.; Zhuang, J.; Raghupathi, K. R.; Thayumanavan, S. A Supramolecular Dissociation Strategy for Protein Sensing. *Chem. Commun.* **2015**, *51* (97), 17265–17268.

Wang, W.; Tetley, L.; Uchegbu, I. F. The Level of Hydrophobic Substitution and the Molecular Weight of Amphiphilic Poly-L-Lysine-Based Polymers Strongly Affects Their Assembly into Polymeric Bilayer Vesicles. *J. Colloid Interface Sci.* **2001**, *237* (2), 200–207.

Webber, M. J.; Appel, E. A.; Meijer, E. W.; Langer, R. Supramolecular Biomaterials. *Nat. Mater.* **2015**, *15* (1), 13–26.

Wong, S.; Shim, M. S.; Kwon, Y. J. Synthetically Designed Peptide-Based Biomaterials with Stimuli-Responsive and Membrane-Active Properties for Biomedical Applications. *J. Mater. Chem. B* **2014**, *2* (6), 595.

Wood, T. A.; Lintuvuori, J. S.; Schofield, A. B.; Marenduzzo, D.; Poon, W. C. K., A self-quenched defect glass in a colloid-nematic liquid crystal composite. *Science* **2011**, *334*, 79-83.

Xiao, Z.; Liu, W.; Zhu, G.; Zhou, R.; Niu, Y. A Review of the Preparation and Application of Flavour and Essential Oils Microcapsules Based on Complex Coacervation Technology. *J. Sci. Food Agric.* **2014**, *94* (8), 1482–1494.

Xiao, Z.; Liu, W.; Zhu, G.; Zhou, R.; Niu, Y.; Tamura, A.; Ikeda, G.; Seo, J. H.; Tsuchiya, K.; Yajima, H.; et al. Micellar Interpolyelectrolyte Complexes. *Soft Matter* **2013**, *8* (21), 6888–6901.

Xie, M.; Wang, S.; Singh, A.; Cooksey, T. J.; Marquez, M. D.; Bhattarai, A.; Kourentzi, K.; Robertson, M. L. Fluorophore Exchange Kinetics in Block Copolymer Micelles with Varying Solvent-Fluorophore and Solvent-Polymer Interactions. *Soft Matter* **2016**, *12* (29), 6196–6205.

Xu, Y.; Wang, L.; Tong, Y.; Xiang, S.; Guo, X.; Li, J.; Gao, H.; Wu, X. Study on the Preparation, Characterization, and Release Behavior of Carbosulfan/Polyurethane Microcapsules. *J. Appl. Polym. Sci.* **2016**, *133* (35), 1–9.

Yamada, M.; Kondo, M.; Mamiya, J. I.; Yu, Y. L.; Kinoshita, M.; Barrett, C. J.; Ikeda, T., Photomobile polymer materials: Towards light-driven plastic motors. *Angew. Chem.-Int. Edit.* **2008**, *47* (27), 4986-4988.

Yamaoka, T.; Tamura, T.; Seto, Y.; Tada, T.; Kunugi, S.; Tirrell, D. a. Mechanism for the Phase Transition of a Genetically Engineered Elastin Model Peptide (VPGIG)<sub>40</sub> in Aqueous Solution. *Biomacromolecules* **2003**, *4* (6), 1680–1685.

Yan, Y.; Huang, J.; Tang, B. Z. Kinetic Trapping – a Strategy for Directing the Self-Assembly of Unique Functional Nanostructures. *Chem. Commun.* **2016**, 52 (80), 11870–11884.

Yang, D.-K.; Wu, S.-T., *Fundamentals of Liquid Crystal Devices*. John Wiley & Sons, Ltd.: Chichester, 2006.

Yefimova, S. L.; Tkacheva, T. N.; Kurilchenko, I. Y.; Sorokin, A. V.; Malyukin, Y. V. Spectroscopic Study of Interactions between Dye Molecules in Micelle and Liposome Nanovolumes. *J. Appl. Spectrosc.* **2013**, 79 (6), 914–921.

Yeh, P.; Gu, C., *Optics of liquid crystal displays*. John Wiley & Sons, Inc.: New York, 1999.

Yesilyurt, V.; Ramireddy, R.; Azagarsamy, M. A.; Thayumanavan, S. Accessing Lipophilic Ligands in Dendrimer-Based Amphiphilic Supramolecular Assemblies for Protein-Induced Disassembly. *Chem. - A Eur. J.* **2012**, 18 (1), 223–229.

Yesilyurt, V.; Ramireddy, R.; Thayumanavan, S. Photoregulated Release of Noncovalent Guests from Dendritic Amphiphilic Nanocontainers. *Angew. Chemie - Int. Ed.* **2011**, 50 (13), 3038–3042.

Yoshidome, T.; Kinoshita, M. Hydrophobicity at Low Temperatures and Cold Denaturation of a Protein. *Phys. Rev. E - Stat. Nonlinear, Soft Matter Phys.* **2009**, 79 (3), 1–4.

You, Y.; Zhou, Q.; Manickam, D. S.; Wan, L.; Mao, G.; Oupicky, D. Dually Responsive Multiblock Copolymers via Reversible Addition-Fragmentation Chain Transfer Polymerization: Synthesis of Temperature- and Redox-Responsive Copolymers of Poly ( N-Isopropylacrylamide ) and Poly ( 2- ( Dimethylamino ) Ethyl Methacrylate ). *Macromolecules* **2007**, 40, 8617–8624.

Young Ju Kim; Seong Jun Han; Shi Choon Kim; Young Kee Kang. Conformation and Sweet Tastes of L-Aspartyl Dipeptide Methyl Esters. *Biopolymers* **1994**, 34 (8), 1037–1048.

Yu, W.; Jiang, Y. Y.; Sun, T. W.; Qi, C.; Zhao, H.; Chen, F.; Shi, Z.; Zhu, Y. J.; Chen, D.; He, Y. Design of a Novel Wound Dressing Consisting of Alginate Hydrogel and Simvastatin-Incorporated Mesoporous Hydroxyapatite Microspheres for Cutaneous Wound Healing. *RSC Adv.* **2016**, 6 (106), 104375–104387.

Yuasa, Y.; Nagakura, a.; Tsuruta, H. Synthesis and Sweetness Characteristics of L-Aspartyl-D-Alanine Fenchyl Esters. *J. Agric. Food Chem.* **2001**, 49 (10), 5013–5018.

Zhai, P.; Chen, X. B.; Schreyer, D. J. Preparation and Characterization of Alginate Microspheres for Sustained Protein Delivery within Tissue Scaffolds. *Biofabrication* **2013**, *5* (1), 1-14.

Zhang, Y.; Cremer, P. S. The Inverse and Direct Hofmeister Series for Lysozyme. *Proc. Natl. Acad. Sci.* **2009**, *106* (36), 15249–15253.

Zhang, Y.; Zheng, Y.; Xiong, W.; Peng, C.; Zhang, Y.; Duan, R.; Che, Y.; Zhao, J. Morphological Transformation between Nanocoils and Nanoribbons via Defragmentation Structural Rearrangement or Fragmentation-Recombination Mechanism. *Sci. Rep.* **2016**, *6* (June), 1–8.

Zhang, Z.; Zhang, R.; Zou, L.; McClements, D. J. Protein Encapsulation in Alginate Hydrogel Beads: Effect of pH on Microgel Stability, Protein Retention and Protein Release. *Food Hydrocoll.* **2016**, *58*, 308–315.

Zhuang, J.; Gordon, M. R.; Ventura, J.; Li, L.; Thayumanavan, S. Multi-Stimuli Responsive Macromolecules and Their Assemblies. *Chem. Soc. Rev.* **2013**, *42* (17), 7421–7435.

Zou, J.; Bera, T.; Davis, A. A.; Liang, W.; Fang, J., Director Configuration Transitions of Polyelectrolyte Coated Liquid-Crystal Droplets. *J. Phys. Chem. B* **2011**, *115* (29), 8970-8974.